Ceramic Component Development

AGT 101

Advanced Gas Turbine Program

Topical Report

October 1979 - July 1987

Prepared by:

Standard Oil
Engineered Materials
Structural Ceramics
Niagara Falls, N.Y.

Under Contract To:

Garrett Auxiliary Power Division
A Unit of Allied-Signal Aerospace Company

For

National Aeronautics and Space Administration
Lewis Research Center, Cleveland, Ohio 44135
Contract DEN 3-167
and
U.S. Department of Energy
Office of Transportation Systems
Heat Engine Propulsion Division
Washington, D.C. 20585

Ceramic Component Development

AGT 101

Advanced Gas Turbine Program

Topical Report

October 1979 - July 1987

Foreword

This report represents a technical summary of the ceramic component development performed by Standard Oil Engineered Materials Company under a subcontract to the Garrett Auxiliary Power Division (GAPD) of the Garrett Corporation as part of the DOE/NASA AGT Project.

The Standard Oil Engineered Materials Company (henceforth abbreviated "Standard Oil"), a business division of the STEMCOR Corporation, is successor to the Carborundum Company.

Acknowledgment is gratefully given to the Garrett Auxiliary Power Division of the Garrett Corporation, The National Aeronautics and Space Administration (NASA) - Lewis Research Center and The U.S. Department of Energy (DOE) for their support of this program.

Also, acknowledged are the contributions of current and former employees of Standard Oil Engineered Materials Company and Carborundum, under the guidance of Dr. Roger Storm and Dr. Truett Sweeting.

Significant technical achievements during major portions of the program were realized through the contributions of Frank Frechette, Roger Ohnsorg in injection molding, Don Gerry in machining and design modifications, Ted Casper in slip casting, Dr. M. Srinivasan, and Diana Tierney in NDE. Additionally, this document could not have been put together without the dedicated help of Darlene Corp.

The comprehensive Final Report for the AGT101 Advanced Gas Turbine Project may be located in NASA publication Contractor's Report CR-180891.

AGT 101

TABLE OF CONTENTS

List of Figures

List of Tables

1.0   Summary

This report describes the component development tasks
carried out by Standard Oil* under the Advanced Gas Turbine (AGT)
project which was funded by the Department of Energy (DOE) and
administered by the National Aeronautics and Space Administration
(NASA) Lewis Research Center. Standard Oil, as a subcontractor to the
Garrett Auxiliary Power Division (GAPD)** of the Garrett Corporation,
conducted development work on ceramic components for the AGT 101
Unique program from October 1979 through June 1987. Additionally
materials and testing methods were evaluated from October 1979 through
March 1981 in the AGT Common Work jointly sponsored by GAPD and the
Allison Gas Turbine Division of General Motors***.

Standard Oil's accomplishments within the AGT 101 program
can be summarized in five key areas:

- Establishment of a design/fabrication interface
- Iterative component development
- Near net shape fabrication of large and/or complex
  shapes
- Availability of hardware for engine testing

Material and fabrication development on silicon carbide
based materials was conducted on the non-bladed rotor during the first
two years of the contract. Injection molding, thixotropic casting and
hot pressing of a molded shell with a suitable core material were
explored. Component integrity and material strength demonstrated in
these efforts showed limited success.

Designs for hot flow path components developed early in the
program were revised periodically to improve the performance
requirements or facilitate fabrication. Continuity of design/
fabrication improvements was maintained through frequent interactive
meetings between Standard Oil and GAPD personnel. The development of
near net shape forming processes for several of the hot flow path
components was in some cases aided by parallel processing routes to
assure adequate supply of good quality, dimensionally satisfactory
components.

Work carried out under the AGT 101 focussed on fabrication
development of sintered alpha silicon carbide (Hexoloy™ SA)
components. Hexoloy™ ST, a titanium diboride particulate reinforced
sintered alpha silicon carbide was introduced for the turbine
backshroud late during the last contract year.

formerly * Carborundum
          ** AiResearch and Garrett Engine Turbine Company
          ***Detroit Diesel Allison

Conventional isopressing/green machining combined with final grinding was chosen for components of relatively simple geometry such as duct spacer, turbine backshroud, regenerator shield, combustor liner and wave springs. An extrusion approach was also investigated to fabricate the regenerator shield and combustor liner but discontinued in favor of the conventional approach.

Fabrication development using the injection molding process was conducted on the turbine shroud and on stator segments as these components have variable wall thickness and a high degree of complexity. Several design iterations were carried out on the turbine shroud which was the largest part fabricated in Hexoloy™ SA. Mold modifications and sintering/fixturing experiments were implemented in an effort to improve dimensional tolerances and reduce warpage. Testing in the 1984/1985 contract years indicated that both components could only marginally withstand the tensile stresses in operation.

The combustor baffle was fabricated first by slip casting and then by injection molding. Design modifications indicated increased need for green machining of the internal slip cast profile, and consequently, injection molding with its near net shape capability was introduced. Machined components made by both forming techniques were supplied and tested.

Development work was carried out for the transition duct using slip casting, isopressing/green machining, and injection molding. The change in fabrication methods was predominantly governed by design iterations incorporating features such as locating tabs, platforms and thermocouple port holes. All components subjected to rig and engine tests were fabricated by isopressing/green machining and dense grinding. Injection molding development was conducted during the latter part of the contract in a parallel effort.

Ceramic components tested in all-ceramic engine tests to 2200^0F have accumulated about 100 hours. Additionally, transition ducts and combustor baffles were successfully screened in 2500^0F rig tests. Several stationary components such as the combustor baffle, regenerator shield, and combustor liner have performed reliably. Testing and resultant failures of other components have lead directly to design modifications or directed attention to material and fabrication improvements.

2.0   Introduction

The Advanced Gas Turbine (AGT) Program was initiated in late 1979 due to growing national concerns regarding energy conservation and critical materials availability, and based on the accomplishments of the earlier Ceramic Applications to Turbine Engines (CATE) Program. The project, funded by the U.S. Department of Energy (DOE) and administered by the National Aeronautics and Space Administration (NASA) - Lewis Research Center, focusses on three major areas:

- Develop technology for a multi-fuel energy efficient turbine engine for passenger cars.
- Determine the feasibility of ceramic components, utilizing easily available, non-strategic materials.
- Assure the end-product is affordable and mass-producible.

The prime contractor of the AGT 101 is Garrett Auxiliary Power Division (GAPD)* a division of the Garrett Corporation with the Ford Motor Company supporting automotive application of the AGT 101 (Figure 1). Standard Oil** has been a principal subcontractor since the project was initiated.
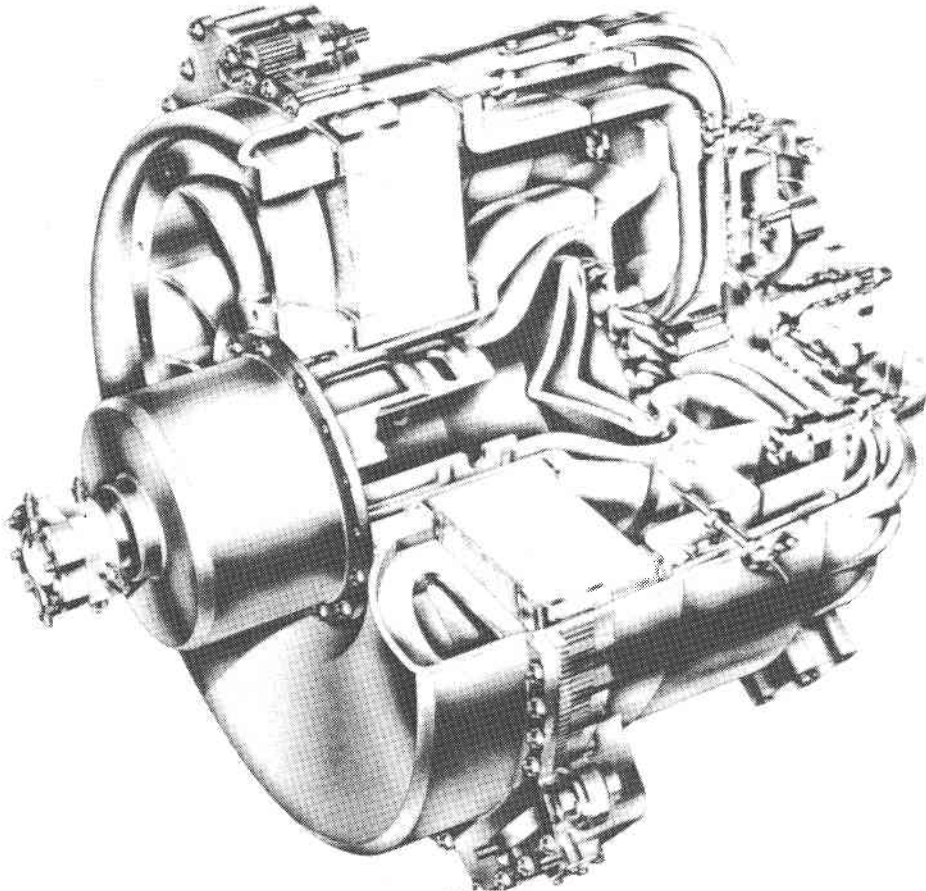
Figure 1. AGT 101 Schematic

* formerly AiResearch and Garrett Turbine Engine Company
**formerly Carborundum

3

2.1 Technical Approach

Within the AGT Powertrain System Development Project, Standard Oil was to provide component development, fabrication, manufacturing feasibility, and cost studies, and participate with the system contractor (GAPD) in performance assessment.

It was essential that development and demonstration of ceramic components for the hot flow path of the AGT 101 be performed as an integral part of the system development project. This would enable both engine development and ceramic component development to proceed with the best possible results.

Key to the technical approach to ceramic component development is the "Closed Loop" development cycle shown in Figure 2. The technologies comprising the closed loop operate in an iterative manner to develop a reliable ceramic.
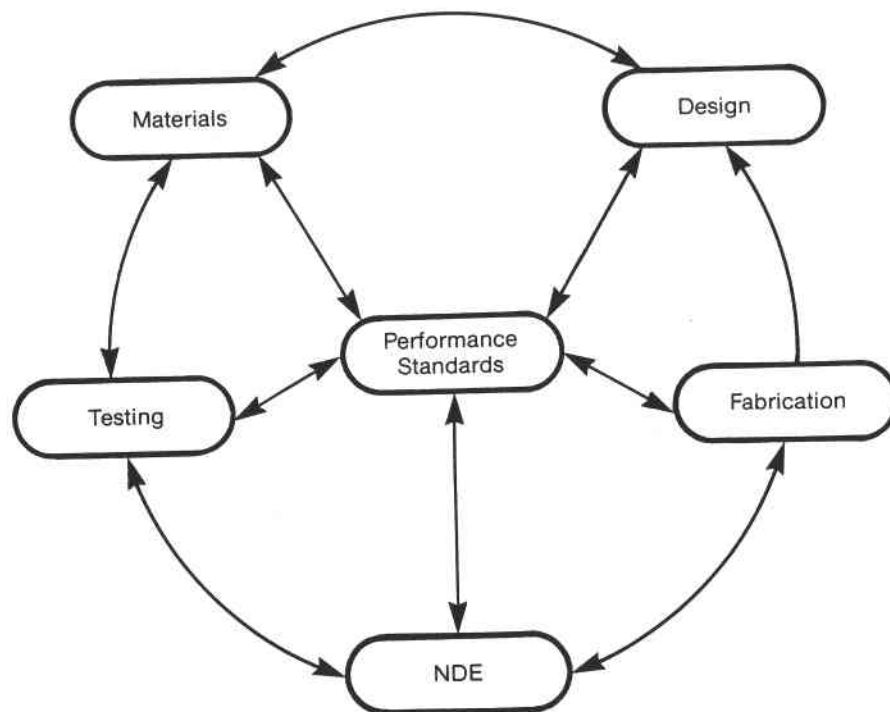
Figure 2. Closed Loop Component Development Cycle

Development of ceramic components requires the talents
available in many disciplines, yet these separate activities must be
closely coordinated. By promoting constant interaction between
specialists in the various disciplines, Garrett and Standard Oil have
developed an effective development process which has achieved
remarkable technical progress.

Performance requirements and design involve establishing the
requirements of environment, reliability, lifetime, stress and
temperature distribution working with the mechanical and aerodynamic
design team to arrive at a viable design, then constantly reviewing
the development program to determine progress toward the requirements.

Materials include the types of ceramic materials and the
physical and mechanical properties of the materials that have
application to the AGT 101 engine. This also includes improving the
fundamental understanding of the materials, their properties, and the
ceramic powders from which they are derived.

Fabrication deals with forming, machining, firing and dense
grinding of ceramic components. A variety of fabrication techniques
are applicable to the various AGT 101 components. Net shape forming
is desirable for most turbine components in order to maximize
performance, reproducibility and eventual manufacture at the lowest
possible cost. Net shape forming can help minimize the incidence of
flaws that may result from machining, grinding or handling.

Non-destructive Evaluation (NDE) involves the development
and use of techniques available to detect critical flaws at current
strength levels, application of these to complex shapes, and the
development of techniques for higher strength material with inherently
smaller flaws.

Testing includes two elements. The first is material
characterization which is required for design, material and
fabrication improvement. The second includes testing ceramic
components under actual or simulated turbine operating conditions in
order to verify or change the design considerations, NDE capabilities,
or material and fabrication requirements.

In summary, the AGT program has represented the most
comprehensive use of all of these approaches to ceramic development.

2.2   Statement of Work

The Statement of Work developed by GAPD and Standard Oil was completed April 11th, 1980. The following is a summary of pertinent sections of this document.

STATEMENT OF WORK
CARBORUNDUM SUBCONTRACT

ADVANCED GAS TURBINE POWERTRAIN
SYSTEM DEVELOPMENT PROJECT

This document defines specific work tasks to be performed by Carborundum as a major subcontractor to AiResearch Manufacturing Company of Arizona, hereinafter referred to as AiResearch Phoenix. These tasks relate to development of selected ceramic components applicable to the development of an Advanced Gas Turbine (AGT) powertrain for automotive applications.

This document addresses the following sections:

AiResearch Phoenix Program Schedule - This section defines key dates when ceramic components are required for Advanced Gas Turbine (AGT) engine development to continue on schedule.

Work Breakdown Structure (WBS) - This section defines the WBS for cost and technical management and is the format to be used by Carborundum to provide a technical work plan and price quotation.

Carborundum Evaluation Criteria - This section defines the milestones and criteria by which Carborundum material and component development will be evaluated. Although the program is organized such that multiple process approaches and materials will be evaluated at the start of the program, the number will be narrowed down at the milestone points.

Work Statement - This section defines specific tasks (according to the WBS) to be included in the work plan, schedule, and Carborundum quotation. To meet the tight schedule of components for rig and engine testing, it is suggested that component fabrication development be initiated, as early as possible after the preliminary design review (PDR), by use of existing or simplified tooling prior to the time prints are released for Design A components.

Component Drawings - Drawings have previously been supplied to Carborundum. The PDR, fixed the engine

6

configuration and served as a release point for initial component development efforts. A list of reference drawings is included and will be updated as configurations are finalized.

Reporting Requirements - The reporting requirements, that are identified in this section, enumerate the different reports and number of copies required.

Specifically, the Work Statement addresses the turbine rotor and ceramic structures comprising combustor transition, combustor turbine baffle and backshroud turbine, turbine stator, turbine shroud, turbine diffuser (duct, inner turbine and duct, outer turbine), and flow separator housing. Carborundum shall conduct work in the areas of design support/fabrication development, component qualification/ NDE/Proof, hardware delivery, and post test evaluation.

3.0   Quality Assurance and Non-Destructive Examination

Quality Assurance, which encompasses the use if not the development of Non-destructive Examination (NDE), is an integral part of any product cycle. Similar to the closed loop approach to development, the quality assurance involvement in the product cycle can be depicted as shown in Figure 3.

Design & Development

Product Planning

Product Use

Quality Assurance Involvement in Product Cycle

Design & Purchase of Mfg. Tooling

Shipment

Production of Product

Purchase of Raw Materials

Receipt of Materials
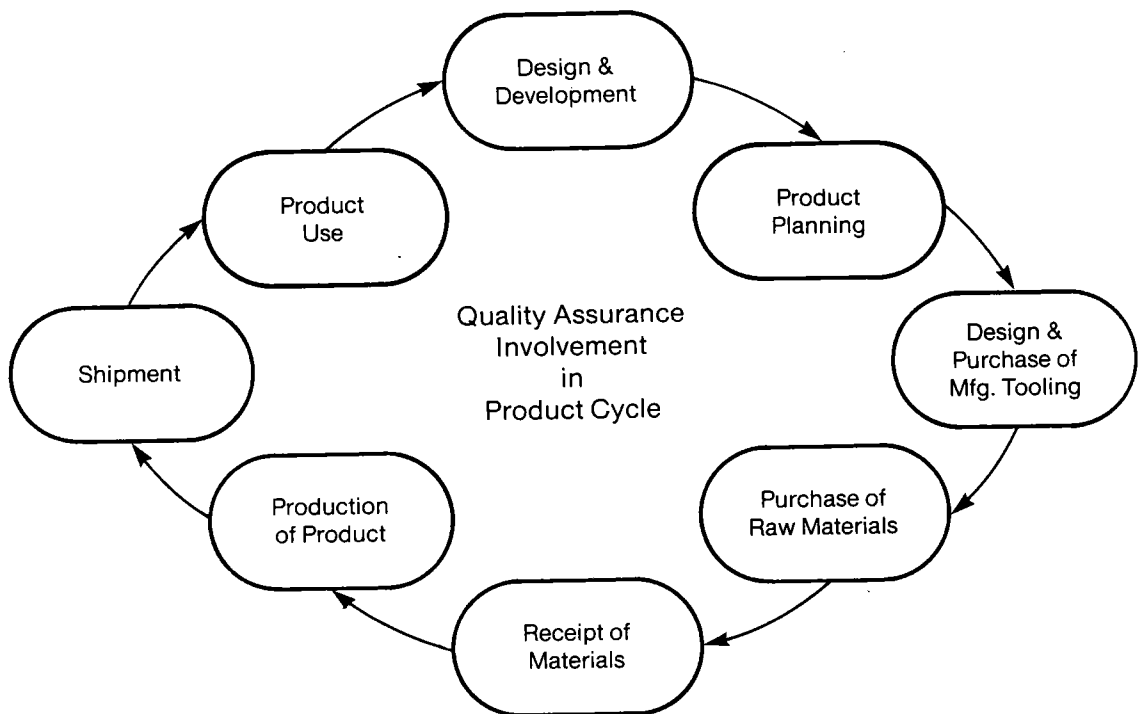
Figure 3.   Quality Assurance Involvement in the Product Development Cycle

Quality Assurance is involved in all stages of the product cycle including design, development, fabrication, inspection, storage and shipment. Q.A. engineering maintains a program for training and certification of personnel who execute special inspection processes. Certification requirements include examination to verify personnel knowledge and proficiency in the inspection process.

For the AGT program, Quality Assurance procedures were used as a screening device to determine the suitability of various NDE techniques. NDE development was largely limited to the AGT Common workscope (Appendix). However, new and promising techniques that have become available during the timeframe of the AGT have been utilized to the benefit of the program.

8

Section 4 includes component specific information regarding how various NDE techniques were used. The following is a brief summary regarding each technique and the types and sizes of flaws that can be detected. The NDE analyses to be discussed include: raw material analyses; visual, dimensional, and surface finish; X-ray radiography; fluorescent dye-penetrant (FPI); ultrasonics; and computer aided tomography (C.A.T.). Table 1 summarizes current NDE capability for several of the available techniques.

Table 1
Flaw Detection
Capabilities of Various NDE Techniques

Technique	Flaw	Detectability	Remarks
Radiography	Porosity	1-2% of part thickness	
	Inclusion Green Sintered	50 µm 25 µm	Depends on Density of Inclusion
X-ray Tomography	Inclusions	50-100 µm	Spatial Information
Ultrasonics	Inclusions Green Sintered Cracks	(100 MHz) 100 µm 25 µm 100 µm	Component Shape Dependent
Dye Penetrants	Surface Defects	250 µm	Surface Finish Dependent
Acoustic Microscopy	Surface and Sub-surface Cracks, Pores, Inclusions	50 µm	Micro-structure Dependent
Photoacoustic Spectroscopy	Surface and Near Surface Defects	50 µm	
NMR	Porosity Binder Distribution	? ?	Needs dopants Provides Spatial Information
Neutron Techniques	Binder Distribution Agglomerates	? ?	

3.1   In Process Quality Assurance

Opposed to merely sorting out project components at the end of the line, in-process Quality Assurance attempts to identify and characterize defects as early in the process as possible. This serves to narrow the scope of investigation when attempting to identify the causes of defects, and prevents the unwarranted expenditure of resources by further processing flawed components.

However, in many instances, flaws in green (unsintered) components are difficult to detect. Flaws that went undetected in green components may manifest themselves much more clearly after sintering. Improved NDE of green components continues to be in need of significant development.

Table 2 shows which NDE techniques may be used in the various steps of the fabrication process.

Table 2
NDE Techniques Utilized During the Fabrication of Components

Raw Material	Spray Dried Powder	Green Components	As-Fired Components	Finish Ground Components
Chemistry Particle Size Surface Area Sinterability	Sinterability Shrinkage Microstructure			
		Density Dimensions X-ray Tomography	Density Dimensions X-ray FPI Contour Tomography	Dimensions X-ray FPI Contour

Individual inspection plans were developed and utilized for each component in accordance with Garrett's specifications: SC 6500 - Drawing Interpretation, EMS 52309 - Penetrant Inspection, EMS 52334 - X-ray Radiography.

3.2   Non Destructive Techniques

3.2.1   Raw Material Analysis

Raw Material is received as submicron SiC which is sampled and subsequently tested for particle size distribution, surface area and sinterability. Chemical analysis is either supplied by the vendor or tested at local labs audited by the Quality Assurance department.

Spray dried powder used for various forming techniques is tested for sinterability (3.13 g/cm^3 minimum), shrinkage

characteristics, and microstructure. Microstructures of sintered test specimens are visually analyzed versus Standard Oil specifications according to maximum flaw size, flaw proximity, and flaw concentration.

In addition to the microstructure examination, lots of premix are graded by shrinkage and their usefulness for particular applications, customer requirements, and forming techniques can be determined. This is particularly critical for fixed dimension tooling or for close tolerance net shape components.

3.2.2   Visual, Dimensional Evaluation and Surface Finish

Prototype components are visually inspected for surface flaws using a Bausch and Lomb binocular microscope with variable magnification of 8-40 times.

Part profiles are checked on selected components (Figure 4) using a double stylus ContouReader model #250 with chart recorder attachment. This unit produces a trace of the part profile at 5, 10 or 20 times magnification which then is compared to a mylar tracing of the part specifications.
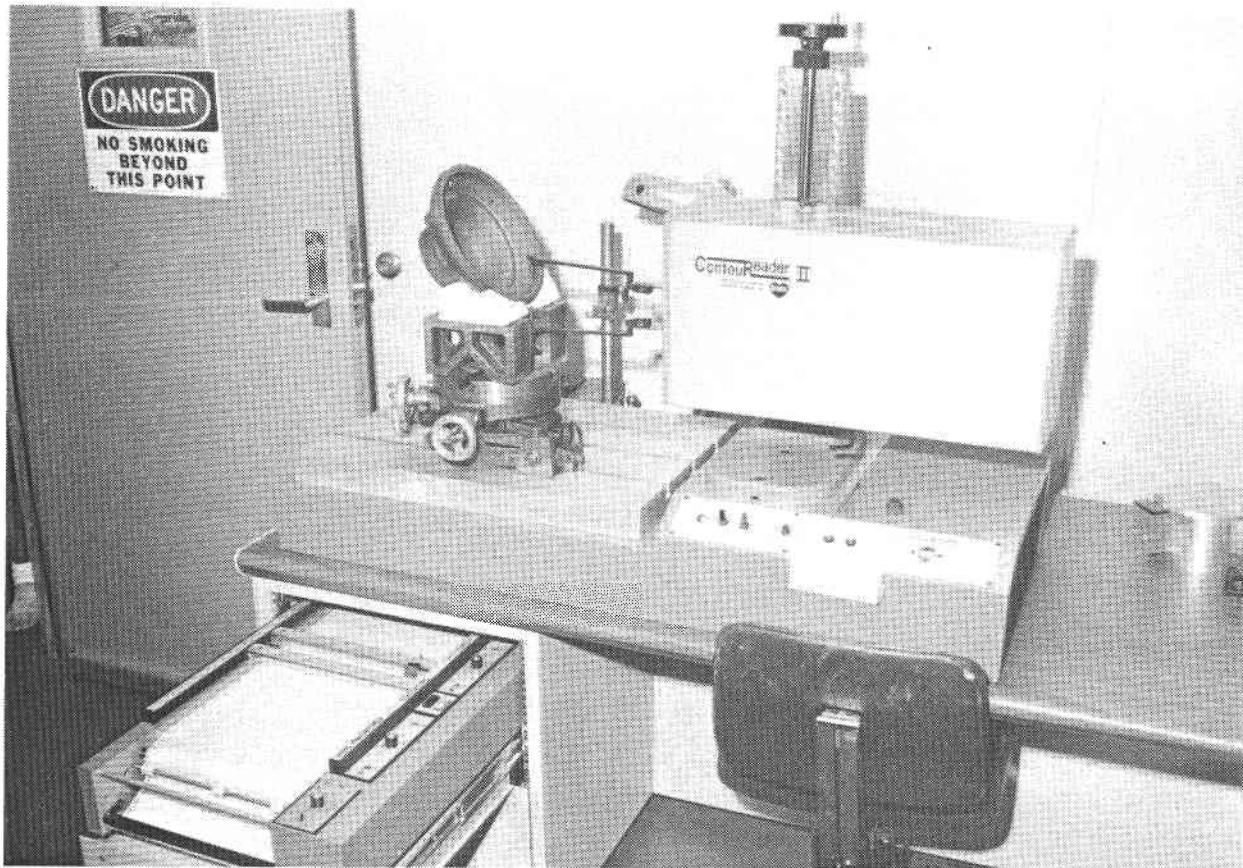
Figure 4. Contour Tracing of Transition Duct

Surface finish on flat sections of components can be measured using a Taylor Hobson Talysurf 10 surface texture measuring instrument. This unit is capable of measuring surface textures from 0.2 to 200 micro inches (0.01 to 5.0 micro-meters).

A Jones and Lampson Epic 214 optical comparator is used to measure some of the more complex shapes having a readability of .00005" and .0001 mm.

3.2.3   X-Ray Radiography

X-ray inspection consists of passing X-rays through a part and documenting, on film, variations in X-ray absorption. Internal discontinuities - cracks, voids, or inclusions - cause a density variation as recorded on film. Typically, voids appear as dark areas, and high density inclusions as lighter areas. Changes in part thickness are other sources of X-ray differential absorption. Section thickness, flaw orientation, X-ray source size, energy and film are all variables to be considered when developing inspection techniques for ceramics which possess low linear attenuation coefficients of X-ray absorptions (as compared to metallics) resulting in low contrast radiographs making indications more difficult to detect.

X-ray inspection at Standard Oil utilizes a Magnaflux MXK-100M microfocus unit with a focal spot size of 50 microns, 100KV and 1.0Ma (Figure 5) for all AGT 101 parts. Fine grain Kodak M and AA film are used with the addition of .010" thick lead screens to increase definition on complex parts by increasing contrast. Table 3 summarizes the detection levels achieved with this instrument on seeded defects within sintered SiC discs dependent on material thickness.
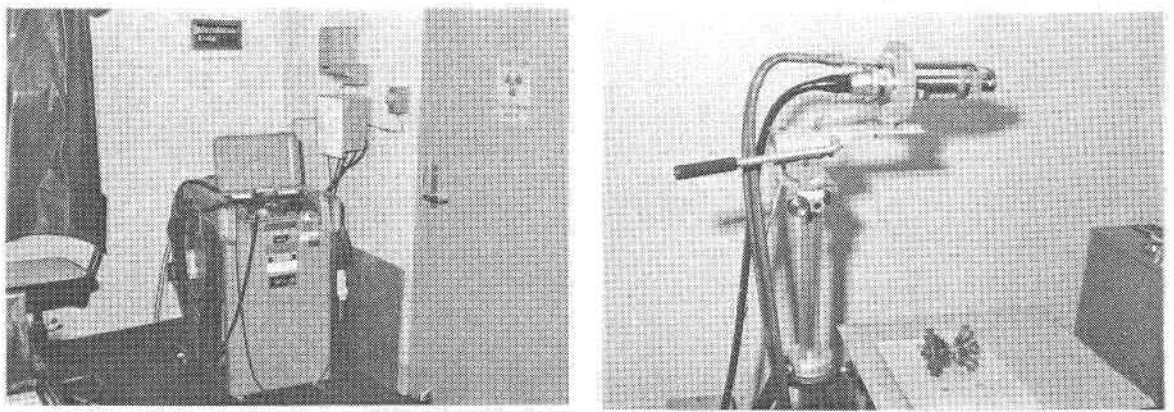
Figure 5. Magnaflux Microfocus X-Ray Unit

Table 3
X-Ray Radiography Detection Levels

Disk Thickness (inch)	Void Size μm		Carbon Inclusion Size (μm)		B_4C Inclusion Size (μm)	
	50-125	125-250	50-125	125-250	50-125	125-250
0.1	D	D	D	D	PI	D
0.125	D	D	D	D	ND	D
0.25	ND	D	—	D	—	D
0.50	—	D	—	D	—	D

D — Detected
ND — Not Detected
PI — Possible Indication

The ability to detect small discontinuities by X-ray is greatly increased when the largest dimension of the discontinuity lies perpendicular to the imaging plane. Knowledge of the typical indications resulting from forming or processing techniques aids the ability to detect flaws since the view imaged will be one which incorporates this knowledge. New parts or processes pose a difficulty since past knowledge although useful may not provide the necessary images.

To further aid in detecting flaws non destructively Standard Oil's R&D Center at Warrensville, Ohio acquired recently a Ridge HOMX 161 real time X-ray unit.

Real-time X-ray allows manipulation of the part and simultaneous viewing of the x-ray image. This system produces X-rays from a 10 micron focal spot which pass through the object to be inspected. The resultant X-rays strike an image intensifier which convert this energy to light. This light is recorded by a video camera, digitized and sent either directly to a video monitor or through an image analyzer and then to the monitor. A Hughes image analysis system is used to average frames to reduce noise, change contrast ratios to produce either greater or less contrast, store images for subtraction and thereby increase the ability to detect discontinuities.

3.2.4   Fluorescent Penetrant Inspection

Fluorescent penetrant inspection (FPI) is used to detect discontinuities open to the surface of materials such as cracks and surface porosity. Fluorescent penetrants employ highly fluorescent dyes suspended in a petroleum based liquid which is highly fluid and can enter surface discontinuities through capillary action (Figure 6). The fluorescent dyes make indications detectable when examined under an ultraviolet light source (Figure 7).

FIGURE (a). Following precleaning, penetrant is applied to test surfaces and seeps into surface discontinuities during the penetrant dwell time.

Penetrant wets clean part surface and seeps into surface defect

FIGURE (b). Angled coarse warm water spray removes excess water-soluble penetrant from test surface but does not remove entrapped penetrant from surface-connected discontinuities such as cracks and pores.

45°

Coarse warm water spray rinse applied at 45° to surface

Penetrant entrapment undisturbed

FIGURE (c). After test parts have been washed, wet developer coating is applied and dried. Porous developer coating acts as a blotter to draw penetrant from entrapments to form indications.

Spreading of indication

Dry porous developer layer

Depletion of liquid penetrant from entrapment

FIGURE (d). Near-ultraviolet light excitation causes fluorescent penetrant indication to glow in dark. Visible color penetrant is observed under ordinary white light conditions and does not require ultraviolet radiation. Following inspection, parts are cleaned to remove developer and penetrant residues.

Fluorescent light emission from indication area

Depleted volume in entrapment

Figure 6. Schematics Showing Fluorescent Penetrant Inspection Treatment of Components

Figure 7. FPI Room - Preparation Area (left),
Inspection Under Ultraviolet Light (right)

FPI at Standard Oil is conducted using a Magnaflux CA28W
testing unit with both water-washable (ZL17C) and post-emulsified
(ZL22C) penetrant testing capabilities. Typical indications can be
detected and categorized to approximately the .005" range regardless
of the configuration (spot or linear indications). Line drawings
(Figure 8) were used to document the location of indications and a
calibrated comparator was used to estimate the size.

Water-washable penetrants are used to inspect as-sintered
components which will be subsequently diamond ground. Since very fine
flaws are less critical to detect on surfaces which will be removed
the water-washable penetrants affords an economical means of detecting
indications which prevent further processing of components of suspect
quality.

The post-emulsified penetrant employs a lipophilic
emulsifier to render excess surface penetrant washable. This testing
system allows detection of both fine flaws and wide shallow
discontinuities.

PART DESCRIPTION **Segmented Turbine Stator**   CUSTOMER P.O. NO. **1931619**

CUSTOMER **Garrett**   PROJECT NO. **489-E5**

PART DWG. NO. **L-3846162**   PART SERIAL NO. **26-586**

	Concave	Convex
Visual P	Blister .005	Pit .005
Zyglo P?		
X-Ray		Spot 0.010
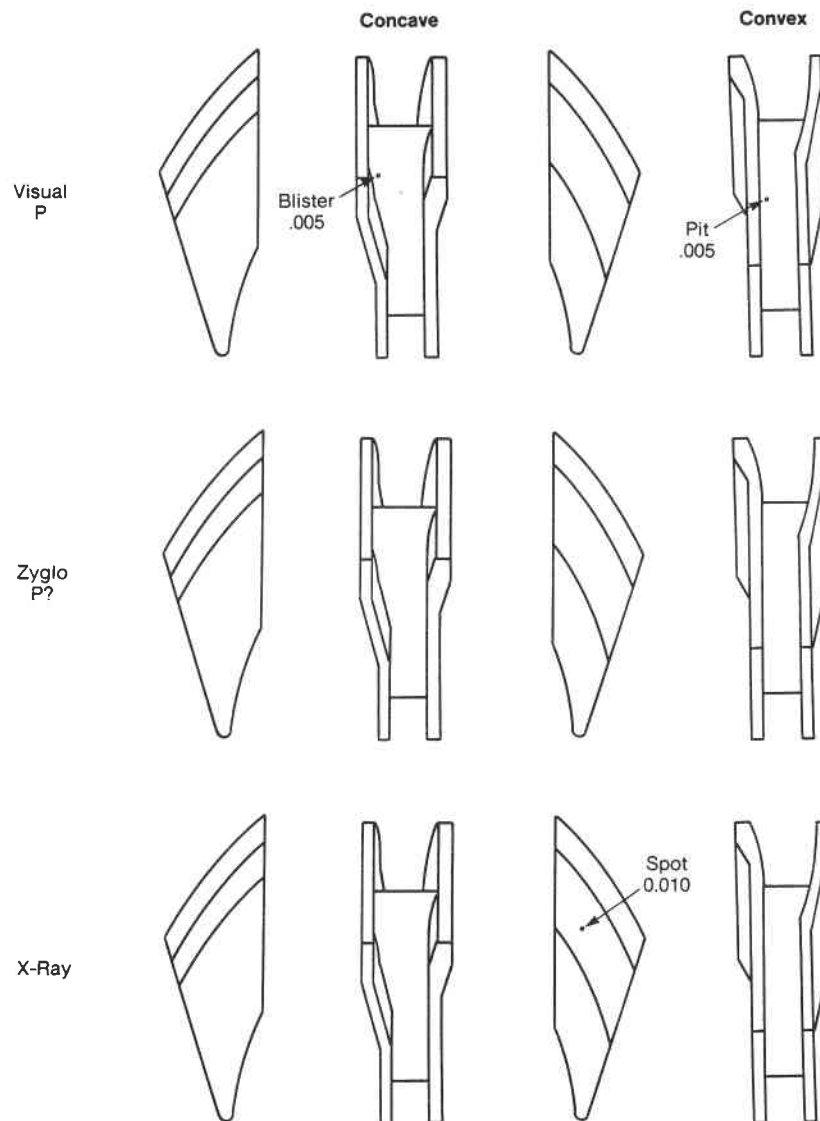
Figure 8. NDE Inspection Summary

3.2.5   Computer Aided Tomography

Computer Aided Tomography (commonly known as C.A.T. Scanning) is an X-ray technology by which the image of the interior of a sample can be analyzed quickly, with little or no sample preparation. Primarily developed for medical use, C.A.T. Scanning has been recently applied to materials analyses.

Tomography is the process of imaging a particular cross-section or "slice" of an object. Various terminologies for "computed tomography" are as follows:

C.A.T.   - Computer Aided Tomography, or Computerized Axial Tomography

C.T.   - Computed Tomography

R.T.   - Reconstructive Tomography

C.T.A.T. - Computerized Transverse Axial Tomography

The latter is the most limited term and refers to cross-section images transverse to the long axis of the sample.

A typical C.A.T. scanning technique uses a collimated X-ray beam and detector array which makes a series of transverse passes across the sample at various angles. Beam attenuation data measured at intervals along the length of each transverse scan is computer processed to generate a 256 x 256 matrix. Each pixel ($1mm^2$ resolution) is assigned a CT or delta number and a gray level is calculated as a function of its attenuation factor.

For example:

Dark Color = Low CT No. = Low Density
Light Color = High CT No. = High Density

Generally, C.A.T. scanning can be used to detect composition variations, density variations, and the presence of voids or fractures.

Early in 1986, Standard Oil's Warrensville (Ohio) R & D Center obtained a Deltascan 100 C.A.T. scanner (Figure 9). This second generation unit consists of a tungsten source X-ray beam that provides three collimated beams and an equal number of detectors for measuring the attenuation of the X-rays as they pass through an object. This type of scanner, a six beam/detector configuration, measures transmitted X-ray intensity during linear translations of the source and detectors at one to six degree increments for a $180°$ rotation (Figure 10). The result is a series of transmitted intensity profiles obtained at multiple angles through all points within the cross section which is being imaged.
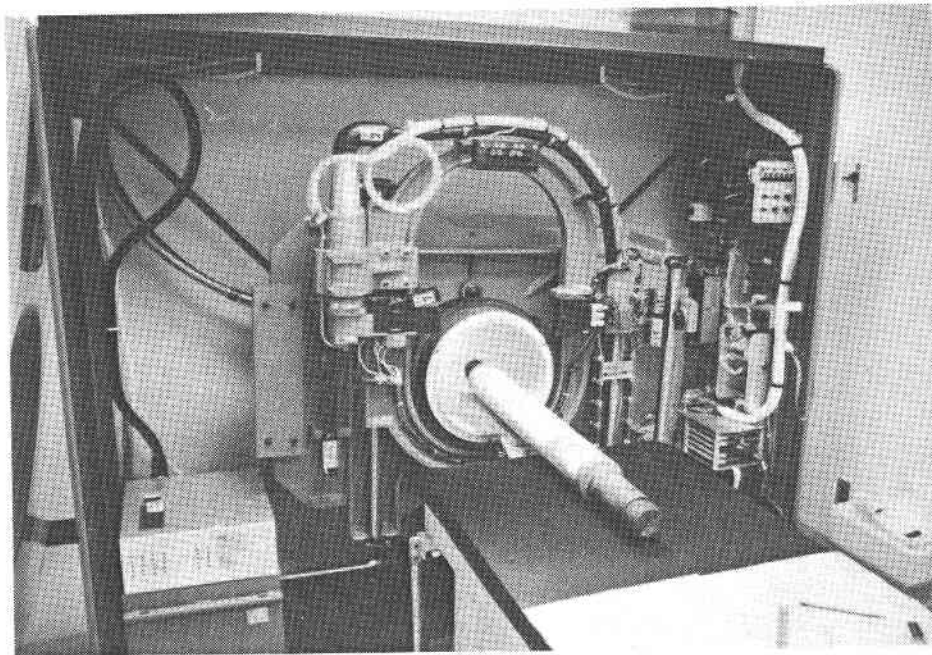
Figure 9. C.A.T. Scanning Equipment
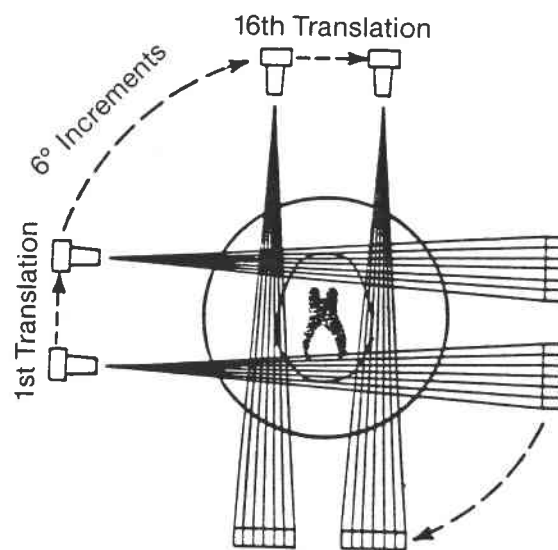
Figure 10. The Combined Rotational-Translational Scan
Sequence with Multiple Detectors Representative
of the Deltascan 100 C.A.T. Scanner

As shown in Figure 11, a slice can be divided into a n X n matrix of voxels (volume elements). The attenuation of N_0 X-ray photons passing through a single voxel with a linear coefficient μ results in N transmitted photons:

$$N = N_0 \exp(-\mu x)$$

where x is the dimension of the voxel in the direction of the X-Rays. Parameters of a material that determine the linear attenuation coefficient of a voxel include density and chemical composition. For n successive voxels, each with its own attenuation coefficient, the number of transmitted photons for one X-ray beam is:

$$N = N_0 \exp \quad - (\mu_1 + \mu_2 + \mu_3 + \ldots + \mu_n) \; x$$
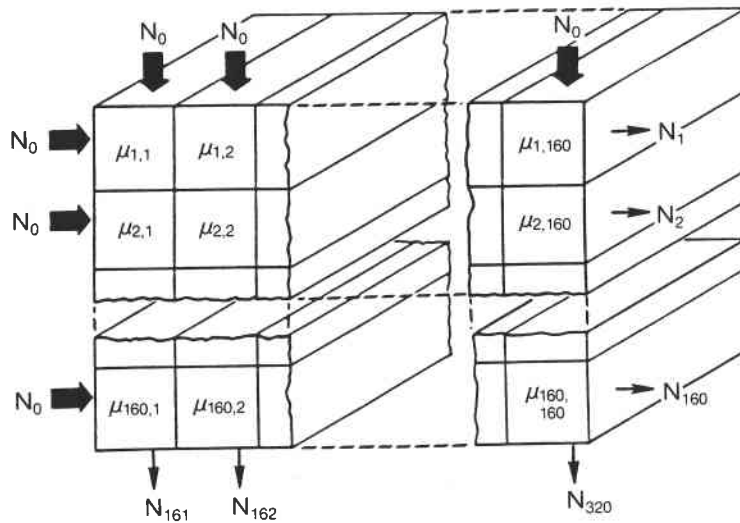
Figure 11. Incident Intensity for a
160 x 160 Matrix of Voxels

The incident intensity is attenuated differently along the various paths the beam traverses, depending on the number and attenuation coefficients of the voxels in each path. Thus, different values of N are obtained as the X-ray beam passes through different series of voxels. An algorithm uses these values to reconstruct an image that is really a matrix of linear attenuation coefficients, termed CT numbers after rescaling. For samples with a homogeneous chemical composition, CT numbers correspond directly to density.

The Deltascan 100 generates a 256 x 256 voxel image with each voxel having dimensions of 1 x 1 x 10 mm (10mm is the thickness of the slice). Each voxel is assigned a gray level based on its CT number with a dark color corresponding to a low CT number (or linear attenuation coefficient) and a light color corresponding to a high CT number.

Ideal sample size is 10 inches in diameter, which is the size of the circle scanned. Samples as large as 17 inches in diameter can be accommodated in the instrument, but a 3.5 inch ring around the perimeter will not be imaged. There is no upper limit on sample length, as samples can be fed through the instrument. The theoretical lower limit on sample size coincides with the dimensions of the voxels making up the image. In practice, resolution decreases as sample size decreases, and only general information can be obtained on samples less than one inch in diameter.

Material samples scanned to date include reservoir rock cores and engineered materials. Internal features discerned in the cores include fractures, drilling mud invasion, and general lithology. Initial studies indicate that for homogeneous intervals, an indirect relationship exists between CT number and rock permeability. This promising relationship potentially could result in C.A.T. scan analysis replacing certain types of costly and time-consuming laboratory core analysis.

Internal features discerned in silicon carbide transition ducts (Figure 12) include density variations and the presence and distribution of voids. In one particular useful related application, rotors were scanned prior to HIPing (hot isostatic pressing), a process designed to increase density and uniformity. Density variations, both within and between rotors, were quantified. The same rotors were scanned again after HIPing. By the comparison of CT numbers, it was determined that the process had been effective. Figure 13 shows the density distribution of SiC rotors before and after HIPing.
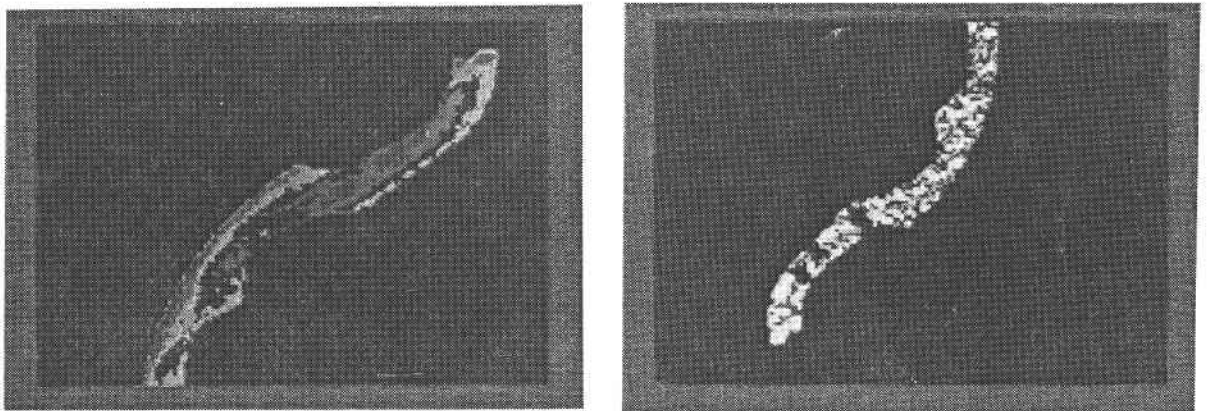
Figure 12. C.A.T. Scans of SiC Transition Ducts -
Molded (left), Sintered (right)

20
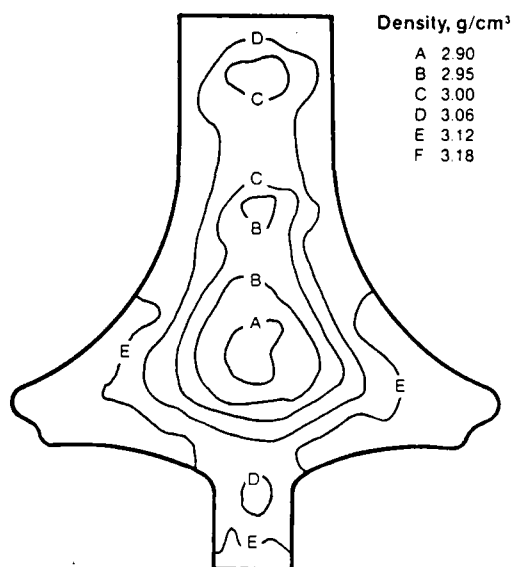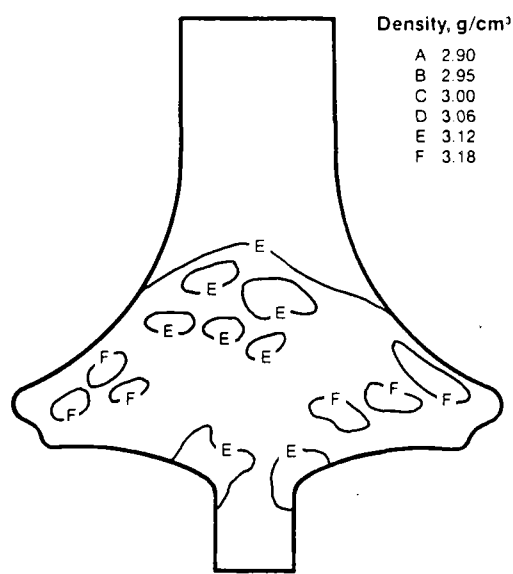
BEFORE HIPing   AFTER HIPing

Figure 13. C.A.T. Scans of SiC Rotors Before and After HIPing

        The Deltascan 100 has two disadvantages: a 1 cm slice
thickness and a fixed scan circle size. This results in a poorer
resolution than what is available on newer generation instruments.

3.3   Material Evaluation

Material performance evaluation is another important means of assuring quality and component reliability. Periodic material evaluation can provide a measure of material consistency and/or development progress depending on the program and technological thrusts. One of the goals of the AGT 101 program was the development of manufacturing processes which are capable of duplicating test bar material properties in complex sintered alpha silicon carbide engine components.

Sintered alpha silicon carbide (SASC) is an essentially single phase material with a fine microstructure having a grain size in the range of 4 to 8 um. Components are made from submicron size alpha SiC powder compacts which are pressureless sintered at temperatures exceeding $2000^{\circ}C$ under inert atmospheres. Most commercial ceramic fabrication techniques such as slip casting, injection molding, isopressing/green machining, etc. have been successfully employed in the manufacture of complex shapes.
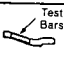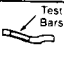
Material properties are commonly determined using modulus of rupture (MOR) bars (1/8" x 1/4" x 2") formed individually or cut from small plates, and tested in a four-point bending mode.

Room temperature and elevated temperature strength data were collected on samples of twenty to thirty bars to develop the Weibull statistics and establish comparative baselines. Lot qualification bars were supplied with components delivered for a threefold property data comparison between baseline, lot qualification, and bars cut from components. This methodology allows a comparative assessment of the various forming methods which are used to fabricate variable profile, complex configurations. However, only a limited number of components were evaluated using this destructive measure. Table 4 provides a summary of the data obtained on two backshrouds and a transition duct, both configurations made by isopressing and green machining, and a slip cast combustor baffle.

An evaluation of these data indicates that the average characteristic strength of MOR bars cut from components is frequently lower than the baseline test bars. However, this table, also indicates that it is possible to fabricate components which exhibit material properties which approach or even duplicate baseline data. The generally high variability of all of the data indicates that further processing improvements and in process controls are necessary to achieve reliability factors suitable for high volume economic fabrication.

Table 4

Room Temperature Flexure Strength Comparison
(GAPD Test Data)

Component/ Source Material	Test Bar Orientation	Component Cut-Up			Certification Bars			Baseline Test Bars		
		No. of Bars	Strength, ksi Characteristic (average)	Modulus (Standard Deviation) Weibull	No. of Bars	Strength, ksi Characteristics (average)	Modulus (Standard Deviation) Weibull	No. of Bars	Strength, ksi Characteristic (average)	Modulus (Standard Deviation) Weibull
Turbine Backshroud S/N 101A	Test Bars	12	41.8 (40.4)	14.2 (3.1)		Not Tested		30	57.7* (54.3)*	7.7 (8.0)
Turbine Backshroud S/N 104A	Test Bars	5	54.4 (49.0)	6.2 (7.7)		Not Tested		30	57.7* (54.3)	7.7 (8.0)
Transition Duct S/N 113	Test Bars	23	34.3 (32.6)	9.1 (4.0)	5	36.9 (34.6)	6.8 (4.6)	30	57.7* (54.3)	7.7 (8.0)
Combustor Baffle S/N 122	Test Bars	5	51.6 (49.1)	8.9 (5.3)	4	67.5 (65.7)	16.6 (3.8)	30	49.4	5.8

All test bars have a 0.250 x 0.125 inch cross section, have been ground in longitudinal direction, and were heat treated 2 hours at 2200° F. Flexure testing was performed at 0.02 inch per minute cross head speed with 1.5 inch outer span, 0.75 inch inner span.

*Not heat treated

4.0   Component Development

4.1   Rotor

Work on the unique rotor development was initiated in late 1979 and continued through November 1981. Sintered alpha silicon carbide and several reaction bonded silicon carbide systems were investigated with respect to their fast fracture behavior at RT and 1200°C. Material development was carried out on individually prepared MOR bars.

Fabrication development was conducted using three distinctly different methodologies. Injection molding of a solid one piece rotor was investigated together with the fabrication of a bonded rotor made of an injection molded shell and a hot pressed core and thixotropic casting of a reaction bonded silicon carbide rotor. All processing activities were carried out on a simulated (non-bladed) rotor. This approach reduced cost and tooling lead time significantly while it permitted assessment of initial fabrication progress.

The non-bladed rotor ("doorknob") as shown in Figure 14 simulates the mass of the bladed rotor and the shape of the rotor hub. Based on future needs to produce a complex bladed rotor (Figure 15) Standard Oil selected the injection molding process to produce the part. An injection molding tool was designed with removable cores to produce two shell configurations as well as a solid hub. The shells represented thicknesses within the processing limits of then current technology while the solid hub provided development opportunities for thick section binder removal and subsequent sintering studies.
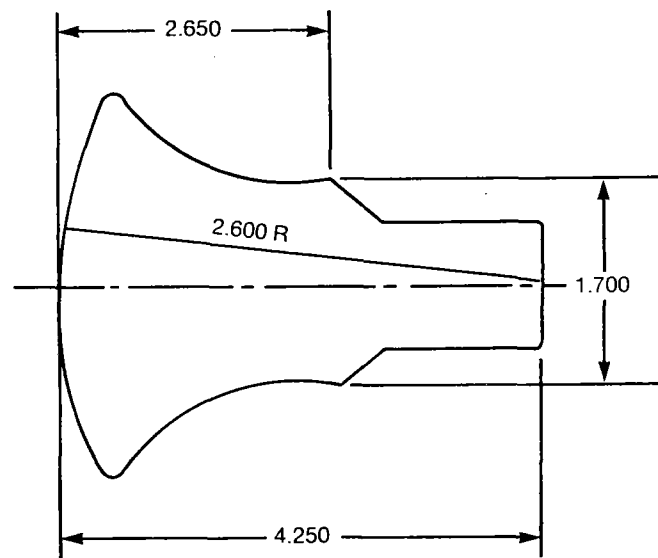
Figure 14.   Simulated Rotor Design

24
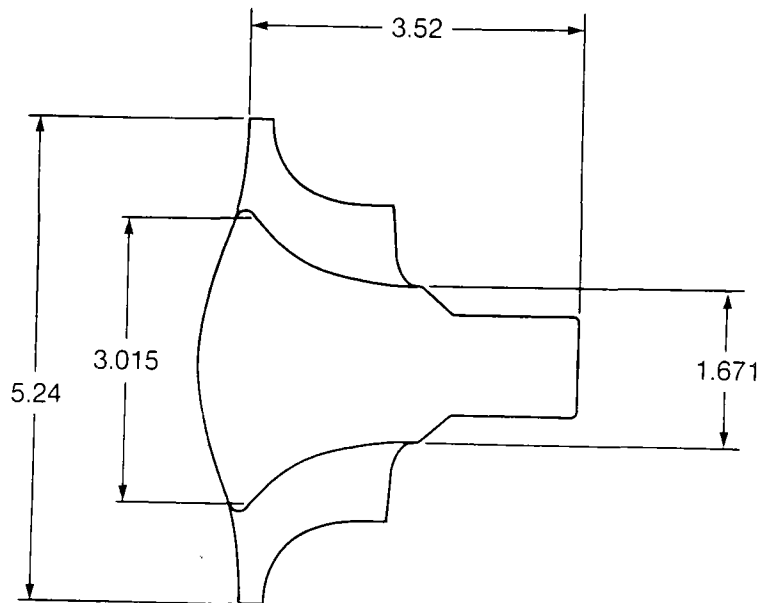
Figure 15. Bladed Rotor Design

4.1.1   Fabrication Development

4.1.1.1   Injection Molding

Rotor Shell Molding

The injection molding tool was designed with the dual molding approach in mind for producing either a single piece solid hub, or by changing cavity inserts, a shell having nominal wall thickness varying from approximately 3/8 inch to 3/4 inch. The design of the tool was completed December 1979 and the tool was received at the end of the first Quarter of 1980.

The tool was installed on a 250T Reed Reciprocating Screw Injection Molding Machine at G-W's (subsidiary of Carborundum at the time) alpha silicon carbide test molding facility. Prior to molding, the ejector mechanism was reworked to provide improved sliding action. The shell configuration was selected for the initial molding trial in April. This molding was conducted to assess functional design and to verify dimensional accuracy of the tool.

The core was designed to seal on four sections of the sprue bushing thereby allowing the cavity to fill through four equally spaced gates. The molding compound has a tendency to jet into the cavity and producing strands which coil and fold during packing. Thus, the defect potential increases unless sufficient pressure is available to compress and weld the strands into a solid mass.

25

All of the rotor shells showed visible flow lines concentrated at the lower section of the inner rim. A sketch of the molded rotor shell is shown in Figure 16 and the arrows indicate the region where the flow lines were predominantly observed. Attempts were made to correct this problem by enlarging the gates to allow maximum pressure transmission for a longer period of time to obtain better packing and minimize the incidence of flow lines. Subsequent molding trials with the enlarged gates produced no noticeable improvements.
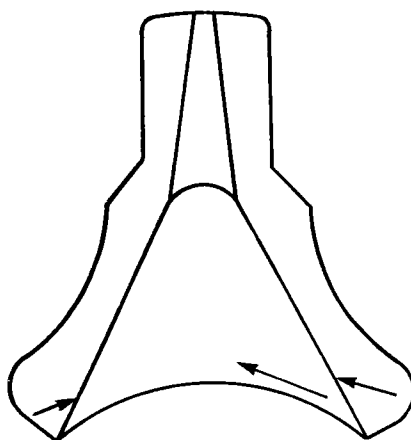
Figure 16. Cross Sectional View of First Generation
Rotor Shell

A total of 39 simulated rotors were molded, 15 of these were produced in the tool after gate enlargement. Attempts were made to optimize the molding conditions by incorporating changes in four basic molding parameters: barrel temperature, pressure, velocity profile, and mold temperature.

The barrel temperature was varied between 300 and 350^0F with the majority of individual molding trials conducted at 310^0F. Essentially three pressure levels were investigated: 1000, 1400 and 1700 psi. The two higher pressure levels were used most frequently. Several velocity profiles were tested with equal importance between a constant and a variable velocity profile utilizing slow, medium and fast speeds. Finally the mold temperature was varied between 80 and 125^0F.

Changes in molding conditions produced only subtle changes in the molded product; a decision was therefore made to modify the core to provide a thinner wall in the problem area. A molding was carried out, and conditions were determined to produce processable parts. The net result of the core modification was a minimization of flow lines. Flow lines that were noticed, were much smaller and closer to the edge of the inner rim.

Two molding trials to produce thin shelled simulated rotors (Figure 17) were conducted during the first half of 1980. Approximately 80 shells were molded. Sixty of these used the standard molding material and the balance used a new molding compound with improved rheological properties and bake-out characteristics.
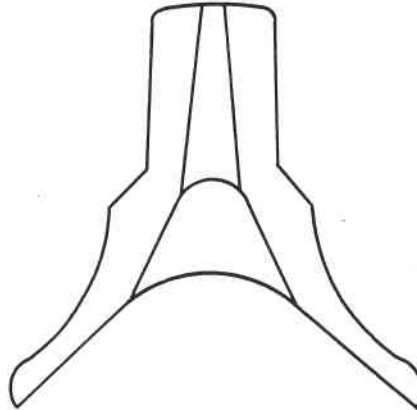
Figure 17. Cross Sectional View of Second
Generation Rotor Shell

Solid Rotor Molding

Preliminary molding trials for producing a solid simulated rotor were conducted in May of 1980. Initially, the thickness of the part posed problems during molding due to shrinkage on cooling and air entrapment during filling. By changing molding conditions, shrinkage could be accommodated and macro-porosity due to air entrapment could be reduced but not completely eliminated (Figure 18).

Even though it was expected that this macro-porosity could completely be eliminated through molding optimization and tooling changes, work continued only on a low efforts basis because of problems in the subsequent binder removal step.
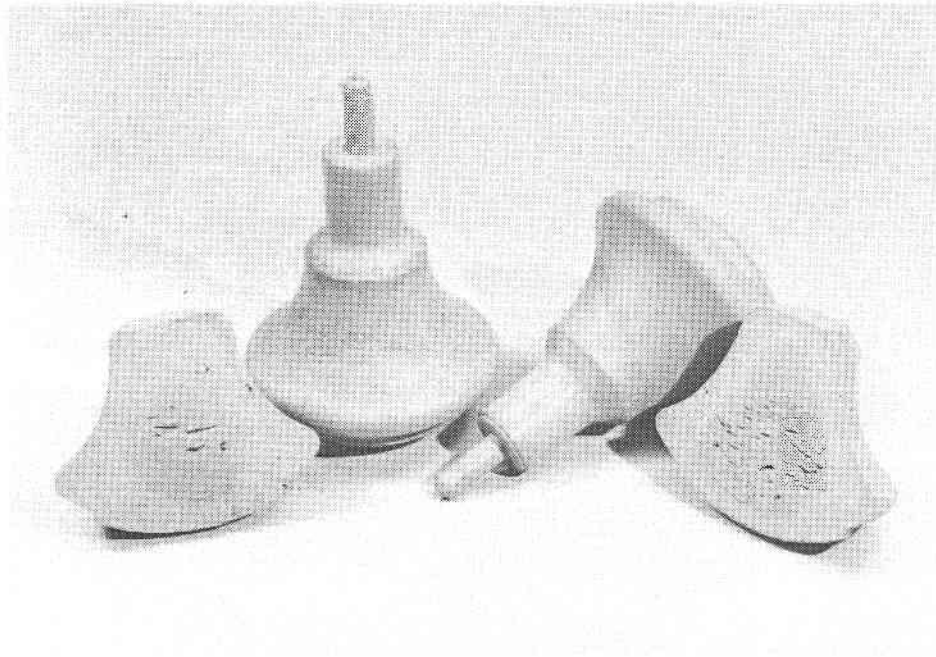
Figure 18. Molded Simulated Rotors with Macro-Porosity

A tool modification aimed at reducing the macro-porosity in the rotor center was completed January 1981. The plate containing the spherical bottom detail was attached to a separate hydraulic system. After packing during the molding cycle, a secondary compaction was initiated and held during cooling. Figure 19 shows the two halves of the mold.

Two molding runs were conducted using two different molding compounds, the previously used compound as well as a newly developed compound which had demonstrated good binder bake out characteristics in thick cross sections. The tool modifications implemented proved to be successful. Dense void-free molded shapes were obtained with both compounds. Several rotors were processed through binder removal and sintering, but each of the rotors exhibited cracks after process completion.
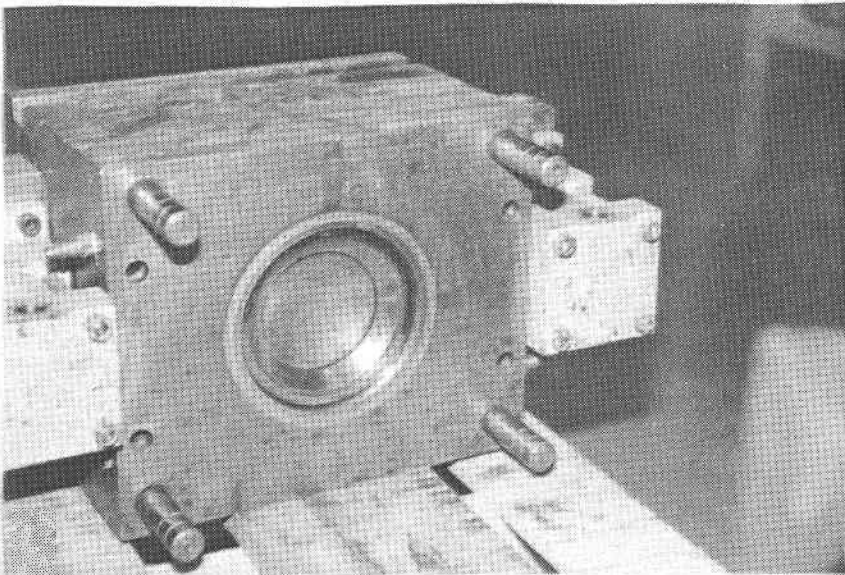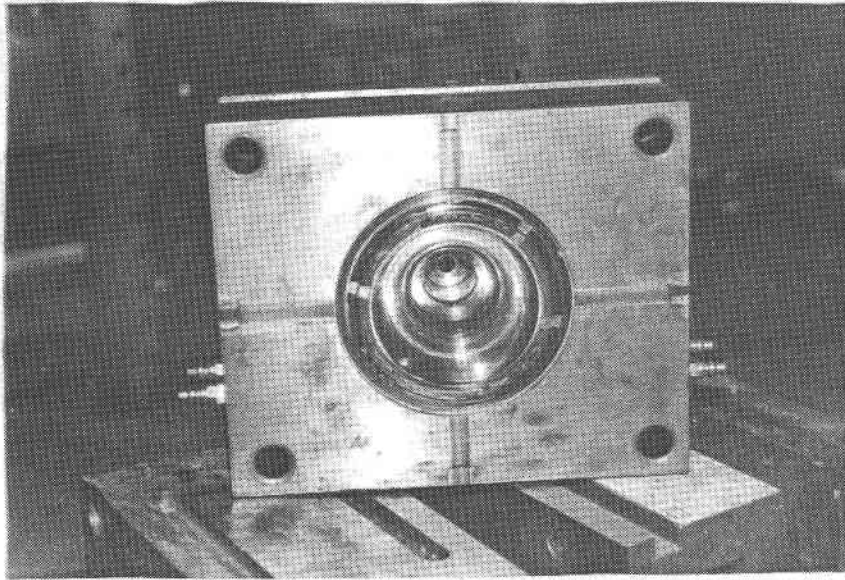
Figure 19. Revised Injection Molding Tool for
Solid Simulated Rotor

Post Molding Processing

Binder removal is one of the most critical steps in the production of sintered alpha silicon carbide shapes. Although other techniques were considered, thermal degradation of the binder was selected since substantial prior experience existed with this method. A comparison of the three molded shapes, thick-walled and thin-walled shell as well as solid one-piece rotor hub, indicated clearly the increased difficulties experienced with larger cross sections.

In order to be successful in the removal of organics from an injection molded silicon carbide body, heat was applied slowly at a gradually increasing rate to produce micropassages which allow the decomposition products from the binder to escape from the body without causing any cracks. An inert environment is required to prevent oxidation of the SiC at peak bake-out temperatures. A uniform temperature distribution is needed in the ovens to remove the binder without introducing cracks in the part. The overall length of cycle and rate of temperature rise is dependent on part size and cross sectional thickness. Cam controlled ovens with percentage on-off timers were used for binder bake-out of the injection molded simulated rotor shapes.

Towards the end of the first quarter of 1981 a successful bake-out procedure had been devised yielding components without cracks prior to sintering. Densification was achieved during sintering but cracking in sintering could not be eliminated. Work on the solid non-bladed rotor was suspended shortly thereafter.

4.1.1.2 Bonded Rotor Development

The goal of the bonded rotor program was to produce an integral simulated rotor having properties equal to or better than the monolithic shape. The major thrust in this development consisted in determining conditions and procedures required to produce a spinnable rotor.

Several different approaches were investigated with respect to forming method and condition of the core material and the procedure applied for joining the core to the injection molded shell by hot pressing. Presintered or fully sintered cores made by isopressing and green machining were used for most of the hot pressing trials in conjunction with a flowable silicon carbide mix to provide the interface. To reduce the porosity in the interface between core and shell after hot pressing, several additional variables such as either cold isostatic precompaction of an assembled unit, increased hot pressing pressure or pulling of a vacuum prior to hot pressing were introduced. In addition, cores were also made by hot pressing or by filling the shell cavity with uncompacted mix and then applying temperature and pressure.

A total of 10 conical segments produced from isopressed stock were sintered in June 1980 to provide core stock for the thick wall shell structure. At that time work was also initiated on the

30

cores for the thin-walled shells. During the same month a graphite mold was designed and procured for hot pressing experiments. The design of the mold could also accommodate a bladed rotor shell in the event that hot pressing techniques were to be used for the fabrication of the final rotor.

Two hot pressing attempts, as depicted in Figure 20, were made during that period using the conical segment and the thick shell configuration.
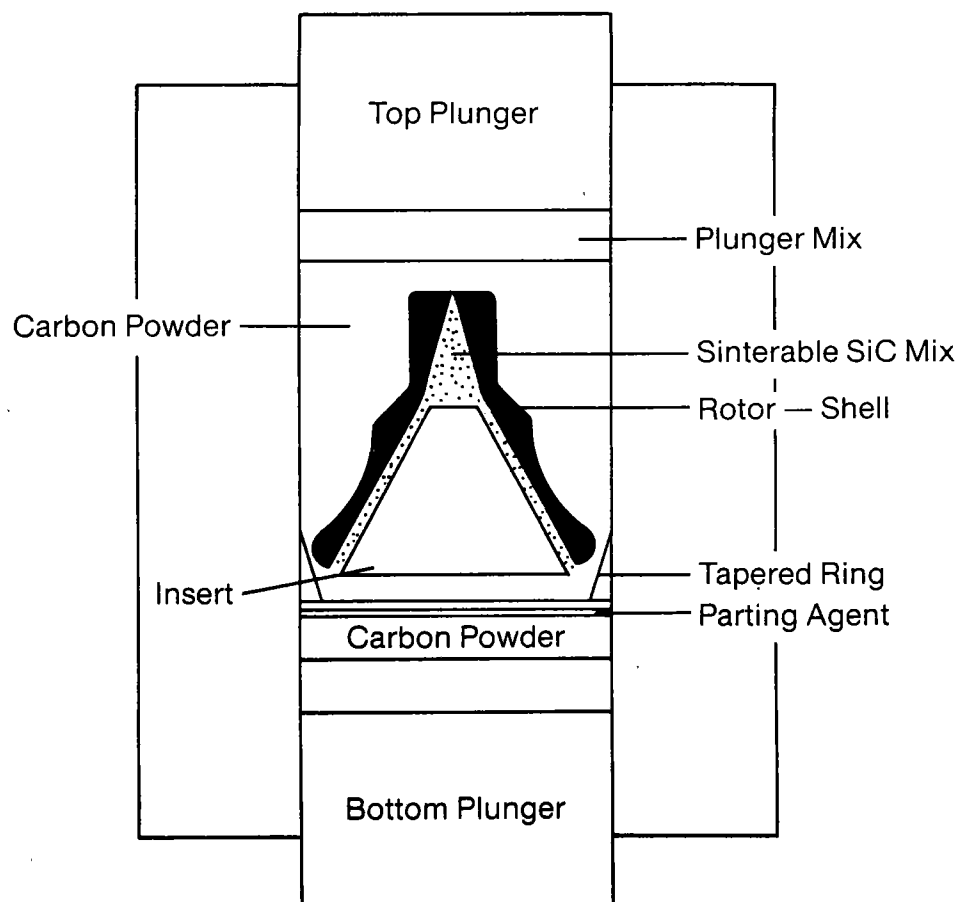
Figure 20. Schematic of Hot Pressing Arrangement

The most frequent problems encountered during this facet of the rotor development program were breakage of the graphite mold and cracking of the injection molded shell during hot pressing. Additional development activities addressed issues such as porous interface between core and shell and inadequate core material strength.

One bonded simulated rotor which had passed X-ray analysis was delivered and spin tested at GAPD. The assembly consisted of an isopressed and machined core, with a non-optimized sintered density of 2.62 g/cm^3 (81.5% theoretical), which was bonded to a sintered injection molded shell. The speed attained at failure was 72,400 rpm. A failure analysis performed by GAPD indicated that fracture originated within the core and that the maximum principal stress attained was 16.3 ksi. The results from the failure analysis indicated the need to improve the strength of the core material.

Work on the bonded rotor development program was suspended at the end of 1980 in favor of focussing additional resources on the material development aspect of the rotor program and on increasing material strength of the core.

4.1.1.3 Thixotropic Casting

A feasibility study and a narrowly defined development program on thixotropic casting of simulated rotors made of reaction bonded silicon carbide was carried out during the second half of 1980. This shape represented the thickest cross section that had been attempted by thixotropic casting. Some mix separation caused during the vibratory casting procedure was observed but could not be eliminated completely. Initial difficulties in obtaining a completely siliconized rotor hub were overcome towards the end of the project. Still, the process indicated a high degree of cracking during siliconizing.

The material selected for this fabrication process was 400 grit SiC grain (37 µ and finer) mixed with resins to form a thick paste which flowed under vibration. Rubber molds were used for forming the simulated rotors and the cast and cured shapes were furnaced at 1850°C. Silicon metal was introduced in form of a preweighed cover mix. These conditions resulted in a relative homogeneous microstructure in the center of the simulated rotor hub. Figure 21 shows a typical etched microstructure at 200 , magnification.

Material representative of these cast rotors had a mean strength of 43.5 ksi (4-point bend test) and a Weibull modulus of 8.3 (48 specimens) at room temperature. This was approximately a 40 percent increase in strength since work began on thixotropic casting. Subsequent cast material showed mean strengths of up to 49.95 ksi at room temperature.
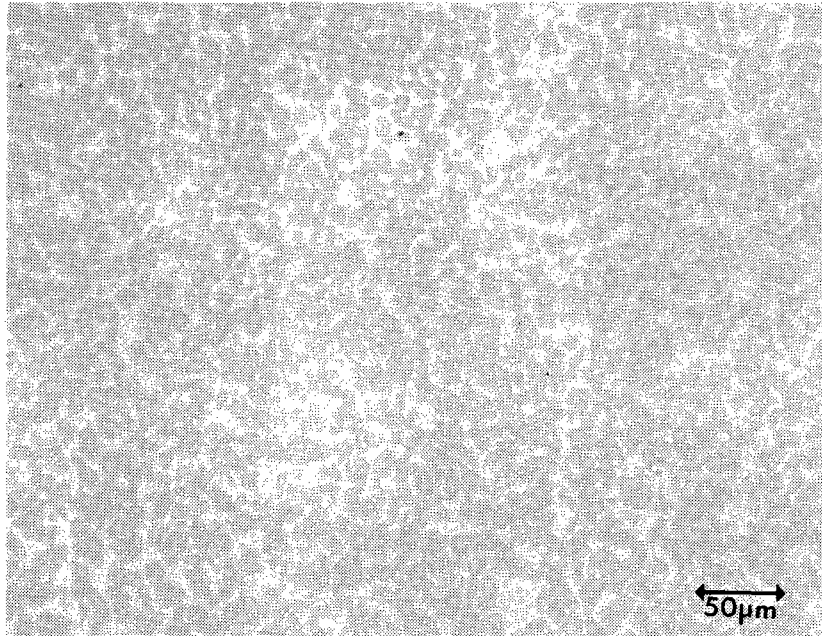
Figure 21. Microstructure of Thixotropic Cast Rotor

4.1.2   Material Development

Material development activities were carried out from mid 1980 through the end of 1981. Table 5 compares flexure strength data of Standard Oil's silicon carbide materials at that time.

Table 5

Silicon Carbide Materials
Evaluated for Simulated Rotor

Material	Trademark	25° C		1100° C		1200° C	
		MOR	m	MOR	m	MOR	m
Sintered Alpha SiC	Hexoloy™ SA	61.5	5.8	—	—	57.5	6.0
Hot Pressed SiC	—	54.0	—	—	—	—	—
Thixocast RBSiC	Hexoloy™ KT	36.9	3.1	—	—	57.7	17.0
Fine Grain RBSiC	Hexoloy™ KX-01	68.6	—	69.5	—	—	—
Ultra Fine Grain RBSiC	Hexoloy™ KX-02	53.6	—	—	—	105.6	—

It was decided to focus material development on the sintered silicon carbide because of its strength at room temperature and its strength retention at high temperatures. A series of alpha SiC mixes containing various sintering aids were prepared and plates made by hot pressing were characterized (Table 6).

Table 6
MOR Data for SA Mixes with Additives

Additive	"A"	"B"	"C"	"D"
Density, g/cm^3	3.181	3.176	3.184	3.160
MOR, ksi	60.2	41.6	49.9	71.1
Std. Dev.	11.7	5.7	6.3	6.2

A Weibull modulus of 10.4 was measured on the mix with additive "D" and a characteristic strength of 74.2 ksi was calculated. Attempts to scale up the procedure for a mix containing sintering aid "D" yielded results with high variability. Six plates were prepared and MOR samples cut from each plate produced the following results from (Table 7).

Table 7
MOR Data for SA with Additive D

	Plate Number					
	1	2	3	4	5	6
Strength (ksi)	73.2	67.3	58.9	47.8	50.0	50.8
Std. Deviation	9.2	15.0	15.0	3.1	5.5	14.1

Experiments conducted to assess the influence of the sintering aid, temperature, and hold times were inconclusive. Work on improving properties of a hot pressed SiC was terminated January 1981 because of the relative low strength levels, about equal to the pressureless sintered material, high variability in strength, and because injection molding became the prime fabrication candidate.

Based on these facts development work concentrated on a high strength material which could also be formed by injection molding. Hexoloy™KX-02, an ultrafine grain RBSiC, was identified in May 1981 as the material candidate. Standard fine grain RBSiC (Hexoloy™KX-01) has an average SiC grain size of 7 μ, while Hexoloy™KX-02 consists of about 1-2 μ SiC grains. Typical microstructures of these two materials are shown in Figure 22 and room and elevated temperature fast fracture data for both materials are given in Table 8.

34
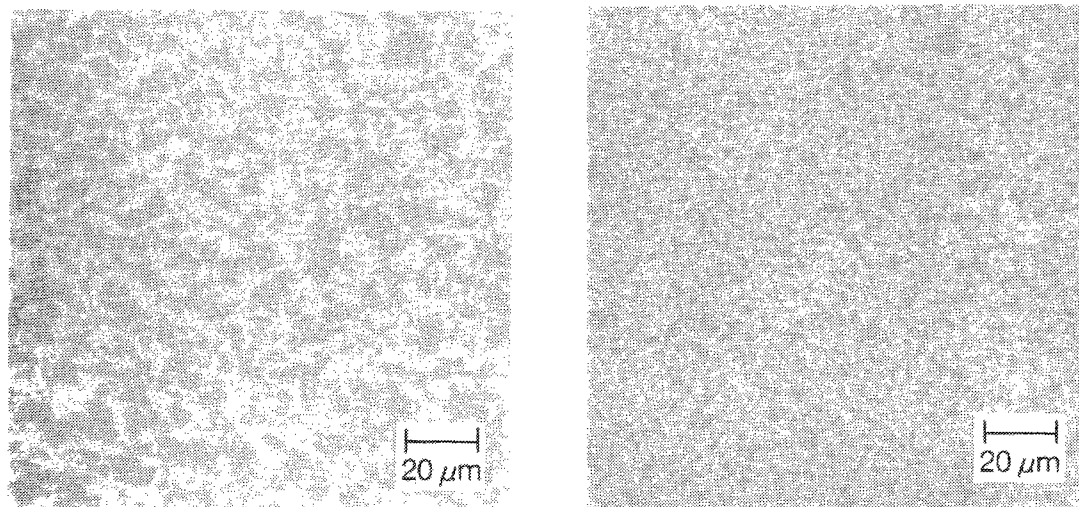
Figure 22. Microstructures of Hexoloy™ KX-01 (left)
and Hexoloy™ KX-02 (right)

Table 8
MOR Data for Hexoloy™ KX-01 and KX-02

Hexoloy KX-01	RT	1100°C	1200°C	1300°C
MOR (ksi)	68.6	69.5		
Standard Deviation (ksi)	9.7	3.8		
No. of Samples	9	10		
Hexoloy KX-02				
MOR (ksi)	55.2		98.0	71.2
Standard Deviation (ksi)			16.3	
No. Samples	3		15	3

Evaluation of the high temperature strength data indicates a
strength versus temperature behavior which differs from that which is
commonly experienced with SiC materials. Figure 23 shows a typical
stress-strain curve for a four-point bend test of sintered alpha SiC
Hexoloy™ SA at room temperature with essentially linear behavior up to
fracture representing a typical brittle ceramic behavior. The loading
curve for Hexoloy™ KX-02 at 1200°C in contrast is shown in Figure
24. This graph shows a concave negative slope as the load increases
followed by an inflection point and a slight concave positive slope,
indicating the material undergoes plastic deformation.

65.4 ksi
Bar size:
0.9540" x 0.0966"

0.02 inch/min →
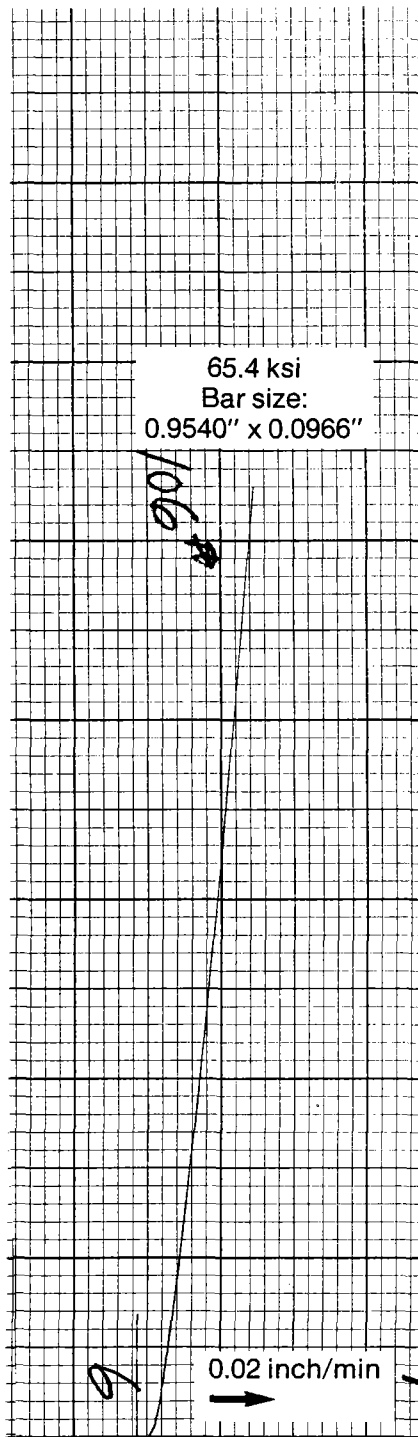
Figure 23. Stress-Strain
Curve for Hexoloy™ SA

105.9 ksi
Bar size:
0.2017" x 0.1023"

0.02 inch/min →
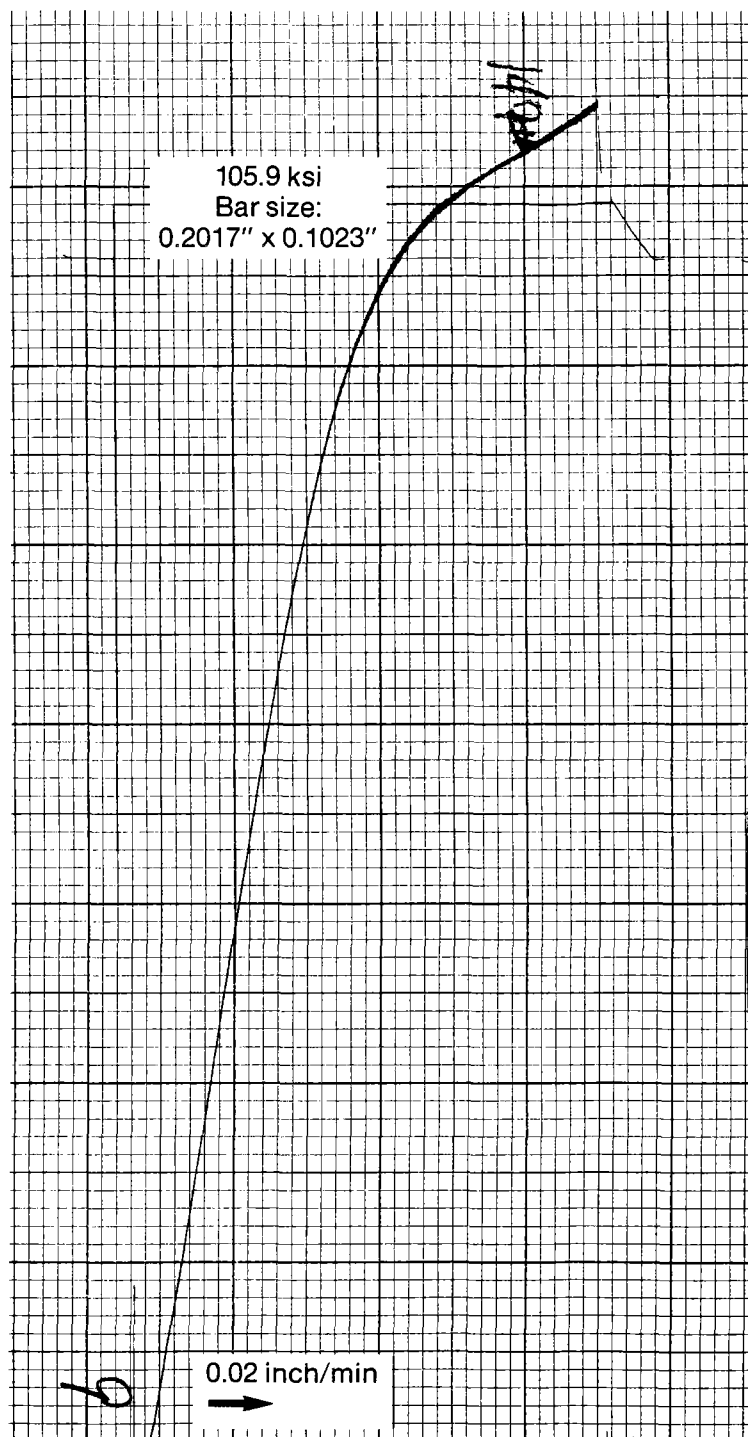
Figure 24. Stress-Strain
Curve for Hexoloy™ KX-02

36

The peak strength of the latter graph is not a breaking point but rather a very rapid decrease in load which corresponds to an upper yield point in metal testing. Typically, the bend test is stopped at this point because of machine displacement transducer travel limitations. Therefore, it is not known whether a lower yield point exists as in the case of low carbon steel tensile testing. It is also not known whether the upper yield strength represents the highest strength of the material.

There are no indications of plastic deformation at room temperature and it is believed that the high strength obtained at high temperature is caused by plastic flow of the silicon phase. Stress concentrations around flaws are reduced by localized plastic flow, thus, the material is stressed more evenly and higher strengths are obtained. Silicon is known to have a brittle to ductile transition point near 700°C.

It was also demonstrated that good material properties can be obtained using fabrication techniques such as cold pressing, hot isostatic pressing, cold isostatic pressing, and injection molding. MOR results given in Table 9 indicate that there is a potential for producing a bladed rotor with this material. However, no additional rotor development program was initiated.

Table 9
Four Point Bend Test Results on Hexoloy™ KX-02

Original Procedure Strength, ksi		New Method of Incorporating Additive		Cold Pressed Strength, ksi		Isopressed Strength, ksi	
25°C .75 Top Span	1200°C .50 Top Span	25°C .75 Top Span	1200°C .50 Top Span	25°C .75 Top Span	1200°C .50 Top Span	25°C .75 Top Span	1200°C .50 Top Span
55.29	77.92	59.82	171.20	85.35	134.5	91.38	134.80
65.33	110.40	84.80	104.40	108.30	152.5	91.34	128.40
55.17	93.75	75.51	140.70	56.68	157.0	87.23	131.30
56.99	115.10	91.32	148.50	59.03	111.9	89.95	134.50
55.19	108.30	94.65	108.20	90.04	158.9	80.07	111.70
75.80	101.60	77.04	184.10	92.63	161.9	94.99	128.00
46.53	121.30	73.70	136.10	65.52	147.1	101.00	122.00
54.06	113.30		186.60	65.83	142.4	87.39	125.70
37.14	106.80		119.00		182.1	104.30	122.70
35.14	107.10					101.90	107.90
Mean: 53.66	Mean: 105.60	Mean: 79.56	Mean: 144.30	Mean: 77.82	Mean: 149.81	Mean: 92.96	Mean: 124.50
S.D. 12.07	S.D. 12.26	S.D. 11.82	S.D. 31.08	S.D. 18.71	S.D. 19.57	S.D. 7.61	S.D. 8.94

NOTE: Test Bar Size = .1" x .2" x 2"
Cross Head Speed = 0.02"/min.

4.2   Static Structures

Several joint meetings were held early in the program to finalize component design and to ascertain that the fabrication route chosen could achieve the desired tolerances on the sintered alpha silicon carbide components. The following Table 10 lists the components which were considered for fabrication development.

Table 10
Component Overview

Component	Fabrication Method
Turbine Inner Diffuser	Slip Casting
Turbine Outer Diffuser	Slip Casting
Duct Spacer	Isopress/Green Machine
Turbine Backshroud	Isopress/Green Machine
Turbine Shroud	Injection Molding
Integral Turbine Stator	Injection Molding
Segmented Turbine Stator	Injection Molding
Regenerator Shield	Isopress/Green Machine
Combustor Liner	Slip Casting
Combustor Baffle	Slip Casting
Transition Duct	Slip Casting

Work on the individual components commenced in May 1980. Three different forming methods isopressing/green machining, slip casting, and injection molding were selected to produce the different shapes in order of complexity. Isopressing/green machining was the preferred method for simple geometrical shapes, whereas injection molding can accommodate highly complex configurations with variable wall thicknesses. Slip casting was chosen for components with complex outside flow configurations combined with constant wall thicknesses. The casting approach employed was based on drain casting principles where only the outside contour can be determined by the fixed mold.

4.2.1   Turbine Inner Diffuser

The turbine inner diffuser, as shown in Figure 25, had been revised during the joint design/fabrication assessment meetings to accommodate the slip casting process. This fabrication technique has been chosen because of the size of the component (17.3" maximum outside diameter), low tooling cost, and the fast turnaround time, especially when compared with injection molding tooling.

The aluminum model was received August, 1980 and a plaster mold was fabricated. A change in the part design, which eliminated six of the originally nine locating lugs, was incorporated in a second mold.
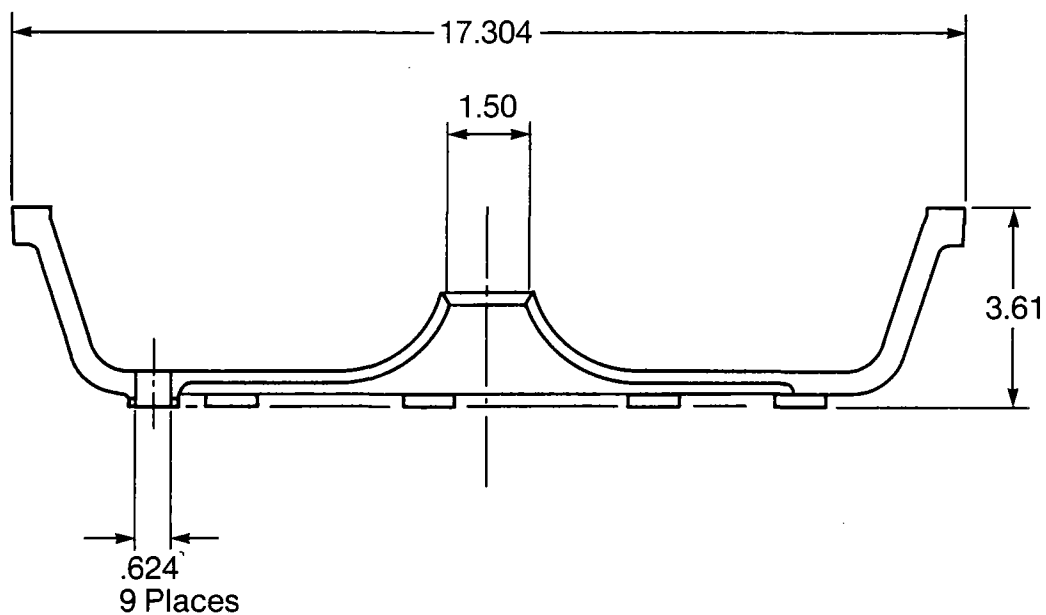
A. Initial Design
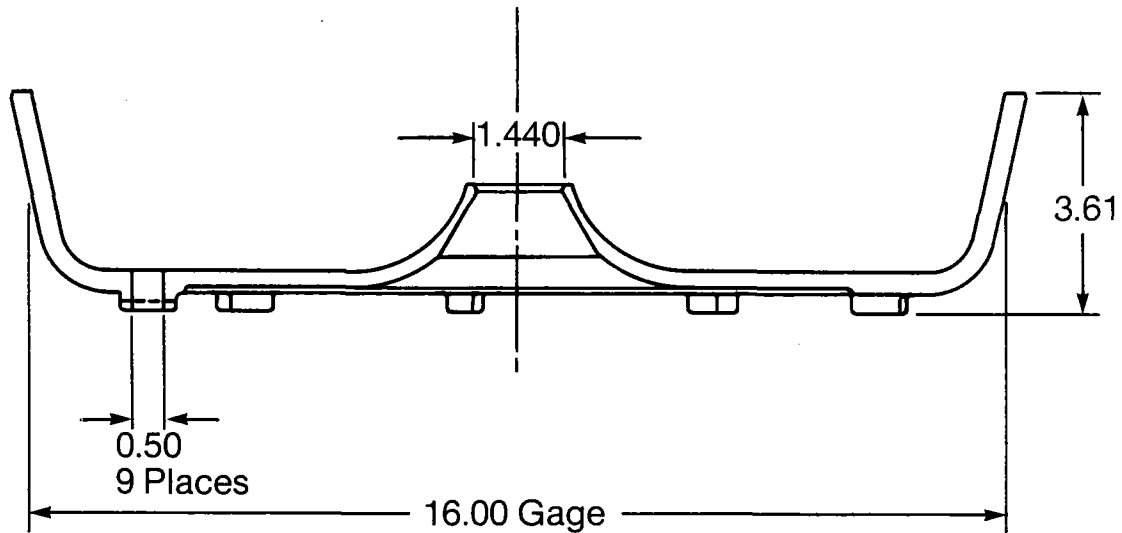
B. Revised Design

Figure 25. Turbine Inner Diffuser
(Initial Design A, Revised Design B)

39

Fabrication development on the slip cast sintered alpha silicon carbide turbine inner diffuser was terminated due to funding limitations at the end of the third quarter.

4.2.2 Turbine Outer Diffuser

The initial design of the turbine outer diffuser, as shown in Figure 26, did not require any configuration changes to accommodate the drain casting approach selected as the preferred fabrication method. It was decided to prepare castings without the location holes, which would be drilled after sintering to minimize anticipated problems due to warpage and cracking near the rim.
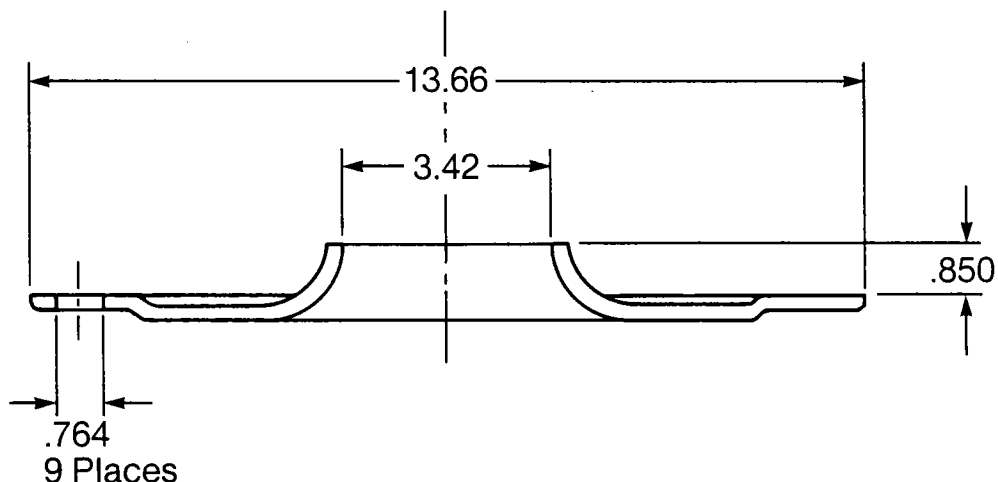
Figure 26. Turbine Outer Diffuser Design

The aluminum model was received in August of 1980. A mold was fabricated and casting resumed shortly thereafter. The first cast unit developed a crack during drying.

Fabrication development on the slip cast sintered alpha silicon carbide turbine outer diffuser was also terminated due to funding limitations at the end of the third quarter.

4.2.3 Duct Spacer

The duct spacer, as shown in Figure 27, did not require any design modifications for better fabricability. This component was fabricated by isostatically pressing alpha silicon carbide tube stock and machining it in the green state to predetermined dimensions. Each component was sintered on a mandrel. After passing X-ray, FPI and dimensional as-fired inspection, units were ground at an outside vendor and resubmitted for final inspection which consisted of FPI and dimensional evaluation.
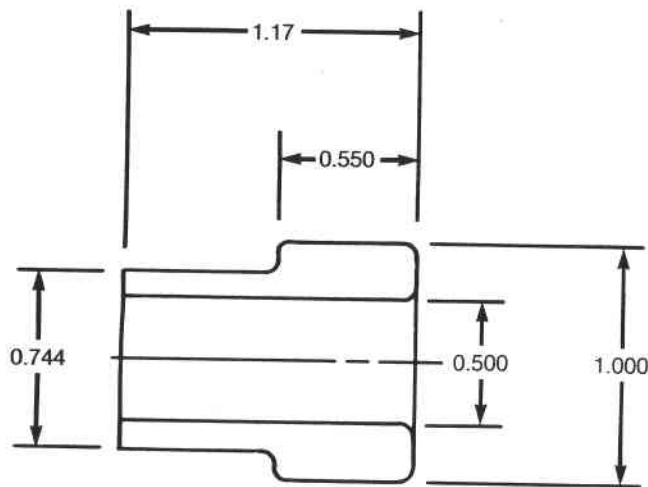
Figure 27. Duct Spacer Design

Work on the duct spacers commenced in July of 1980 and continued through November 1980. The shipment of 30 finish ground components completed this program task.

4.2.4   Turbine Backshroud

The initial design of the turbine backshroud, as shown in Figure 28, required no fabrication related design modifications. Isopressing of cylindrical stock combined with green machining was selected as preferred fabrication route. The green machined components were sintered per established procedures and subjected to dense grinding to obtain final dimensions and contour.

Work commenced in June of 1980. Six components were delivered for evaluation during the second quarter of 1981. Results of the evaluation revealed that the machined contour facing the rotor was not within print tolerances. Consequently, the fabrication of a second set of components was initiated in October of 1981.

The first six articles were produced on a lathe equipped with a template tracer attachment. The template was developed from coordinates having 12 points/inch. The contour of the second group of turbine backshrouds was produced on a CNC lathe incorporating 50 points/inch for improved accuracy. The new coordinates were used to generate a program for the CNC lathe. Precise sintering fixtures to eliminate distortion during densification were fabricated utilizing a similar CNC lathe machining procedure. Two finished components were used to develop the lapping and grinding procedures to produce a precise contour within the tolerance band.

41
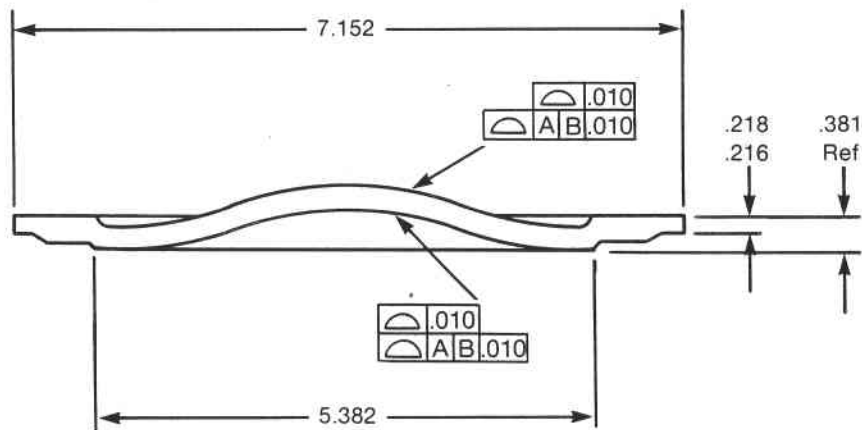
Figure 28. Turbine Backshroud
(Initial Design)

Close green machining control of the contour and the use of the newly developed sintering fixtures, however, resulted in components which were close to the desired tolerance band and required no additional contour grinding (Figure 29). Six finish ground turbine backshrouds were delivered in June of 1982. This shipment completed the contractual requirements per the established work plan.
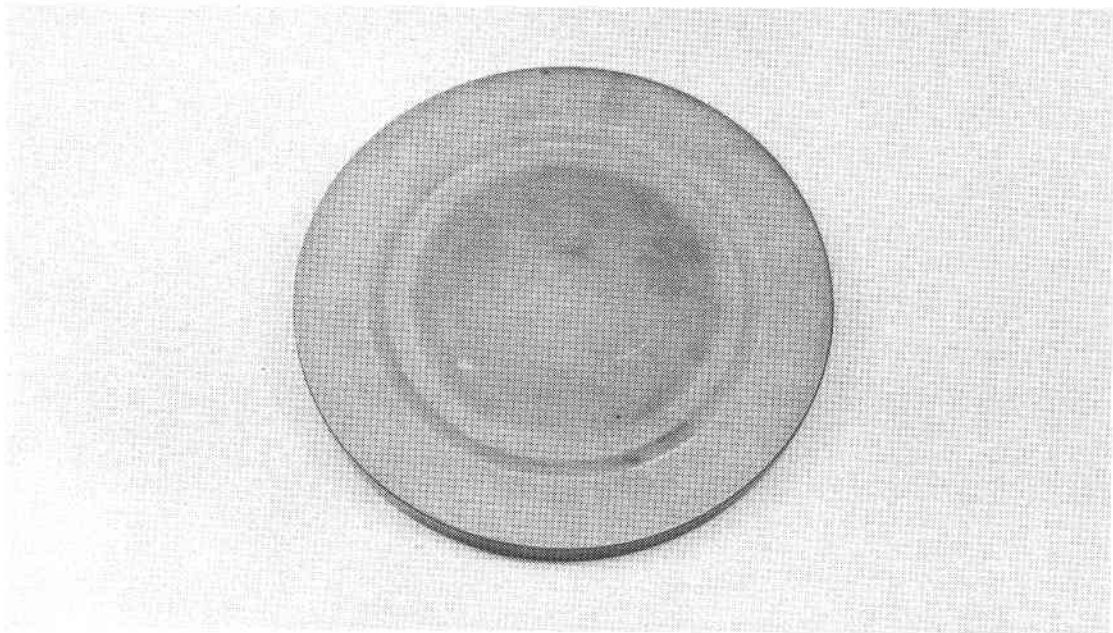
Figure 29. Sintered Backshroud

During rig testing at Garrett it was found that the regular heating rate during start-up created excessive tensile stresses in the center of the turbine backshroud causing crack development and failure of the component. To allow for further testing of this component in SASC GAPD pursued two alternatives. One alternative was to change the sintered components by removing the high stressed center portion. As a trade-off, however, an increase in leakage had to be tolerated. The second alternative was a modified design combined with lower transient stresses during start-up by utilizing a slower heat-up rate. This approach increases the performance at maximum test temperature because of reduced leakage over alternative one.

Work on the new design (Drawing PA3611439), as shown in Figure 30, was initiated in August of 1986. Four backshroud blanks were made of isopressed alpha silicon carbide and were supplied between August and October of 1986. The 1987 shipments consisted of 2 sets of three fully ground components (Figure 31) supplied towards the end of the program. The first set consisted of pressureless sintered alpha silicon carbide (Hexoloy™ SA) and the second set of a pressureless sintered particulate composite of a silicon carbide matrix with discrete particles of titanium diboride (Hexoloy™ ST).
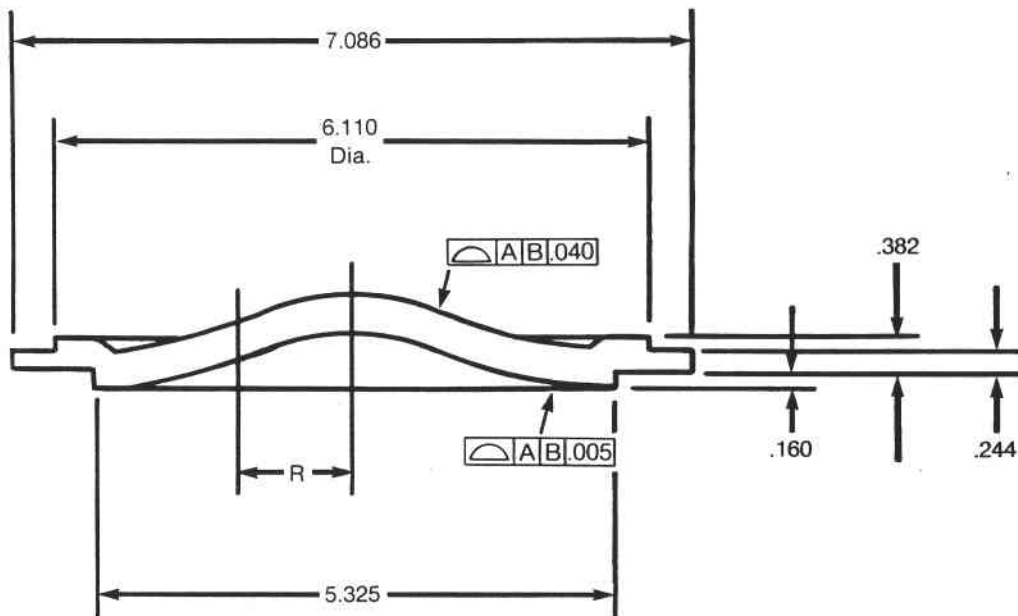
Figure 30. New Backshroud Design
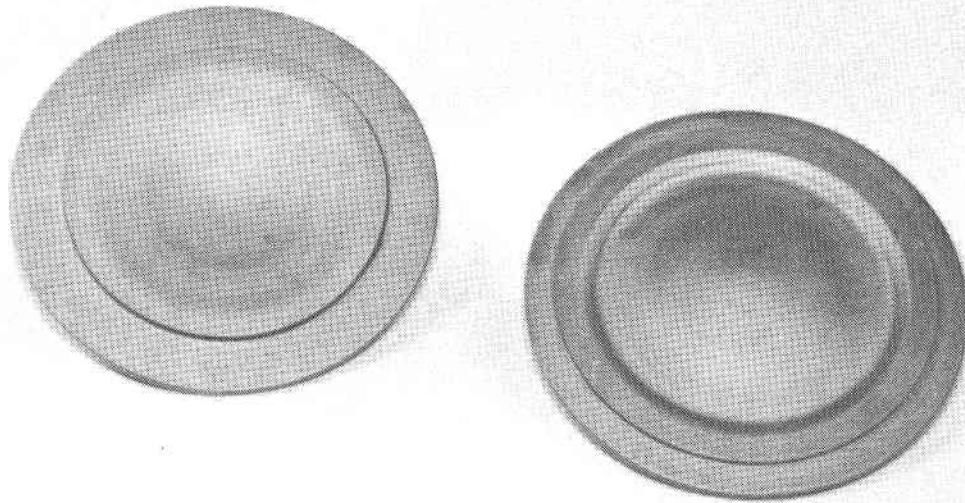
Figure 31. Sintered Backshrouds - New Design

Several backshrouds have been evaluated in rig and engine tests. One component, machined from a sintered disk, accumulated 13 hours in a rig test at 2500^{0}F in October of 1986, and backshrouds 105 and 106 were tested successfully in 2100^{0}F engine tests in different engine builds and multiple cycles.

4.2.5   Turbine Shroud

The initial design of this component, as shown in Figure 32, combined the turbine shroud and turbine diffuser. In order to fabricate this component in one piece, it was suggested that a cold pressed block be green machined. Because of the part size and shape, low yields and long machining times would prohibit low cost/high volume production. Consequently, it was decided to produce this item in two sections and incorporate additional small changes on the individual drawings.
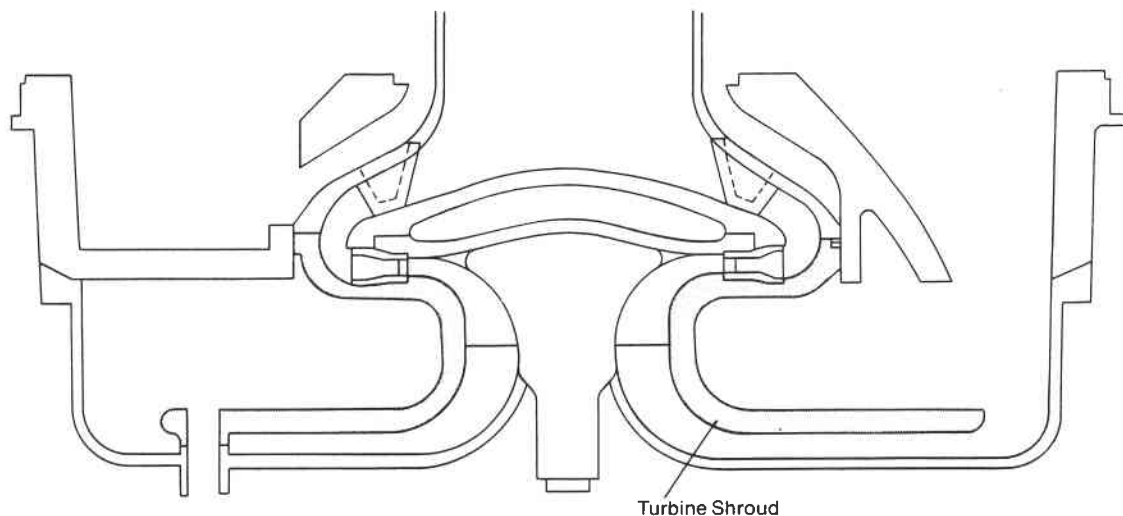
Figure 32.   Initial Turbine Shroud Design

Subsequently, it was decided to fabricate the turbine shroud in the redesigned form (Drawing L3846151), as shown in Figure 33, using injection molding as the primary approach. The slip casting process with extensive green machining and final grinding was to be used as a back-up in the event that insurmountable problems would surface with the injection molding process. The slip casting process in this case was based on a drain casting approach where a constant wall thickness is produced. To generate a component as shown below, a thick walled component would have to be cast first and additional features would be introduced through machining.

45

.755-.760 Dia. Thru
Typical 3 Holes
Equally Spaced

1.007-1.009
Typical 9 Place
Equally Spaced

9.808

8.843

5.331

2.495

2.807

3.409

1.231

.510

13.700
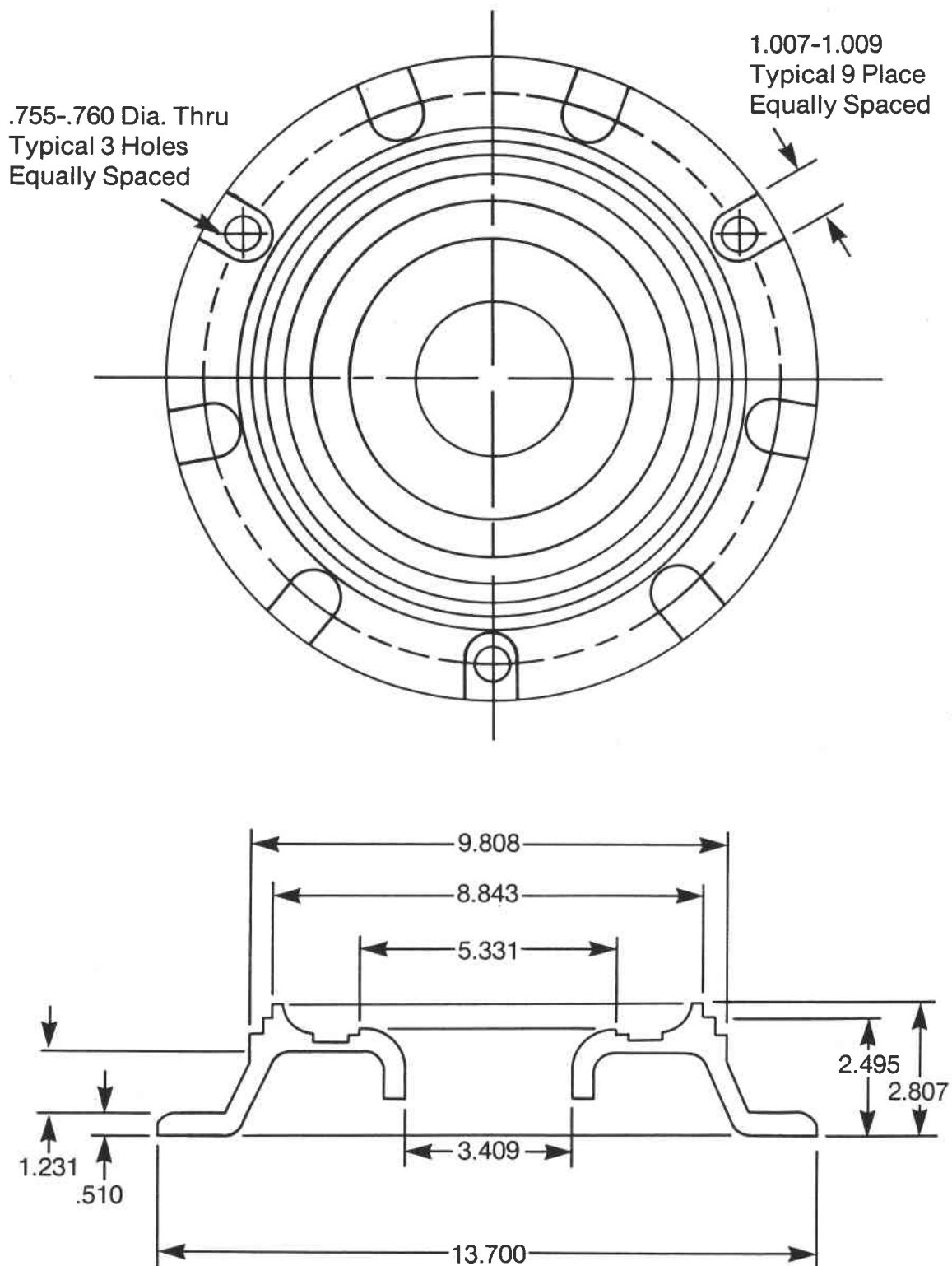
Figure 33.   Revised Turbine Shroud Design

The final turbine shroud design presented a major challenge for the fabrication technology of sintered alpha silicon carbide components, especially in the beginning of the AGT program. The selected forming approach of injection molding is capable of near net shape fabrication. However, in early 1980 there was considerable risk involved, because, at that time, components of this large a size and mass had not yet been fabricated using the injection molding process.

Design discussions on the injection molding tool were initiated with an outside mold maker in June 1980. The tool was designed to mold a near net shape component with excess stock for final grinding in tight tolerance areas. The tool was completed in September and a wax replica of the cavity was supplied by the vendor for approval. The component passed evaluation and the tool was shipped to an outside molding facility. Problems with the mixing and compounding equipment caused delays in the preparation of several hundred pounds of plasticized compound and the first molding trial had to be postponed until January of 1981.

The initial molding trials were conducted using a microprocessor-equipped 300 ton Reed RS machine. The volume of the molded shroud was estimated at approximately 150 cubic inches which was greater than the single shot size available on this machine. Therefore, a flow molding sequence through the microprocessor control system had to be used to deliver sufficient volume of material to the shroud cavity. The flow molding operation consisted of partially filling the mold by extrusion and screw rotation for a predetermined length of time. The forward motion of the screw was then used to complete filling and provide final compaction.

Machine settings were determined to produce completely filled parts. Four of these parts were judged suitable for further processing. However, the mold filling pattern could not be optimized during the molding trial. The shrouds contained many flow and weld lines, which were the result of improper fusing of compound injected under pressure caused by the delay in the injection stroke. The delay between flow and packing allowed the injected material to cool which prevented subsequent fusing. Three of four parts were baked successfully with no visible cracks present. After sintering, cracks developed along the flow or knit lines.

In response, the tool was returned to the machine shop where the sprue and diaphragm gate were enlarged in order to facilitate an improved flow pattern with fewer and less pronounced flow lines.

A second molding trial was carried out in April with the reworked tool using the flow molding technique. A total of 13 individual moldings were carried out under a variety of conditions. The slow fill obtained by flow molding showed some improvements due to the tooling modifications, however, a high incidence of weld lines was observed which posed problems in subsequent processing steps. The best two shrouds were processed in an attempt to learn the special handling techniques required for a part of this size. Both components developed several cracks on pronounced flow lines.

At this point the flow molding process was abandoned in favor of single shot injection molding using a sufficiently large machine at a custom injection molding facility. Conventional injection molding machines of at least 800 ton clamping pressure and 145 ounce shot size (based on polystyrene with 1 ounce equivalent to 26.5 cm^3) were considered suitable.

Approximately 700 pounds of molding compound were prepared in the June/July 1981 timeframe. The compound was delivered to the custom molder for injection molding trials in July on a 1000 ton, 165 ounce reciprocating screw machine equipped with microprocessor controls.

A total of 48 turbine shrouds were molded using a variety of conditions. The machine adjustments were made utilizing personnel from the custom molding facility skilled in molding plastics and highly familiar with the behavior of the individual machine, as well as our own technical personnel familiar with the behavior of plastic filled alpha silicon carbide compound.

All parts were visually better than those produced using the flow molding technique. Closer inspection showed that minor linear indications were still present on the surface of some parts. It was thought that these indications could be eliminated by further enlarging the gate and adding vents at the parting line at the shroud rim. Additional tool modifications were postponed until some of the turbine shrouds were processed through sintering to better assess the actual shrink factors.

Two shrouds were successfully baked in August and one was sintered (Figure 34) without any of the cracks typically observed on the components made with the flow molding process. To assess the true shrinkage behavior without introducing interference, it was decided to sinter this unit without any high temperature fixtures which resulted, as expected, in some distortion on the flange.

Two additional shrouds were sintered in September. After measurements were taken, one was delivered to GAPD for evaluation. The second shroud was approximately 0.100" smaller in diameter than the previous two units. Further evaluation of the processing history showed that a different set of molding conditions was used which had resulted in a part weighing 0.5 lbs less and having a lower green density. Densification during sintering, however, reached about the same level as for the other turbine shrouds. Thus, the reduced green density caused an increase in final shrinkage producing a smaller part.

Another two shrouds were sintered in October of 1981 without the benefit of fixturing in order to calculate the dimensional changes required for tool rework.
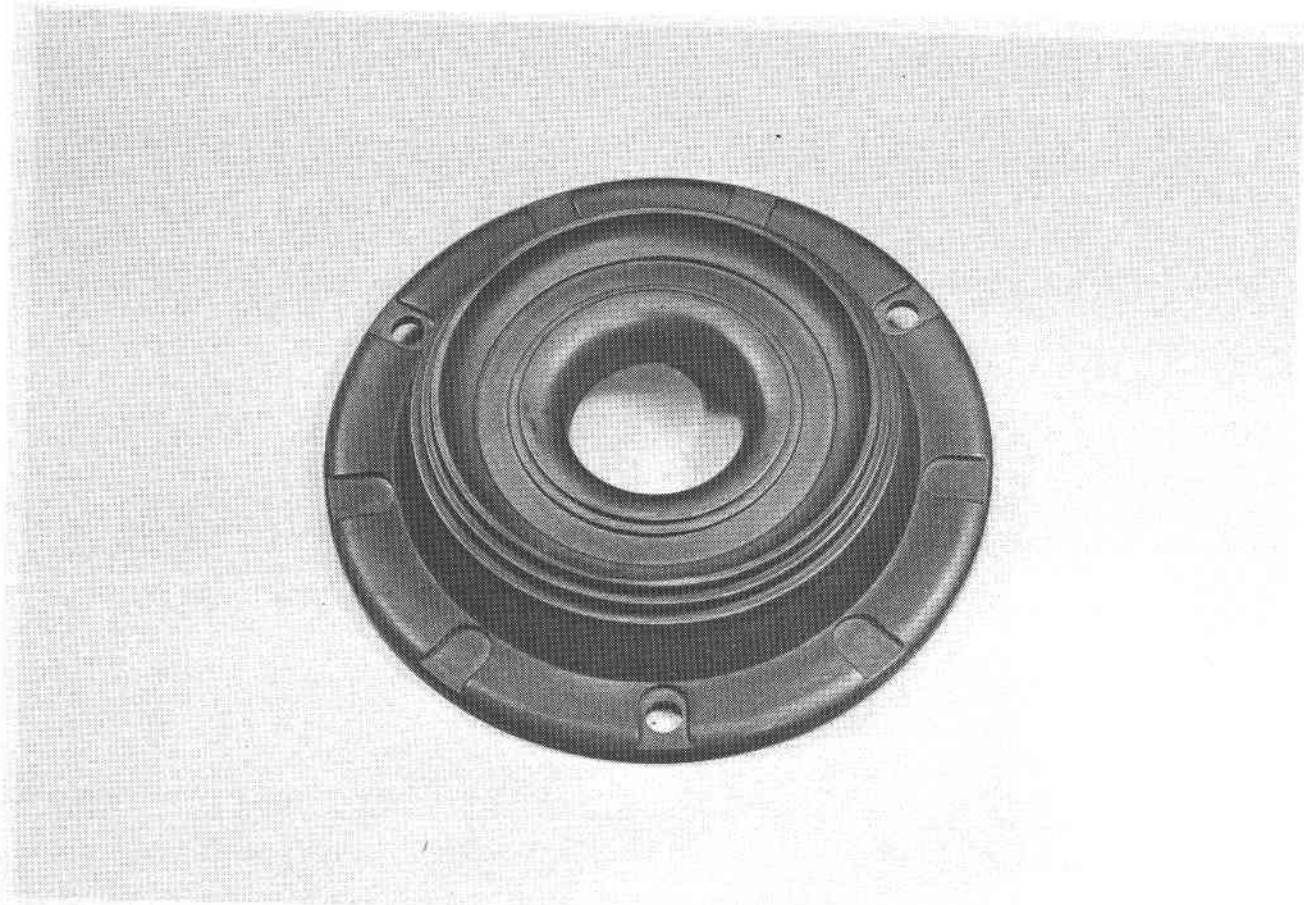
Figure 34. Sintered Turbine Shroud

The above five turbine shrouds were sintered in a resistance heated furnace and some of the observed flange distortion was attributed to the closeness of the heating elements. To further assess shrinkage behavior during sintering, a sintering trial was conducted in a large induction furnace which can hold components of up to 22" diameter using a traditional three column setter arrangement. No change in shrinkage behavior was observed when comparing parts from both sintering furnaces. Dimensional data were taken on the six sintered components and shrink factors were calculated for tool modification.

A new drawing (3846212) reflecting a revised flange design was received during the fourth quarter of 1981. The new design showed three locating pads versus the nine pads on a solid flange of the previous design. The tool rework was completed late 1981 and a molding trial was carried out during January of 1982 using the same 1000 ton molding machine as for the previous molding run.

A total of 43 shrouds were produced using two compositions varying in shrink factor. A matrix of molding conditions was applied to each composition. The first shroud selected for processing cracked severely during baking for undetermined reasons since the baking procedure was identical to that used for the old design. Four more pieces were baked and three parts showed cracks which originated in the positioning slots on the flange in the turbine shroud/outer diffuser interface. The fourth component which did not exhibit any cracks in this region after baking was sintered and subsequently showed also cracks in this region (Figure 35). Prior to baking additional shrouds, a generous fillet radius was applied to the slot detail on the flange to minimize stress concentrations. The first crack free sintered shroud (Figure 36) having the revised design was produced in March of 1982, proving the theory of a sharp corner as a severe stress riser as correct.
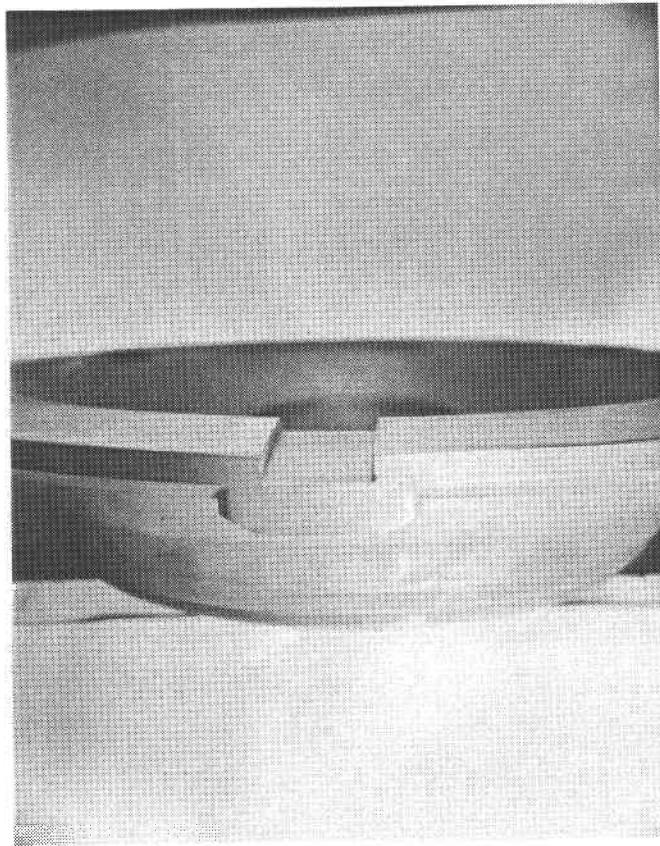
Figure 35. Slot Detail on Turbine Shroud Flange
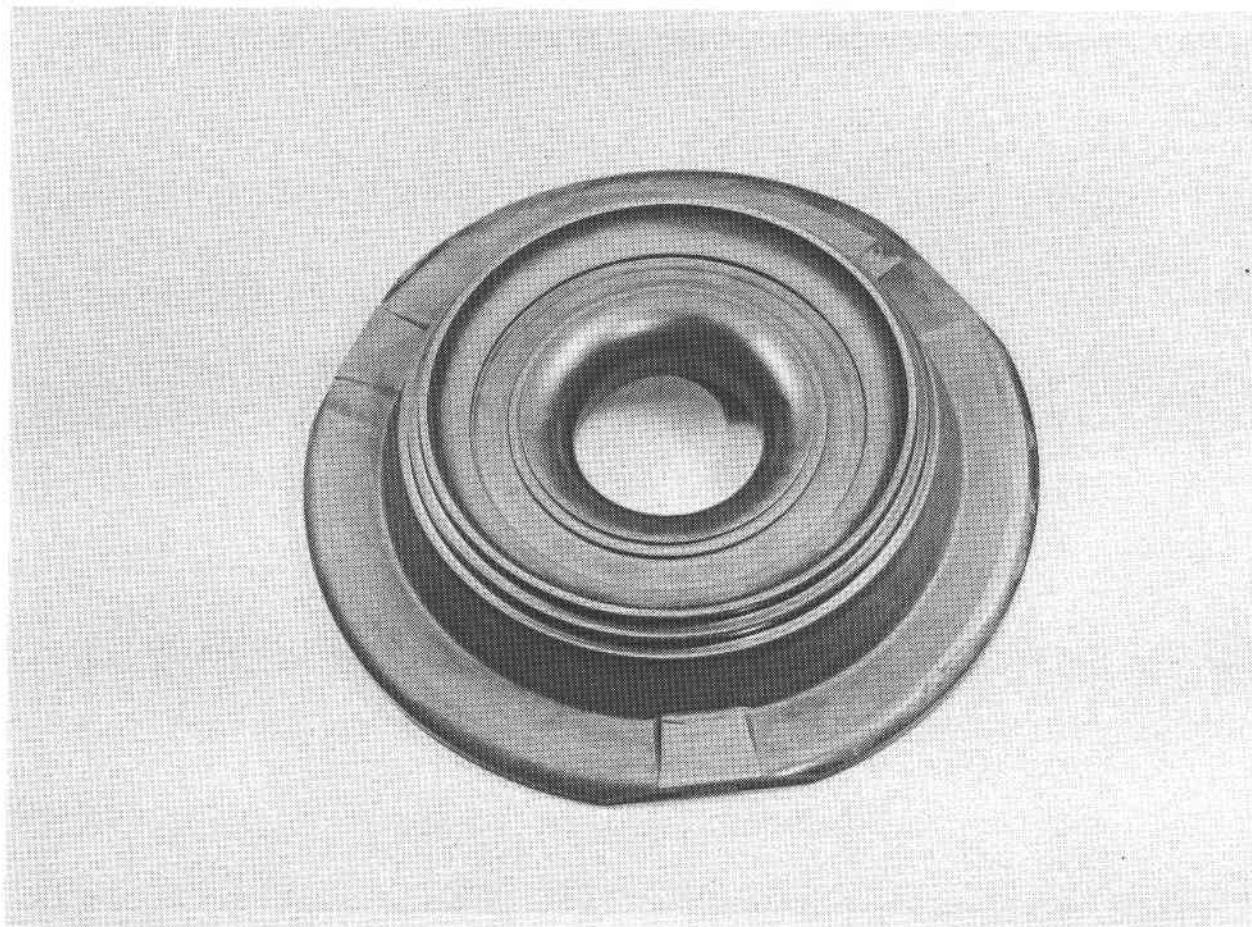
Figure 36. Sintered Turbine Shroud with 3-Slot Flange Design

For future moldings it was therefore planned to either mold in a generous radius on the positioning slots or to completely eliminate this flange detail during molding and incorporate it during final grinding.

Sintering of the turbine shrouds with generous fillet radii was carried out on graphite rollers to minimize frictional drag. However, flatness on the face of the flange continued to be a problem and a study to determine the cause of this distortion was initiated. Microscopic examination of radially sliced samples, 4 microns thick, taken from a molded part, did not detect significant packing density differences. In addition, green density measurements taken in the same area indicated no differences. Two approaches for correcting the flange distortion were then suggested:

1. Removal of flange sections between the mounting locations or tabs to show if circumferential shrinkage is different from radial shrinkage or if the radial shrinkage differs depending on its circumferential location.

2. Deliberate distortion of the flange in the opposite direction
    while in the molded state, to be accomplished by applying
    pressure to the flange while the freshly molded part is still
    warm and pliable.

A total of four shrouds were green machined in April of 1982
to remove flange sections between the mounting locations (Approach 1).
The expected benefit on the sintered components was not achieved as
the mounting flange sections showed about the same degree of
deflection as on the parts with full flange.

One of the above shrouds (2-101) was shipped to GAPD in
May for evaluation. One of the remaining modified shrouds was refired
using a hot pressing procedure in an attempt to straighten the tabs.
A noticeable improvement was noted on two tabs while the third
remained essentially unchanged. Subsequently, the remaining two
shrouds (16-1 and 16-3) having some flange distortion were shipped to
GAPD the following month.

Turbine shroud 16-3 was thermally screened at GAPD. It
successfully passed light off cycles from 1200 to 1600°F. However,
the part fractured during heat up from 1600°F to 1800°F. The fracture
originated at an internal void. Pictures taken from fracture surfaces
(Figures 37, 38) indicated also severe exaggerated grain growth.

A set of trials to reduce flange distortion using Approach 2
was conducted in the May/June timeframe. Steel fixtures to aid warm
deformation of the shroud flange were obtained.

The injection molding tool was changed to eliminate the
three slots on the flange and a new molding trial was conducted. A
total of 53 shrouds were molded using two compositions. Attempts to
purposely distort the flange at the molding site were unsuccessful.
The parts were apparently too cool to respond to pressure, even
directly out of the tool. A more successful technique was developed
by placing a shroud with the steel fixture and a suitable weight on
the flange into an oven for several hours near the injection molding
temperature. The flange showed distortion conforming to the fixtures
upon completion of this trial. However, after sintering it was noted
that the same amount of flange distortion occurred indicating that the
stresses developed during molding or the material characteristics
producing distortion were not eliminated.

Flange distortion caused by heat gradients during sintering
was investigated as another alternative cause. Individual graphite
crucibles were fabricated for sintering purposes and it was attempted
to insulate the components in such a way so as to minimize any heat
gradients. This method showed promise but did not completely correct
the distortion problem.

In parallel to the efforts on reducing flange warpage, work
was initiated in April on the design and fabrication of grinding
fixtures. Grinding and ultrasonic cutting of the first turbine shroud
(Figure 39) was completed in July. Some areas of the shroud

flange face had insufficient stock and did not clean up, however, because of the very localized and shallow unground areas it was not projected to cause problems in evaluation and rig testing.
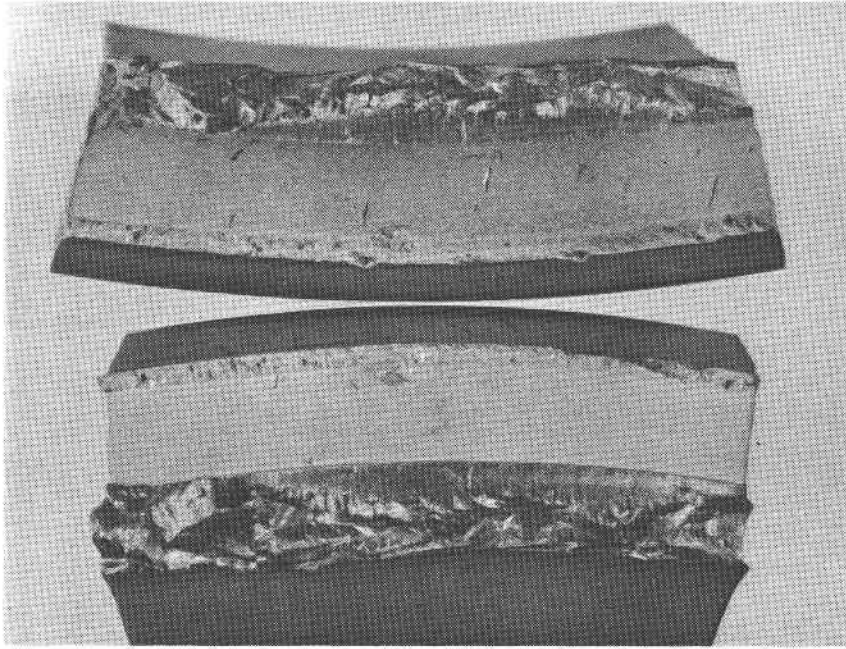
Figure 37. Fracture Surface
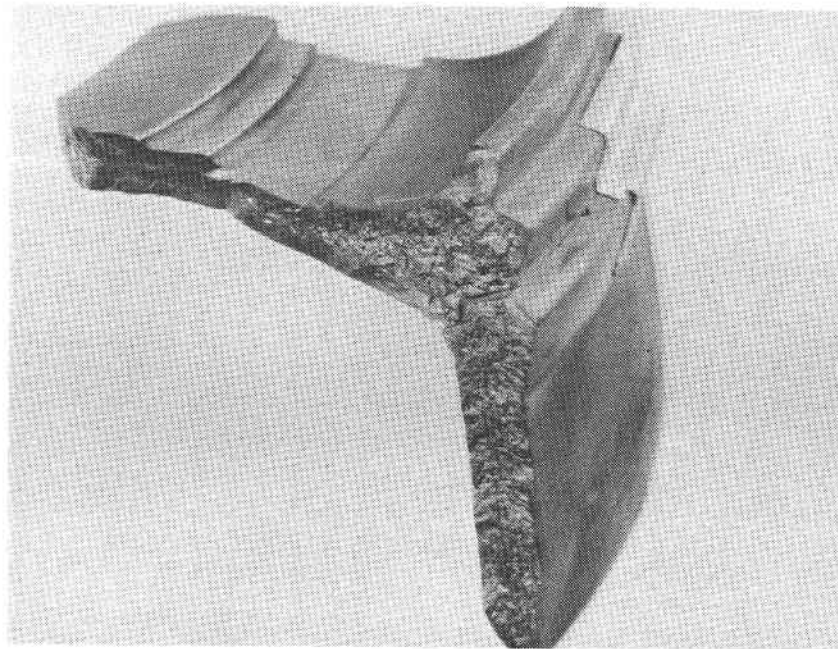
Figure 38. Exaggerated Grain Growth on Fracture Surface
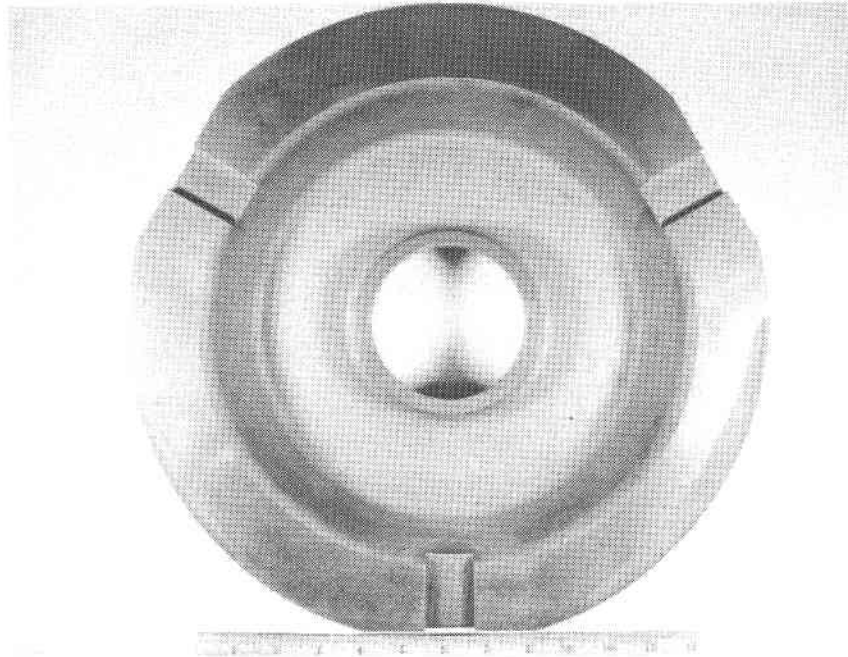
Figure 39. Ground Turbine Shroud

Work continued on the development of several sintering fixtures in an effort to gain control over the distortion predominantly observable on the flange. An alternative route of using fixtures during a second sintering step to reduce warpage obtained during the initial sintering step was also pursued.

Turbine shrouds molded during the May/June trials were processed through the system and data were collected on individual components to assess the influence of the various fixturing approaches.

The post-sintering fixtures for correcting flange distortion were designed and fabrication was completed in August. Testing was conducted on three sintered shrouds with mixed results. The first two trials resulted in severe shroud cracking with little or no straightening of the flange. Subsequently, the fixturing configuration was altered for the third run which resulted in visible improvements. The shroud from this run exhibited a full flattened flange, however, the minor cracks that were detected in this part prior to the test had grown in severity.

A comparison of results of the post-sintering procedures for straightening flange warpage showed that even though some warpage reduction could be determined the introduction of cracks could not be eliminated. Work on this development task was terminated in October of 1982.

Four additional shrouds were sintered in November of 1982. Evaluation of these parts showed that most of the dimensions were slightly oversized, however, densities were acceptable. All four parts exhibited minor flange warpage. Two of these parts exhibited no detectable linear flaws and were submitted for final grinding.

Dimensional evaluation of all sintered shrouds indicated that in general a lower shrinkage factor was observed than initially planned for. The injection molding tool was therefore modified to produce grinding stock in critical areas and a new molding trial was conducted late that month. Twenty-eight shrouds were molded using two different compositions. Detailed visual inspection of these parts showed that sixteen were of better molding quality than the remaining parts.

In December of 1982 GAPD advised they were considering several design changes to reduce thermal and mechanical stresses for SASC. Therefore, parts in the processing system were completed and the molding of additional shrouds was suspended pending the results of the redesign.

Two turbine shrouds completed grinding early in 1983. One component was rejected because of a crack discovered on the ground flange close to the I.D. The second component (80-8) was NDE acceptable and was shipped to GAPD in February. Three additional components completed grinding. Only one of these (105) passed NDE and was submitted to GAPD for evaluation and testing in April. The unit was tested at GAPD but an operational error resulted in fracture of the part.

The new drawing (PA3609679) for the modified scalloped design (Figure 40) was obtained in June and the remaining parts in the system were sintered and evaluated. It was concluded that the former design yielded insufficient stock in the vicinity of the reinforced rotor contour and all remaining parts of the old design were discarded.

Design considerations for a new injection molding and/or transfer molding tool were subsequently initiated but actual fabrication was put on hold until October of that year. At that time it was decided to not invest in a new injection molding tool but revise the old tool and remove steel where additional stock is required (Figure 41). Excess stock was also added in the flange area to allow for some warpage. In addition green machining was employed to remove details from the molded components to meet new print requirements.

12.080 Dia. Gage

10.800 Dia.

.467-.475 Dia.
Thru 3 Holes

9.836 Dia.

8.872
8.866 Dia.

2.568
2.566

1.905
1.895

67.500°

3.409 Dia.
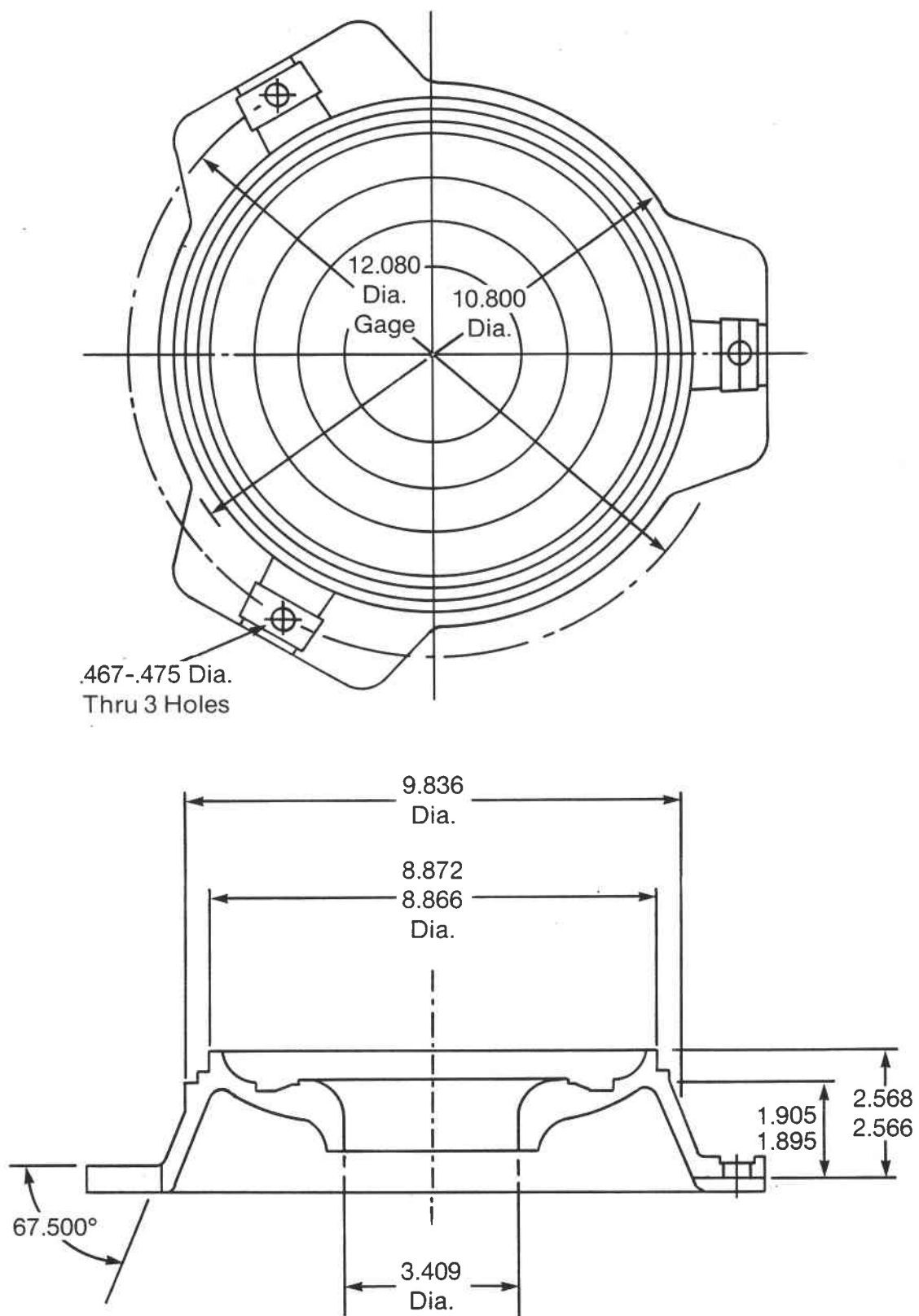
Figure 40. Scalloped Turbine Shroud Design
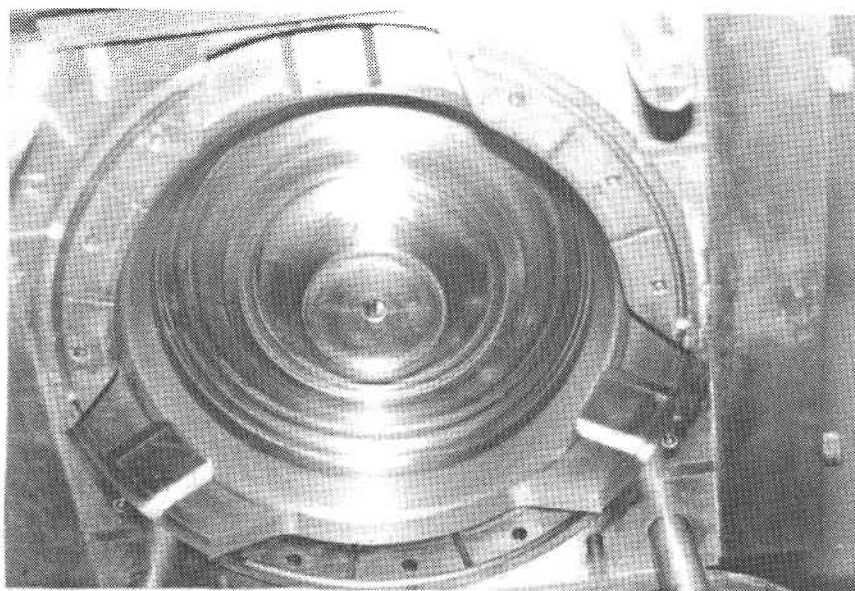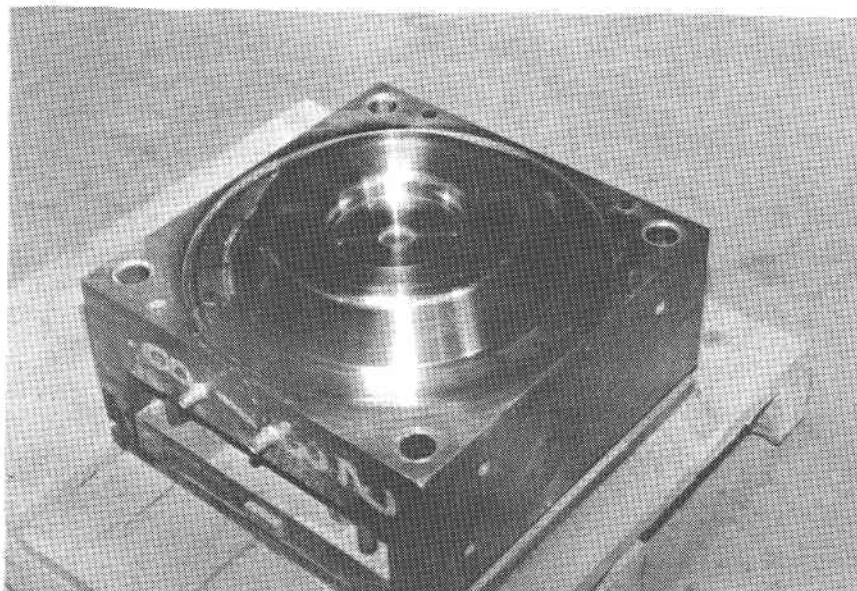
Figure 41. Injection Molding Tool

The tool revision was completed in November and a molding run in December yielded a total of 29 components. All parts showed some flow lines, most of these, however, were in areas where stock was to be removed during green machining. Nine shrouds were green machined in the as-molded state and submitted for initial NDE inspection. X-ray evaluation of the green machined parts revealed plastic and metal contamination. Burn-out of these foreign materials, depending on the location, would lead to pores or blow-outs in the sintered parts. It was decided to use these green parts only for fixturing trials and to schedule a new molding run.

The new molding trial was carried out in March of 1983 and yielded 45 components. Particular attention was placed on the preparation of the molding machine at the custom molder to reduce the possibility of contamination originating from plastic (previous molding material on the machine) or metal (possibly used to clean up sections of the machine).

Components of the last two molding trials having the most recent design with three locating tabs instead of a full flange were processed to develop a better understanding about the fixtures required during sintering to minimize tab warpage. Two parts from the December molding were sintered in March. Both parts were out-of-round with the three massive locating tabs seemingly acting to restrict radial shrinkage. Another three parts were sintered in April using different fixturing techniques in order to better control flange or tab distortion. In addition, an isopressed blank was cut into plates for the shroud to rest on. The shrinkages of both materials were matched and the plates and the tabs of the turbine shroud were pinned together in an attempt to force the shroud to shrink with the plates. In this way both out-of-roundness and flange distortion were reduced.

A total of three parts were sintered in April of 1984 using slightly modified fixturing techniques. One part without visual defects was submitted for as-fired X-ray and FPI inspection. The dimensional inspection showed good agreement with the print and sufficient stock in areas intended to be ground with the exception of the diameter in the turbine shroud/outer diffuser interface, where a slightly oversized inner diameter was observed.

Development work continued to address various fixturing techniques to reduce tab warpage, I.D. out-of-roundness and cracking which appeared to be caused by excessive force on the tabs. By September two components had passed X-ray and FPI inspection. Warpage on the tabs was minimized and sufficient stock on the I.D. of the turbine shroud/outer diffuser interface was present. Both components were considered grinding candidates. Figure 42 shows turbine shrouds of the new scalloped design in the as molded state and after sintering where approximately 20% of shrinkage is observed.
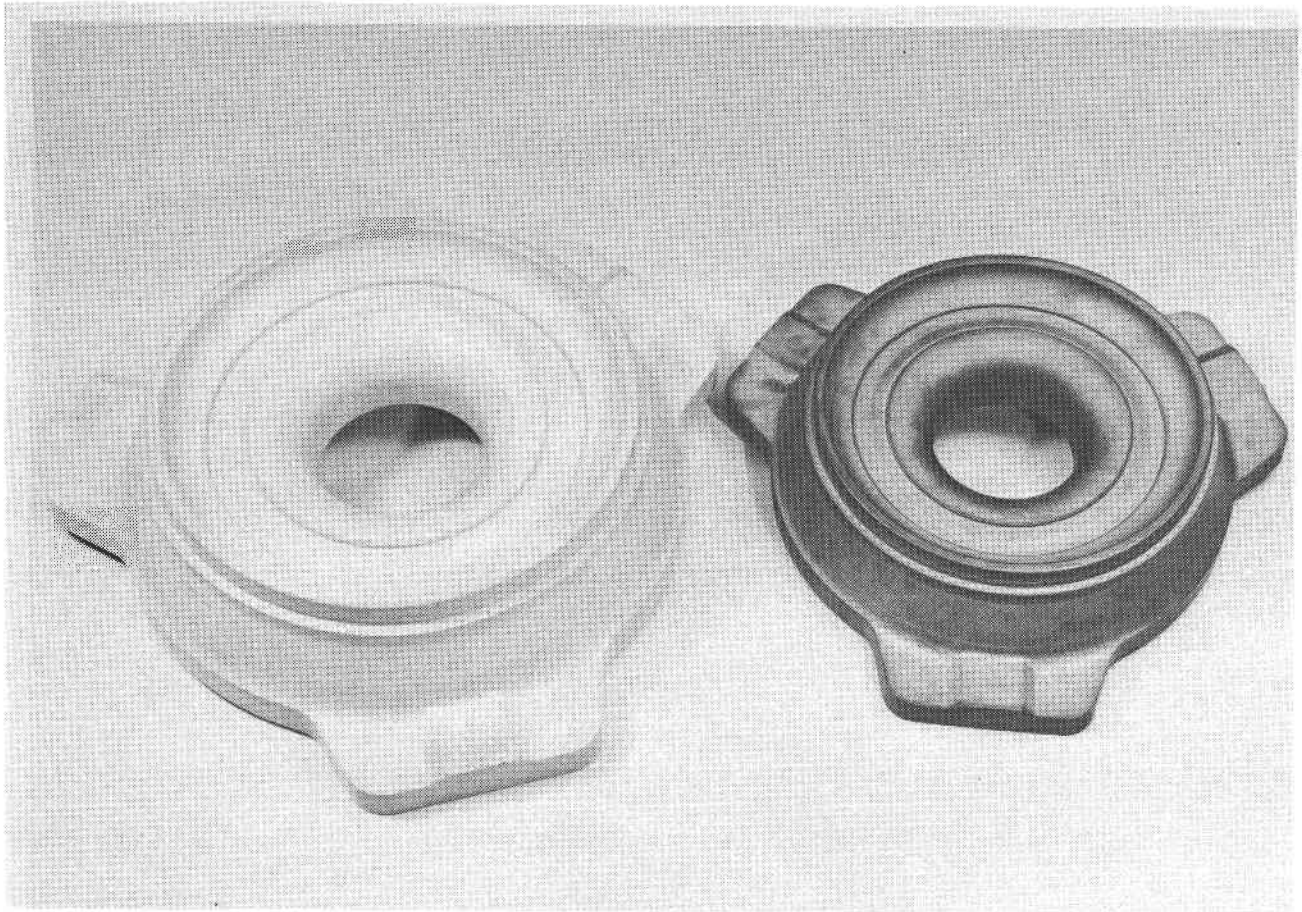
Figure 42. Scalloped Turbine Shroud
Green (left), Sintered (right)

GAPD had conducted additional stress analyses on the most recent design of the turbine shroud using alpha silicon carbide generic performance characteristics. It was determined that even the redesigned form of the turbine shroud still exhibited too high a stress for successful completion of the desired test program. Subsequently all work was discontinued after October 1984.

4.2.6   Turbine Stator

Both a segmented and an integral design (Figure 43 and 44) were initially considered for the stator section of the engine. For aerodynamic efficiency, the airfoil shape contains both convex and concave contours. In order to fabricate a functional injection molding tool to produce the integral stator, concessions on the airfoil contours would have been required. Aerodynamically, these concessions were undesirable and not allowed. Therefore, it was recommended to pursue the segmented approach which will produce the preferred airfoil shape. A single cavity tool was designed and ordered in May of 1980.
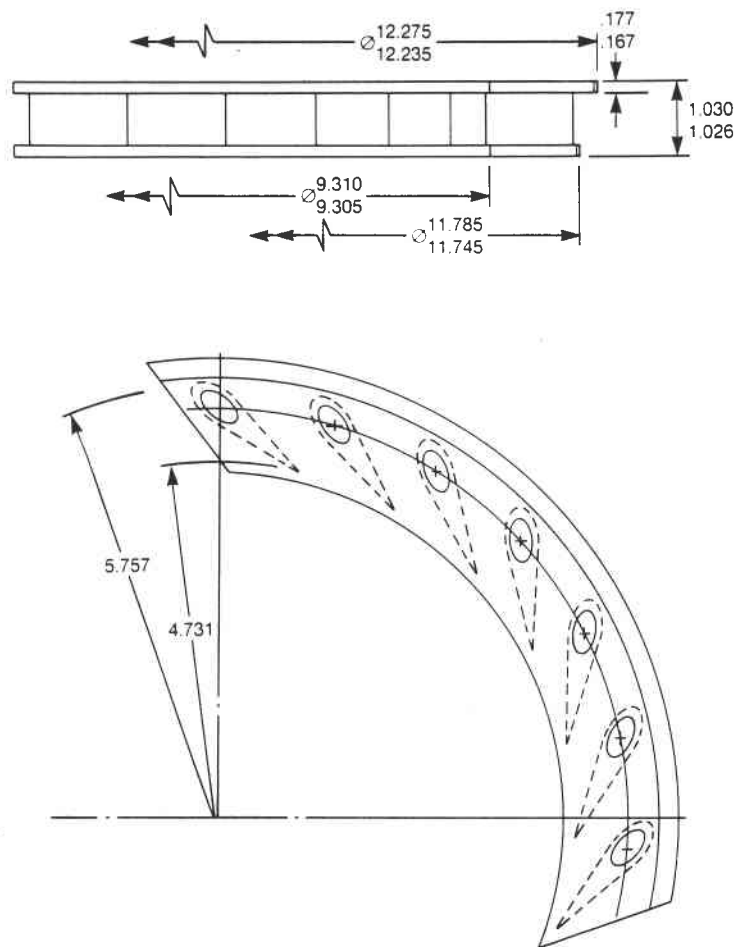
Figure 43.   Integral Stator Design
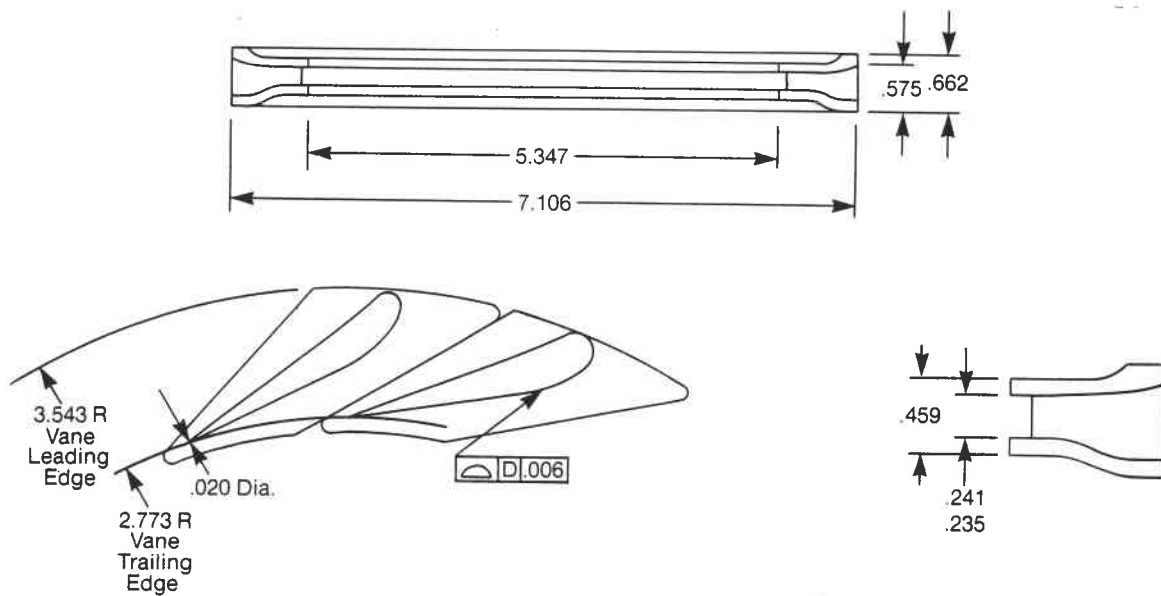
Figure 44. Individual Stator Segment Design

A wax replica of the stator segments formed in this injection molding tool was obtained in September. Inspection of the molded piece revealed the incorrect location of the gate on the leading edge of the vane. The gate location was changed to the more massive upper platform with an option to relocate at a later date.

Initial molding trials were conducted during the same month using an experimental molding compound. The filling pattern was satisfactory and the segments were processed through sintering. Low density and some distortion on the inner shroud were experienced.

A matrix of molding variables was selected and 20 segments were produced from each set of conditions. All molded parts were visually acceptable. However, after baking one group had a 60% yield, a second group had 10% and the remaining two groups had all defective segments. The predominant defects were small cracks in the gate region on the upper platform. Crackfree vane segments were sintered (Figure 45) and a density of 3.14 g/cm^3 was achieved. All parts exhibited some platform distortion. Simple fixturing techniques using plates or pins were not effective.

Development activities during the first half of 1981 focussed on designing, building, and evaluating support fixtures to prevent platform distortion during sintering. Six different sintering fixtures were evaluated. The most effective method was a reusable fixture which employed a fixed spacer at the trailing edge of the airfoil between the platform tips. The remaining five methods showed inconsistent results and were largely ineffective in assuring the parallelism of the platforms near the trailing edge.
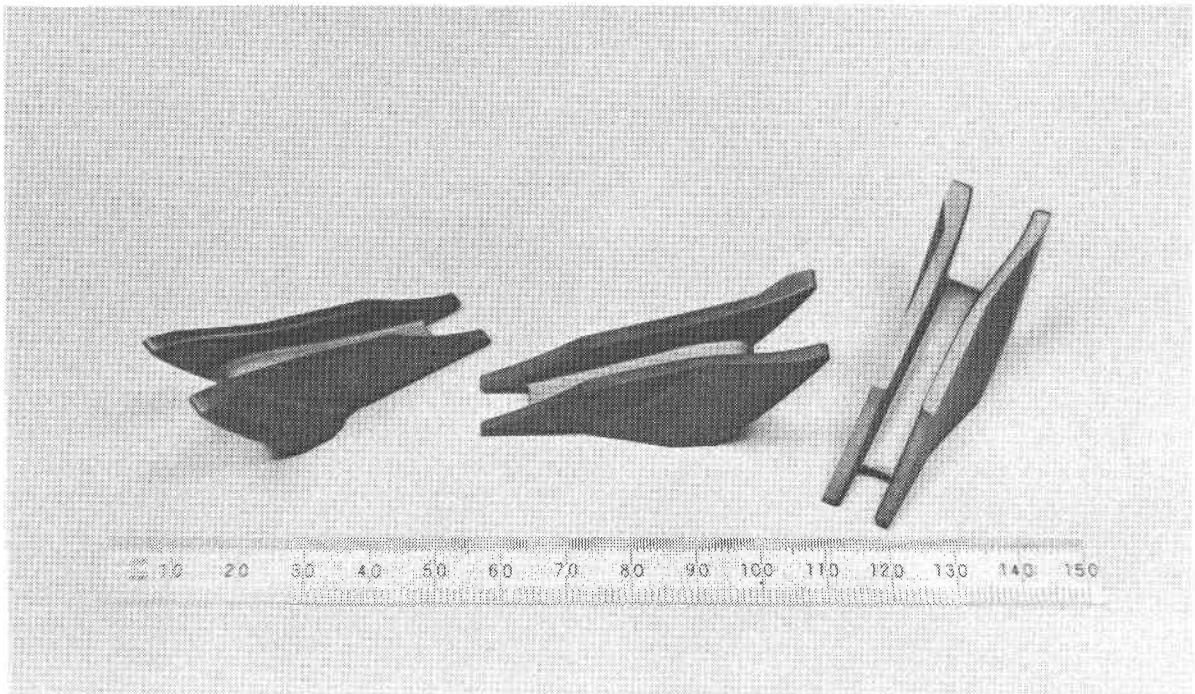
Figure 45. Sintered Stator Segments

Grinding fixtures were designed and fabricated in parallel to the sintering experiments. Sintered stator segments were used to finalize the grinding fixtures and assure proper set-up during grinding. The first grinding trial commenced in June of 1981. However, insufficient stock was present to finish the components to print. A second set of stator segments was completely ground to provide an undersized stator unit with correct interfacial tolerances to further assess the grinding capability, the amount of grind stock necessary, and shrinkage/warpage related dimensional deviations. Even though the platforms were smaller than required for finish grinding it was found that the airfoil shape and size corresponded well with the drawing dimensions. Figure 46 shows an as fired and a ground stator segment for comparison.

Compositional adjustments to provide platforms with a minimum of .010" grinding stock resulted in airfoils whose chord lengths were approximately .050" longer than print specifications, indicating anisotropic shrinkage during sintering. Similar behavior has also been observed on other complex injection molded shapes and is attributed to a variation in packing and green density.

Consequently, it was decided to rework the tool. An air vent in the trailing edge region was added to eliminate flaws in that region and the shroud platforms were enlarged to provide the necessary grinding stock while using standard injection molding compound.
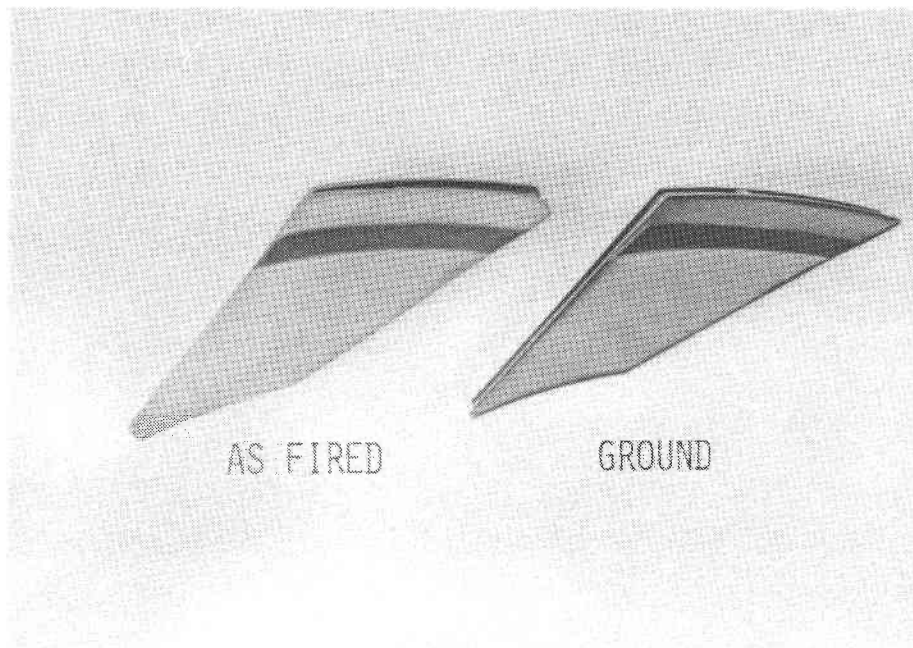
Figure 46. Stator Segments, As Fired and Ground

Molding activities were resumed in December and approximately 200 stator segments were produced. Airfoil contours and dimensions were verified on the sintered segments and overall platform dimensions were found to be adequate for grinding. However, visual and dye penetrant inspection revealed surface imperfections in the trailing edge region on approximately 50 percent of the segments. Air vents were subsequently enlarged on the mold and an additional 250 segments were molded. These components were processed through sintering during the first quarter of 1982.

In February a group of 30 segments was delivered to the grinding vendor where a precise grinding and fixturing procedure was established with substantial input from Standard Oil's development group. Four segments were used to work out the procedure.

Finish grinding was completed on the first of three sets of segments (19 individual stator segments per stator and one spare). To verify the O.D./I.D. dimensions as an assembly, a sizing fixture was produced and dimensionally certified. Identical fixtures were fabricated for the grinding facility, as well as Standard Oil's and GAPD's Quality Control.

63

The first set fit the fixture with less than .0015" total gap in the assembly. Review of this information with GAPD and further clarification of the drawing revealed that a .020" gap is necessary in the assembly to accommodate circumferential growth during heat-up to engine operating temperatures. The first set was reworked by removing an additional .005" from each side of the contact faces. After annealing and inspection this first set of ground stator segments was delivered to GAPD in April of 1982. A second set was provided during the following month. A minor grinding change was incorporated in the next two sets to be ground. The radius at the intersection of the O.D. arc and the flat of the shroud platform was increased.

During the second half of 1982 development work addressed grinding of individual stators. It was noted that several components had grinding induced flaws. Most of these components could be reworked to eliminate chips and small cracks through hand blending. The grinding procedure and execution at the grinding vendor were reevaluated to minimize rejects and improve the quality and also the yield of finish ground components. All potentially usable parts in inventory, ground as well as unground, were shipped to GAPD in October 1982 for evaluation, completing the project for FY 1982.

Work on this project was reinitiated at the beginning of FY 1983. An improved injection molding compound with a different plastic system and a somewhat higher plastic content was used to make stator segments in the mold designed for the previously employed system which exhibited a 17% shrink factor.

The new compound (B) is superior to the old one (A) by producing parts with less molding defects or flow lines. Parts made of compound B also exhibit less sintering distortion. A set of parameters was investigated to alter and sufficiently influence shrinkage during sintering to obtain parts to print.

The initial molding trial with the new compound (B) conducted in January yielded components which were substantially undersized. Various molding compounds (B_1, B_2, B_3) with decreased plastics content to reduce overall shrinkage were subsequently investigated.

Several groups of stator segments were molded during the first half of that year. All compounds derived from the B composition yielded visually excellent molded parts without apparent flow lines or excessive flaws in contrast to a control group of segments from composition A which showed some unfilled areas and also some flow lines. At that time 20 plastic stator segments were also molded to verify the consistency of the mold dimensions and to check specifically the vane shape, vane length, and the profile of the sidewalls. Inspection indicated extremely good agreement with drawing dimensions.

64

Various sintering schedules were investigated using stator segments of the B_2 composition to determine the exact relationship between sintering temperature, density and dimensional tolerances. A matrix approach was used in determining the sintering temperature which would yield the best dimensions in connection with an acceptable final density. Six stator segments were used for each experiment which involved three temperature levels: T_1, T_2, T_3, and two compositions: B_2 and B_3. It was concluded that B_3 at T_2 and B_2 at T_3 gave the best results.

Evaluation of the stator segments made from the B compound versus the modified compounds B_2 and B_3 indicated superior quality parts from the former. Subsequently it was decided to design a new mold with increased shrink factors.

Compound B was used for molding 250 stator segments. All parts were processed under standard procedures and conditions and some of these parts were used to determine mold dimensions for a new injection molding tool. The remaining parts were utilized for fixturing experiments during sintering. Warpage of the sidewalls, flaring at the ends and some distortion in the trailing edge necessitated additional design work on the sintering fixtures. A configuration was developed which was successful in minimizing these deviations.

The new molding tool (Figure 47) was received late 1983 and 400 stator segments were molded in January of 1984. A total of 190 parts were processed through sintering. All parts had good densities and showed good dimensional stability but exhibited sharp filet radii and a thin trailing edge. GAPD received three as sintered stator segments and verified the deviations.

The molding tool was reworked and two groups of stator segments were molded consisting of 300 parts of compound B and 400 parts of compound C. Latter varies from compound B only in the particle size distribution of the submicron alpha SiC powder which results in slightly reduced shrinkage as experienced on isostatically pressed shapes. However, processing either one of the SiC injection molding compounds exhibited essentially the same shrinkage characteristics.

All parts had good densities and shape integrity but exhibited vane profiles which were too short and thin on the trailing edge. Consequently, the injection molding tool was sent out for a second rework in the trailing edge.

The tool was returned in July of 1984 and a large molding trial was conducted. The parts were processed using standard conditions. Virtually no parts were rejected due to X-ray flaws. Some visual defects on the trailing edge were removed through minor touch-up grinding. The good correspondence of the vane profile with the print was verified by both GAPD as well as Standard Oil.
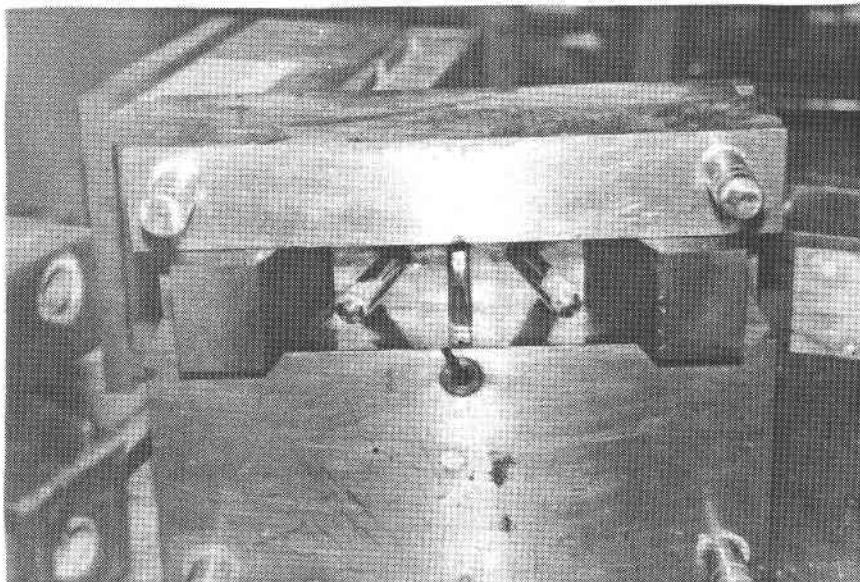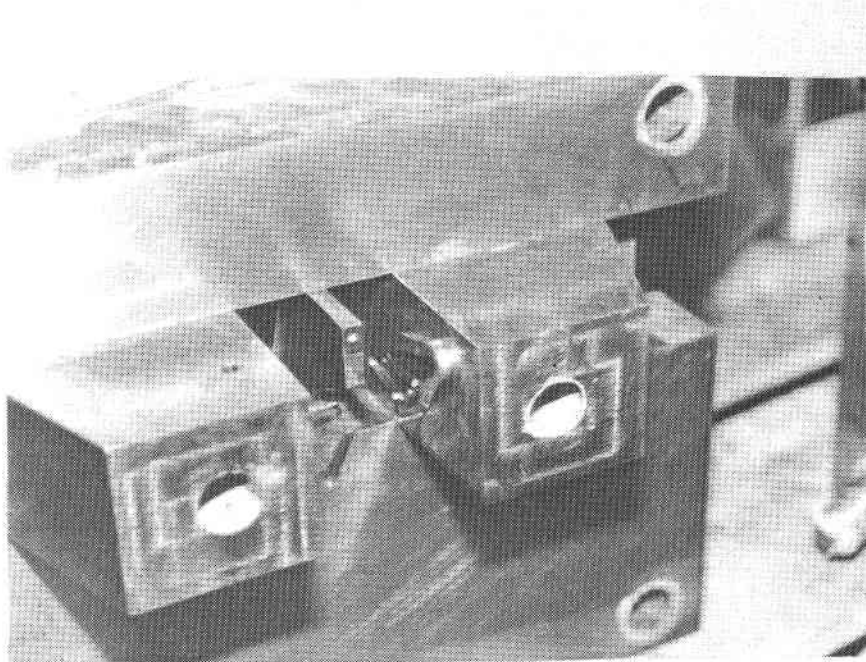
Figure 47. Injection Molding Tool

Four sets of as fired stator segments (Figure 48) were shipped to GAPD in September, two sets in November and the remaining seventh set in December to complete 1984 delivery requirements. Work for FY 1985 was scaled down substantially, one small molding trial and several fixturing experiments were conducted to obtain better control over the platform distortion near the leading edge as depicted in Figure 49 which shows the platforms opposite the gates bending inward. New fixtures were designed and fabricated. However, no substantial improvement could be observed. At that point it was felt that a change in gating and maybe some integrally molded fixtures would resolve these difficulties.
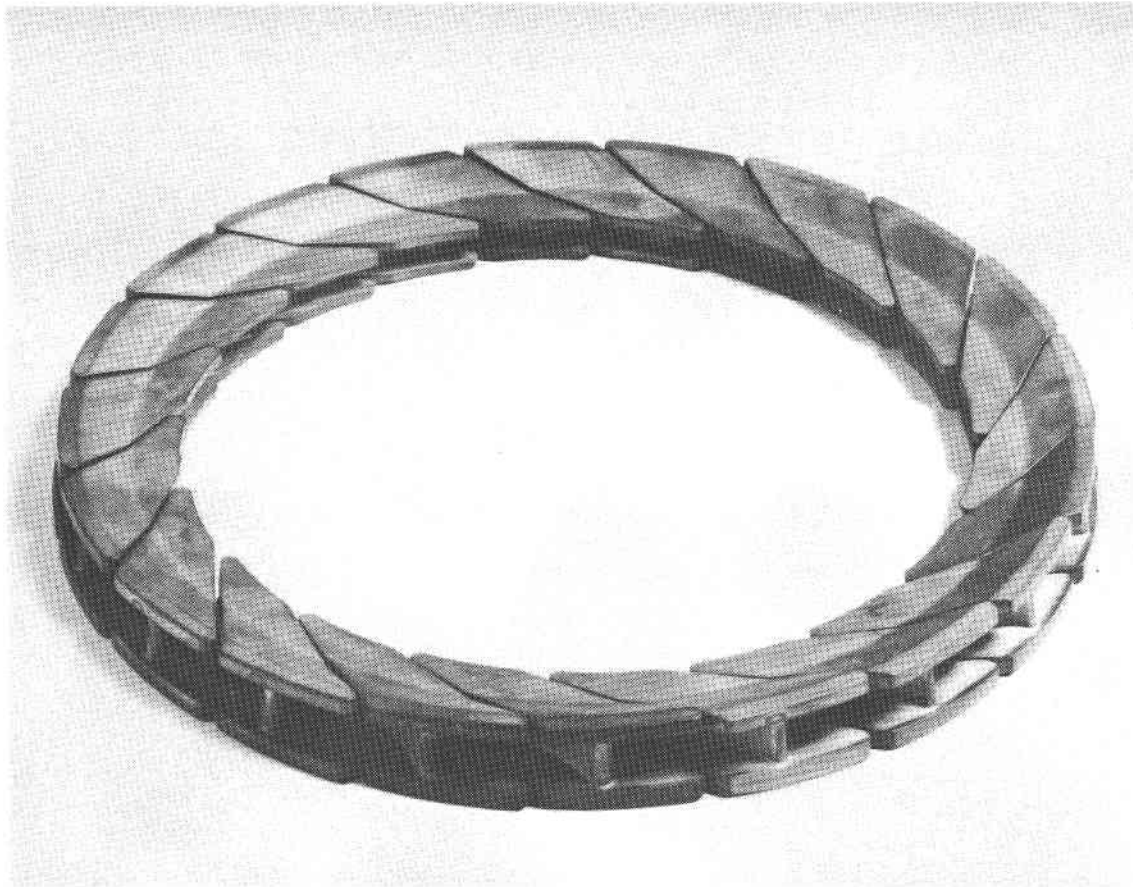
Figure 48. As Fired Stator Set

Testing at GAPD during the first half of 1985 revealed frequent cracking of segments in the center of the trailing edge. Subsequent detailed stress analyses indicated that stresses of up to 44 ksi can be present in the trailing edge depending on test sequence. These stresses could be reduced by cutting back the trailing edge, as shown in Figure 50. A set of stator segments was modified accordingly and passed thermal screening. However, this modification results in reduced engine performance. It was therefore decided to conclude this development project and not to invest in additional tooling rework.
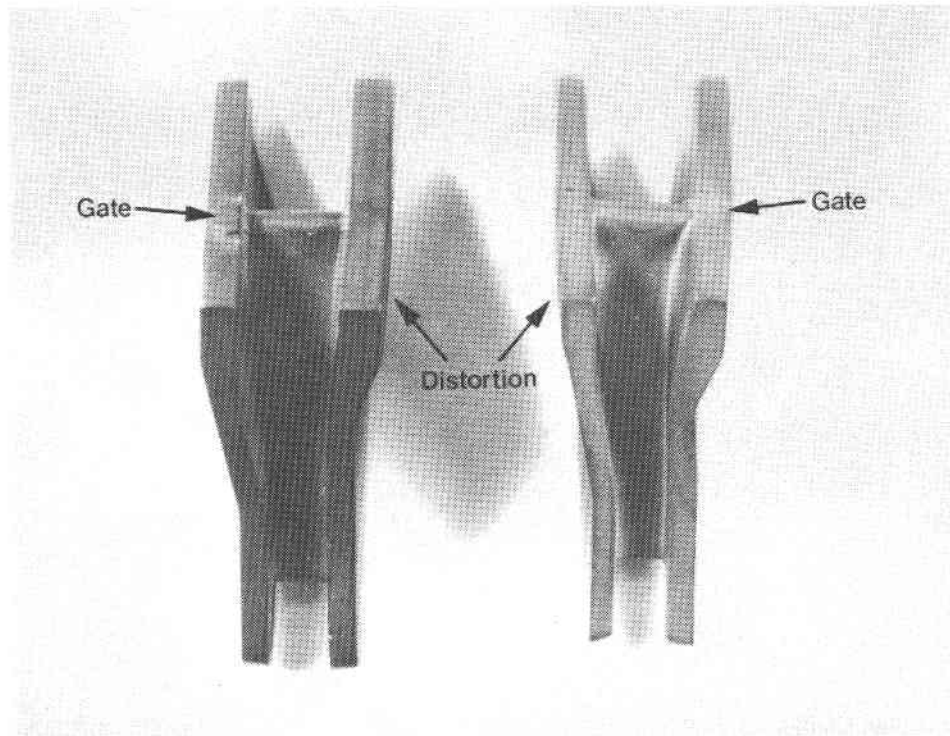
Figure 49. Distortion on Stator Segment
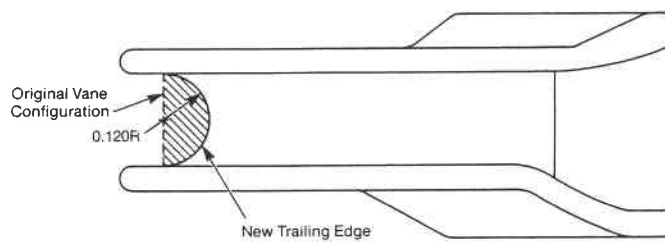
Figure 50. Cutback of Stator Vane Trailing Edge

4.2.7   Regenerator Shield

Design discussions on the regenerator shield (Figure 51) were initiated in January of 1980 with Drawing L3646114. Initially it was suggested to produce this component by slip casting, followed by green machining of the I.D. taper and some final grinding after sintering. However, it was decided to use isopressing and green machining instead to obtain components for testing.
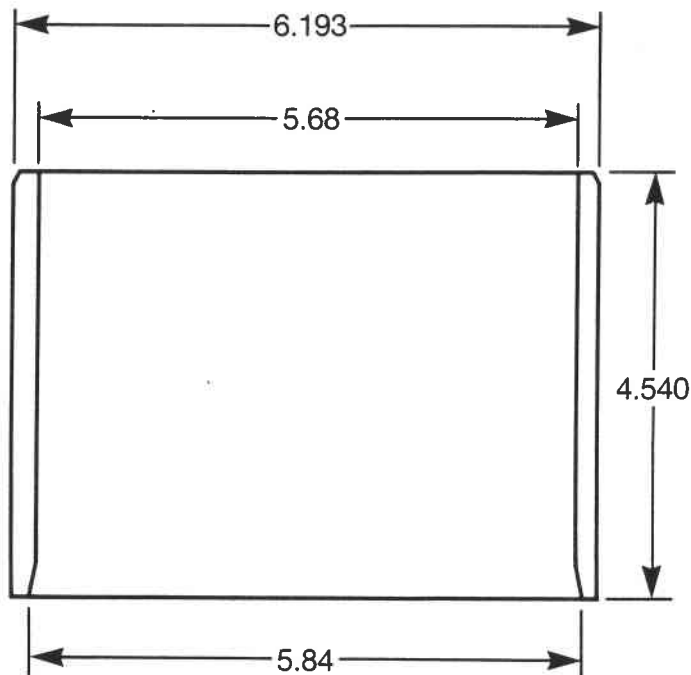
Figure 51. Initial Regenerator Shield Design

Isopressing and green machining of tube stock has been a standard fabrication method used routinely for high performance ceramics and development work was only required for exact shrink factor determination and fixturing during sintering to reduce grinding time/cost or completely eliminate grinding in certain areas such as the I.D.

Fabrication of isopressed billets was started in July. Five components completed sintering and as fired inspection during the 3rd. Quarter of 1980 and were submitted for grinding to an outside vendor. Fixturing and grinding methodology difficulties on this relatively large component delayed the actual completion of these first deliverables. Additional five components were processed through as

fired NDE, dimensional inspection and submitted for final grinding during the 4th Quarter. A total of nine ground components were delivered in February of 1981 completing the delivery requirements for the 1980/1981 AGT 101 schedule.

Development work was reinitiated on a modified design (Drawing 3846154) in May of 1983. Figure 52 depicts overall characteristics of this new design.
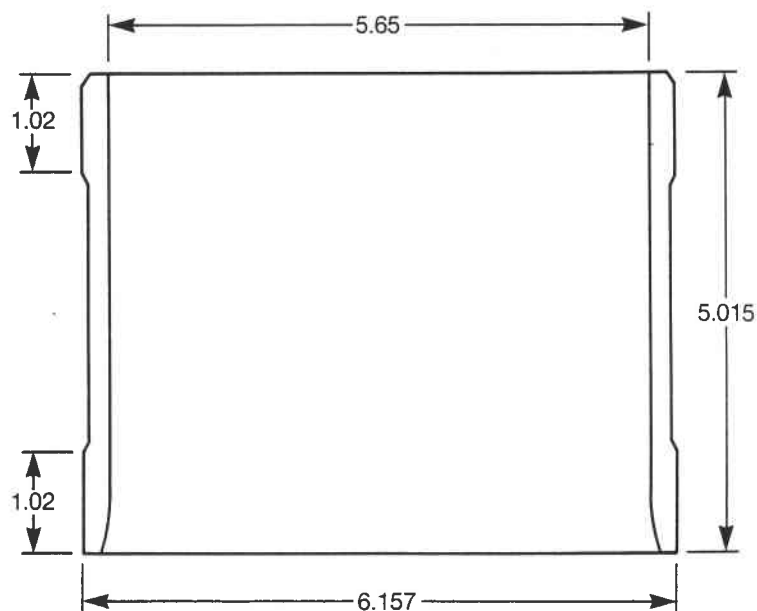
Figure 52. Modified Regenerator Shield Design

Extrusion was chosen as a viable fabrication method which would reduce material cost significantly because of increased material yield. Additionally, this method is capable of producing large quantities of the basic tubular shape very cost effectively with little manual labor necessary.

The relative large diameter required on the green shape, approximately 7.75" (197 mm), and the extrusion compound available at that time, determined that plastic extrusion should be developed instead of aqueous extrusion. Plastic extrusion has higher green strength which aids in handling and reduces green losses. However, it requires an additional binder removal step which is very critical for the quality of the sintered component.

70

Initial shrink factor determination on plastic extrusion mix was conducted during May and an extrusion die was designed in cooperation with an outside extrusion vendor. Difficulties were experienced in first scheduling an extrusion trial at the outside vendor site and second in having the proper take-up equipment in place.

The first extrusion trial conducted in October was unsuccessful because of insufficient pressure to fill the large diameter die. A second trial on a larger extruder during the following month proved to be successful. Tube stock to yield 26 individual thick walled liners was produced. Four sections were cut to size, visually examined, dimensionally checked, and placed into binder removal.

The first extruded regenerator shield blank was sintered in December of 1983. Subsequently it was ground and submitted for final inspection. It was found that insufficient stock was present due to out-of-roundness, thus, dimensional requirements were not met. In addition, subsurface flaws were exposed during grinding.

Processing experiments were conducted on several of the remaining cut-to-length sections. Each of the parts showed blow outs or cracks. Reevaluation of the extruded green stock using X-ray microfocus examination indicated that internal voids and inhomogeneities were present throughout the whole charge. Subsequently, a reassessment of this development program was conducted in light of the funds available and the delivery requirements. In February of 1984 it was decided to terminate this aspect of the program and place increased emphasis on supplying ground regenerator shields made by isopressing and green machining.

Parallel processing had been initiated in September of 1983 after scheduling problems with the large extruder were experienced. Two units were isopressed and processed through as-fired NDE. These parts were submitted for grinding as it became apparent that the extruded tube stock would not yield engine quality components.

One ground component (3-101), as shown in Figure 53, supplied in December was followed by a second unit (4-101) in January. Staying with this proven prototype fabrication technique two additional units (4-102 and 4-103) were supplied in March followed by a single shipment (4-104) in June which completed the FY 1984 requirements.

Activities on this program task were reinitiated in November of 1984 to meet FY 1985 delivery requirements of components throughout the year. Work addressed precise shrinkage determination on a specified lot of alpha silicon carbide to minimize final grinding cost through the elimination of I.D. grinding on the straight section. Green machining of the I.D. radius proved to be unsuccessful because of the close tolerances required and subsequent alignment and set-up problems during final grinding.
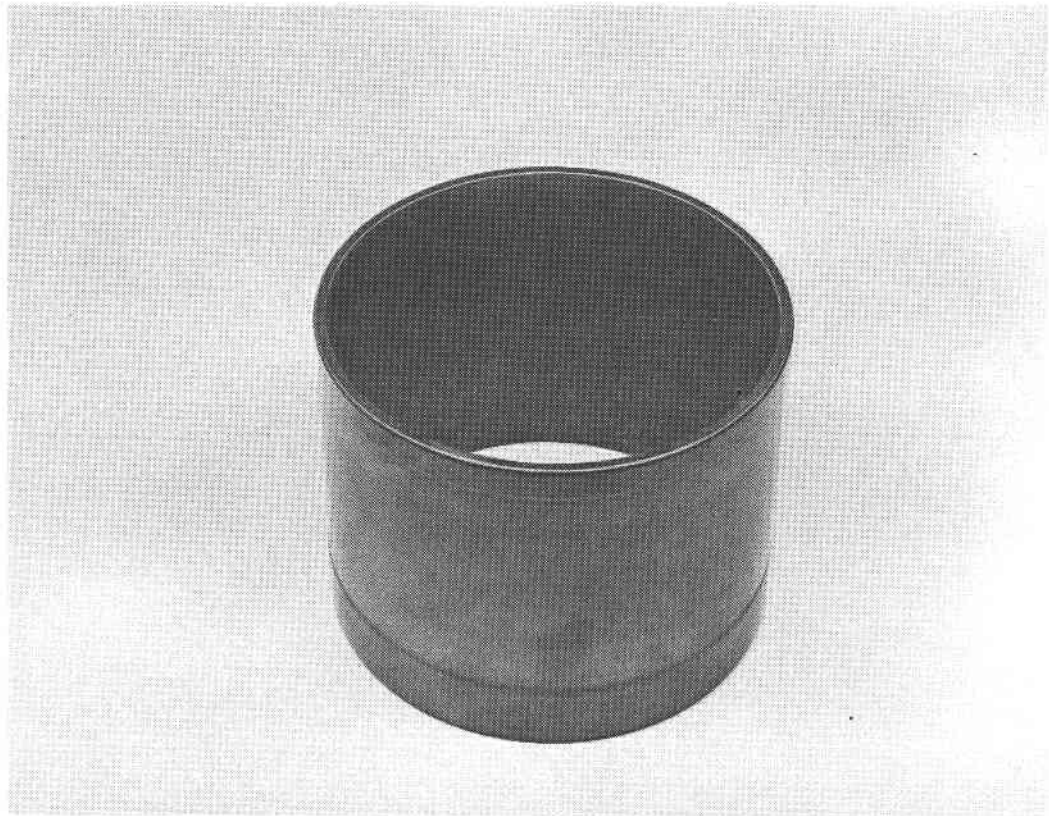
Figure 53. Finish Ground Regenerator Shield

Six preforms were isopressed in January of 1985 and shrinkage determination was conducted on one tube blank. The shrink factors used for calculating green dimensions were adjusted accordingly and four units were processed through sintering. All units were ground after passing NDE and dimensional evaluation. Two ground, annealed regenerator shields (5-105 and 5-106) were shipped in February and two additional parts (5-107 and 5-108) in March.

A revised drawing (3846154-A), as illustrated in Fig. 54, was obtained during the following month. Partially processed regenerator shields were evaluated if they could be reworked to meet the new more stringent requirements on one of the O.D. bands. Grinding difficulties were experienced on the first part to be machined according to the new drawing. The component was machined undersize.

New preforms were isopressed and processed. Two regenerator shields (5-109 and 5-110) completed processing through grinding, final NDE and dimensional evaluation and were shipped to GAPD in June of 1985.

Component fabrication from isopressing through sintering and as fired inspection continued to follow routine procedures. Grinding was accomplished by an outside vendor. A total of four finish ground regenerator shields were supplied from September through November completing FY 1985 requirements.
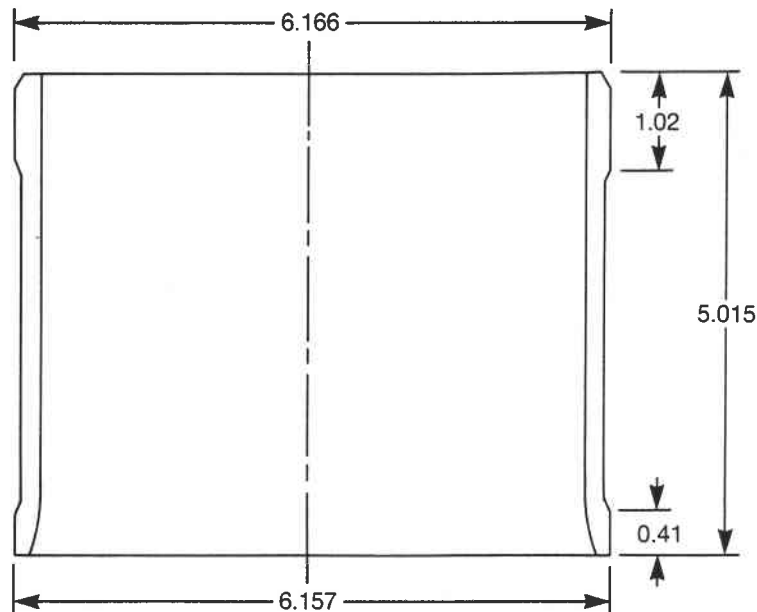
Figure 54. Revised Regenerator Shield Design

Difficulties, however, were experienced in obtaining the tight O.D. tolerances and closer inspection of the close tolerance O.D. band indicated some additional grinding related irregularities. Evaluation of the ground O.D. dimensions using a Talyrond tracing machine (Figure 55) was conducted. It was found that grinding patterns similar to those shown in Figure 56 were present. The grinding vendor was advised of the deviations and close interaction with the grinding vendor resulted in marked improvements, as shown on the Talyrond tracing in Figure 57.

After establishing shipping requirements for FY 1986 in late 1985, new preforms were pressed and processed according to the new schedule. Due to malfunctioning of the grinding machine one part was chipped and had to be rejected. This resulted in a delayed shipment of the first two components. Four components (6-115 through 118) were completed in March of 1986 and were shipped after they were subjected to an annealing step.

Figure 55. Talyrond Tracing Machine
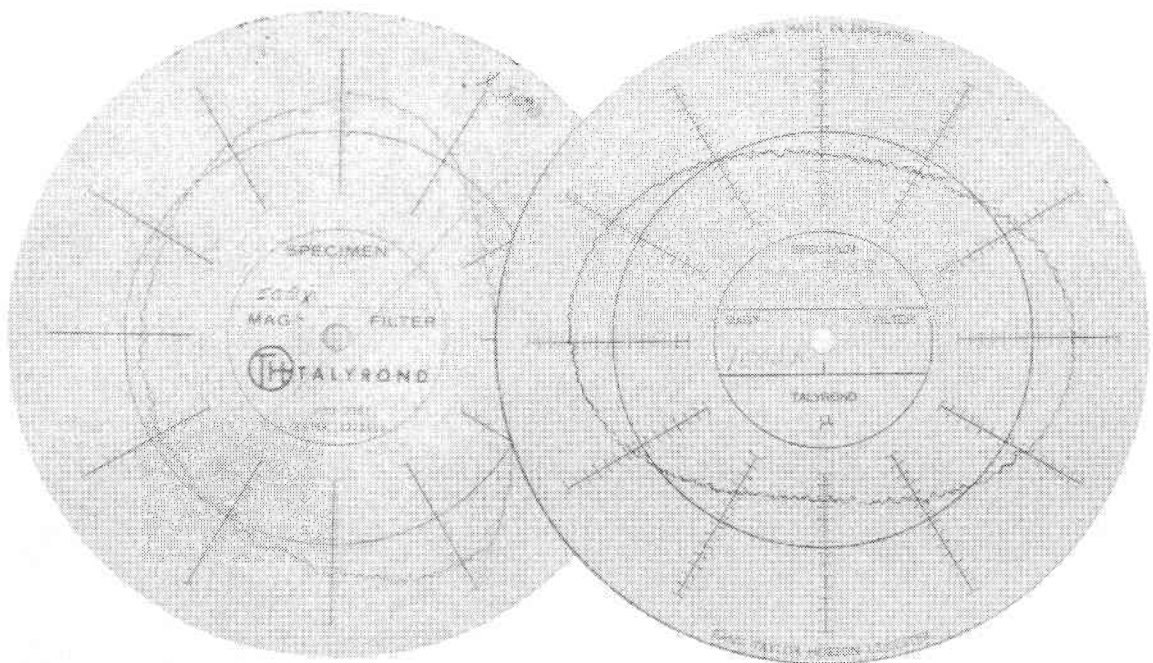
Figure 56. Talyrond Tracings of Unacceptable Grinding Patterns
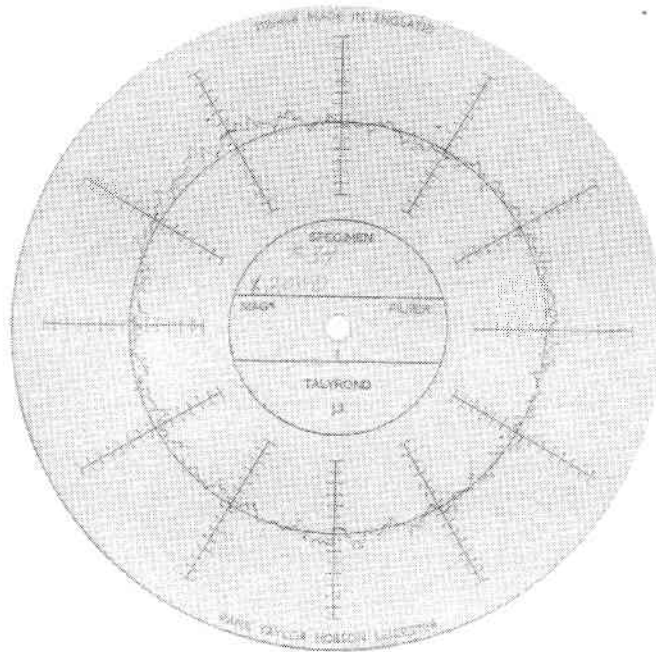
Figure 57. Tracing of an Acceptable O.D. Band

Drawing revision B (Figure 58) was obtained shortly thereafter and three units which had been ground to revision A were reworked accordingly. The best two components (6-119 and 6-120) were shipped in May completing FY 1986 requirements. Figure 59 shows a regenerator shield ground to drawing revision B.

Table 11 summarizes the component shipment for the complete program. Sintered alpha silicon carbide regenerator shields have repeatedly performed well within the AGT-101 during mechanical qualification and engine testing with no known failures.

Regenerator shield 103, for example, was tested in engines at $2200^{\circ}F$ and had accumulated almost 100 hours of testing prior to a major engine failure where it was damaged with most of the ceramic hardware. A second regenerator shield (108) has been successfully tested at $2100^{\circ}F$ for over 100 hours.
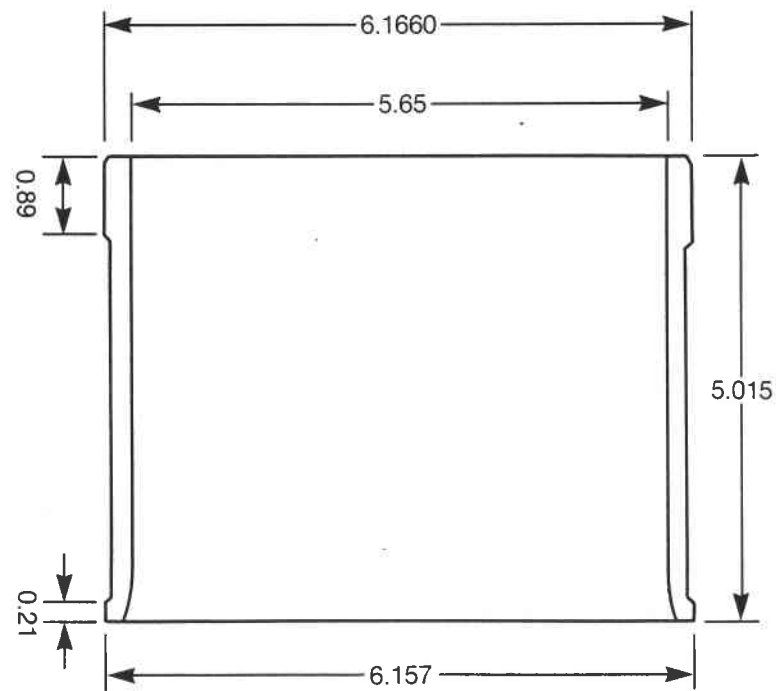
Figure 58. Regenerator Shield Design - Revision B
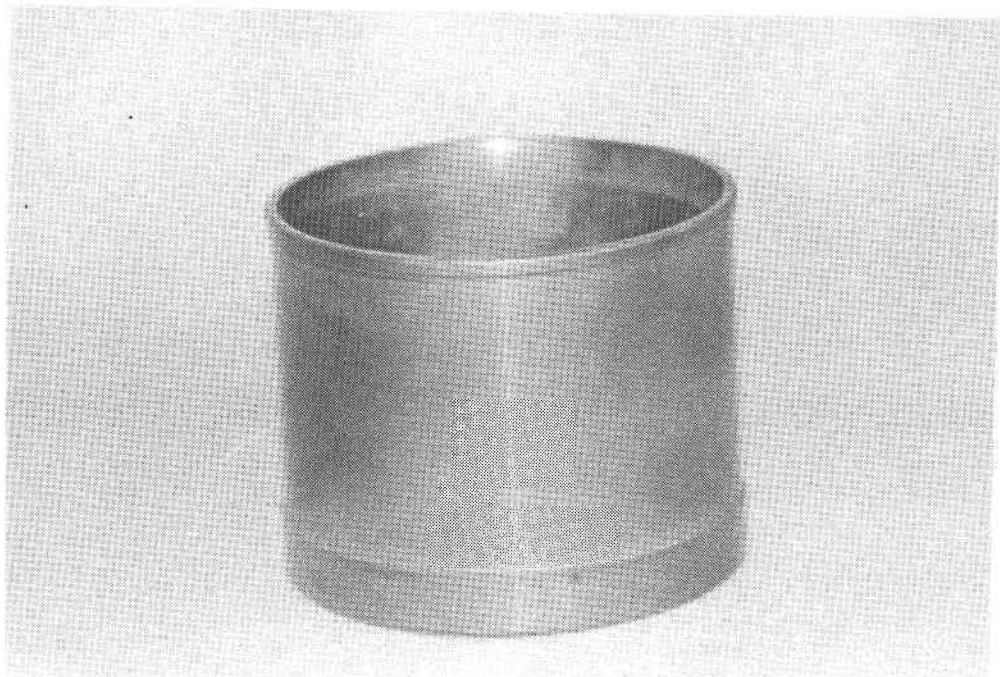
Figure 59. Ground Regenerator Shield
(Revision B)

Table 11

Regenerator Shield - Component Deliveries

FY

	1980	1981	1982	1983	1984	1985	1986
Dec.					1		
Jan.					1		
Feb.		9				2	
March					2	2	4
April							
May							2
June					1	2	
July							
Aug.							
Sept.						2	
Oct.							
Nov.						2	

4.2.8   Combustor Liner

Work on the combustor liner, as shown in Figure 60, (Drawing 3830148) commenced mid 1982. The components were made of isopressed green machined tube stock. After furnacing each component was ground to dimensions.

Two material systems had been selected for this component: Hexoloy™SA, pressureless sintered alpha silicon carbide, and Hexoloy™ KX-02, a silicon infiltrated silicon carbide material. Two ground combustor liners from each material were supplied first in August and then in October of 1982.
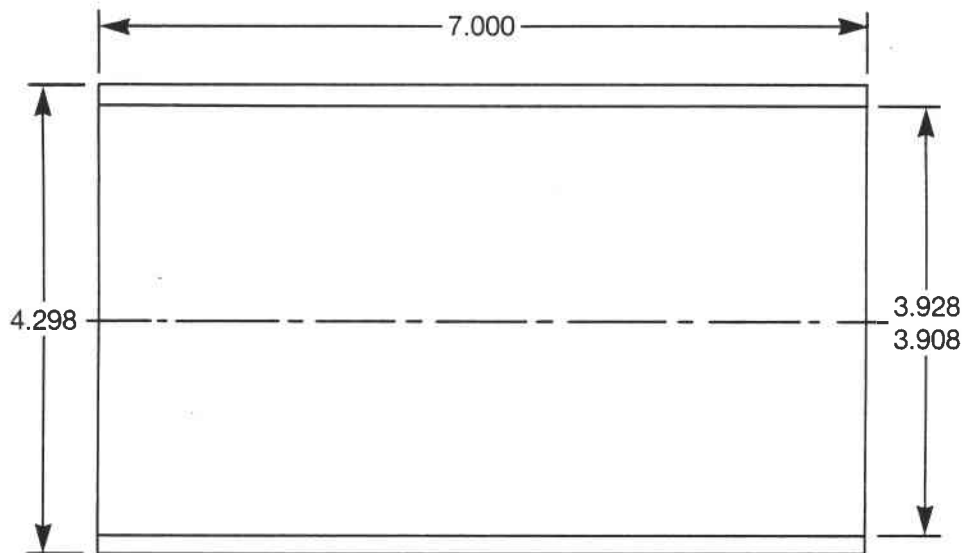
Figure 60.   Combustor Liner Design

Development work on extruded and sintered silicon carbide combustor liners was initiated in May of 1983 in parallel with the extrusion development on the regenerator shield. The combustor liner with its straight tube section is ideally suited for high volume/low cost fabrication by extrusion.

Compound was prepared and tested for shrinkage and an extrusion die was designed in cooperation with the extrusion vendor. The first extrusion trial was carried out in July. Three 5 foot long tube sections yielding 20 individual liners were successfully extruded. Several liners were subjected to binder removal. The

78

initial sintering test resulted in blow outs and warpage. The fixturing method was revised and inside mandrels were used during the following sintering trials. The observed warpage was greatly reduced, however, all parts from this first extrusion trial exhibited surface flaws.

A second extrusion trial was conducted in September. Additional stock on the O.D. and I.D. was incorporated in the die and the extrusion machine variables were changed to eliminate surface flaws. Initial visual inspection revealed no surface flaws were present on this second group of liners. Still, sintered liners showed a rough surface and blow outs. The remaining baked liners were subjected to X-ray inspection to check for a possible contamination problem. Most parts showed substantial metal contamination. Two parts without metal contamination were sintered and submitted for final grinding. The components did not clean up completely and voids were uncovered during grinding.

Material from a third extrusion run under new extrusion conditions, conducted in December of 1983, yielded tube stock for 26 individual liners. Several components were processed, however, none of these were of engine quality.

Additional grind stock was incorporated in the die prior to the fourth extrusion trial carried out in February. Four of these components showed good dimensional control and material quality and were sent after grinding and final NDE to GAPD during the second quarter of 1984.

Subsequently, the direction of this development project was reexamined. Based on schedule, financial impact and extrusion progress it was decided to discontinue the extrusion development effort and fulfill hardware requirements with isopressed/green machined units.

Plastic extrusion was considered to require more extensive development than the combustor liner project would warrant. In the near term, especially with the use of an outside vendor and the limited number of trials, it was felt that net shape of the O.D./I.D. dimensions could not be achieved. Thus, extensive diamond grinding would be necessary while no grinding is required in the case of isopressed/green machined units. In addition, material quality of plastic extruded material was inferior to isopressed material. Figure 61 shows a comparison of etched photomicrostructures at 200 magnification.

Due to the slow progress of plastic extrusion development isopressing and green machining was initiated in March 1984. Work was carried out in parallel for about four months, first to assure timely hardware delivery and second to evaluate and finish extruded work in process.
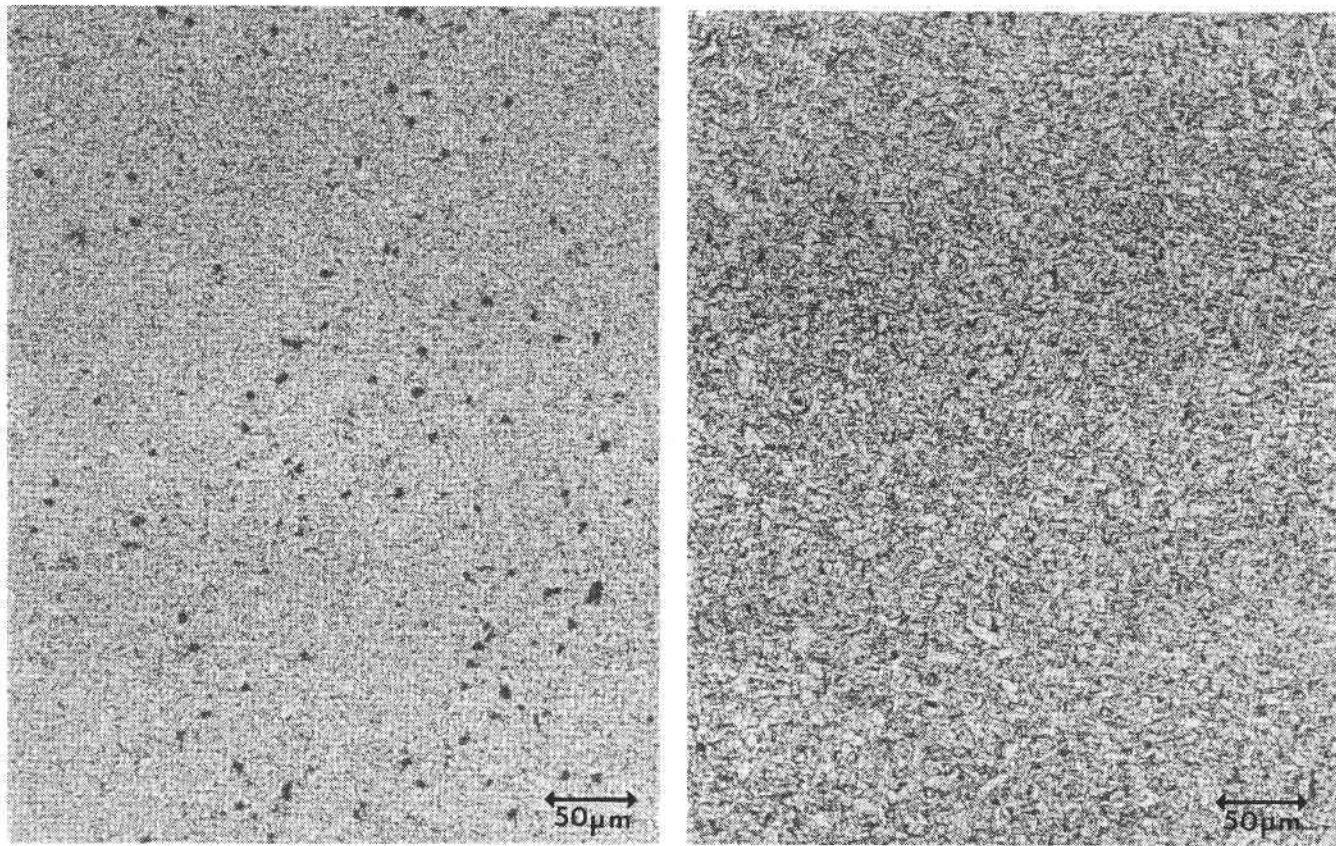
Figure 61. Photomicrostructures of Sintered Silicon Carbide
Extruded (left), Isopressed (right)

Deliveries for FY 1984 consisted of four extruded (4-105 through 108) and six isopressed (4-101 through 104, 109 and 110) and green machined combustor liners delivered from April through July. The latter liner (Figure 62) required no grinding after the initial shrink factor determination was completed.

Work resumed in December of 1984 with isopressing/green machining as the selected fabrication method. Eight units (5-111 through 118) meeting drawing specifications in the as fired state without additional grinding were delivered in regular intervals between February and August.

Two new designs (Drawings PAP254020 and PAP255863) were received in October. These components had the general tubular shape, however, varied in diameters and length from the originally delivered combustor liners. A total of nine liners (5-119 through 127) were delivered in October and November of 1985.
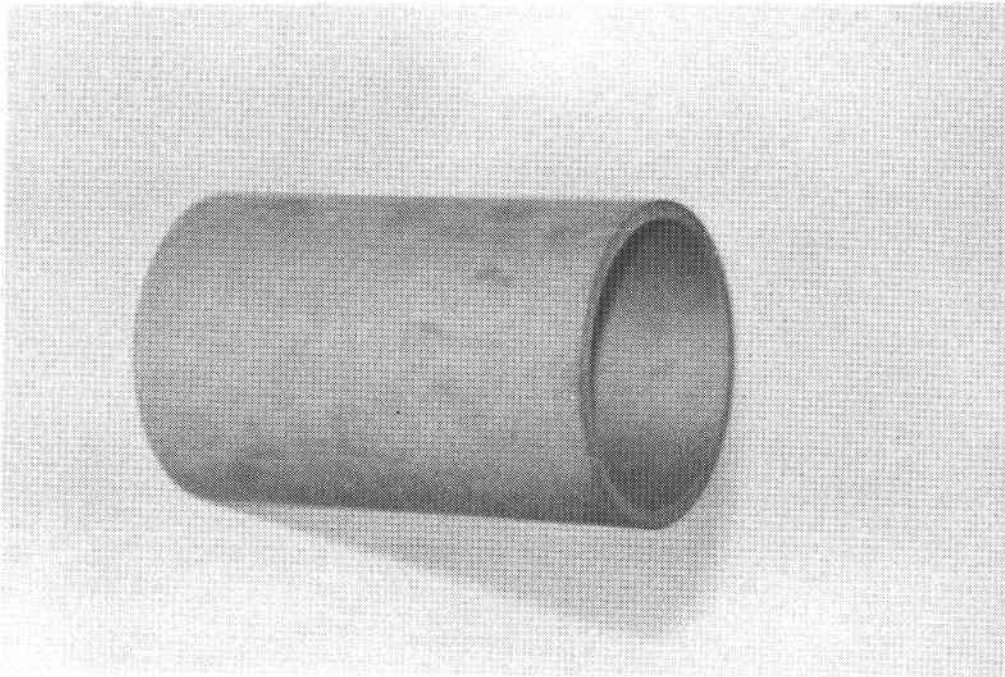
Figure 62. Sintered Combustor Liner

The plan for FY 1986 called for ten deliverables per drawing PAP254020. The first two shipments consisted of two liners each (6-128 through 131) in January and March.

A new drawing (PA3611755) was received in March. The major distinction between this and the previous designs was the closer tolerance control of all the dimensions (Figure 63). Four units (6-132 through 135) supplied in March represented a hybrid design because they consisted of reworked units which had been green machined and sintered prior to receiving the new drawing. They were followed by a shipment of two liners (6-136 and 6-137) which corresponded completely to drawing PA3611755.

Component deliveries for this project, summarized in Table 12, were completed in May of 1986. No additional fabrication development activities have been carried out.

Testing of combustor liners was initiated in October of 1985. Several components have been qualified in engine tests. Combustor liner 132 accumulated about 100 hours at 2200°F during tests from September of 1986 through January of 1987.

81
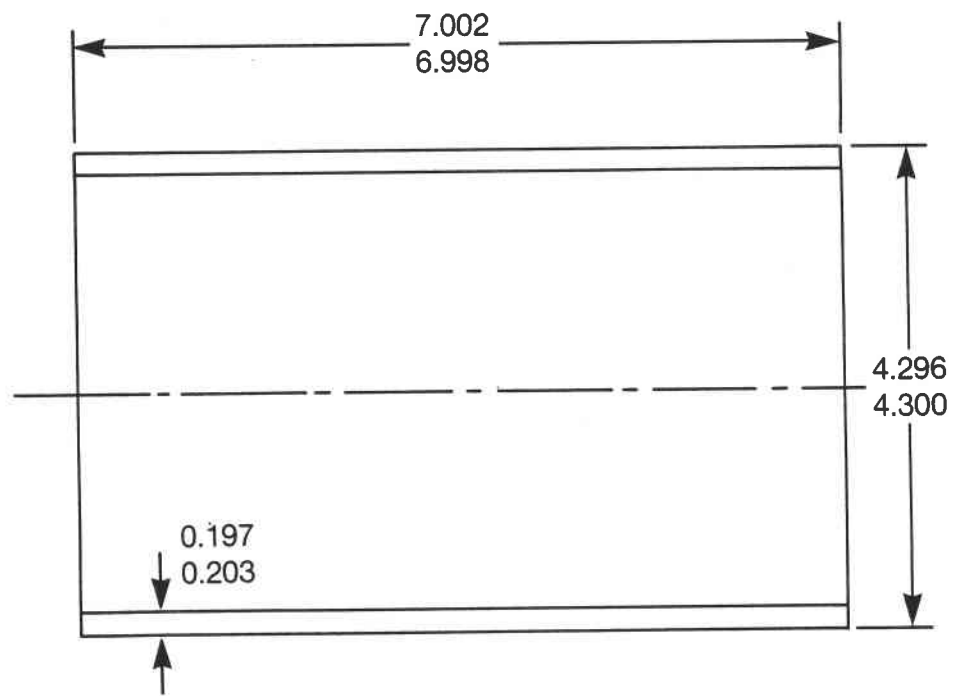
Figure 63. Revised Combustor Liner Design

Table 12

Combustor Liner - Component Deliveries

	1980	1981	1982	1983	1984	1985	1986
Dec.							
Jan.							2
Feb.						2	
March							2
April					4	2	4
May					1**		2
June					3**	2	
July					2		
Aug.			2/2*			2	
Sept.							
Oct.			2/2*			5	
Nov.						4	

*Hexoloy™ KX-02

**Extruded

4.2.9   Combustor Baffle

Design discussions on the combustor baffle (Drawing L3846109), as shown in Figure 64, were initiated in January of 1980. Initially it was thought to fabricate this component in two sections, a ring and an inner face, joined by brazing. Critical final dimensions would be incorporated through diamond grinding.
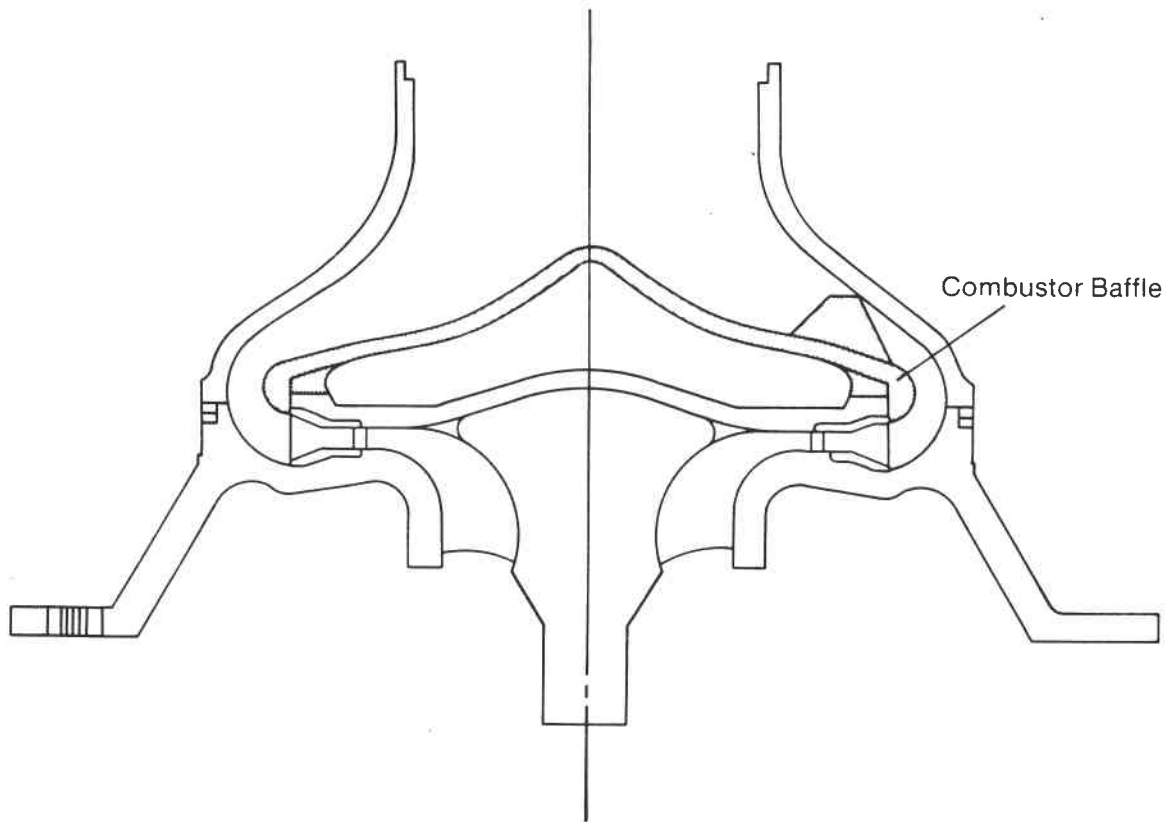
Figure 64.   Initial Combustor Baffle Design

Several design/fabrication capability meetings were held during the first half of 1980. As a result the combustor baffle design was modified to allow fabrication in one integral piece. During these design discussions it became apparent that slip casting would be the preferred forming method. Subsequently, work was initiated on simple shapes to determine processing characteristics for a variety of casting mixes.

84

4.2.9.1   Casting Formulation Development

Two slip compositions, one of a submicron SiC and the second of a bimodal SiC had been used for a wide variety of parts. The bimodal composition consisted of 65 wt% of submicron SiC powder and 35 wt% 1000 grit SiC grain (mean particle size $\approx$ 7 μ). A comparison of these two mixes showed that the casting rate increased with the addition of the coarse SiC grain. On the other hand, the submicron composition exhibited better draining qualities resulting in a superior internal surface finish. Parts made from this composition showed about 18% shrinkage in comparison to parts from the bimodal composition which had about 12% overall shrinkage. Final sintered density is proportionally related to overall shrinkage. Consequently, parts made from the submicron mix had higher final densities than parts from the bimodal composition, assuming comparable green densities were obtained as was the case in the two systems investigated. Fired densities ranged from 3.08 to 3.15 g/cm^3 for the former and 2.75 to 2.90 g/cm^3 for the latter.

Mix studies on seven compositions were conducted with the goal to reduce shrinkage and minimizing distortion problems while still obtaining adequate densification. Table 13 summarizes the results obtained on cast crucibles.

Table 13

Evaluation of SiC Slip Compositions

Mix	Sub Micron %	Coarse %	Density g/cc	Shrinkage %	MOR (ksi) RT	MOR (ksi) 1200°C
1	0	100	1.93	3.32	—	—
2	10	90	1.98	3.30	—	—
3	20	80	2.42	7.44	22.5	17.0
4	35	65	2.59	9.51	26.0	24.0
5	65	35	2.85	11.31	42.0	42.0
6	75	25	3.02	—	—	—
7	100	0	3.08	15.15	54.0	61.0

The major problem associated with Mixes 1, 2, and 3 were the poor drain properties. The surface finish of the crucibles improved as the amount of submicron SiC was increased. The crucibles from Mixes 4 through 7 showed a satisfactory inside surface. Mix 4, which corresponds to the bimodal composition mentioned above, and Mix 5 presented the best compromises with respect to drain qualities versus shrinkage characteristics. For further evaluation MOR strength at room temperature and at 1200°C were measured on four of these mixes.

This interim slip evaluation program was completed by May of
1980 and work was subsequently directed towards individual component
development.

4.2.9.2   Slip Casting

Work on a finalized design (Figure 65) based on Drawing
L3846149 was initiated in June. An aluminum model designed with grind
stock on the three locating tabs and the height was obtained in August
and component fabrication development was initiated during the
following month.
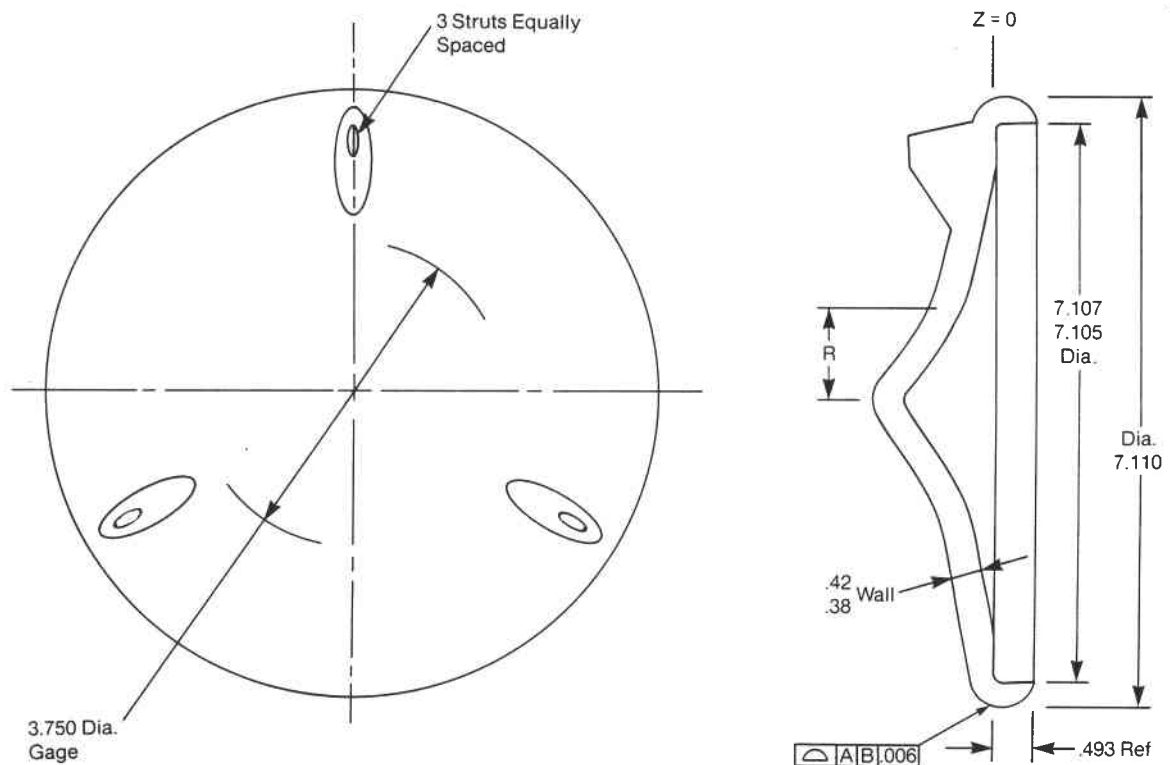
Figure 65. Combustor Baffle Design

The first plaster mold consisted of a one-piece
configuration which produced a cracked part during drying. It was
believed that a constraint at the tripod regions during shrinkage was
responsible for the crack. A second mold was therefore fabricated
with removable plaster sections surrounding the three projections.
After the appropriate drying time, the sections were removed to allow
further shrinkage without constraints. Variables such as casting,
draining, and drying times were investigated.

Attempts were made to cast the components approximately 0.5 inches thick to obtain the desired final wall thickness of 0.40" (nominal) and assure sufficient grind stock for machining the inside platform, which presents a mating surface for the turbine backshroud. Even at this casting thickness depressions opposite the three locating tabs on the outside flow path could not be avoided. This discrepancy from the print was permissible and according to GAPD personnel non critical to the performance of the part.

Development efforts centered on casting and obtaining sintered crack free components using molds with inserts. Additionally it was attempted to obtain an acceptable inside profile to avoid any profile green machining. The slip had the tendency to fill in the cone shaped center portion of the component. This tendency was further promoted and exaggerated because of the thick wall and the increased water retention within the cast wall.

The first crack free components (Figure 66), as determined by X-ray radiography and fluorescent dye penetrant inspection, were obtained in December of 1980. However, the components produced had insufficient grinding stock on the O.D. Consequently, the model was modified and a new mold was produced in January of 1981. Several components were cast, successfully demolded and green machined. Achieving sufficient wall thickness, especially near the outer diameter, remained a problem. Components which had passed early processing steps showed frequently cracks after sintering on the inside of the nose cone.

Slip development and the introduction of a new binder system during the first half of 1981 resulted in the ability to obtain thick walls more consistently. The incorporated changes resulted also in better yields through drying and sintering.

Additional development work during this period addressed difficulties experienced in green machining. New fixtures for machining the internal profile were designed and fabricated. Attempts in green machining the locating tabs to near net shape failed due to the relative low green strength of the parts. Bisque firing was conducted to improve the strength for green machining. In addition, several sintered test components were submitted for grinding to develop a method to grind the profile of the locating tabs.

These machining attempts failed to produce the desired results and indicated the need for a near net shape casting especially with respect to the locating tabs. By November of 1981 it had been decided to obtain a new model and to eliminate a large portion of the earlier machining requirements. The details on the three airfoil shaped tabs and the O.D. radius were incorporated in the new model.
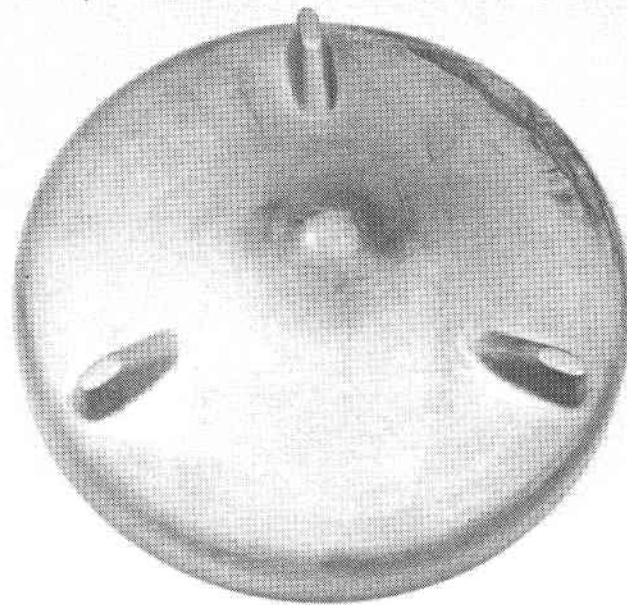
Figure 66. Slip Cast Combustor Baffle with Grind Stock
on Locating Tabs

        The first baffles cast in the new mold design (Figure
67) were processed during December. Four sintered components which
had passed as fired NDE were selected for grinding based on their
dimensional evaluation even though they were somewhat oversized as all
the other baffles because of insufficient densification. The O.D.
radius contour was hand blended between the struts on one of the
ground baffles. The components (2-103 through 2-105) were delivered
to GAPD for review in March, April of 1982. Figure 68 shows an
as-sintered combustor baffle with closely profiled locating tabs.

        The problem of oversized parts was addressed through two
different development paths. One involved compositional variations to
obtain increased shrinkage during sintering and the second involved
fabrication of models using castable mold materials (epoxies) with
increased shrinkage.
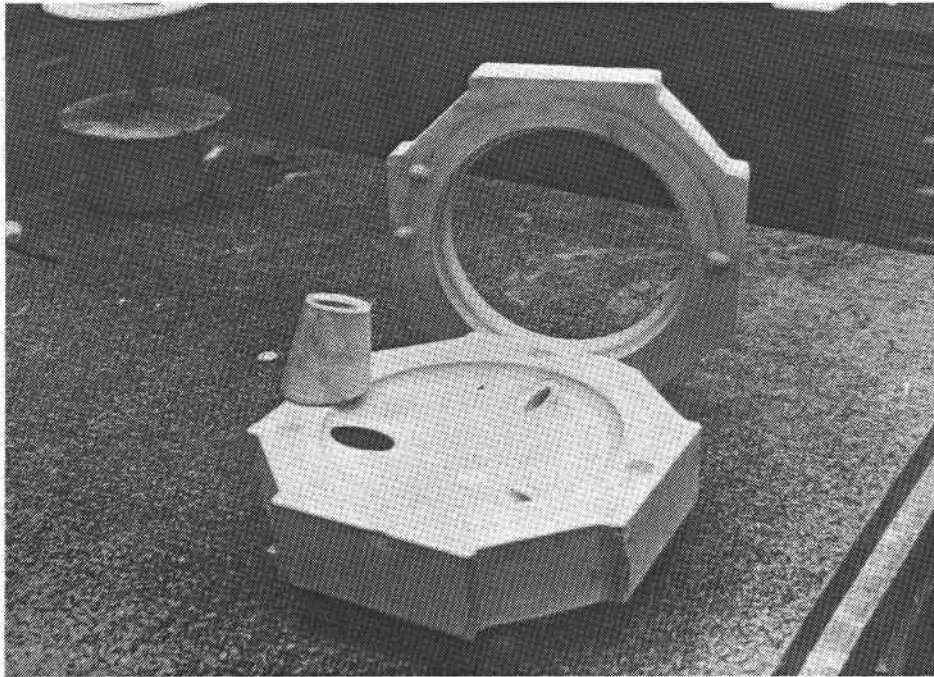
Figure 67.   Plaster Mold
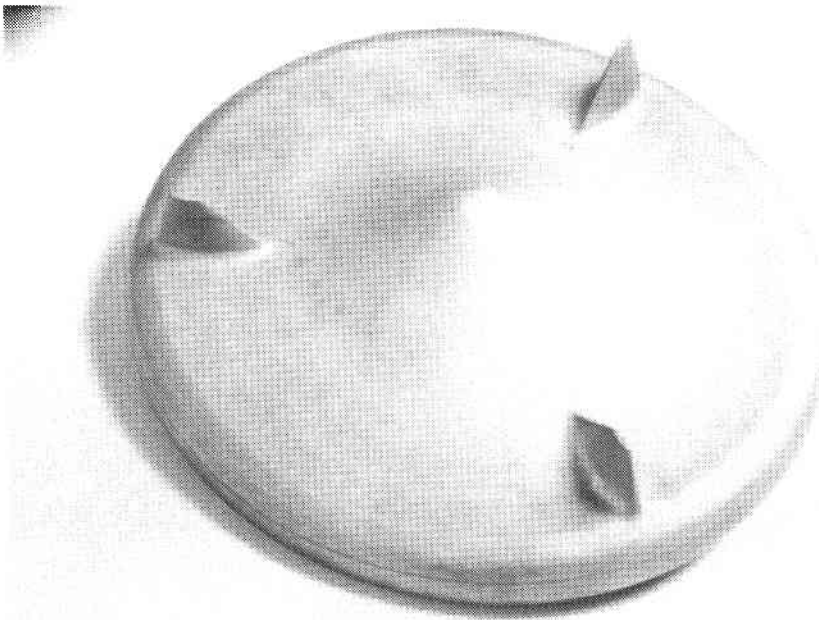
Figure 68. Combustor Baffle with Profiled Locating Tabs

The bimodal compositions with an increased submicron powder to grain ratio initially produced parts which were prone to cracking during green machining or handling. The first acceptable sintered component was obtained in May. This unit was ground, hand finished and inspected together with a second acceptable component. Both parts (2-107 and 2-108) were completed and shipped in August. A third combustor baffle (2-109) made of the same composition was shipped in October. Even though several dimensionally good components were obtained it was found that the process had an unacceptable high variability. Measures to obtain better control about shrinkage and final density on these bimodal cast combustor baffles were not successful.

Combustor baffles made in the smaller molds were processed using the original bimodal composition. However, the shrink factor deviations were over compensated and sintered components were undersize. Sintering cycle modifications were investigated on several cast baffles made in the smaller mold to determine if the desired size could be attained. An optimized sintering cycle was determined yielding components with sufficient stock for grinding. One combustor baffle (2-110) was completed through grinding and shipped in December.

Fabrication development continued in parallel on both casting mixes throughout 1982 and the first half of 1983. No problems were encountered in obtaining the proper wall thicknesses. Some of the baffles exhibited surface flaws after demolding. The main areas of concern were the tab bases and the circumferential seam area. More frequent mold turnover improved the surface quality and the integrity of the tabs on the as cast baffles significantly and a slightly larger radius on the tab bases decreased further the occurrence of linear flaws. Edge chipping and cracking observed during the green machining operation were eliminated through a modified holding fixture and a precleaning step to remove flash acting as stress riser from the seam area. Two as fired baffles (3-111 and 3-112) were supplied in April of 1983. Six other baffles (3-113 through 117) with some dimensional deviations and FPI indications were supplied to GAPD for evaluation the following month.

Casting development was continued until August of 1983 and subsequent finishing of work-in-process was concluded by February of 1984. A total of nine as fired combustor baffles (3-118 through 125 and 4-126) were supplied between June of 1983 and the end of this development program, yielding excellent candidates for engine testing.

Combustor baffle 112, for example, was extensively tested between July of 1983 and October of 1985 in engine tests at 1600^0F and at 2100^0F. It has accumulated over 130 hours of engine test time with 79 hours of continuous operation at cruise speed. Combustor baffle 122 was successfully screened at 2500^0F in October of 1984 and combustor baffle 124 has been tested in 1985 in several engine runs predominantly at 2100^0F prior to damage because of other ceramic hardware failure.

90

4.2.9.3 Plastic Forming

Plastic forming of combustor baffles was initiated in June of 1983. This method was chosen as a means of developing a near net shape forming capability which could replace the drain casting approach and eliminate the time consuming, relative low yield green machining operation which had been necessary to obtain a constant wall thickness.

Initial molding tests were conducted with a converted epoxy mold which had previously been used to fabricate a size reduced casting model. Two plastic compositions with varying plastics content and a grain distribution equivalent to the standard bimodal casting composition were prepared. This composition which sinters to about 90% of theoretical was chosen because of the good test results achieved on cast components. A molding trial was carried out on a vertical plunger machine. However, because of the relatively low strength mold material molding pressures had to be reduced drastically resulting in components with inadequate packing, a large parting line in the seam area, and too much overall thickness.

The components were processed through sintering in an attempt to define the shrink factor for a suitable bimodal plastic composition. Additional shrinkage data were collected on test bars processed in parallel. Room temperature MOR strength of these early compositions exhibited lower values than anticipated (Table 14).

Table 14

Evaluation of Initial Plastic Molding Compositions

Composition	Avg Density	Mean Strength	Weibull Modulus
P-1	2.90 g/cm^3	36 ksi	10.4
P-2	2.66 g/cm^3	28 ksi	9.1

These data together with the observed cracking and blistering of the molded components indicated the need for additional compositional development in parallel with the fabrication development.

A steel mold, designed with the option for conversion to an injection molding tool, was obtained in October of 1983. Molding trials using extruded preforms and reshaping them in the compression molding tool were carried out. The first trial conducted in October indicated the need for an increased radius on the O.D. of the plunger because of similar I.D. cracking pattern on all molded parts. Further minor tool modifications were carried out to incorporate vent holes and improve upon the integrity of the molded parts. At the same time other development work was addressing preform fabrication, integrity, and reheating means to assure reformability. Molding trials were conducted with 3/4" thick extruded preforms and also with stacked 1/4"

thick sheets because evaluation of the extrusion stock had shown significantly increased defect levels with increased thickness.

All compression molding development work was terminated in February of 1984 in favor of converting the tool into an injection molding mode because difficulties with the quality of the preforms and in obtaining a homogeneous elevated temperature throughout the preform just prior to reforming could not be overcome.

4.2.9.4   Injection Molding

The steel mold was reworked during the first quarter of 1984 to incorporate additional injection molding features (Figure 69) and to obtain a design of reduced wall thickness (0.2" versus 0.4"). Molding on a 250 ton horizontal screw machine was initiated in March yielding 32 parts suitable for further processing. New sintering mandrels were fabricated and the first injection molded combustor baffles were sintered in June. The parts showed good surface finish, tab definition, and overall integrity. In addition, the baffles had good densities, and sufficient grind stock on the O.D. but were slightly oversized on the I.D. and showed some distortion on the profile of the hot flow path.
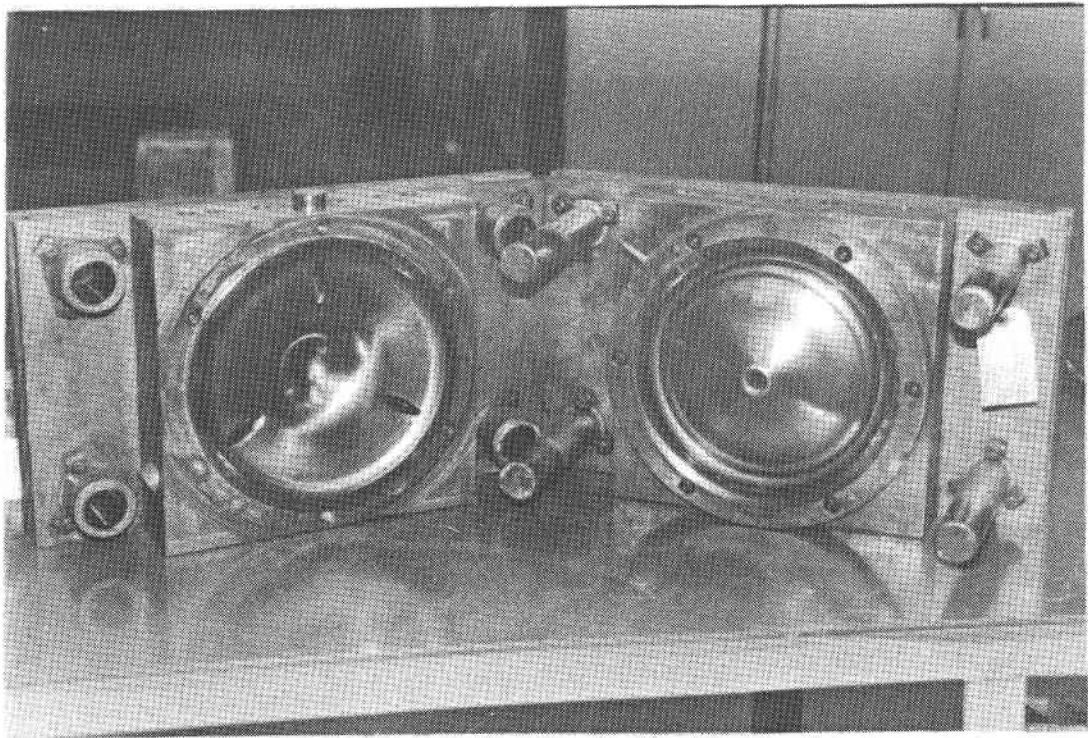
Figure 69.   Injection Molding Tool for Combustor Baffle

Subsequently, the tool was reduced on the I.D. and a new molding trial was conducted in August. Several modifications in the presinter treatment, sintering schedule, and fixturing were investigated. Three different bimodal plastic compositions were used in an attempt to optimize dimensions and have sufficient grind stock for finishing.

Sintered parts, evaluated during the latter part of 1984 and early 1985, showed high variability in dimensions and density (Table 15). The flow profile on some of these components showed circumferential distortion in the vicinity of the locating struts. Several iterations of fixturing mandrels were required to eliminate this problem. One component (5-127) was sent to GAPD for evaluation in the as fired state.

Table 15
Density Variations - Injection Molded Baffles

Composition	Part No.	Density g/cm^3
P2	261	2.77
	270	2.67
	300	2.70
P5	362	2.96
	368	3.03
P6	396	3.02
	397	3.00
	415	2.92

Further investigations into the presinter treatment and sintering conditions indicated that significantly higher densities could be obtained with the P2 composition than shown earlier. Increased consistency and increased density with the optimized conditions was also verified on three sets of MOR bars (Table 16).

Table 16

Bimodal Injection Molded MOR Bars

Compound	No. of Specimens	Density Range (g/cm^3)	RT-MOR (ksi)
P2	23	2.86-2.95	42.77 $\pm$ 6.98
P5	20	2.87-2.94	40.96 $\pm$ 7.35
P6	5	2.92-3.00	43.13 $\pm$ 3.72

The MOR data indicate no significant difference between the three compounds. However, compound P6 exhibits a higher density as a result of increased sintering shrinkage than either P2 or P5 rendering the compound unsuitable for the current mold.

A new drawing (PA3609614) was obtained in April of 1985. It incorporates a variable wall thickness to reduce thermal stresses by having considerable thickness on the backshroud interface and having a relative thin wall in the nose cone to reduce thermal stresses during operation (Figure 70). The configuration of this new design further manifested the need for a reliable advanced forming method with variable wall thickness capability such as injection molding. Figure 71 depicts major steps within the processing sequence used for the combustor baffle.
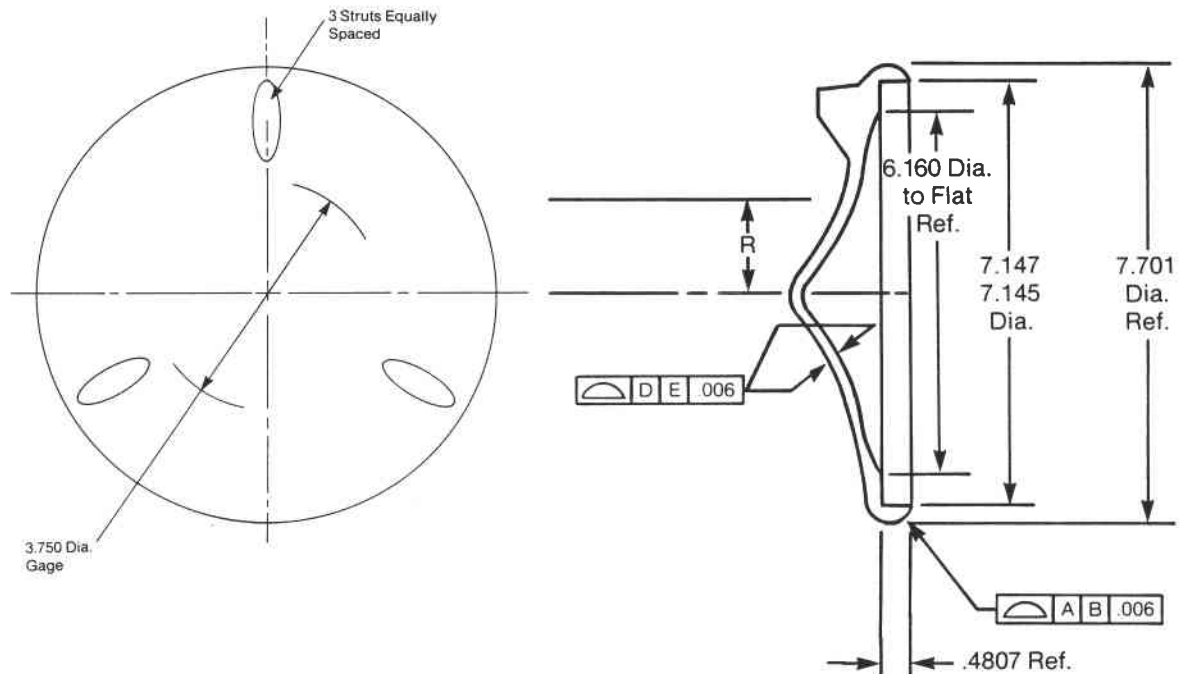
Figure 70. Combustor Baffle Design with
Variable Wall Thickness

The injection molding tool was modified during the second quarter of 1985. A molding trial at a 500 ton machine was conducted at an outside vendor site in August. It followed an inhouse molding trial where it appeared that for the modified tool the clamping pressure (250 ton) was on the borderline for this configuration. Incomplete filling and flow lines were experienced.

Each molded combustor baffle was processed through a sprue removal step in the green state. Difficulties experienced during this step were attributed to the chuck arrangement and also to the process sequence, e.g. before or after binder bake out. The optimized procedure provided for components with sufficient green strength to avoid cracking during handling and machining.
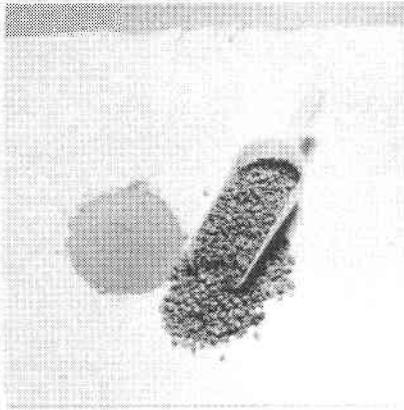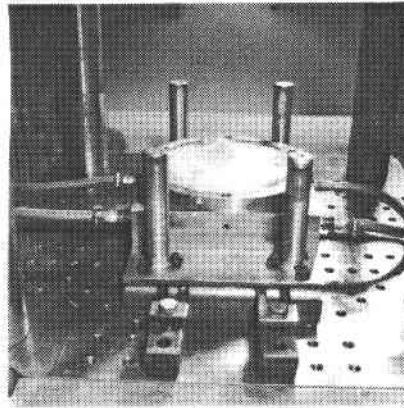
Premix	Injection Molding	Demolding
Trimming	Cleaning	Sintering Furnace
Component	X-ray	Contour Reader
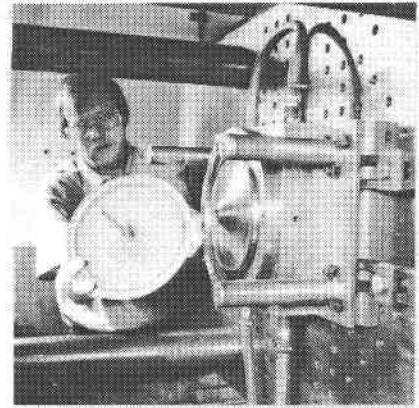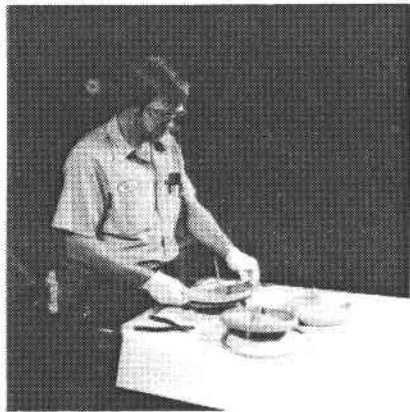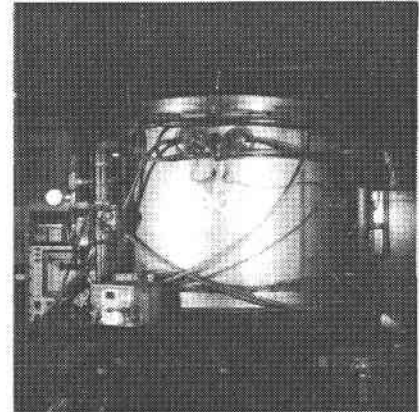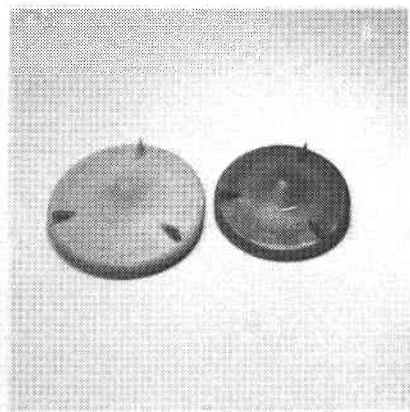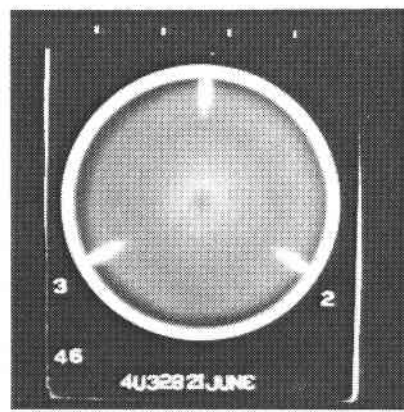
Figure 71. Processing Sequence for the Injection
Molded Combustor Baffle

New contoured internal sintering fixtures were obtained. Initial sintering tests indicated some interference which led to distortion and some minor rework on the O.D. and the radius near the backshroud interface was required. Subsequently, fired components showed good profile consistency. Four as fired components (5-128 through 131) and one ground unit (5-132) were delivered to GAPD during the fourth quarter of 1985.

A new molding trial was conducted in January of 1986. Thirty-nine combustor baffles were molded after satisfactory adjustment of the molding conditions. A group of these components showed cracking predominantly in the nose cone area after binder removal. The program and procedure of this processing step was reevaluated and modified. Additional components were processed successfully. One combustor baffle (6-133) ground to PA3609614-A was shipped in April followed by a second ground component (6-134) in July. A third ground component was rejected in final Q.C. (Figure 72) because of FPI flaws which could not be removed through grinding. No additional work was carried out on this project after October of 1986.
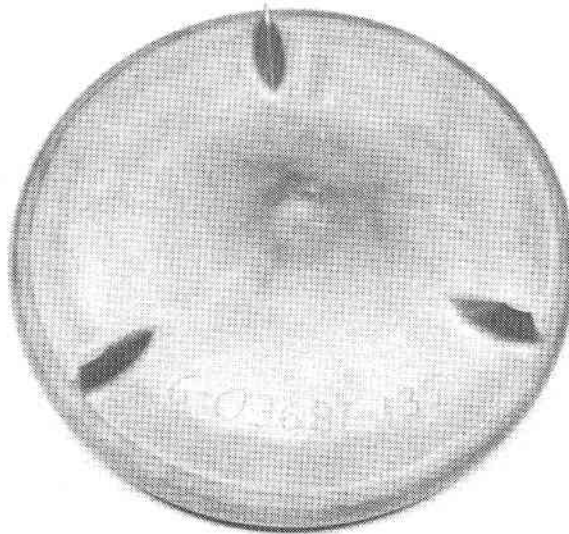
Figure 72. Injection Molded Combustor Baffle

The first injection molded combustor baffle (128) was successfully tested in a rig test at 1800^{0}F in November of 1985 and combustor baffle 132 was qualified at 2300^{0}F in April of 1986. To date, a total of four injection molded components have been qualified for engine tests and no failures have been reported.

4.2.10 Transition Duct

Design discussions on the transition duct were initiated
late 1979. The initial design in Drawing SKP33401 showed thin walls
attached to a thick flange which would pose problems for slip casting,
the preferred fabrication route for this component. An updated
approach, as shown in Figure 73, has an improved design, however, the
variable wall thicknesses were still beyond the slip casting
capability. It was therefore suggested to fabricate this item in two
pieces which are subsequently joined by brazing.
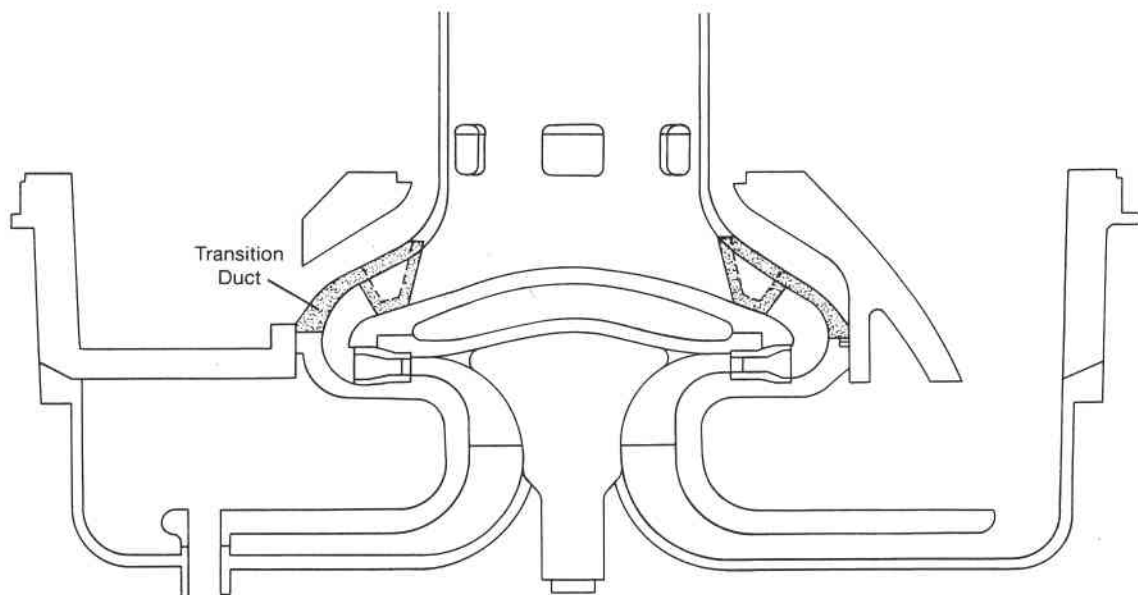
Figure 73. Early Transition Duct Design

Revised drawings (L3846119 and L3846159) were obtained in
January and in March of 1980, latter reflecting essentially a
component (Figure 74) of constant wall thickness with three locating
tabs on the combustor baffle interface. Slip casting was initially
pursued for fabrication development together with final grinding to
incorporate interface details.
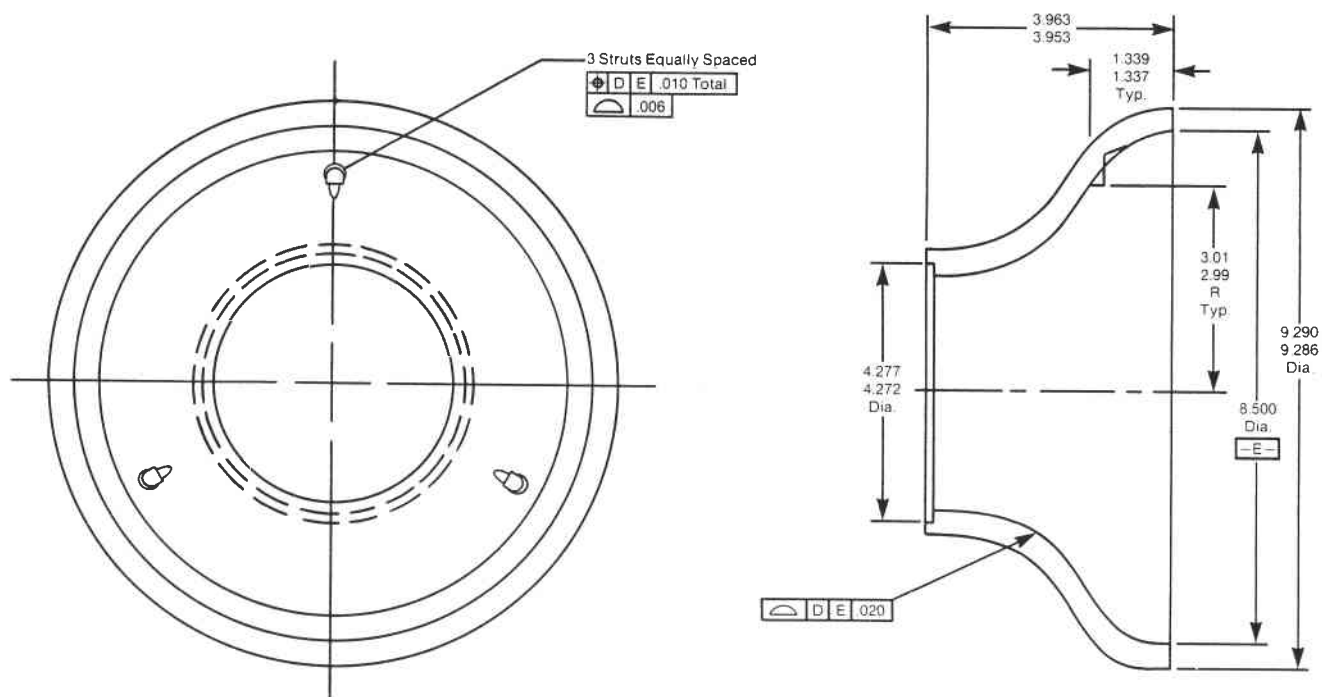
Figure 74. Transition Duct Design with Individual Locating Tabs

4.2.10.1 Slip Casting

Casting formulation development work, as described under 4.2.9.1, was carried out during the first half of 1980 in preparation of focussed component development which was initiated for the transition duct in June of 1980. The model was received in September and a single piece plaster mold was fabricated. The first articles were cast during the same month. Initial parts were cast without the three locating tabs on the inside profile. A special casting fixture was designed in October to allow for casting in place the three tabs. The tabs are thereby attached to the inside surface of the transition duct after the main contour has been cast and drained but before the component is demolded and dried.

Cracks which frequently developed in the interface between the main body and the attached tabs and obtaining a constant thick wall were the main areas of concern. Due to the casting direction, which is dictated essentially by the transition duct design itself, a relative thin casting was obtained on the large I.D. and a thick casting on the small I.D., as depicted in Figure 75.

98
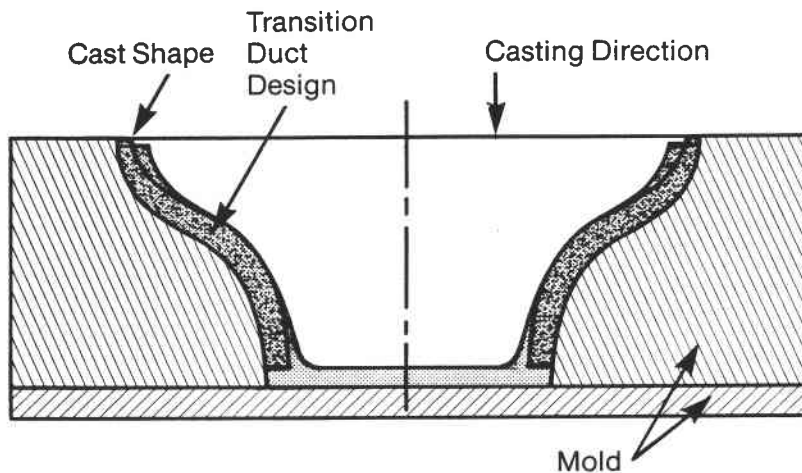
Figure 75. Slip Casting Schematic

Development work on the slip cast transition duct continued through the first quarter of 1980. The problems with respect to the wall thickness could not be resolved within that time period and it was decided to use the isopressing/green machining approach for fabricating transition ducts with the desired details. Initially this method was considered the alternate fabrication method because of its high material usage and extensive green machining time.

4.2.10.2 Isopressing/Green Machining

Green machining of isopressed thick walled tube stock was initiated in February of 1980. Special isopressing bags and pins, green machining templates and sintering fixtures were procured within the following two months. Billets with about a 17" outer diameter and a 4" inner diameter were isopressed starting in April. Each of these billets consumed roughly 120 pounds of spray dried alpha silicon carbide material.

The isopressed billets were first rough cut to approximate size, then, using templates on a tracking attachment to the lathe, the I.D. and O.D. profiles were green machined incorporating a predetermined shrink factor. Individual tabs were also green machined from the same material and a ceramic to ceramic bonding technique was employed to attach the three protruding tabs to the I.D. after the tabs as well as the main transition duct body had been sintered. Subsequent dye penetrant inspection of the first assembly revealed several small cracks at the joints. Additional dimensional assessment indicated that the flow profile had been machined incorrectly.

Since new templates had to be prepared, it was decided in
June of 1980 to form the projections by isopressing onto a suitably
contoured mandrel. The first four pressings resulted in wall cracks
during removal from the mandrel. The first good blank obtained in
July was green machined and sintered in August and ground in
September. The unit was rejected in final Q.C. because of excessive
chipping in grinding.

Process development using the contoured isopressing pin
continued throughout the second half of 1980. Progress was slowed
because of tooling failure and deformation of the aluminum pin. Green
machining advances were realized starting in December of 1981 when a
CNC lathe became available for machining the I.D./O.D. profiles.
Stock was allowed for milling of the tab details. Two units, one
ground as shown in Figure 76, the other as fired were completed with
some dimensional deviations in January. Both components (101 and 102)
were supplied to GAPD for evaluation.
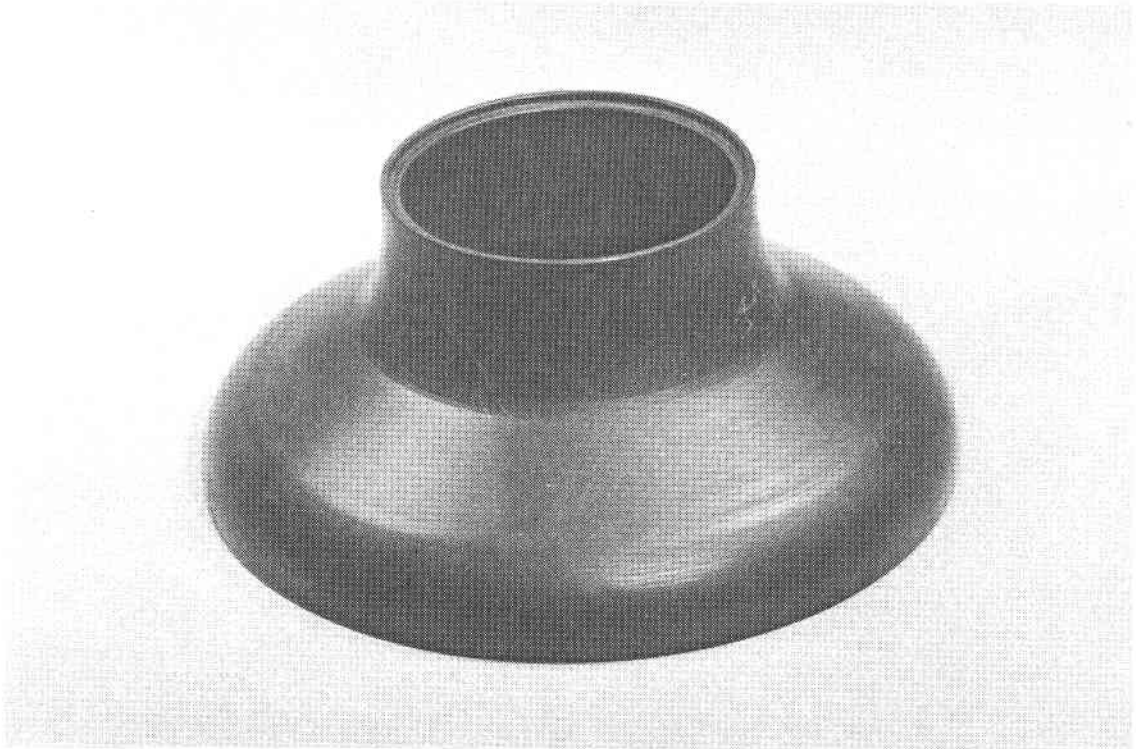
Figure 76. Ground Isopressed Transition Duct

Design discussions between GAPD and Standard Oil with
respect to machining difficulties of the individual locating tabs on
the inner profile resulted in a modified print (Drawing 3846232) with
a continuous inside platform to replace the tab details and an outer
contour change to provide for wall thickness uniformity as illustrated
in Figure 77.

100
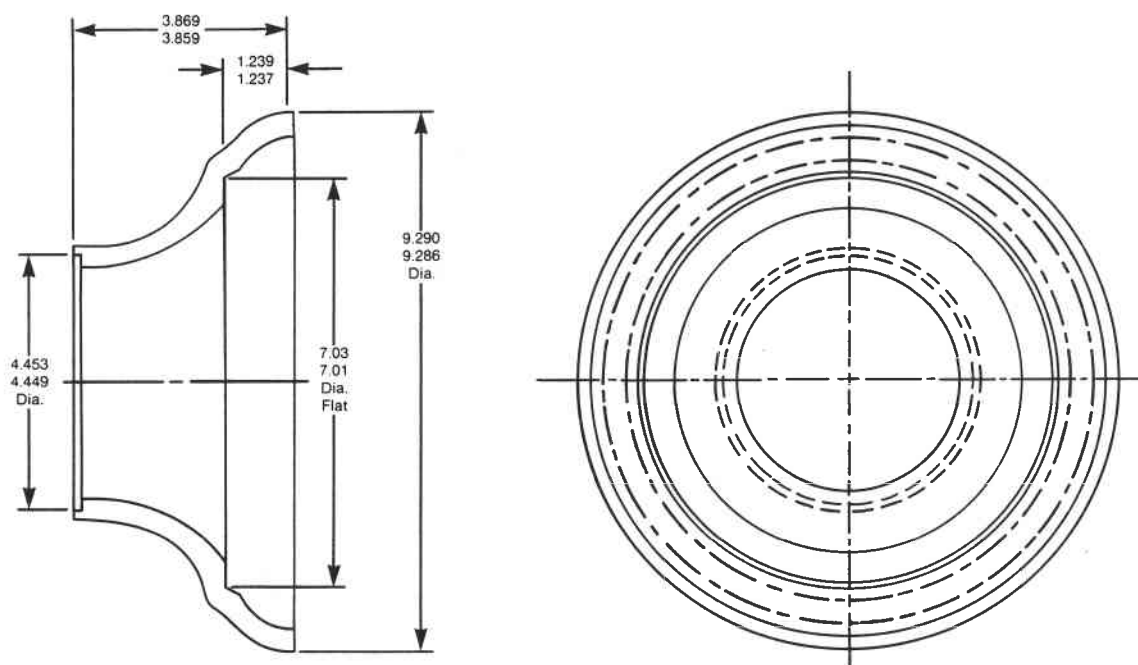
Figure 77. Transition Duct Design with Locating Platform

Seven ground transition ducts (104, 105 and 107 through 111) and one as fired component (106) were supplied to GAPD during a five months time period from April to August completing FY 1982 requirements. These components were fabricated according to the modified print using standardized procedures. No major fabrication difficulties became apparent during this time period and high component yield was realized in each processing step.

Development work on FY 1983 requirements was initiated in February of 1983. Progress on part fabrication was slowed because of cracks in the isopressed billets and because of failure of the isopress tooling.

Additional minor grinding changes were incorporated as soon as it became feasible. The first ground transition duct (3-112) with reduced stacking clearance towards the combustor baffle was delivered in August. Two additional components (3-113, 114) with the same design features were delivered the following month.

Stock added on the height on the turbine shroud interface was incorporated on the following delivery of a ground component (3-115) in November of that year and two additional deliveries (4-116, 117) in March and April of 1984.

Meetings held between GAPD and Standard Oil indicated the necessity of the introduction of thermocouples for monitoring purposes during testing. Previously supplied transition ducts had been reworked by GAPD and three tube inserts had been machined for each transition duct for close tolerances to minimize leakage during operation.

Two new designs were received in March of 1984 consisting of Drawing PA3609649, simplified shown in Figure 78, and Drawing PA3610213 (Figure 79). The latter represents an ideal advanced configuration with its integral thermocouple port design for reduced leakage and improved flow and its 180° air flow diverter for more symmetrical flow distribution of air exiting the flow separator housing. Drawing PA3609649 on the other hand with its attached ports represents a compromise design with respect to functionality and fabricability.
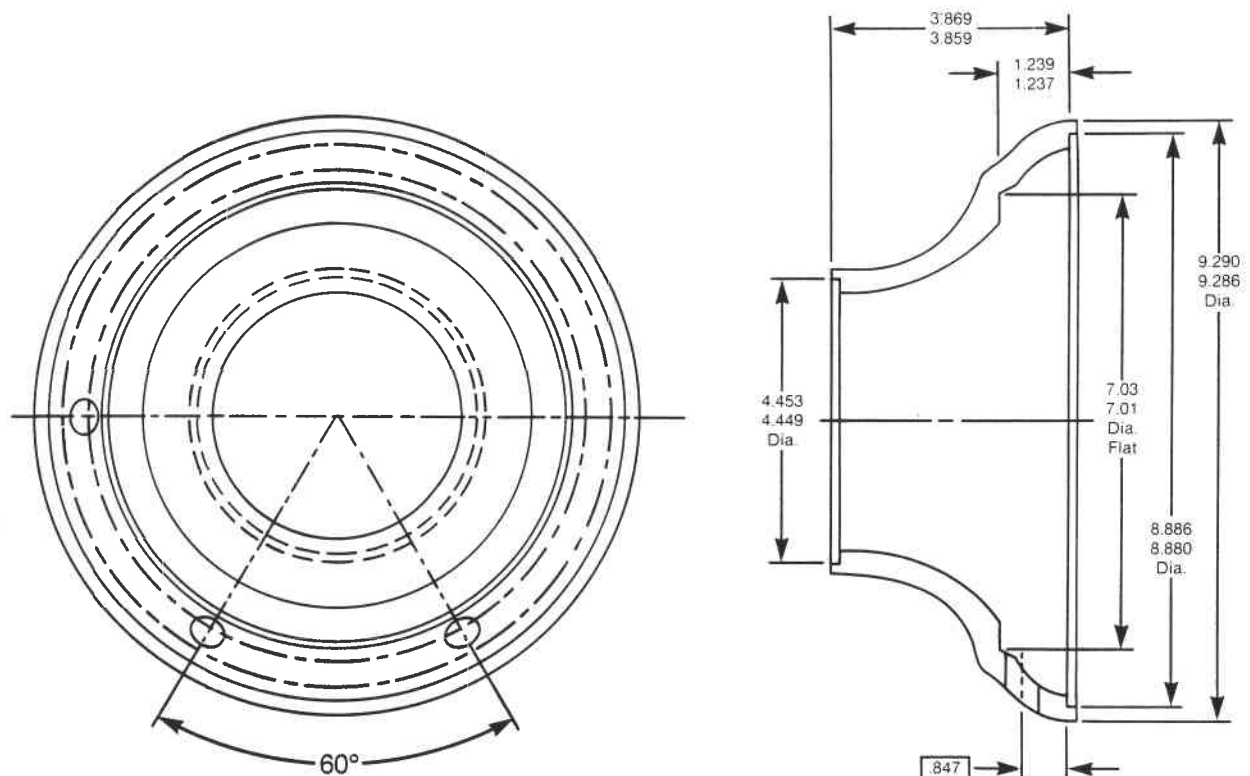
Figure 78. Transition Duct Design with Thermocouple Holes
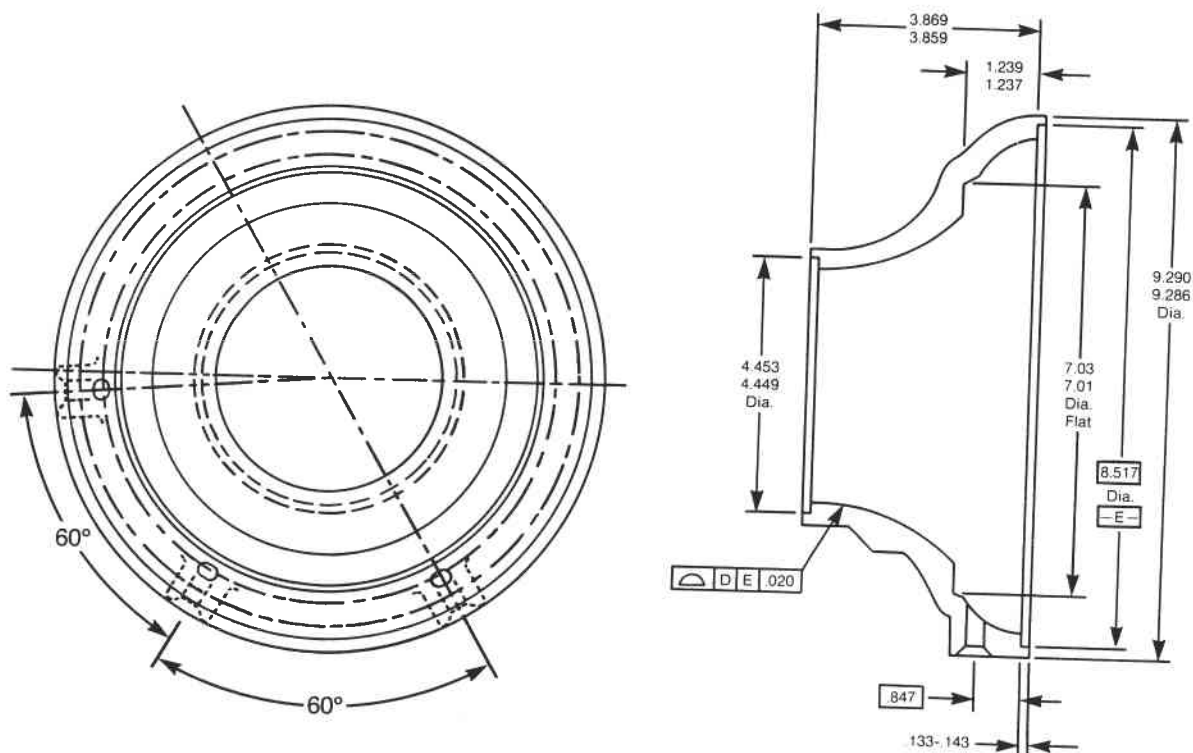
Figure 79. Integral Transition Duct Design

Work on the less advanced design was initiated in March and development work addressing issues of shrinkfit and/or brazing of the thermocouple port inserts was conducted during the following 18 months. A shrinkfit approach which was thought to deliver the quickest and best results was investigated first.

Several trials with tubular sections made from the same powder lots as transition duct bodies and inserts as to be used for the final transition duct assembly were fabricated and joined. Materials with sufficient shrinkfactor difference to form a close interference fit without introducing cracks and green machined to close predetermined tolerances were subsequently selected for shrinkfit trials with transition duct bodies. The first unit assembled with green inserts was sintered in June. It was of acceptable visual quality but revealed slight leakage at one of the tube joints when air pressure tested at 5 psi. Subsequently the unit (Figure 80) was subjected to a brazing operation during a second furnace operation. The brazing was successful in sealing the joint and the unit (4-118) was delivered to GAPD in October of 1984 after grinding and NDE.

Figure 80. Transition Duct with Shrinkfit Thermocouple Ports

Shrinkfactor deviations and brazing difficulties during the fourth quarter of 1984 rendered two additional units non-usable and a third shrinkfit/brazed unit broke during grinding set-up. In addition, in depth investigations of the flow profile using an optical pyrometer was conducted during the first quarter of 1985 on the various surfaces in relation to the inside and outside profiles. It could be shown that the contours on part 4-118 and 4-119, a second completely ground part, were very close to the tolerance limits when considered independently of other height dimensions. However, in order to obtain correct stacking dimensions, it had been necessary to move the contour outside its tolerance band. Subsequently, the CNC programs were revised to allow for additional grinding stock on the inside platform as well as the turbine shroud interface.

During grinding it had been found that the shrinkfit ports showed some misalignment. Steps were therefore undertaken to use a graphite locating fixture during the following sintering trials. The fixture was marginal effective and reevaluation of the shrinkfit approach indicated the need for an improved attachment method. Joining with a $MoSi_2$ braze and using closely machined interfaces was considered the preferred approach.

Development work carried out during the first nine months of 1985 resulted in the delivery of four ground transition ducts (5-120 through 123) with brazed port inserts in October. Only minor leakage at 2 psi air pressure was observed. Testing conducted at GAPD on three of these four components indicated failure at low stress levels. Further analyses indicated cracks originated near or directly from the brazed joints. Additional test bar work conducted on MOR bars with a thin layer of braze applied showed a reduction in flexure strength of up to about 50%. It was therefore concluded that interfacial stresses caused the failures of the components. One unit (5-122) with brazed ports was returned from GAPD and reworked with loose fitting ports.

During 1985 work had also been initiated on obtaining the integrated advanced design by using more sophisticated green machining programs to first generate the 180° diverter and then second to machine the integrated ports as shown on Drawing PA3610213. A transition duct (4-124) consisting of a hybrid design with loose fitting port inserts and a diverter (Figure 81) was completed in February of 1986.
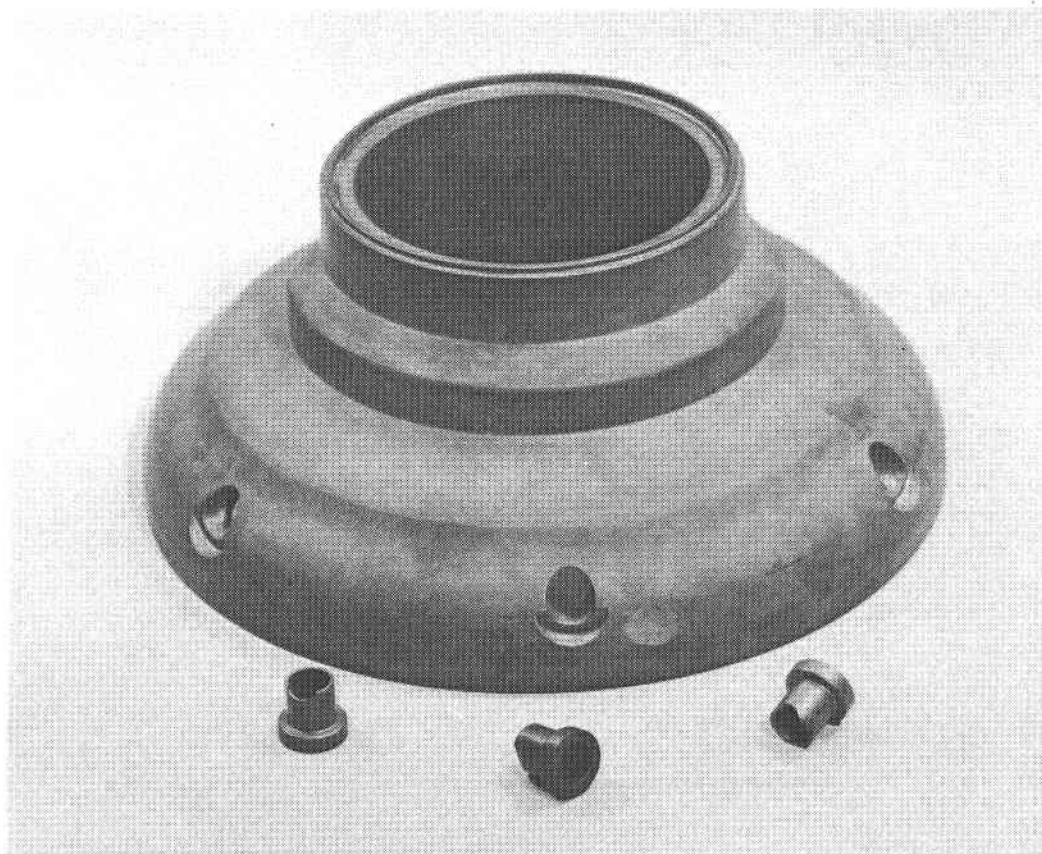
Figure 81. Transition Duct with Diverter and Loose Fitting Ports

The first ground transition duct (6-125) having all integral features (Figure 82) was delivered to GAPD in May. Extensive CNC green machining using a lathe and a mill is required to generate these non symmetrical features on isopressed blanks. All subsequent component work concentrated on the integral design and development work on shrinkfit and brazing was discontinued. Shipments during the remainder of 1986 and the first half of 1987 consisted of four non machined transition ducts (6-127, 128 and 131, 132) and three ground components (6-127 and 7-133, 134).
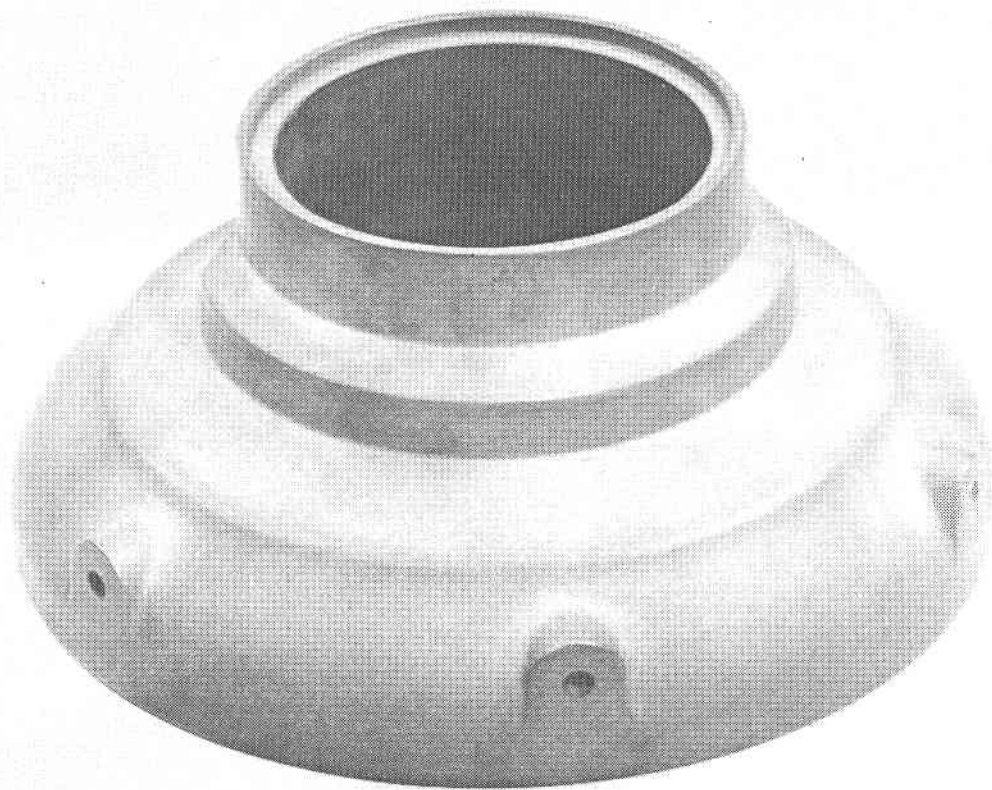
Figure 82. Integral Transition Duct

Work on an improved isopressing procedure was initiated late in 1986. A shaped isopressing bag and pin for increased powder yield per blank and reduced green machining time were designed and fabricated. The first pressing trials were conducted in March of 1987 and resulted in blanks with I.D. circumferential cracks as shown in Figure 83.
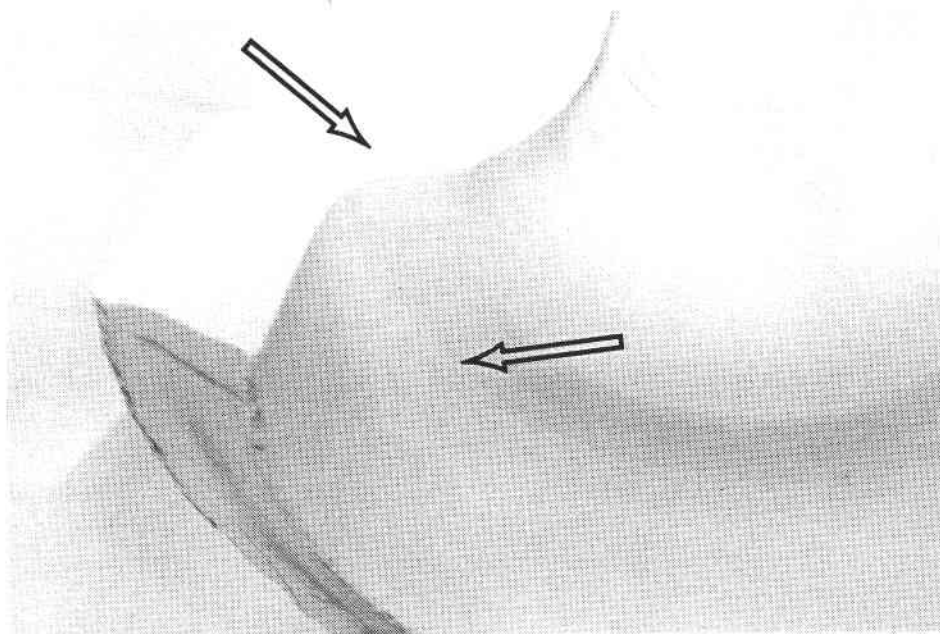
Figure 83. Isopressed Shaped Blank

Several minor tool and set-up modifications were required to eliminate cracking. The first crack free blank was obtained in May and several additional units were fabricated in June and July. Progress on the contoured blank eliminated the need for the large straight blanks saving thereby about two-thirds of the initially required amount of spray dried material. In comparison, the contoured blanks require about 35 pounds of material while the straight blanks require about 120 pounds.

Additional isopressed and machined components are being processed under the AGT extension to fulfill FY 1987 shipping requirements of four components.

With the exception of the brazed components, sintered alpha silicon carbide transition ducts have performed well in rig and engine testing. Component 109, for example, has successfully accumulated in a test rig 25 hours at 2500°F and component 111 has been subjected to 10 cycles at 2100°F within an engine test. In addition, component 6-125 accumulated almost 100 hours of engine test time at 2200°F prior to being damaged during a major engine failure.

4.2.10.3 Injection Molding

Development of injection molding as a near net shape forming method for the transition duct had been discussed since the integral design was introduced in March of 1984. Injection molding development was subsequently started at the beginning of FY 1985 and the injection molding tool (Figure 84) was received at the end of the first quarter. Minor revisions with respect to corners, fillet radii, and size of sprue bushing were incorporated after a nylon replica had been molded using a 700 ton machine.
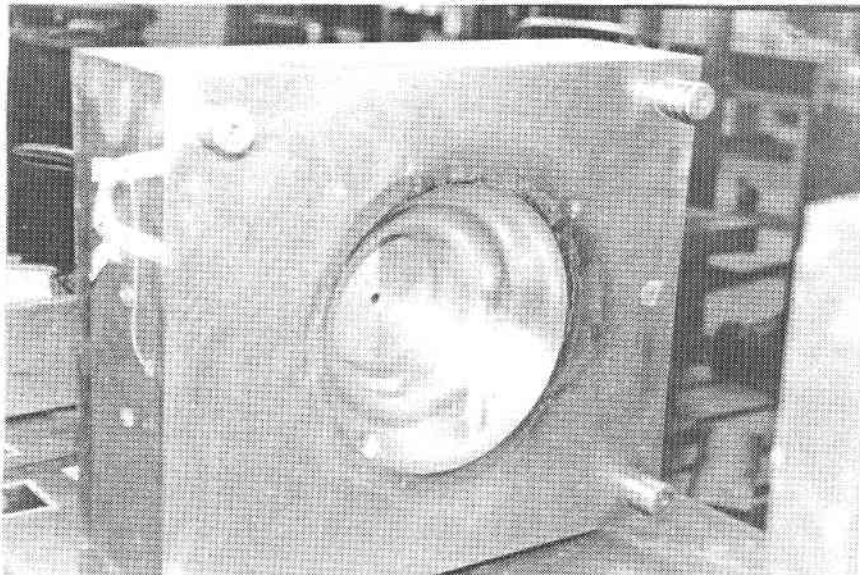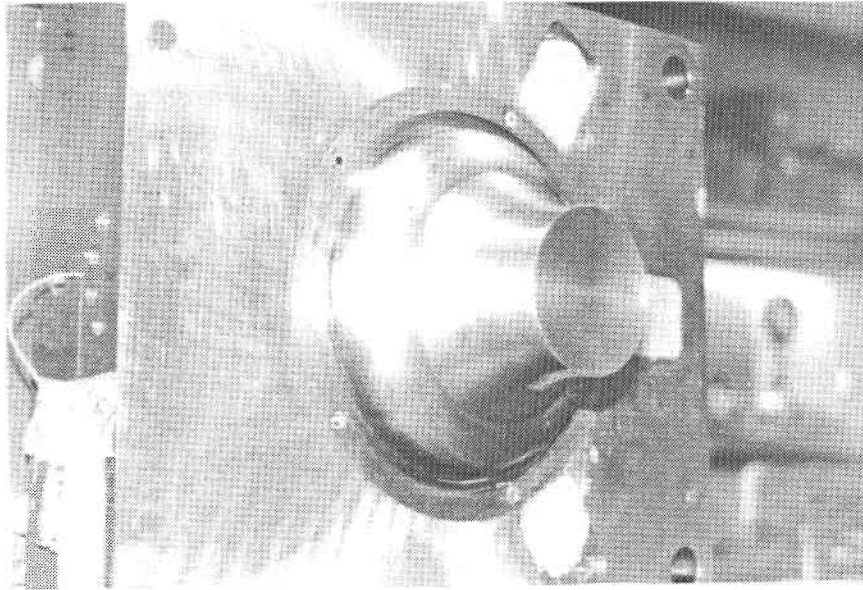
Figure 84. Injection Molding Tool for Transition Duct

The mold was designed with removal inserts for forming of the thermocouple ports. These inserts allowed for molding transition ducts with or without holes within the thermocouple port bosses. Latter was thought as a precautionary measure because of the possibility of weld lines formed below these holes giving rise to defects.

An extended molding run over a two day period conducted in May yielded 35 transition ducts with port holes and 22 without port holes. Several of these components were processed during June through September through sintering and as fired NDE.

Dimensional evaluation indicated insufficient shrinkage was obtained even though the components had achieved densities up to 3.17 g/cm^3. A detailed reexamination of the shrinkfactors was conducted indicating the need for a tool revision to obtain sufficient stock on ground dimensions and to achieve as fired tolerances as required on the contoured profiles. Additionally, it was found that in some cases the weld lines below the port holes (Figure 85) contained defects as detected by dye penetrant inspection.
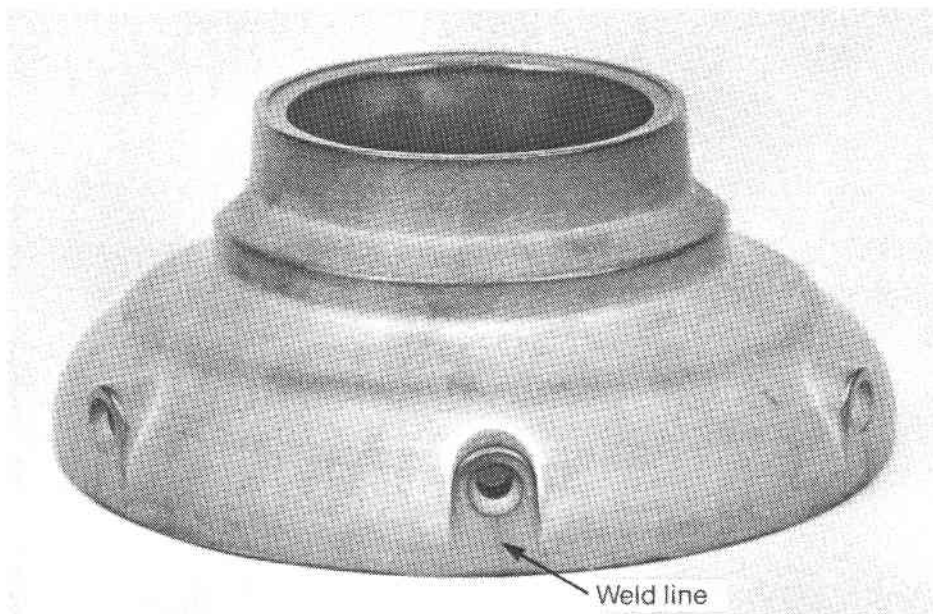
Figure 85. Injection Molded Transition Duct

The injection molding tool was revised at the end of 1985 using shrink factors which showed some variation with direction. A molding run on a 1000 ton horizontal screw machine was conducted at an outside vendor yielding 79 components. All units were molded with solid thermocouple bosses to eliminate the weld lines that had previously occurred.

An initial group of 20 transition ducts was designated for evaluation and optimization of the binder removal and the presinter treatment procedures. In addition, it was planned to process some of these parts through sintering and conduct in depth dimensional analysis even though this lot consisted of components which were produced early during the molding trial when the packing pressure and the ejection mechanism had not been optimized. Unexpected difficulties were experienced during binder removal. Over 50% of the components exhibited cracks after bake out. The majority of rejects were located in one specific bake oven. Additional investigations were conducted and it was concluded that the standard loading procedure was inadequate. Special measures had to be implemented to allow for sufficient support of the components during binder bake out and to accommodate the thermal expansion/contraction movement during the bake cycle.

Following the binder removal procedure the components were subjected to a presinter preparation. Units exhibited an unusual amount of fragility and susceptibility to blow outs. Steps were implemented to modify the cycle and an additional group of 20 transition ducts was processed using the revised procedure.

These transition ducts showed after sintering some flow lines which held dye penetrant fluid and cracks in the push-out pin locations. Otherwise the units exhibited good densities and showed good consistency on the flow profile. Evaluation of the stacking dimensions showed that only marginal stock was present on these initial components.

Evaluation of several sintered transition ducts revealed X-ray defects in the vicinity of the platform. Figure 86 represents a close-up picture of one of the units, showing defects after firing which appear to be a result of insufficient green density in localized areas. Green density measurements on sectioned components indicated variations of up to 0.03 g/cm^3 (Figure 87), however, no defects could be detected on green components destructively by slicing select components or nondestructively by using microfocus X-ray.

Units molded towards the end of the molding run exhibited improved green density consistency. This quality improvement was attributed to optimized molding parameters and better packing. The internal cracking problem observed on the earlier molded components was no longer apparent. Two injection molded as fired units (6-129, 130) were supplied to GAPD for progress evaluation in September and October respectively.

The injection molding tool was revised in November to allow for additional stock on the height dimensions and to change the push-out mechanism from individual pins at the inner platform to a full size ring at the large diameter end. The radius on the inner platform was enlargened for improved material flow and to minimize the probability of having processing related defects in this high stressed area.

110
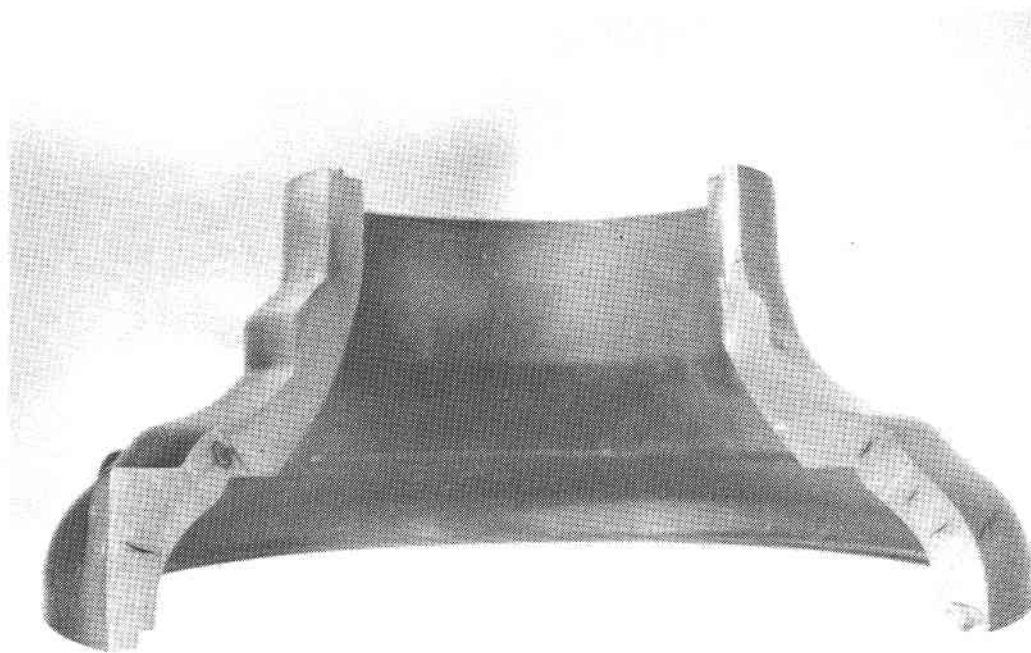
Figure 86. Defects in Sintered Transition Duct
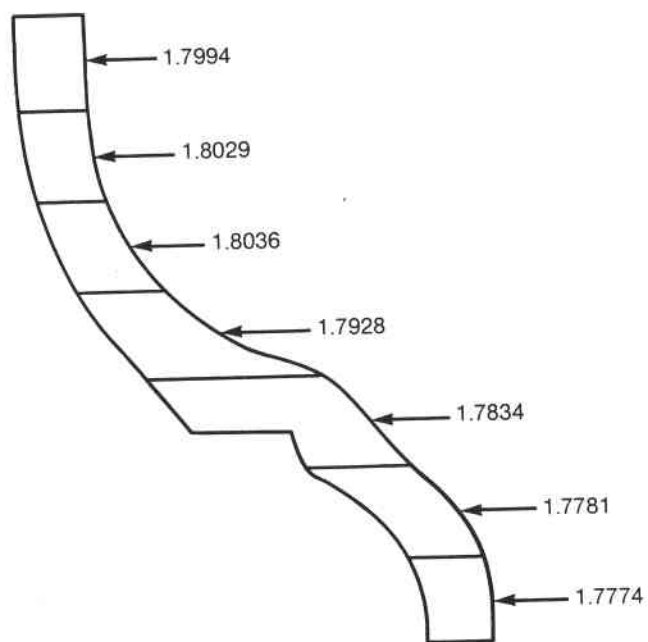
Figure 87. Green Density Determination Through Sectioning

An injection molding trial was conducted at a custom molder site in December. A 700 ton horizontal screw machine with a 110 ounce shot size (equivalent to about 2900 cm^3) was used and the molding parameters were adjusted to obtain maximum green density without excessive flashing. The molding run was conducted with two molding compounds (SX-05 and SX-09) and yielded 68 parts (Figure 88) suitable for further processing.
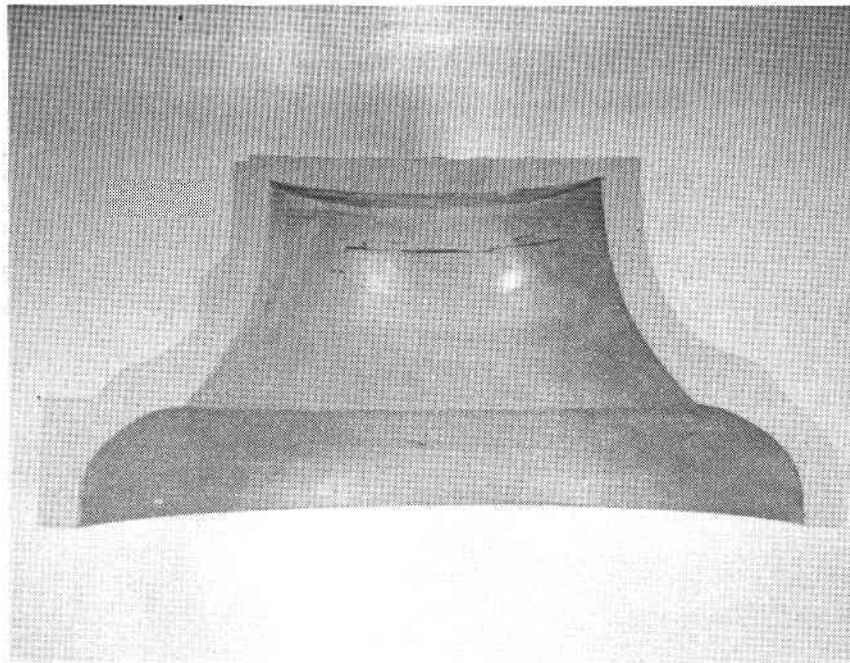
Figure 88. Cross Section of As Molded Transition Duct

Components from this last molding run have been processed during the first half of 1987, most show flow lines after sintering. One NDE acceptable component was ground to specifications but revealed cracks within the wall on the small diameter end. Additional transition ducts from this lot will be processed under the AGT extension during the third quarter of 1987. The following Table 17 summarizes all transition duct deliveries, isopressed as well as injection molded.

112

Table 17

Transition Duct - Component Deliveries

FY

	1980	1981	1982	1983	1984	1985	1986	1987
Dec.								
Jan.			2					
Feb.							1/1*	1
March					1			
April			2		1	2		1
May			3				1	
June							1	1
July			2				1	
Aug.			2	1			1	
Sept.				2			1**	
Oct.				1	1	4	1/1**	
Nov.								

*Reworked

**Injection Molded

113

4.2.11   Wave Springs

The ceramic wave springs used in all engine tests to date have been fabricated of Si_3N_4 materials. However, at a test temperature of 2500^0F, some of the wave springs have shown unacceptable plastic yield. Garrett has therefore redesigned three wave spring configurations to take in account the different material properties of the SiC material. Figure 89 shows their location within the engine.
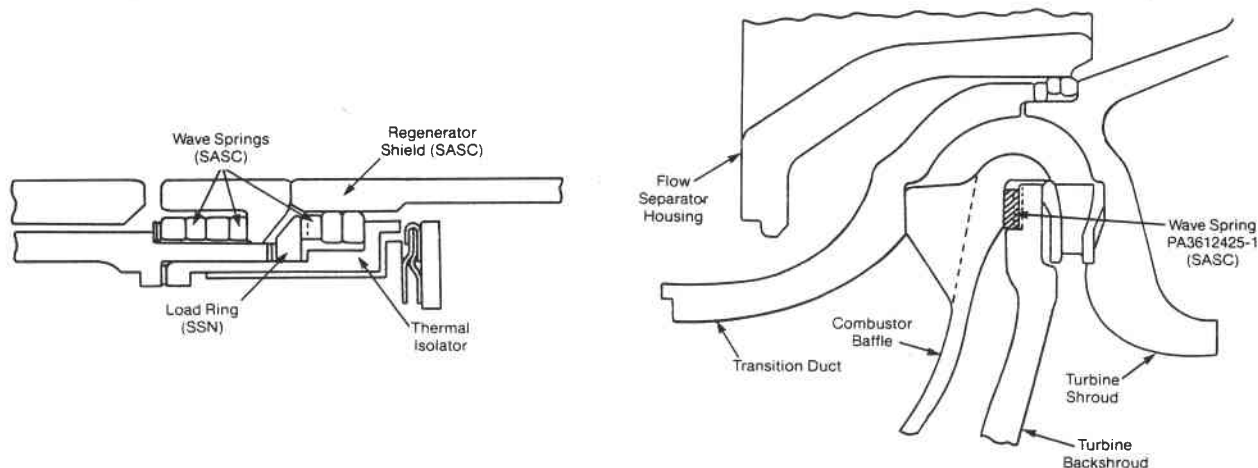
Figure 89.   Location of Wave Springs

        Drawings for three different wave spring designs, as shown in Figure 90, were obtained in January of 1987 for the fabrication of sintered alpha silicon carbide parts. Based on the tolerances required it was decided to use isopressed tube stock and green machine it into flat rings allowing for grind stock on all surfaces. A grinding methodology was devised which took into account drawing requirements as well as the capability of inhouse equipment.

        Isopressing of the tube blanks was initiated in February and new attachments for grinding the sinusoidal wave forms were designed and fabricated. The first sintered rings became available for O.D./I.D. grinding in May and wave grinding was started in June, 1987.

        Figure 91 shows two completely ground wave springs. Grinding completion is scheduled for August under the AGT extension.

114
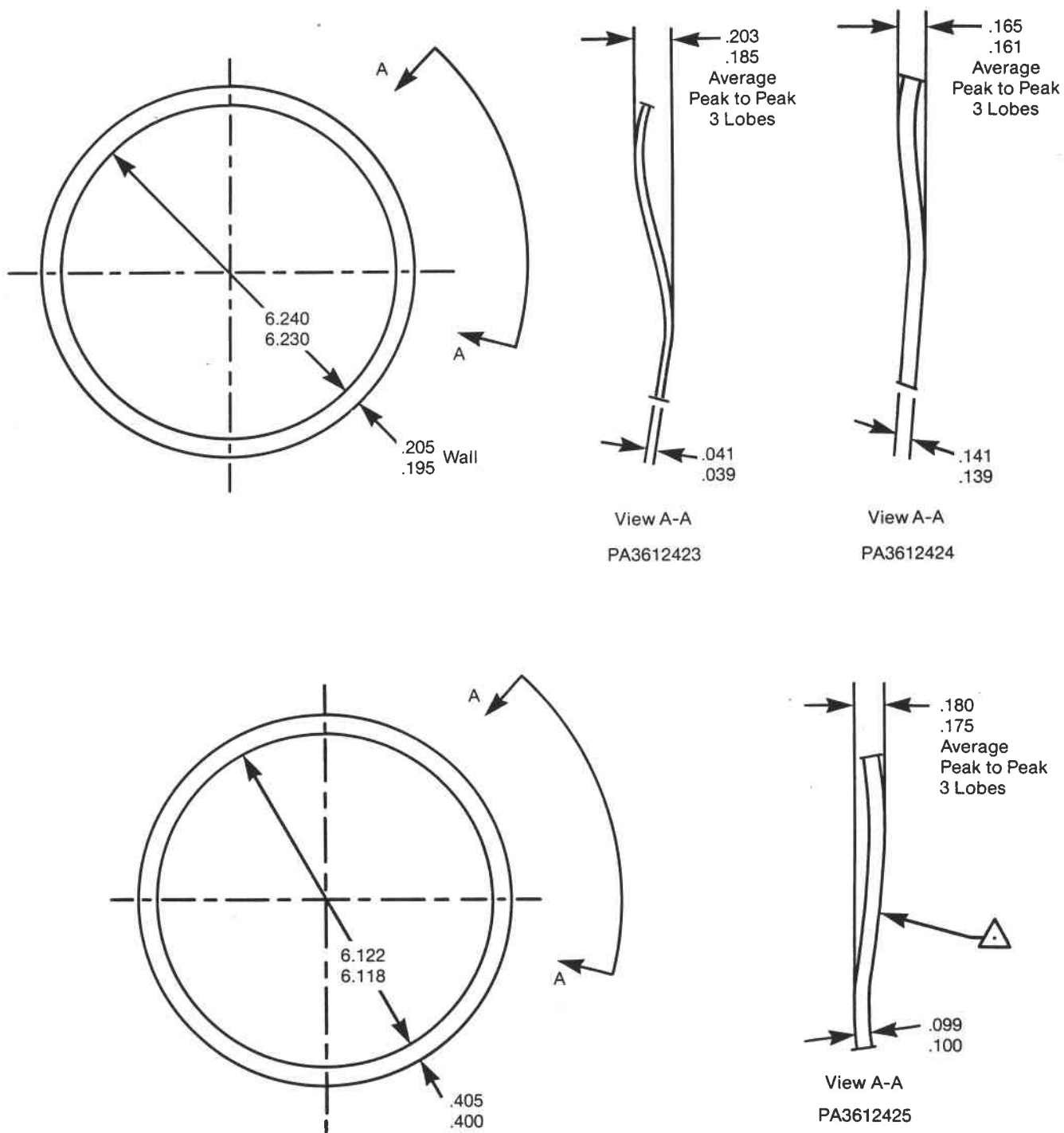
Figure 90. Wave Spring Designs
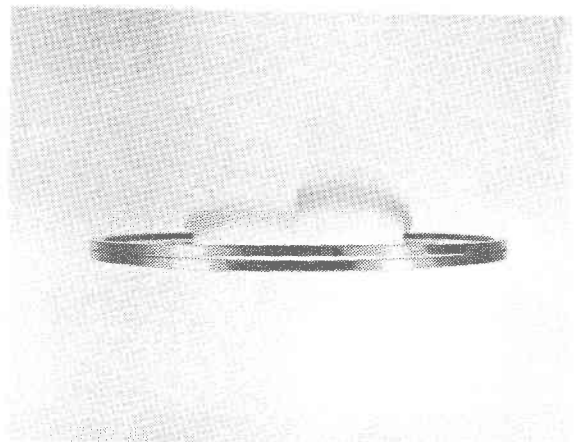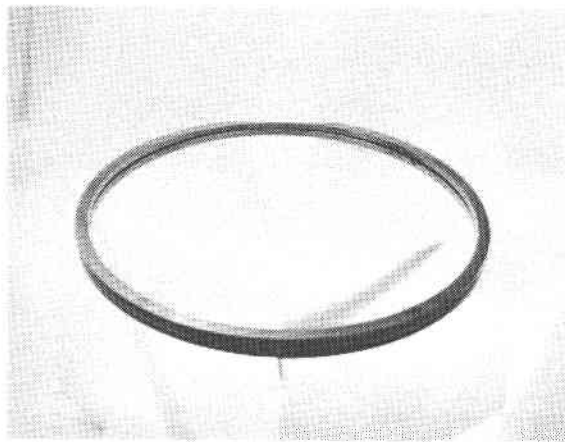
Figure 91. Ground Wave Springs
(Design PA3612424)

5.0   Conclusion

Standard Oil has developed fabrication processes for several hot flow path components of the AGT 101 program. Figure 92 shows the ceramic components which have been supplied to GAPD for testing and Figure 93 identifies the location of these components within the engine and in addition it also depicts components, such as the turbine rotor and the inner and outer diffuser, which were included in the work scope for only a limited time, early in the program, without resulting in components suitable for testing.

Figure 92. Sintered Alpha Silicon Carbide
AGT 101 Components
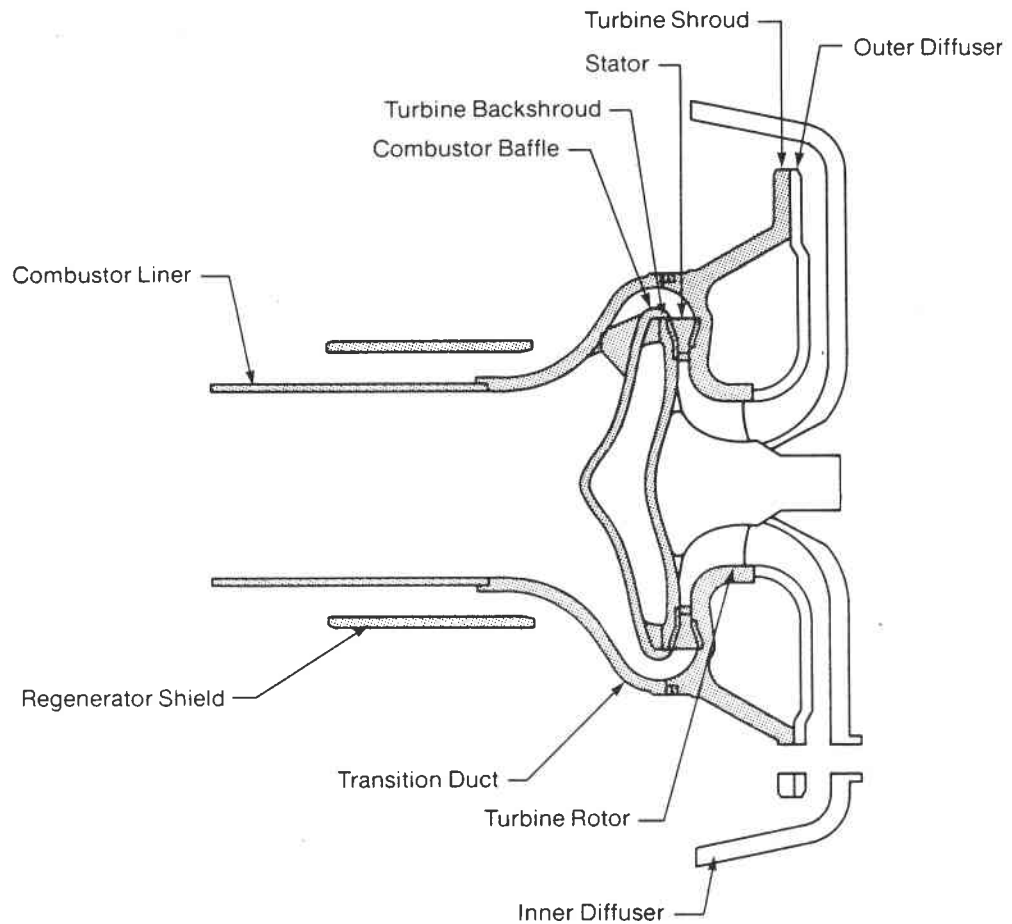
Figure 93. Hot Flow Path Components

Standard Oil's accomplishments with respect to ceramic component development within the AGT 101 program can be summarized in five key areas:

o   Establishment of a design/fabrication interface
o   Iterative component development
o   Near net shape fabrication of large and/or complex shapes
o   Material properties duplicated in some of the fabricated components
o   Availability of hardware for engine testing

Design/Fabrication Interface

Direct one-on-one interaction of engineers of the required disciplines from GAPD and Standard Oil resulted in components with fabrication and assembly advantages without reduced performance in the engine. One of these components which benefitted from this close interface is the transition duct, as shown in Figure 5.3. The design modification from initially three locating tabs requiring either a separate joining step or complicated hand machining to one continuous ring which is incorporated through a routine lathe machining operation represents only one of the changes successfully implemented within the AGT 101 program.
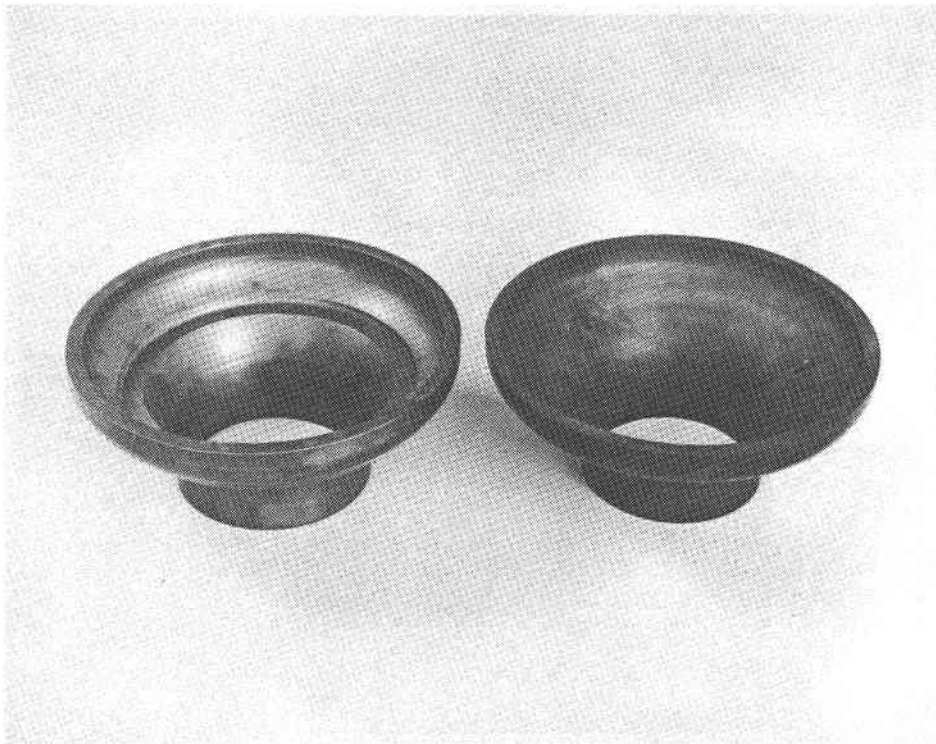
Figure 94. Transition Duct - Fabrication
Induced Design Change

Iterative Component Development

Engine development carried out by GAPD to reduce leakage, improve temperature capability, and optimize ceramic component interfaces to improve overall performance resulted in several design modifications of the individual ceramic components. In some cases these changes could be accommodated very easily during final grinding

or through a revised green machining procedure. In other instances, however, a new forming process or CNC green machining had to be developed to produce components to satisfy these new requirements.

The transition duct, for example, underwent several design modification during the course of the program. Figure 95 shows only the four major design changes, several minor changes addressing stacking heights were implemented as soon as feasible. The rotational symmetry of the early parts which could easily be handled by lathe green machining of isopressed tube stock were modified for performance reasons to incorporate a 180^0 diverter and three integral thermocouple ports. As a result of these design changes CNC green machining had to be implemented and injection molding development was initiated to arrive at a more cost effective near net shape fabrication method.
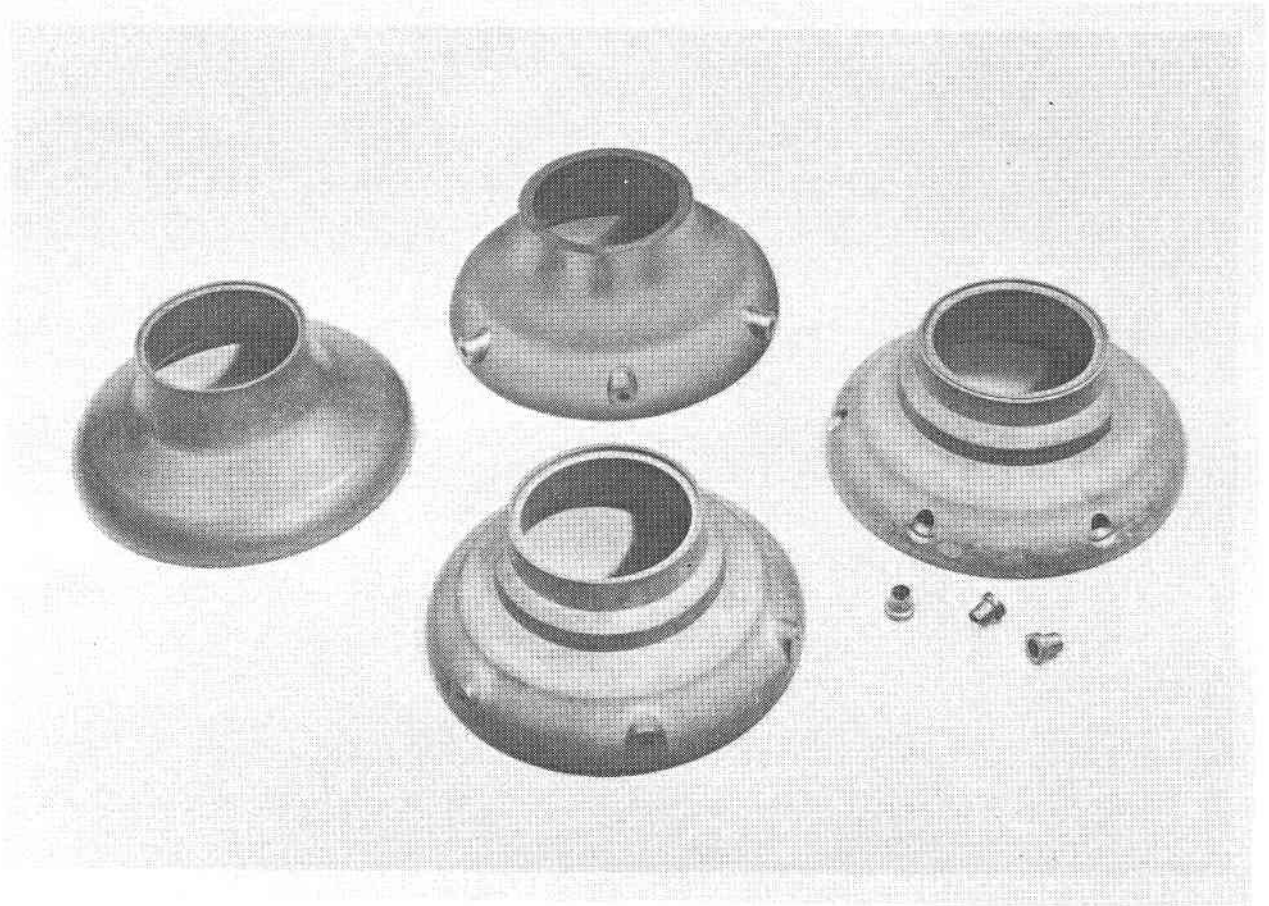
Figure 95. Transition Duct - Iterative Component Development

Near Net Shape Fabrication

Net shape processing is ultimately essential to achieve high reliability at minimum cost. Significant progress has been demonstrated with injection molding in components such as combustor baffles, transition ducts, stator segments, and turbine shrouds where

a wide span of complexity, overall size, and cross sectional thickness is required to produce components suitable for rig and engine testing. Additional development, however, is required to further reduce molding induced density gradients which can lead to some distortion and warpage after sintering.

The development of net shape components is frequently costly and time consuming and can require high tooling cost, thus, not all components fabricated under the AGT-101 program were attempted using net shape forming techniques. Several components such as combustor liner, regenerator shield, backshroud and transition duct were either solely fabricated by isopressing and green machining or this fabrication technique was used to assure adequate and timely supply of components for testing. Figure 96 shows the two parallel forming approaches of injection molding and isopressing used for the fabrication of transition ducts. It clearly depicts the advantage of near net shape forming with respect to material usage and machining time.
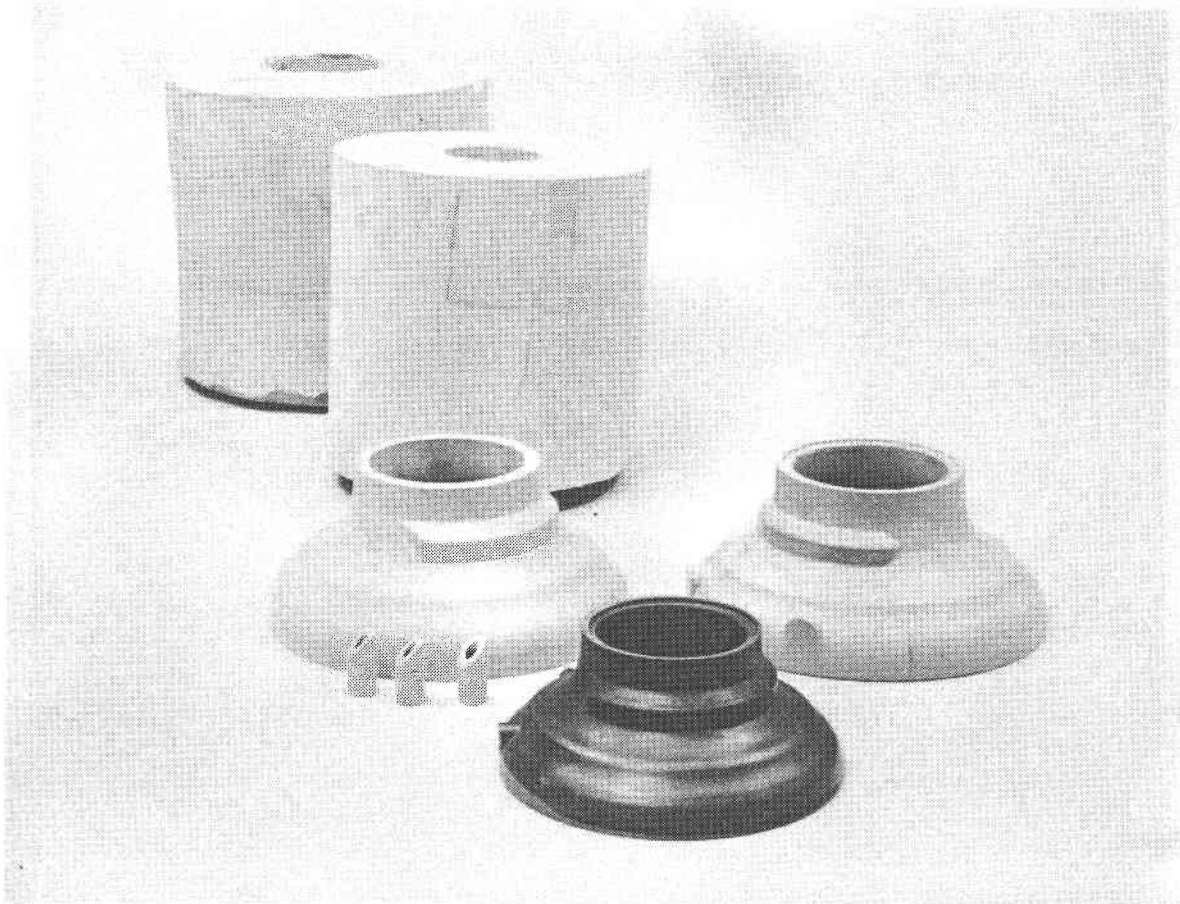
Figure 96. Transition Duct - From Isopressing/Green Machining to Near Net Shape Forming by Injection Molding

Material Properties in Fabricated Components

Material properties of components were evaluated by testing modulus of rupture (MOR) bars cut from the fabricated, sintered components and comparing these data with lot and baseline MOR data. It has been shown that it is possible to obtain material properties within select components which approach or even duplicate baseline performance. However, the generally high variability in average strength and Weibull modulus indicates the need for further processing improvements and more stringent in process control during further development efforts.

Availability of Hardware

Sintered silicon carbide components suitable for rig and engine testing were supplied throughout the program. In some cases parallel processing of isopressed/green machined and near net shape formed components was implemented to first provide components early in the program and second to assure an adequate supply of good quality components while the more cost effective forming technique was being developed. A summary of all hardware deliveries for the AGT·101 is given in Table 18.

The above table shows that a relative large quantity of complex components has been made available for testing and each of these components underwent several design changes to further improve on its fabricability and/or performance within the rig and engine environment. This shows that the question of determining the feasibility for utilizing high performance ceramic components within gas turbines has been affirmatively answered during the course of the AGT 101 project.

Table 18

AGT-101 Hardware Deliveries

October 1979 - July 1987

	FY							
	1980	1981	1982	1983	1984	1985	1986	1987
Turbine Rotor	1							
Duct Spacers	30							
Backshroud		6	6				4	6
Turbine Shroud			4	2				
Turbine Stator			4		7			
Regenerator Shield		9			5	10	6	
Combustor Liner			8		10	17	10	
Combustor Baffle			9	17	2	4	3	
Transition Duct			11	4	3	6	8	3
Wave Springs								4

APPENDIX

Common Work - Final Report

July 14, 1981

M. Srinivasan

Project Manager

1 - INTRODUCTION

This topical report of the AGT Program Common Work narrates the technical activities between October 1979 and March 1981. The report has four areas of activity: (1) developmental efforts in rotor fabrication, (2) non-destructive materials evaluation, (3) determination of mechanical properties, and (4) determination of physical properties.

The rotor developmental efforts were completed with an earlier modified Chrysler tool. This report details the efforts including injection molding, thixotropic casting, and joining of rotor segments. Also included is a limited effort investigating chemical vapor deposition (CVD) coatings on sintered alpha silicon carbide and hot isostatic pressing (Hipping) of partially pre-densified alpha SiC.

The application of the state-of-the-art non-destructive evaluation (NDE) techniques are detailed including high frequency pulse-echo ultrasonics, micro-focus x-ray, scanning laser acoustic microscopy (SLAM), and scanning photo-acoustic microscopy (SPAM).

The mechanical properties investigations resulted in baseline data on alpha silicon carbide manufactured by cold pressing, slip casting, and injection molding. The mechanical strength of both thixocast and warm compression molded reaction sintered SiC was also investigated. Limited experiments characterizing the oxidation effects, possible slow crack growth effects, and elevated temperature creep were conducted.

The thermal diffusivity and specific heat of both alpha SiC and reaction bonded SiC were determined as a function of temperature.

2 - SUMMARY

As a result of discussions between The Carborundum Company and the Prime Contractors (Detroit Diesel Allison*and Garrett Turbine Engine Company) during October - December 1979, a number of developmental activities were defined under the AGT Program Common activity. These were classified broadly into five major areas: rotor fabrication, non-destructive evaluation, mechanical properties, physical properties, and machining studies. Work areas were identified in each of the above topics, and a work plan was submitted to the Prime Contractors during the middle of January 1980 which included a brief narrative for each of the tasks in the work plan with schedules and milestones.

2.1 - Rotor Fabrication

A number of rotor fabrication methods were studied during this period. In the injection molding task, a rotor tool from an earlier Chrysler program was modified so that separate segments of an unbladed rotor could be injection molded. By selective variation of injection molding parameters, visually defect-free rotor segments were injection molded, baked, and sintered to high densities (>98% theoretical).

Baking studies on large segments were conducted by employing an extended baking cycle, plasma baking, and a vacuum bake approach. Crack-free baking was not accomplished with any of these approaches. This cracking was attributed to either the inherent limitation in the then existing process or to deficiencies of the rotor tool which gave rise to inherent molding defects.

Joining of rotor segments was examined by various techniques. These included establishing a silicon carbide bond between isopressed and sintered alpha silicon carbide cyclinders by using sinterable submicron powder and an extrudable alpha silicon carbide mix, and also bonding reaction bonded silicon carbide to alpha silicon carbide. Excellent results were achieved with the extrudable mix consistently achieving final assembly densities of >3.13 g/cc. An inorganic braze material was also used in isolated brazing attempts. Flexural MOR bars were sliced from cylinders joined with sinterable powder. Room temperature strength testing demonstrated that some joints withstood 50,000 psi flexural bend stress with failure occurring outside the joint. Microstructural examination revealed excellent microstructure of the hot pressed silicon carbide and evidence for grain growth across the joint interface.

Considerable effort was also directed to the fabrication of a reaction bonded silicon carbide rotor by thixotropic casting. The challege was to form a thixocast rotor of adequate green strength which could be cured without cracking and to then achieve through-the-section siliconization. These goals were attained during this period. Joining of a reaction bonded SiC shaft to the reaction bonded SiC hub of a rotor was also demonstrated. Centrifugal casting

*now: Allison Gas Turbine Division of General Motors Corporation

126

attempts were made by using a laboratory centrifuge. The results were inconclusive in that void-free castings could not be made reproducibly.

Hot pressed silicon carbide was investigated as a hub material for the AGT rotor program. Room temperature MOR (modulus of rupture) results indicated that very high strengths are possible for certain compositions. These high strengths were obtained on small hot-pressed disks. However, translating these strengths to large, thick sections needs further development. The results have indicated the potential of hot pressed SiC as a core material for the AGT rotor.

Alpha SiC substrates were coated with SiC by CVD process and evaluated by for room temperature strength, microstructure, and failure analysis. There was no significant strength enhancement or a reduction in the variability of the original strength distribution. Microstructural examination revealed that, in general, coatings are well bonded to the substrate with an absence of microporosity in the CVD coatings. Therefore, these coatings can perform a useful sealing function.

Hipping of partially sintered alpha silcion carbide resulted from a joint participation of NASA and Carborundum. The results have indicated density increases by hipping of up to 98.5 percent of the theoretical value. The strength determinations have indicated that significant improvements in room temperature strength cannot be achieved for an initially 98 percent theoretically dense sintered alpha silicon carbide.

2.2 - Non-Destructive Evaluation

The advanced NDE methods, scanning laser acoustic microscopy (SLAM) and scanning photoacoustic spectroscopy (SPAM), were investigated for both sintered alpha silicon carbide and reaction bonded silicon carbide.

Significant progress was made in detection of approximately 0.004- to 0.005-inch voids in 0.1-inch thick disks. The defect detection capability level was increased to 4.3 to 3.5 percent of section thickness by using microfocus x-ray radiography. Although surface roughness of as-fired surfaces causes difficulties for both methods, useful NDE signals can be obtained from both SPAM and SLAM. Complex shape examination seems to be very feasible by SLAM. The SPAM method is also applicable to complex-shaped components by appropriate cell design. However, both methods require extensive experience for correct interpretation of NDE signal. In addition, it is not yet possible to describe the type, size, and location of defects directly from the primary data.

The applicability of high frequency ultrasonics (35 MHz) to examine B_4C inclusions and voids in sintered alpha silicon carbide was demonstrated.

2.3 - Mechanical Properties

The two-parameter Weibull distribution, the three-parameter Weibull distribution, and the method of moments were all considered. The effect of nonuniform stress distribution that occurs along the depth of a bend specimen was incorporated. Computer codes were generated to analyze strength data by each of the above methods. Significant progress was made in understanding the statistical strength distributions. The test data dictates the applicability of each of the above methods. These statistical techniques were applied to the baseline data obtained on injection molded, cold pressed, slip cast and isopressed sintered alpha silicon carbide.

Failure analysis of baseline strength bars produced by injection molding sintered alpha SiC has indicated that greater than 60 percent of the failures occurred from processing-related volumetric flaws located at or close to the tensile surface. Similar results were observed also with slip cast silicon carbide.

The characteristic strength of 64,700 psi at room temperature of injection molded test bars is among the highest observed in our laboratories, and the characteristic strength slip cast test bars was found to be 59,400 psi at room temperature. The strengths of dry pressed sintered alpha silicon carbide and fine grain reaction bonded silicon carbide are approximately 20-25 percent lower than that reported earlier and have been traced back to processing anomalies. Corrective measures were subsequently implemented. The excellent retention of room temperature strength at 2192°F for all silicon carbide materials investigated in this program was demonstrated.

The time-dependent mechanical properties investigations such as creep and stress rupture were also conducted. Compression molded reaction sintered silicon carbide exhibited no time-dependent failure in 100 hours at applied stress levels of 40,000 to 56,000 psi in 4-point bend at 1000°C (1832°F). Creep deflections ranging from 3500 to 8000 micro inches were observed; however, time-dependent failure in stress rupture occurred at 1200°C (2192°F) for applied stresses $\geqslant$54,000 psi. Creep deflections ranging from 5,900 to 25,900 micro inches were also observed.

Four-point bend creep experiments at 1200°C (2192°F) were completed for compression molded reaction sintered silicon carbide for three applied stress levels. Minimum creep rates ranged from 7.44 x 10^{-7} in/in-h to 3.32 x 10^{-6} in/in-h, with an experimental value for stress exponent, n $\geqslant$ 3. A reduction in densities up to approximately two percent was noticed, perhaps owing to cavitation during creep.

The static stress rupture experiments conducted with dry pressed sintered alpha SiC at 1500°C indicated limited failures within 100 hours for applied stress levels greater than 45,000 psi in four-point bend. Fractography indicated no oxidation-related slow crack growth phenomenon. These results indicated the difficulties in applying the traditional known life predictions established via stress rupture tests in ceramics to the failure of SiC ceramics. A more fundamental understanding with respect to mechanisms causing the stress

128

rupture of silicon carbide materials needs to be established before undertaking life-predictive data reduction.

Selected oxidation experiments, conducted at 1260°C for 200 hours has revealed that room temperature flexural strengths of inherently low strength fine grain reaction sintered silicon carbide can be increased by up to 63 percent.

2.4 - Physical Properties

Thermal diffusivity and specific heat measurements were made as a function of temperature for both sintered alpha silicon carbide and fine grain reaction bonded silicon carbide.

3 - SCOPE OF THE AGT COMMON WORK

The scope of the AGT Common Work was defined in a series of meetings between Carborundum, DDA and AiResearch. The Common Work was to involve developmental activities in the rotor fabrication area which were to aid in defining the best combination of processing techniques which were to allow fabrication of DDA and AiResearch unique rotors respectively. The Common Work was also to involve examination of the applicability of available NDE methods to silicon carbide and also detailed mechanical properties data base acquisition which was to aid both the designer and silicon carbide processing. With these objectives, the Common Work plan consisted of the following five major areas:

- Rotor Fabrication
- Non-Destructive Evaluation
- Mechanical Properties
- Physical Properties
- Machining Studies.

The early termination of funding precluded the completion of some tasks and precluded the achievement of latter program scheduled goals. Those areas and/or goals specifically affected by early fund curtailment are indicated.

3.1 - Rotor Fabrication

The objective of rotor fabrication activity was to develop techniques to produce integral rotors such as the ones in the AGT program. The approach was to fabricate rotor segments which were to be joined by appropriate means. Various joining methods were investigated such as alpha silicon carbide bonding, high temperature brazing, and bonding by using hot pressing. One-piece molding and insert molding with a porous ceramic core were approaches which were examined. Development efforts also included studying the use of alpha silicon carbide shell which can be filled with a reaction sintered silicon carbide material. Alternate fabrication methods included thixotropic casting and centrifugal casting of reaction sintered silicon carbide. Hot pressed silicon carbide core with expected high mechanical strength was investigated as a possibility. The merits of chemical vapor deposition and hot isostatic pressing (hipping) was investigated as a means to increase mechanical strength.

3.2 - Non-Destructive Evaluation

The objectives of the advanced NDE effort in the AGT Common pool were to:

130

(a) Apply existing advanced NDE technology for flaw detection, and characterization in candidate SiC materials;

(b) Examine the role played by NDE in increasing the reliability of AGT components, such as rotors, by coupling NDE with fracture mechanics approaches; and

(c) Feed back the NDE information to processing to achieve processing improvements.

The NDE tasks involved fabrication of seeded defect specimens and evaluation by different NDE techniques such as x-ray radiography, high frequency ultrasonics, scanning laser acoustic microscopy (subcontracted to Sonoscan, Incorporated), and scanning photoacoustic spectroscopy (subcontracted to Wayne State University). Also, acoustic emission as a NDE technique was evaluated. The effectiveness of the NDE methods in screening critically defective bars was to be established by NDE-fracture mechanics coupling. The last two tasks could not be completed during the contract tenure due to funding revisions.

3.3 - Mechanical Properties

The objectives of the mechanical properties evaluation efforts were to:

(a) Extend the design data base of prime candidate materials, sintered alpha silicon carbide and reaction sintered silicon carbide. The need is particularly acute in the area of time-dependent high temperature properties.

(b) Conduct some supportive testing of advanced material efforts.

(c) Perform cold spin tests to characterize the materials and processes, and to evaluate joining methods and materials.

(d) Evaluate the interaction between silicon carbide materials and thermal transient environments.

(e) Test materials cut from fabricated components to correlate results with both baseline data and properties of test bars fabricated with the components.

The mechanical properties studies were to include baseline properties determination, fracture mechanics, proof testing/spin testing, oxidation, slow crack growth studies, creep, mechanical fatigue, thermal fatigue, strength distribution, failure prediction, joint evaluation, and property translation on components.

Tasks (c), (d), and (e) were not completed during the contract tenure.

3.4 - Physical Properties

For both alpha silicon carbide and reaction sintered silicon carbide, baseline physical property measurements were to be made. These properties were to include thermal diffusivity, heat capacity, coefficient of thermal expansion, and elastic modulus and Poisson's ratio which are important parameters governing thermal stress resistance. Measurements of residual stresses and coefficient of friction were also to be made.

Of these properties, only the thermal diffusivity and the specific heat measurements were made during the tenure of the contract, additional planned work was not undertaken due to funding revisions.

3.5 - Machining Studies

The objective of this study was to investigate the effects of different methods of machining on the residual strength of SiC candidate materials for AGT components.

An investigation was to be carried out to determine the value of alternate and/or new machining methods as compared to traditional diamond grinding which was to serve as control. The methods to be investigated were to include, but not be limited to, ultrasonic machining, EDM, ECM, and laser machining. Residual strength measurements after machining by various methods were to be the basis for evaluation.

The machining studies task could not be accomplished during this contract tenure due to funding revisions.

132

4 - ROTOR FABRICATION

The rotor fabrication task investigated the most promising processing methods for both the single-phase sintered alpha silicon carbide and the dual-phase reaction sintered silicon carbide. The fabrication of a single-piece rotor presents unique material and process problems. For example even though large pieces of the alpha SiC ceramic can be easily injection molded, the maximum allowable cross section in order to obtain a crack-free component after baking was 1 inch during the contract period (Oct. 79 - Oct. 80). A similar limitation can be envisioned for a uniform and complete siliconization during the processing of a reaction sintered silicon carbide rotor.

Therefore, the basic development approach consisted of:

(a) Injection molding a thick rotor hub and investigating various baking technology (for alpha SiC).

(b) Thixocasting a rotor, with blades, of reaction sintered SiC composition and investigating the optimum siliconization conditions.

(c) Injection molding segments of a rotor hub (alpha SiC), baking and sintering, and investigating joining of segments by subsequent elevated temperature hot pressing (by using both sinterable alpha SiC powder and extrudable SiC mix as joining medium). A study consisting of filling the pre-sintered outer shell with sinterable alpha SiC powder which can be hot pressed to obtain a hot pressed alpha SiC core joined to the outershell, and an effort to fill the outer shell of alpha SiC with a reaction bonded SiC core which were then joined by hot pressing were included in this task.

4.1 - Injection Molding of Segments

An earlier Chrysler rotor tool was modified such that a series of inserts when placed into an existing tool cavity allowed an outer shell, an inner core, and a bottom plate to be formed separately. The segments could then be used for bonding studies.

The inserts in place in the mold tool assembly is shown in Figure 97. The three segments of this modified Chrysler tool is shown individually in Figures 98 through 101. In the initial molding trials, many defective moldings were made. Because of the fact that the original tool design was not intended for molding inserts, these defects were introduced during molding. The solid hub segments were molded with fair results (no gross cracking). The outer shell segment after molding had circumferential cracks on the inside where the sprue feeds the wall. Again, after molding, the inner core pieces cracked radially from center with the separation of the bottom lip.
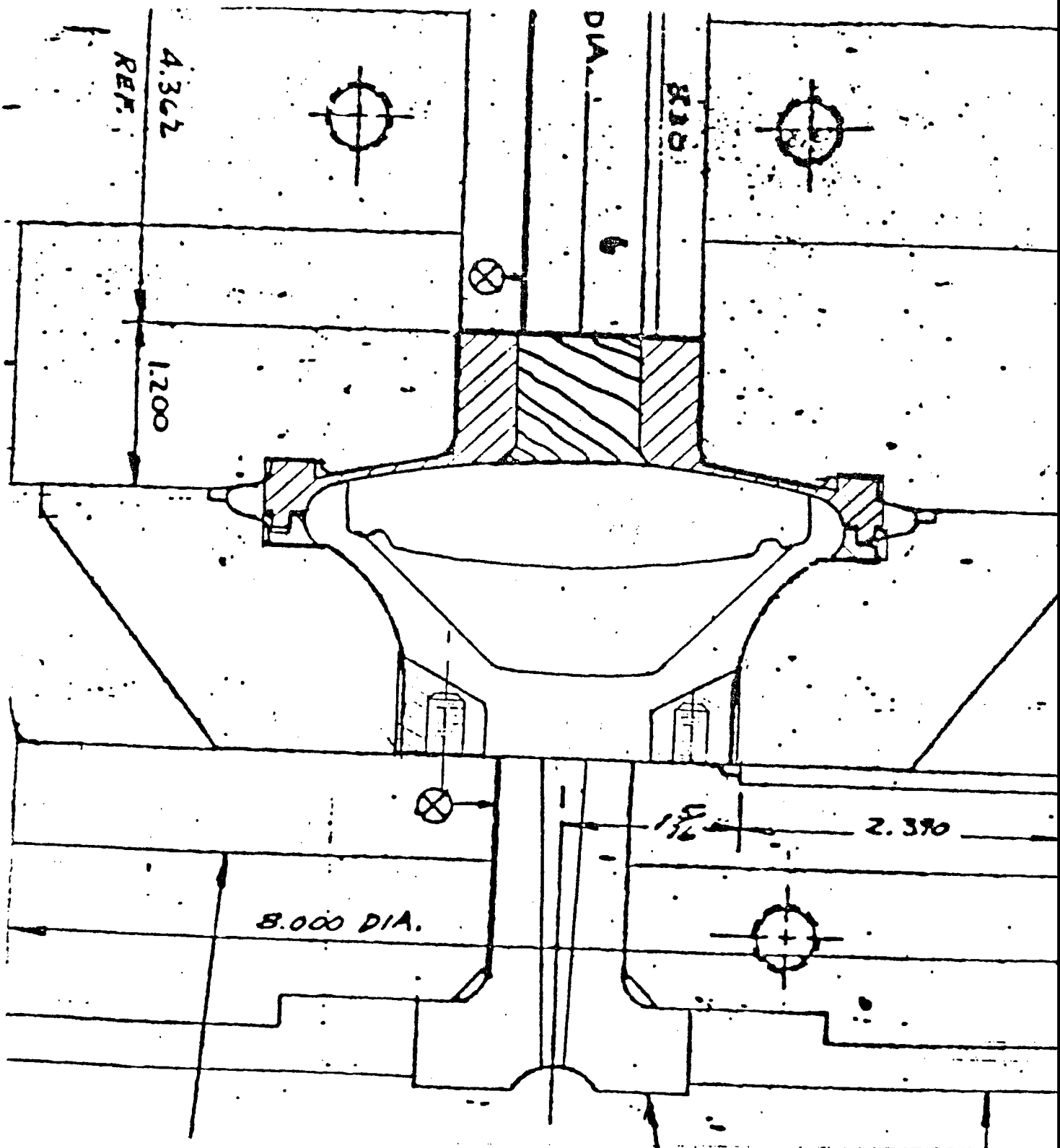
133

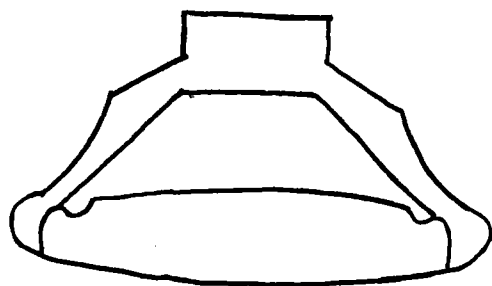Fig. 97 - AGT Common Rotor Mold Tool Assembly

Fig. 98 – Segment Assembly in
the Chrysler Tool

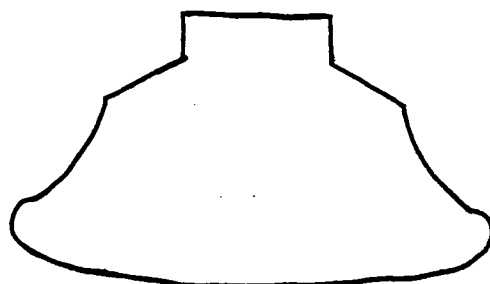Fig. 99 – Solid Hub Segment
(One Large Piece)

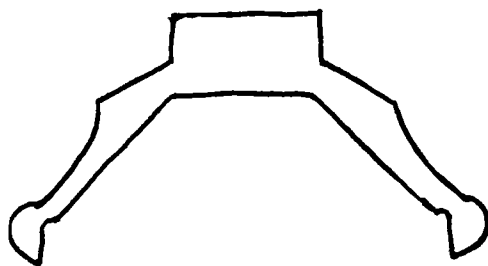

Fig.100 – Outer Shell Segment

Fig.101 – The Inner Core Segment

During May-June 1980 after optimization of processing variables, several pieces of outer shell, inner core, and bottom plates were molded, baked, and sintered to densities greater than 3.13 g/cc with no visual cracks after any of the processing steps.

4.2 - Baking Studies (One-Piece Rotor)

Studies were undertaken to modify the standard bake cycle to yield crack-free solid hub segment components on cross sections in excess of one inch. These studies were:

- Extended Bake Cycle,
- Plasma Bake Approach, and
- Vacuum Bake Approach.

None of these were completely successful and a crack-free baked rotor could not consistently be obtained.

4.3 - Joining Studies

Joining studies were conducted by using both complex shapes, rotor segments of the modified tool, and simple cylinders of isopressed and sintered alpha silicon carbide. The latter was performed to characterize the strength of the joints and to study the microstructural development across the joint interface by optical microscopy.

4.3.1 - Segments Joining

The objective here was to obtain an integral rotor by joining the segments by various means.

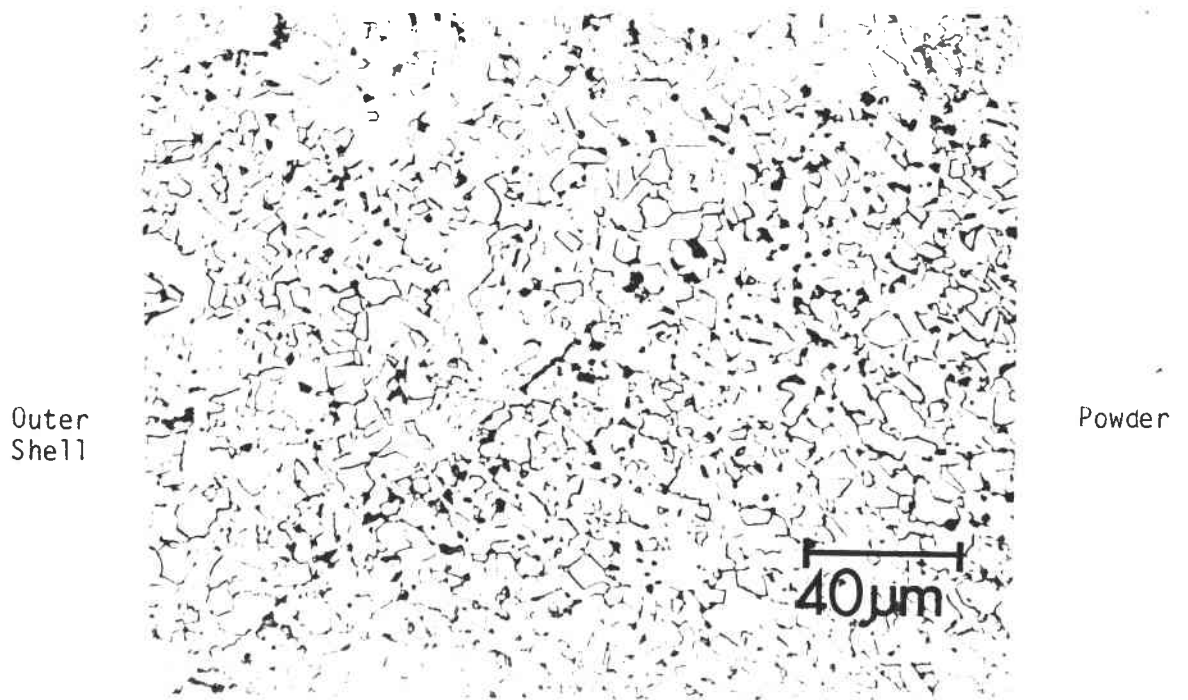#### 4.3.1.1 - Filling the Outer Shell with Alpha SiC Powder and Hot Pressing

This technique involved several combinations of plunger and carbon powder. Eventually, carbon and phenolic resin were hand mixed and used as plunger material, and the outer shell filled with alpha SiC powder prior to hot pressing (Figure 102). After hot pressing, the surface of the bell was slightly deformed. This method produced a piece with a density of 2.83 g/cc.
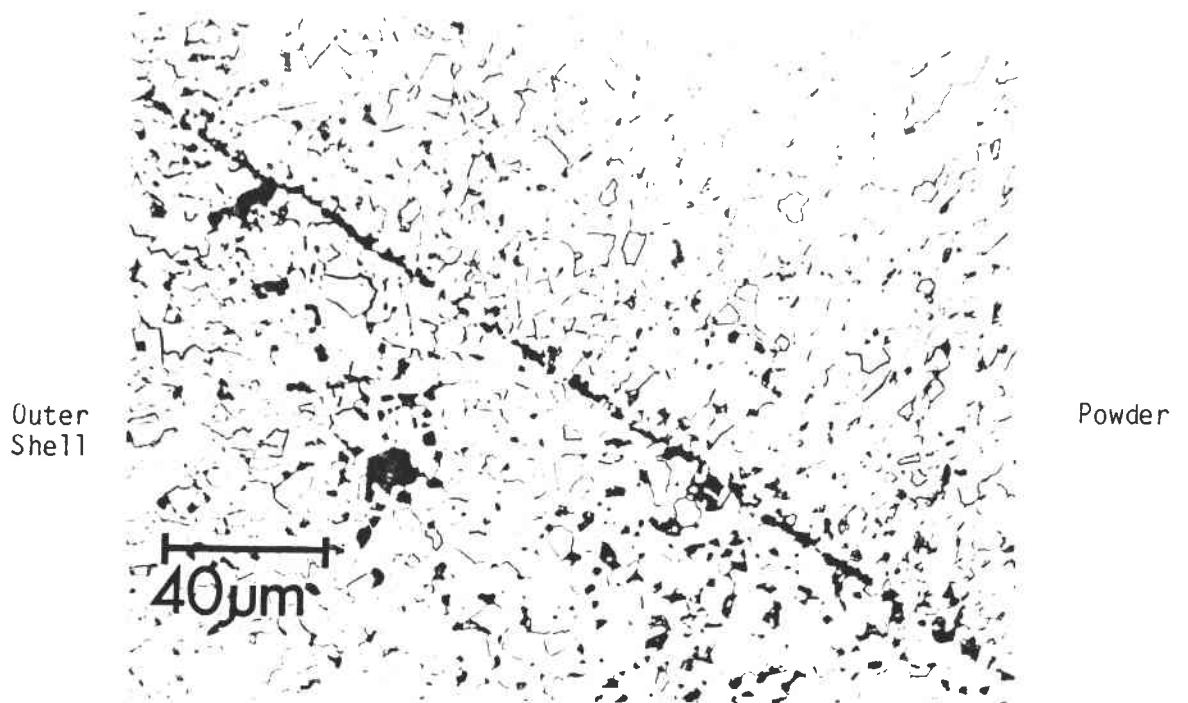
Fig.102- Insert of a Sinterable Alpha SiC Powder and Sintered Outer
Shell and Hot Pressed. Density of Final Body = 2.83 g/cc

The microstructural development across the hot pressed joint was
also examined in a rotor fabricated by filling the outer shell with
sinterable powder and hot pressing. The results are shown in Figure 103.
In Figure (a), a poor joint area is evident. Figure (b) shows a
good area in which there exists good bonding and grain growth across
the joint interface. Also, the microstructural development is such
that there exists no essential difference in the microstructures of
the hot pressed sinterable powder and the sintered outer shell
segment. In Figure (c), microstructural differences exist between
the two materials. The hot pressed powder shows finer grain size and
perhaps lower density. These three examples have demonstrated that
there exist temperature and pressure variations during hot pressing in
different areas of the interface which result in varying degress of
bonding, and microstructural development across the interface.

It must be pointed out that the hot pressing direction is not
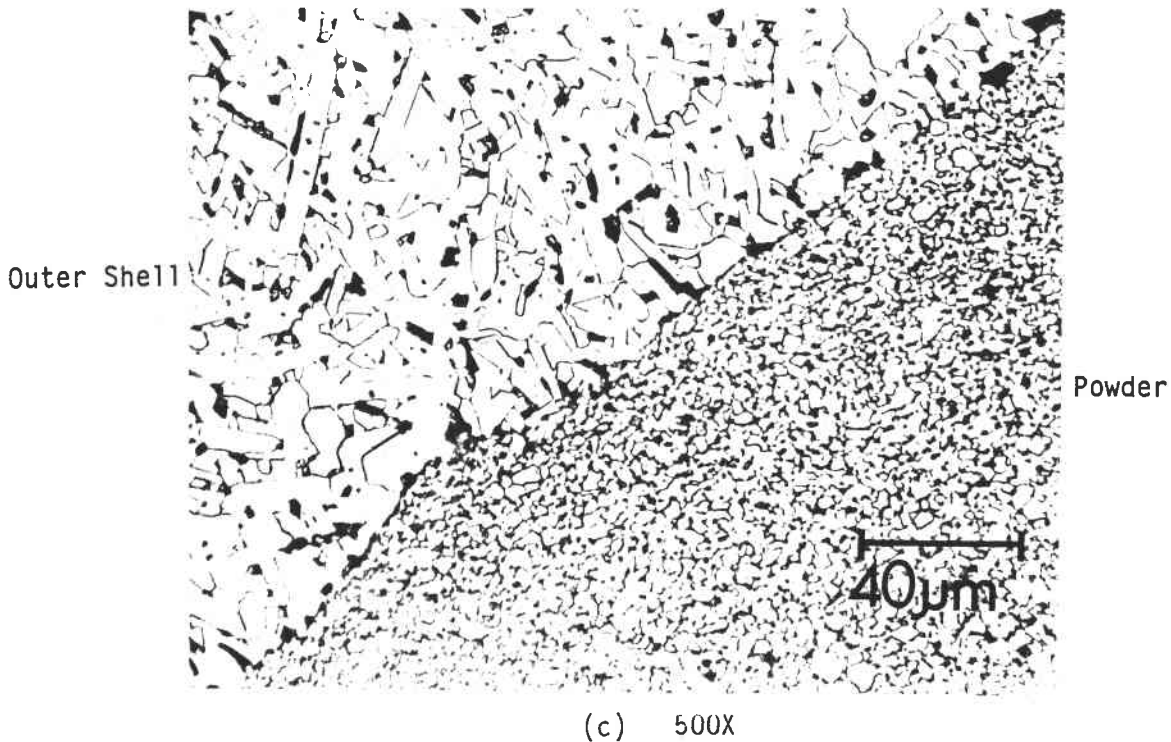perpendicular to the joint interface in these segment joining
investigations.

Outer
Shell

Powder

(a) 500X

Outer
Shell

Powder

(b) 500X

Fig.103- Microstructure Across the Hot Pressed Interface of a
Sintered Outer Shell Filled With Sinterable Alpha
SiC Powder

138

Fig. 103 (Continued)

Outer Shell

Powder

40μm

(c) 500X

4.3.1.2 - Filling the Outer Shell with Reaction-Sintered SiC Mix and Hot Pressing

An injection molded sintered alpha SiC rotor shell can also be filled with a reaction sintered SiC material. A resin-SiC grain mix is compacted into the hollow rotor shell and heated. The filled portion is infiltrated with molten silicon to form reaction sintered SiC.

The reaction sintered SiC mix must be carefully formulated to minimize shrinkage. Large shrinkage results in a weak pure silicon interface between the sintered alpha SiC shell and the RBSiC core. Also the thermal expansion rate of RBSiC material and the sintered alpha SiC shell must closely match to prevent the presence of residual stresses.

In an initial attempt, a reaction bonded SiC piece was used to fill the bell-shaped segment before hot pressing. The RBSiC mix was hand tamped and cured. The cured segment was removed from the bell, siliconized, and the siliconized segment was reinserted into the bell

Fig. 104- Outer Segment Filled With RBSiC And Then Hot Pressed

and hot pressed. The result (Figure 104) was that the insert filled in quite well, but the insert was not as dense as required. The bell-shaped segment exhibited some cracking which was present before hot pressing. In other attempts, pieces also cracked during hot pressing. Some cracks were filled with silicon while others were not. Thermal expansion mismatch are considerable for these materials.

An example of microstructural development across the joint is shown in Figure 105. The large grains of SiC in the reaction bonded SiC region is due to the nature of the mix used. Good bonding can be seen in the region examined. However, there existed regions in which porosity was present at the joint interface.

4.3.1.3 - Alpha SiC Bonding
Between Rotor Segments

In initial attempts, sinterable powder was used as a joining medium which surrounded the segments to be joined by hot pressing.

Here a presintered inner core segment was used as an insert into the outer shell. Sinterable powder surrounded the insert and then the
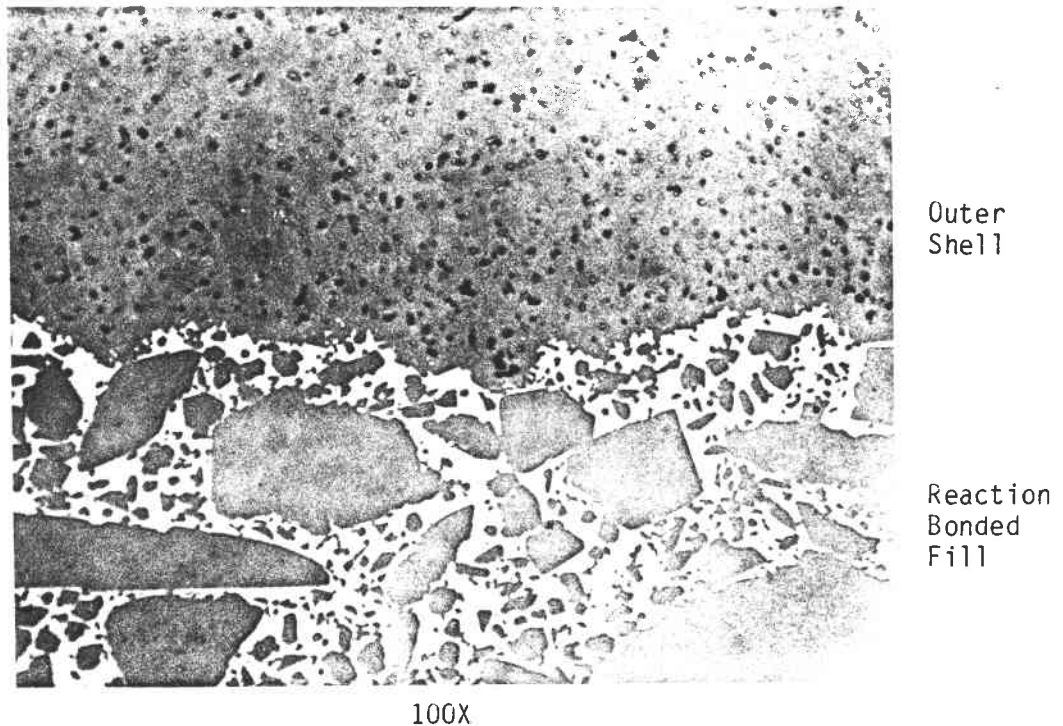
140

Outer
Shell

Reaction
Bonded
Fill

100X

**Fig.105- Microstructural Development Across The Sintered
Alpha SiC And Reaction Bonded SiC Interface**

whole assembly was hot pressed. The results indicated an unexpected
amount of large porosity in the joining material. This porosity is
the result of some presintering at the hot pressing temperature before
the application of pressure. In subsequent experiments, pressing
began at even lower temperatures to eliminate this problem.

In another trial, the bell-shaped segment was filled with sin-
terable powder and also a presintered insert. Pressure was applied at
lower temperatures and final hot pressing was done at an elevated
temperature. The final density of the piece was 3.13 g/cc and deve-
loped no cracks during hot pressing. A cross section examination
(Figure 106) indicated that the joint areas appeared sound. However,
there exists many large pores in the joint material. Also, cracks in
the insert, which were introduced during sintering, did not heal
during hot pressing.

In the preceeding experiments, carbon powder filled the clearance
between the hot press mold and the outer bell segment. It was con-
cluded that pressure transfer was not optimum in these experiments,
and that the side pressure of the carbon powder caused some hot press
mold breaks.

141

Fig. 106 – Hot Pressing Of A Sintered Alpha SiC Outer Shell With Presintered
Inner Core And Sinterable Powder Surrounding The Inner Core.
Final Density Of The Assembly = 3.13 g/cc

In subsequent experiments, some rigidity was sought for the
plunger material next to bell. This requirement was achieved by using
a plunger made of carbon and phenolic resin. In an experiment, the
two halves of a cracked insert (cracked due to molding flaws) were
inserted into the outer bell and sinterable powder was placed between
the segments and the entire assembly was hot pressed. An excellent
final density (3.15 g/cc) was achieved (Figure 107). The bond appeared
to be good and no cracks were seen. The only defect was a small non-
dense region between sections of insert. However, a considerable sur-
face deformation of the outer shell was evident. It was then decided
to change the plunger material. In subsequent experiments, the
plunger material was carbon powder next to the bell and carbon-phenolic
resin above this (Figure 108).

In addition to the use of sinterable powder as the joining
medium, investigations were also carried out to utilize extrudable
alpha SiC mix as the joining medium between the segments. The hot
pressing arrangement shown in Figure 108 was used with some modifica-
tions to make the bell fit tighter. The results were excellent
(Figure 109). The joining of segments by hot pressing by using an
extrudable alpha SiC mix was developed and achieved consistently
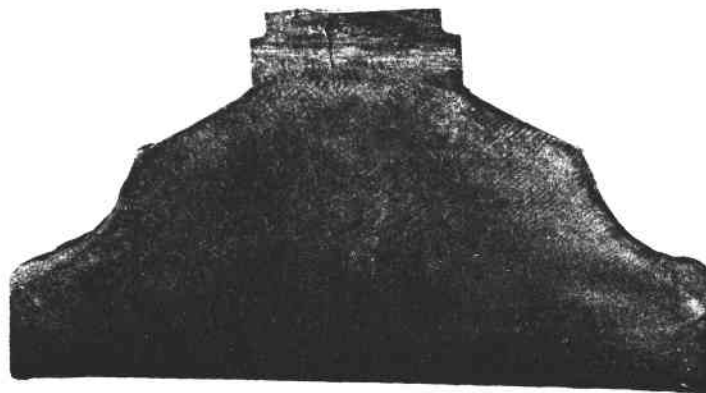higher (3.10 g/cc) final assembly densities.

Fig. 107 - Hot Pressing of Sintered Alpha SiC Outer Shell Filled
With Sinterable Alpha SiC Powder. Plunger Made of
Carbon and Phenolic Resin. Final Density of Body =
3.15 g/cc. Good Bonding Across Joint Interface

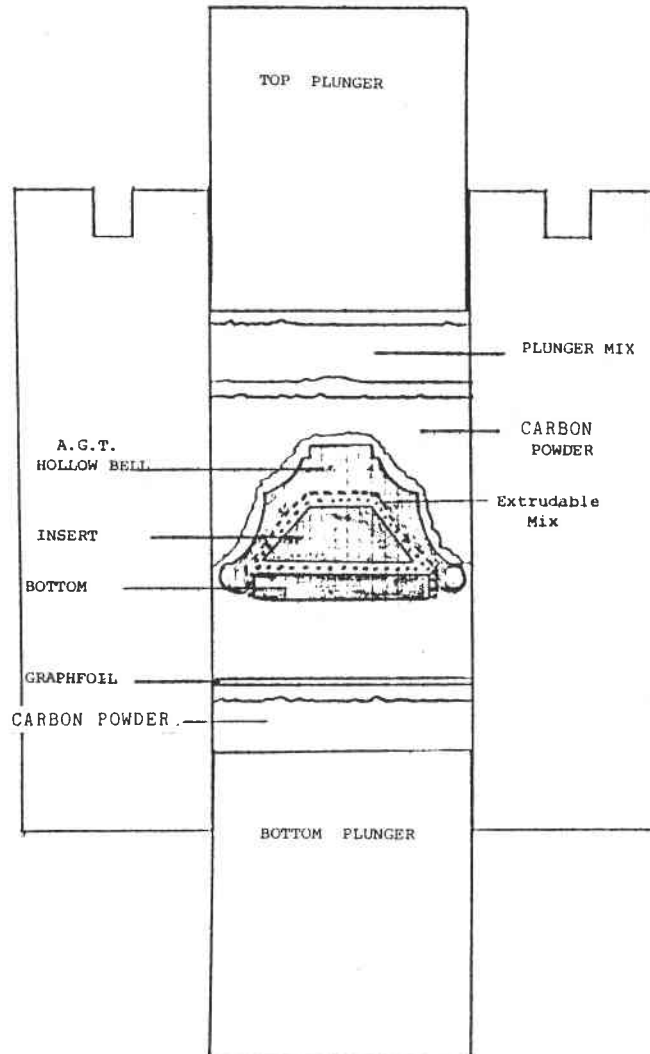HOT PRESS LOADING ARRANGEMENT: A.G.T. COMMON

TOP PLUNGER

PLUNGER MIX

CARBON
POWDER

A.G.T.
HOLLOW BELL

Extrudable
Mix

INSERT

BOTTOM

GRAPHFOIL

CARBON POWDER.

BOTTOM PLUNGER

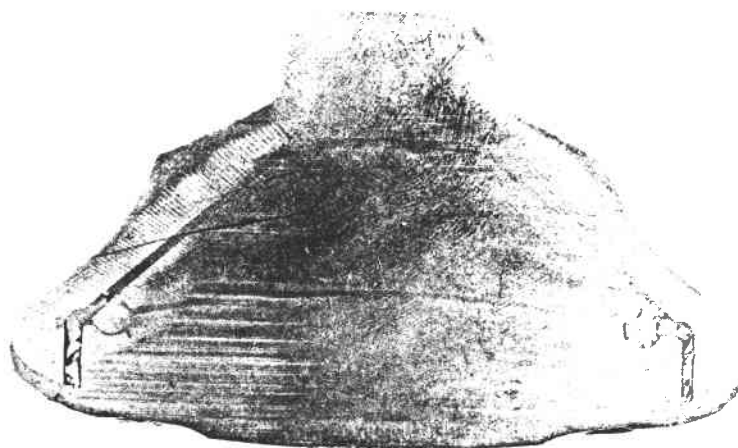Fig. 108 - Schematic of the Arrangement
Used for Hot Pressing

144

Fig. 109 - Hot Pressing by Using Extrudable Mix Between Sintered Segments (Outer Shell, Inner Core, and Bottom Plate). Note Absence of Bonding Between Bottom Plate and Outer Shell in the Region Parallel to Hot Pressing Direction. Final Body Density = 3.08 g/cc

4.3.2 - Joining of Simple Cylinders and Characterization

4.3.2.1 - Alpha Silicon Carbide Bond

Efforts were directed to obtain bonding by hot pressing by using sinterable alpha SiC powder at the interface. In various attempts, different amounts of powder were used to obtain different thicknesses of hot pressed silicon carbide between two isopressed and sintered silicon carbide (Figure 110). The average strength of isopressed material used for this joining study was 48,160 psi with a high of 52,870 psi and a low strength of 40,090 psi. The joined cylinders were cut into MOR bars of the cross section 0.125" x 0.25". These were tested in 4-point bend with 0.5" inner span and 1.5" outer span at room temperature. The results are shown in Table 19. Although the average bond failure occurred at 37.3 $\pm$ 8.51 ksi, the indication that some joint interfaces withstood stresses approximately 50 ksi when failure occurred in joint material (hot pressed SiC) is noteworthy.

145

Table 19- Strength Data for Joints Established by Hot Pressing Isopressed and Sintered Alpha SiC

Sinterable Alpha SiC Powder Was Joining Medium

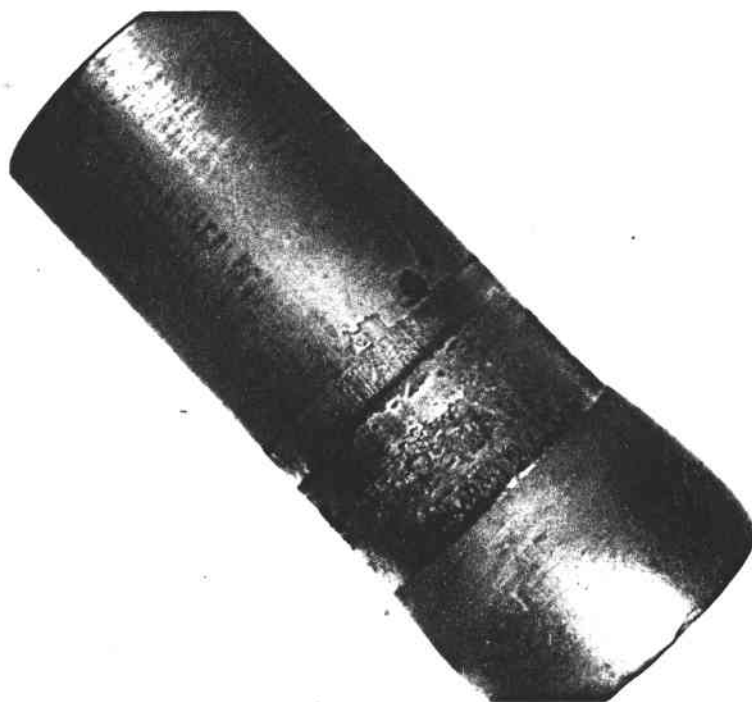| Bond Failure (10^3 psi)	Joint Material Failure (10^3 psi)	Base Material Failure (10^3 psi)	Unknown (Unable to Locate Bond by Radiography) (10^3 psi)
D434-14*	D434-14	A	B
47.09	33.23	50.28	29.48
40.48	38.38		
40.51		B	79
38.28	79	40.00	34.79
47.09	29.88	43.06	42.83
52.87	(Surface Void)		
		79	
A	80	48.19	
36.66	56.35		
40.32	(No Obvious	80	
	Fracture Origin)	35.01	
B	50.38	42.22	
31.11	(Internal Void)	35.01	
	52.60	41.23	
D589-60		(Surface Void)	
42.74		45.08	
36.16		44.44	
41.49			
35.02			
79			
25.31			
80			
17.18			
28.34			
30.57			
(Surface Damage)			

* These are cylinder identification numbers.

Fig. 110 - Hot Pressing of Two Sintered Pieces with
Sinterable Powder as Joining Material

Figure 111 shows the microstructural development for No. 80-U
(σ_f = 56,350 psi). The hot pressed SiC microstructure (right) is
denser than isopressed material (left). No obvious failure origin
could be located by SEM investigation for this specimen. Figure 112
shows the microstructure for another specimen (σ_f = 30,570 psi). The
joint appears sound; however, failure occurred at one of the joints
due to surface machining damage as seen by SEM failure analysis.
Figure 113 shows the microstructure for No. 80-6 (σ_f = 50,380 psi).
This specimen, which failed in the hot pressed SiC region, had an
approximately 100 μm subsurface void as the fracture origin, as shown
in Figure 114. In Figure 115, the microstructure of No. 80-08 is
shown. Here again, good bonding is evident. No obvious fracture
origin could be located by SEM fractography for this specimen.
Finally in Figure 116, the poor microstructure of hot pressed silicon
carbide (higher porosity) is shown for No. 79-5 (σ_f = 29,880 psi). In
general, the bond identification by x-ray radiography for specimens
cut from cylinder No. 79 was not feasible because of the almost
equivalent densities of hot pressed SiC and isopressed and sintered
SiC. Failure of this specimen was due to large subsurface pores shown
in Figure 117. Failure occurred in the hot pressed silicon carbide
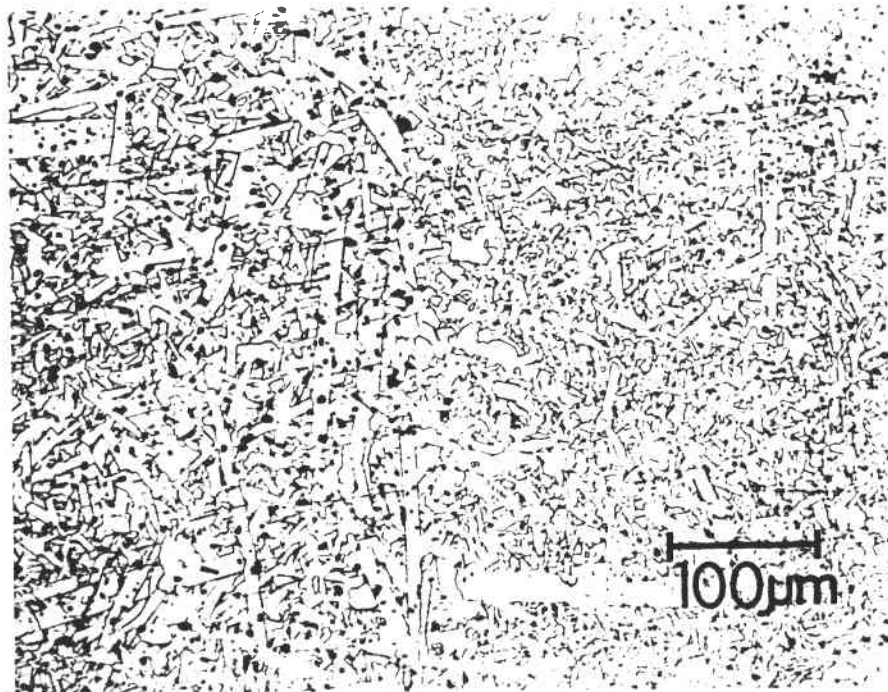region.

Fig. 111 -   No. 80-U. Isopressed SiC Microstructure (Left) and
Hot Pressed SiC Microstructure (Right). Evidence of
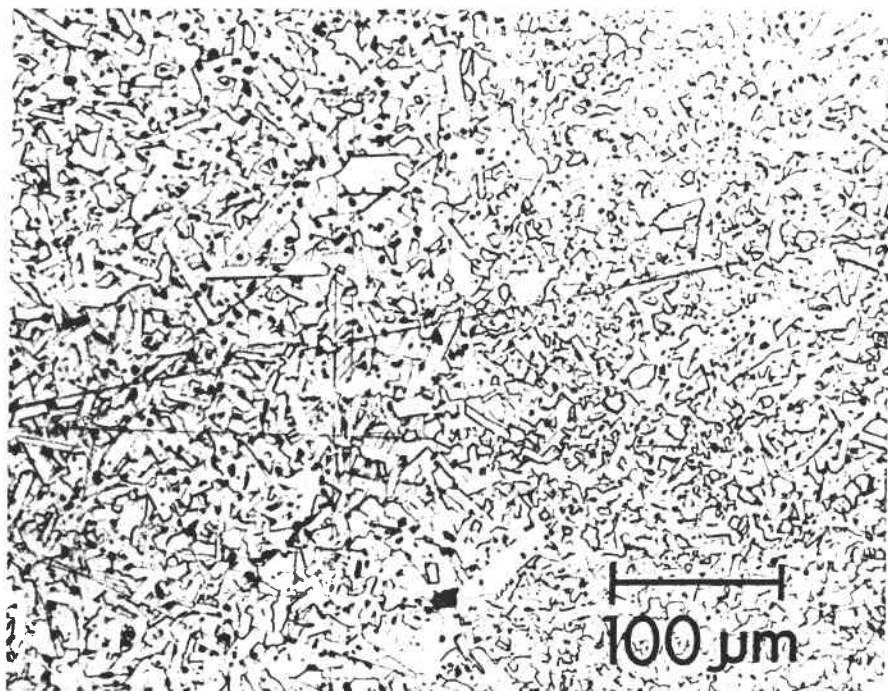Grain Growth Across Joint Interface Seen

Fig. 112 -   No. 80-5. Microstructure of Isopressed Sintered
Alpha SiC (Left) and Hot Pressed SiC (Right)

Fig. 113 – No. 80-6. Isopressed SiC Microstructure (Left) and Hot Pressed SiC Microstructure (Right). The Specimen Failed in the Hot Pressed SiC Region.
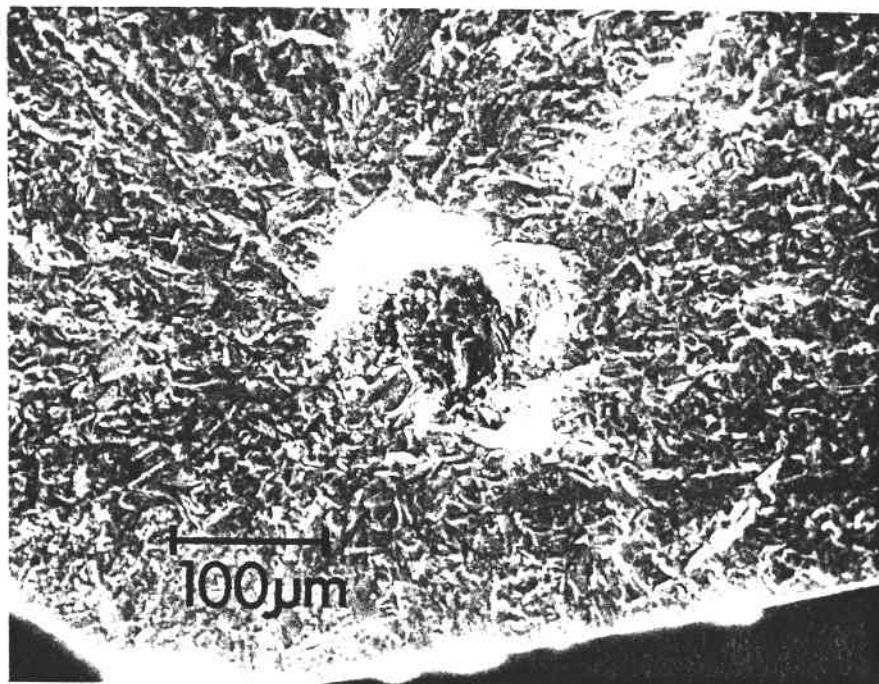

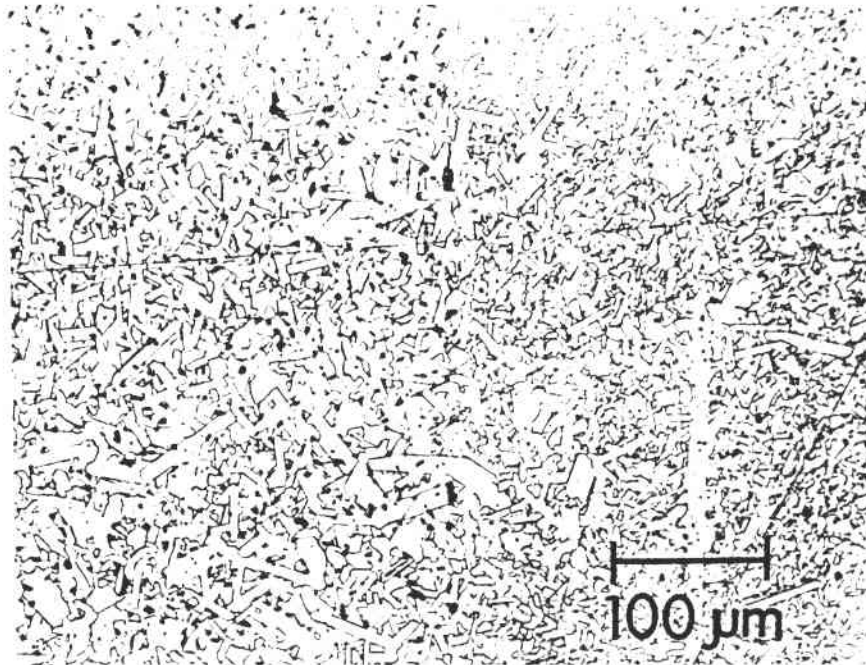Fig. 114 – No. 80-6. Failure Origin Within The Hot Pressed SiC Region

Fig. 115 – No. 80-8. Microstructure of Isopressed Sintered Alpha SiC on the Left and Hot Pressed SiC on the Right. No Obvious Fracture Origin was Located on the Fracture Surface
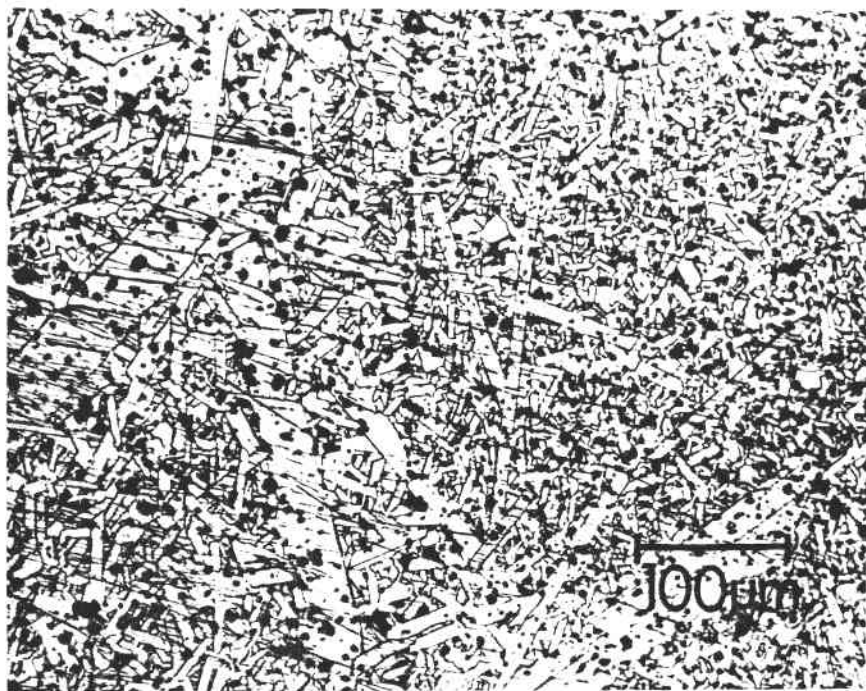

Fig. 116 – Microstructure of No. 79-5. On Left is Isopressed SiC and on Right is Hot Pressed SiC
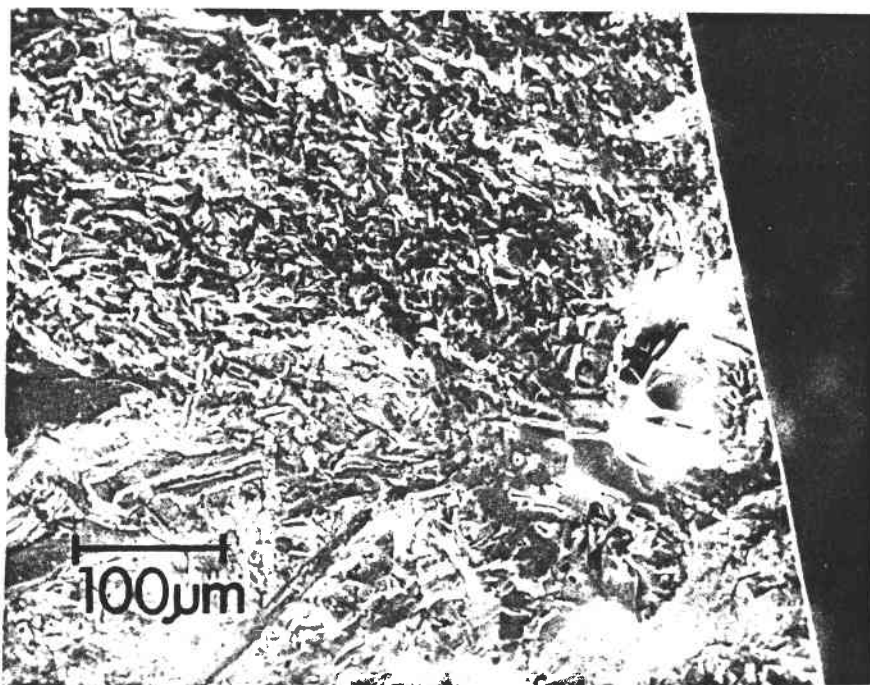
Fig.117 - Failure Origin for No. 79-5. Failure Occurred in the Hot Pressed Silicon Carbide Region

4.3.2.2 - Reaction Bonded SiC Bond

Five cylinders of 1.5-inch diameter were made by using fine grain reaction bonded silicon carbide mix by pressing. After siliconization, segments of these cylinders were used to join two isopressed and sintered alpha silicon carbide cylinders. In one attempt, a segment of the reaction bonded silicon carbide cylinder was placed in between isopressed and sintered alpha silicon carbide cylinders and hot pressed under standard conditions. The results indicated that only one of the alpha silicon carbide cylinders was bonded to the fine grain reaction sintered silicon carbide and that bonding was poor. In two subsequent attempts which used lower temperatures and lower pressures, bonding was never established. It is not understood as yet why bonding was not been achieved between alpha SiC and RBSiC in simple cylinder forms by hot pressing; perhaps, thermal expansion mismatch between the two silicon carbides prohibit bonding during cool down.

4.3.2.3 - High Temperature Braze

Work in this area involved joining studies by using an inorganic high temperature proprietary braze developed by The Carborundum Company.

The major considerations in the selection of a successful braze for SiC were:

- Good wetting of the SiC by the braze
- Close match of thermal expansion coefficients
- Chemical compatibility
- Oxidation resistance, and
- Strength at use temperature.

The proprietary braze meets the above requirements. This technique was successfully applied to alpha SiC by attaching a shaft onto the hub of a simple wheel. The brazing material was placed on the part in such a manner that when heat was applied, the braze flowed into the space between the hub and the shaft. An excellent bond was formed between the two parts, as can be seen in Figure 118.

In the initial trials of joining cylinders which were conducted although bonding appeared to be good externally, when the cylinders were sliced for MOR bars, the existence of voids at the interface was obvious. The method, therefore, needs further development.

4.4 - Alternate Fabrication Methods

4.4.1 - Thixotropic Casting

The general approach was to use a pattern of the turbine rotor to make a rubber mold. A thick mud-like mix consisting of a resin and SiC grain is cast into the rubber mold. Vibration is used to make the mix fill the mold, and the rigid part is removed from the mold and subsequently siliconized to form reaction sintered silicon carbide.

DDA provided Carborundum several large truck turbocharger rotors which have the general shape of the turbine rotors in the AGT program. They had approximately the desired hub section thickness. One of these rotors was used as a pattern for making a cast mold. The rotor blades were increased 0.050 inch in thickness with laminations of wax sheets. This thickness increase was done to aid in filling the blades during thixotropic casting.
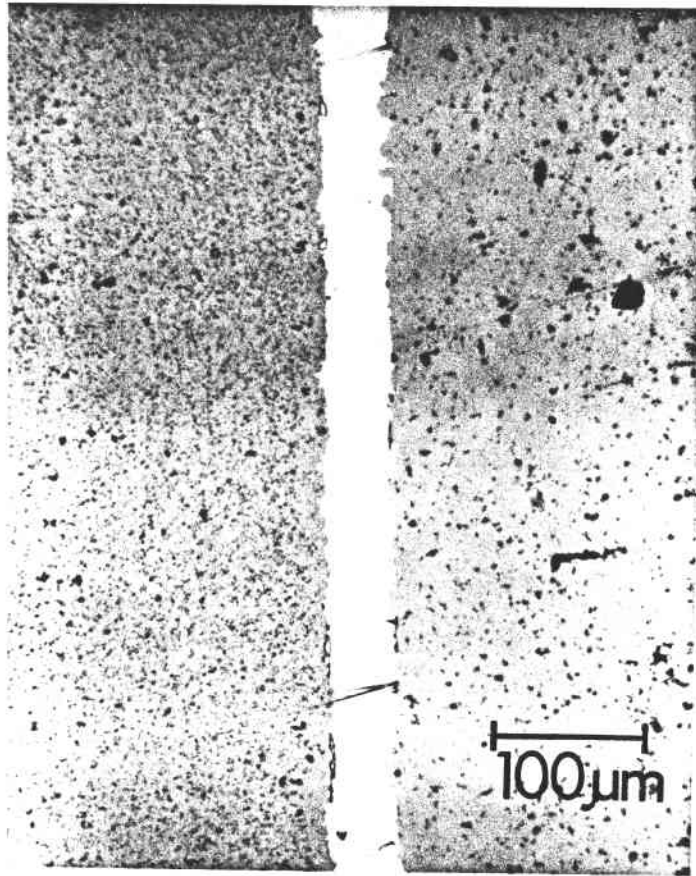
Fig. 118 - Joining by Use of an Inorganic Braze

Figures 119 and 120 show the metal rotor with its cast blade inserts, and the inserts and mold barrel assembly.

Initially, two RBSiC rotors were cast and fully processed. The first was cast with Carborundum's standard coarse-grain thixotropic casting mix. Typical 4-point bend strengths are only about 30,000 psi. Nevertheless, this mix was chosen as a baseline point to gain experience with the mold.

A rotor was cast without difficulty and siliconized in a routine furnace run. A gradual resin bake-out oven run was not used, yet the piece was siliconized without any apparent cracking. The part was diamond wheel sectioned to reveal the interior which is shown in Figure 121. This photograph is life size.

This rotor was not fully siliconized through the entire hub section. This shortcoming was anticipated to be the major problem of this forming method. The top surface of the rotor has numerous bubbles and cracks. These kinds of defects were eliminated in subsequent castings.
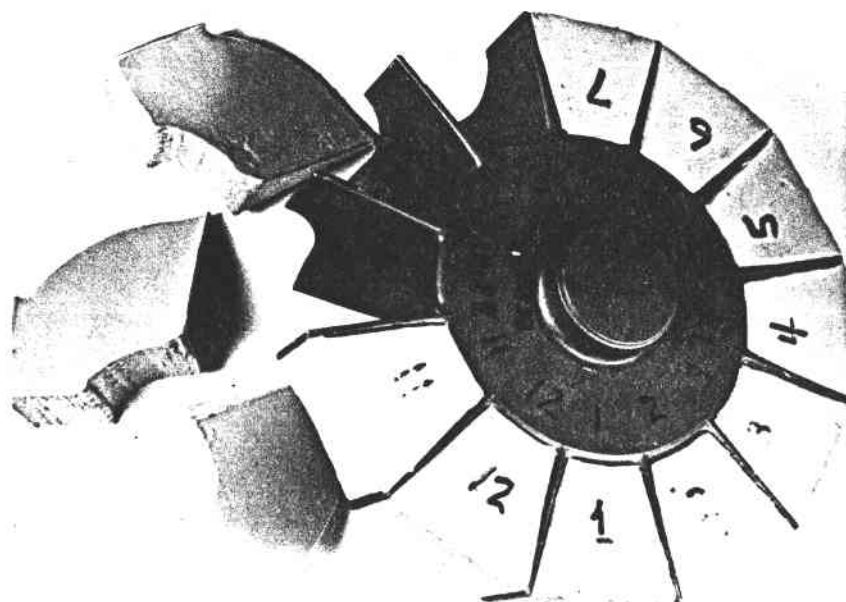
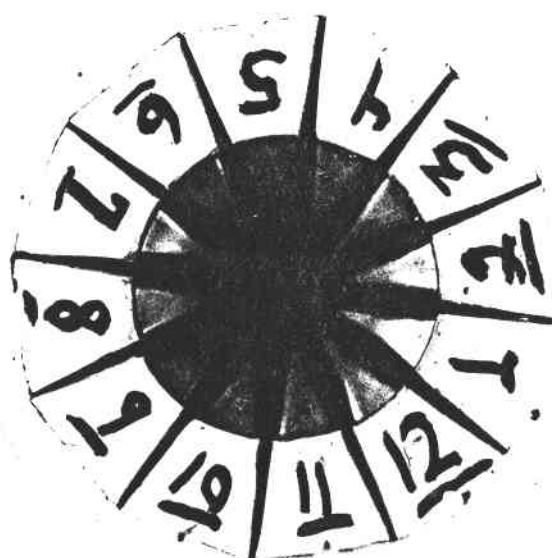Fig. 119 - Metal Rotor and Cast Blade Inserts

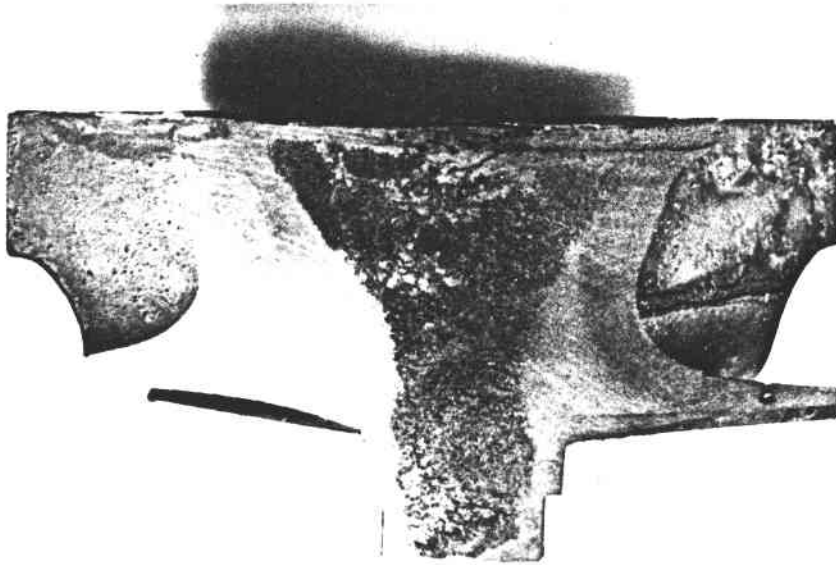Fig. 120 - Inserts and Mold Barrel Assembled

154

Fig. 121 – Siliconized Coarse Grain Thixotropic RBSiC Rotor

Another rotor was cast by using a much finer casting mix. The processing was identical to the previously described rotor. Figure 122 shows the rotor as cast and Figure 123 shows the rotor as siliconized.

The top surface of the siliconized rotor (Figure 123) has shallow "mud cracking". This occurred due to shrinkage of a thin layer of resin which rises to the top during casting. This resin-rich layer could easily be removed before siliconizing and this problem was eliminated in future castings.

Figure 124 shows the cross section of the rotor. Again, the hub was not completely siliconized through the section thickness, but it was much better than the first attempt.

Subsequently, four more thixotropic cast fine grained RBSiC rotors were cast and furnaced. The first was cast with a 3/8-inch center through-hole to reduce the thickness that had to be siliconized. This rotor had a 2.98 g/cc final density and had a very good surface finish.

The other three rotors were all solid cast and siliconized by various techniques. Figure 125 shows a cross section of a rotor which was siliconized in a vacuum furnace with a standard furnacing cycle. This furnacing was identical to that used for the first two rotors made. The only variaton was that extra siliconizing mix was used. The depth of silicon
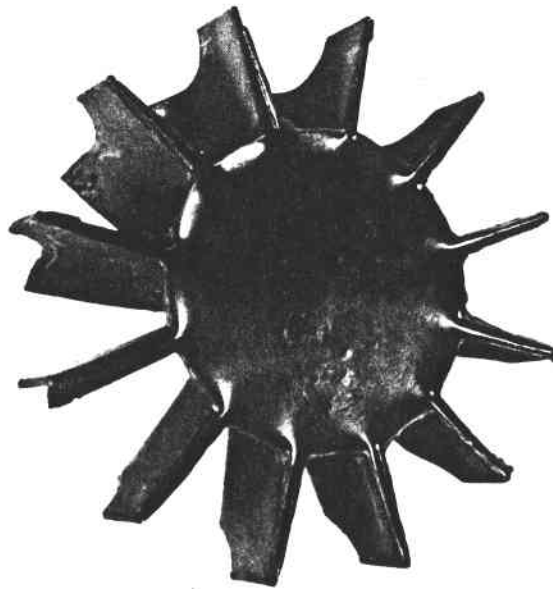
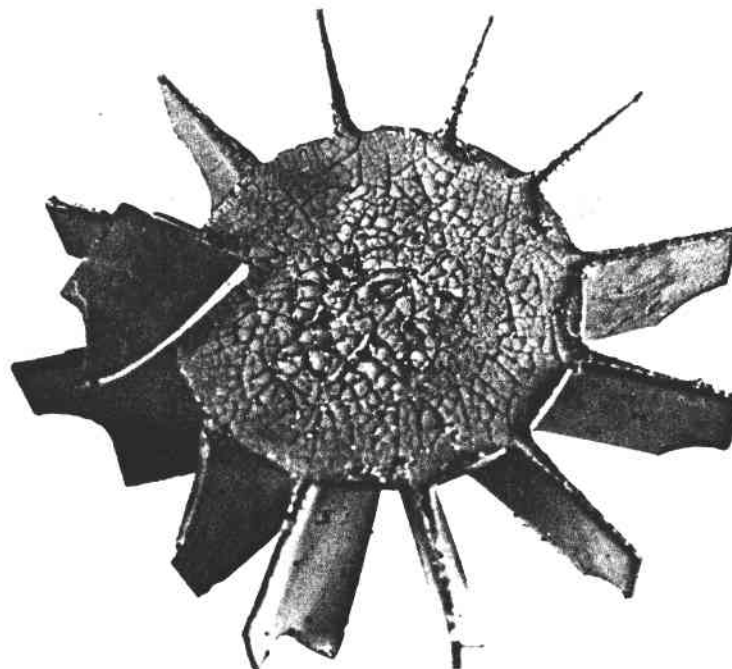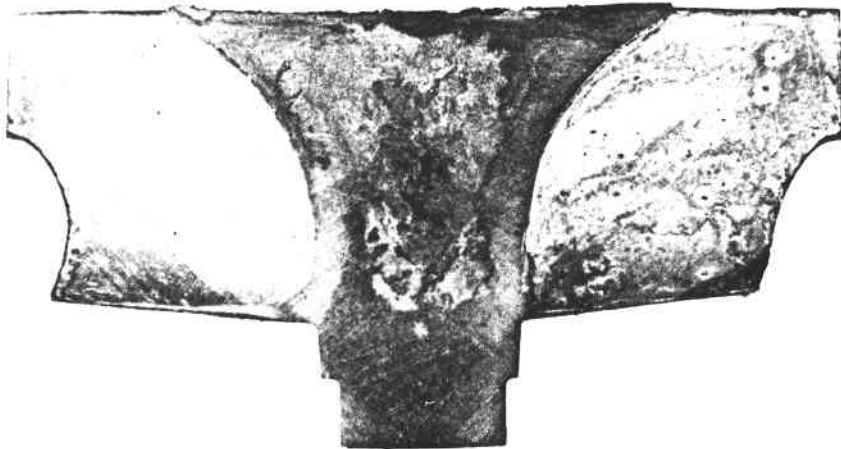Fig. 122 – Top Surface of Fine Grain Thixotropic Cast Rotor

Fig. 123 – Bottom Surface of Fine Grain Thixotropic
Cast Rotor After Siliconizing

Fig. 124 – Cross Section of Fine Grain Thixotropic
Cast Rotor After Siliconizing

Fig. 125 – Cross Section of A Thixotropic Cast Vacuum
Furnace Siliconized RBSiC Rotor

penetration was greatly improved and the entire thick section was completely siliconized. Ironically, the small diameter portion of the hub was not fully siliconized.

One rotor was siliconized with optimized furnacing conditions in a large production induction furnace with argon atmosphere. This rotor was completely infiltrated with silicon (Figure 126). There are apparently two regions: an outer layer approximately 1/8- to 1/4-inch thick which has a large amount of free silicon, and a central zone with less free silicon in the microstructure. This variation occurs because the furnace does not have good atmosphere control and even though the furnace is purged with inert gas, some air leakage occurs. The oxygen oxidizes the surface of the rotor and removes carbon. When the rotor is silicon infiltrated, there is no new silicon carbide formed at the surface from a silicon-carbon reaction. Thus the outer zone has a higher free silicon amount. Further attempts eliminated this effect. The induction furnace with argon thus demonstrated that thick sections of fine grain material can be siliconized.

4.4.2 - Shaft Attachment

Two attempts were made to attach a shaft to the rotor body. In both cases, the rotor was machined at the hub surface to accept a cast shaft in a shallow locating recess. The rotor and shaft were cast and cured separately, machined, and joined together by using thixotropic mix as a cement and filler. After curing the filler mix, the unit was furnaced in the standard way.

In the first attempt, there were voids at the interface possibly as a result of incomplete removal of machining dust.

With the second piece (Figure 127), care was taken to thoroughly clean the joining surfaces, and a finer particle size mix was used as a filler. With the exception of small casting voids near the surface of the hub, this part looked good, with complete siliconization and joining of shaft and rotor (Figures 128 and 129).

4.5 - Hot Pressed Silicon Carbide

Hot pressed alpha silicon carbide was investigated because of its potential higher strengths than sintered alpha silicon carbide.

Submicron alpha silicon carbide powder was hot pressed at 1700°C (3092°F) to 2000°C (3632°F) temperature range into approximately 1.25-inch diameter disks using four different additives as hot pressing aids. MOR bars were sliced out
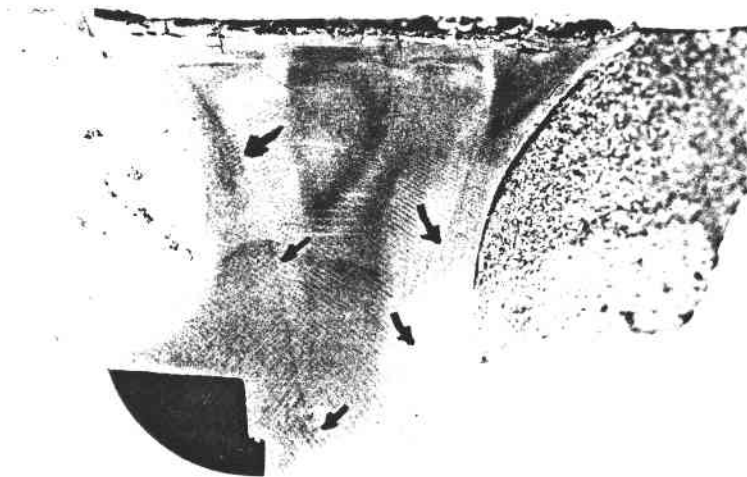
Fig.126 - Cross Section of A Thixotropic Cast Induction
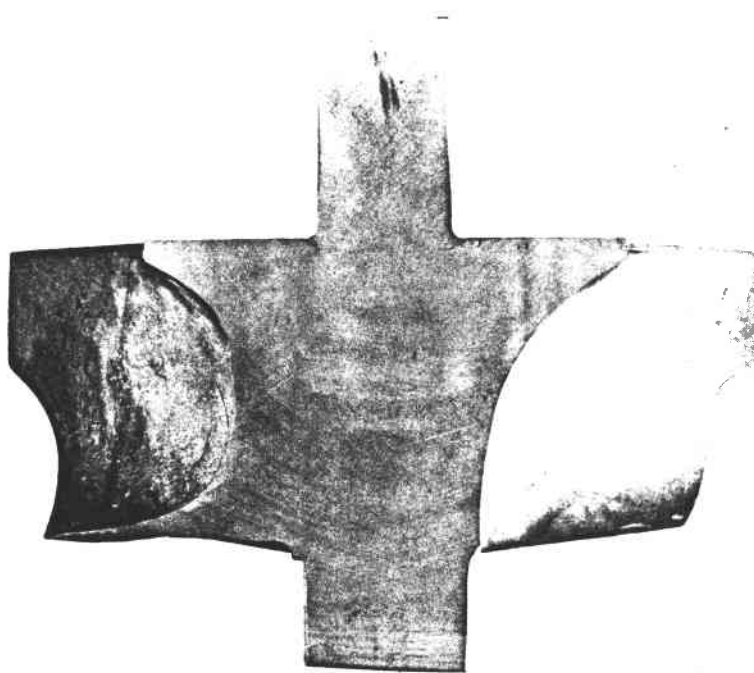Furnace Siliconized RBSiC Rotor

Fig. 127 - RBSiC Thixotropic Cast Rotor Sliced to Show Shaft
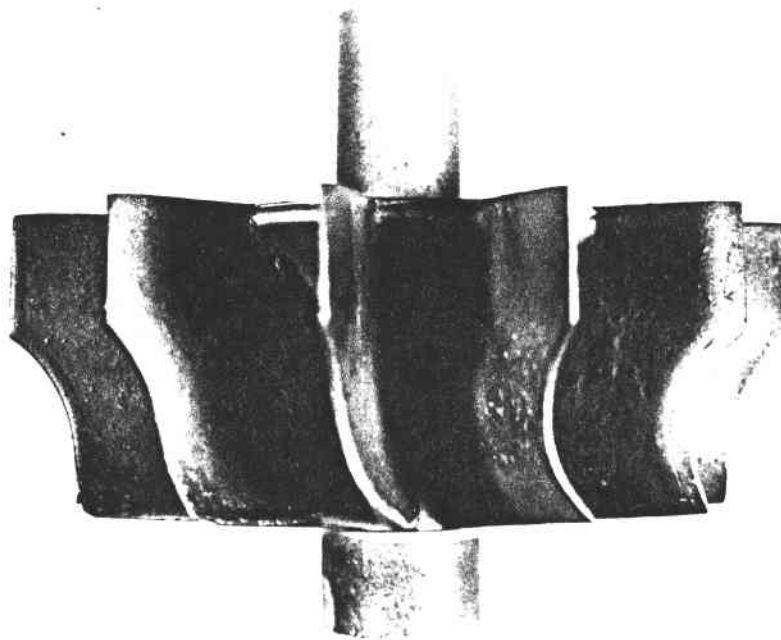Attachment and Complete Siliconization

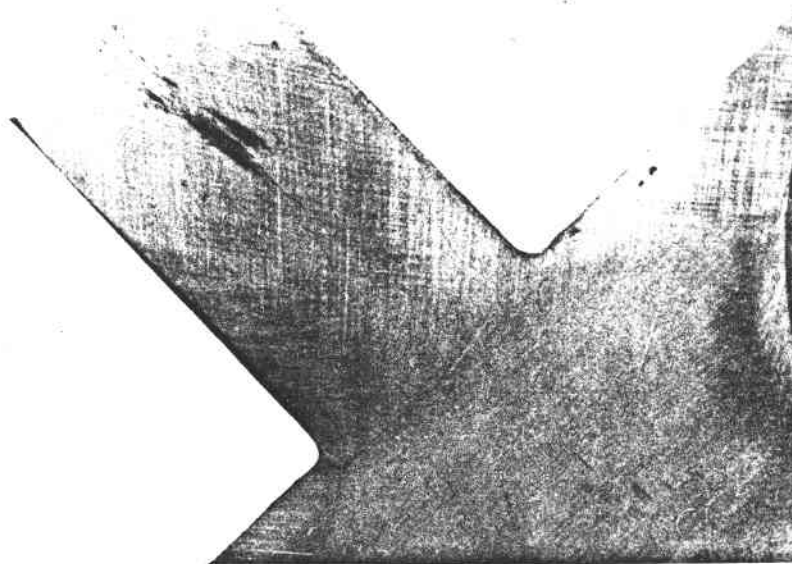Fig. 128 - Fired RBSiC Thixotropic Cast Rotor With Shaft Attached

Fig. 129 - **Close-Up of Shaft Attachment.** Apparent Crack at Left Interface Area is Light Reflective Difference in Photo. No Crack was Evident.

of these disks to 0.1" x 0.05" cross section with edges chamfered. Room temperature flexural strength was measured in 3-point bend by using a span of 0.75 inch. The effect of compositional variation is summarized in Table 20.

Table 20- Effect of Chemistry on Strength of Hot Pressed Alpha Silicon Carbide

Additive		Hot Pressing Temp, °C	Bulk Density, g/cc	Strength σ_f, ksi
1%	A	1800	3.10 - 3.15	63.68 + 5.08
1%	A	2000	3.18 - 3.19	80.85 + 5.48
1%	B	1800	3.14 - 3.17	84.78 + 18.48
1%	B	2000	3.18 - 3.19	119.96 + 13.90
1%	C	1800	2.90 - 2.94	85.01 + 4.75
1%	C	2000	3.10 - 3.15	110.06 + 14.13
2%	C	1800	3.05 - 3.10	112.40 + 7.87
2%	C	2000	3.17 - 3.18	95.90 + 2.88
2%	D	1700	3.16	67.51 + 6.70
2%	D	1800	3.20 - 3.24	103.39 + 13.58
2%	D	1900	3.20	101.85 + 13.24
2%	D	2000	3.20	107.11 + 8.82

Flexural strengths of over 100,000 psi indicate the potential of this approach. The hot pressing efforts were halted after these efforts under the common work and were transferred to an appropriate unique program. The challenge there will be to hot press thicker and larger bodies with homogeneous microstructure and to translate the high strengths obtained on specimens machined from hot pressed large bodies.

4.6 - Evaluation of CVD Coatings

Earlier Carborundum work, which has been confirmed by work done under this contract has demonstrated that a majority of failure-causing flaws are processing-related, void-like defects lying at or close to the tensile surface of a flexural bend bar. Therefore, it was hypothesized that chemical vapor deposition of silicon carbide could offer an attractive technique for potential strength enhancement.

The adverse effects of machining on strength could be significantly decreased with a theoretically dense surface coating. Additionally, the resistance of less than theoretically dense materials to various types of atmospheric attack and corrosion including oxidation may be significantly

enhanced with theoretically dense coatings. The state-of-the-art of chemical vapor deposition of silicon carbide has advanced to the point where a "final" and comprehensive evaluation of its utility for high performance structural materials should be made.

In this study, 125 injection molded test bars were fabricated and inspected, and were divided into 5 groups of 25 bars. Twenty-five (25) bars were retained as a control to evaluate strength. Thirty (30) bars each (which included 5 each for establishing coating conditions) were shipped to:

- ° San Fernando Laboratories
- ° Materials Technology Corporation
- ° Deposits and Composites, Inc.
- ° Refractory Composites, Inc.

After the bars were coated, they were tested at room temperature in 4-point bend with a 0.75-inch inner span and a 1.50-inch outer span. The complete strength results of CVD coatings on injection molded and sintered alpha SiC in the as-fired condition are as shown in Table 21. The strength of the control population is lower than the 61.5 ksi for injection molded bars reported elsewhere in this report. The bars for the CVD study were fabricated at an earlier date when 50 ksi was the strength obtained by injection molding.

Table 21- Strength Evaluation of CVD-Coated Alpha SiC Bars

Vendor	Average Coating Thickness (inch)	Number of Specimens	Weibull Parameters				
			σ_f + S.D. (ksi)	m	σ_θ (ksi)	Low σ_f	High σ_f
Control	--	25	48.86 + 5.75	8.9	51.49	34.47	60.77
DCI-Coated	0.004	24	43.89 + 8.80	4.8	47.91	22.80	59.15
MTC-Coated	0.012	25	47.47 + 5.51	9.0	49.70	35.87	55.98
RCI-Coated	0.003	20	52.52 + 7.78	6.9	56.04	37.17	63.77
San Fernando Labs (CNTD)	0.004	23	49.68 + 14.00	3.0	56.32	18.42	65.59
San Fernando Labs (CNTD)	0.004	21	52.58 + 10.65	4.9	57.31	32.02	65.59

It can be seen that the changes in both room temperature strength and Weibull modulus are mixed on CVD and CNTD coated alpha SiC bars. It should be noted that coating thickness varied significantly for specimens from the same vendor precluding meaningful comparisons. In the case of CNTD bars, two bars have unusually low strengths of 18,000 psi. Elimination of these two specimens from the group increases the Weibull modulus to 4.9. Figure 130 shows the strength levels achieved in various density ranges for CVD coated bars. For the
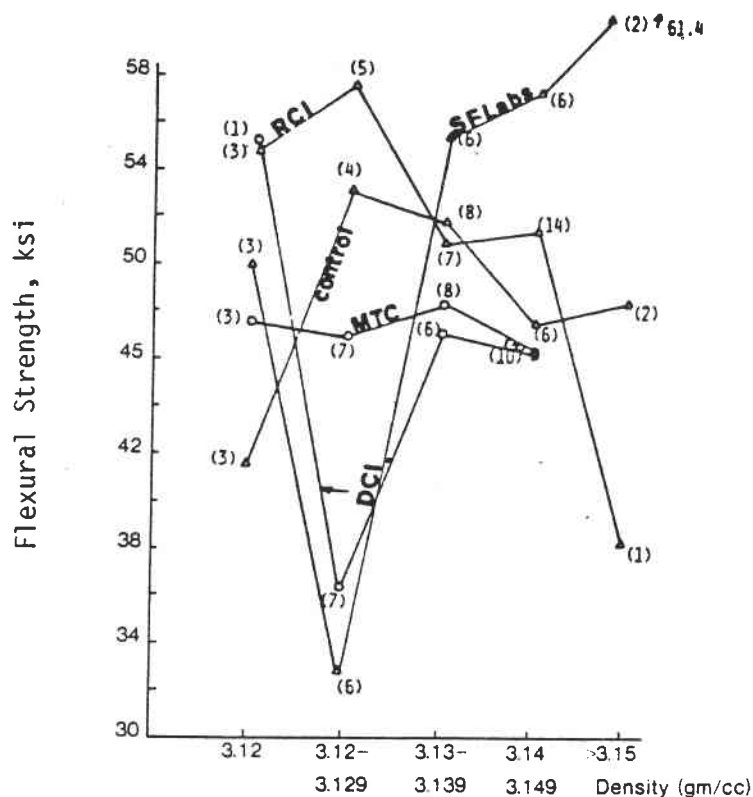
Fig. 130 - Strength Levels Achieved in Various
Density Ranges for CVD Coated Bars

RCI-coated bars, strength enhancement is observed for low density specimens.
In the case of the San Fernando Lab CNTD-coated bars, strength enhancement is
seen for all density ranges except for the 3.12 - 3.129 g/cc density range.

In Figure 131, the microstructure and failure origin for injection molded
and sintered alpha silicon carbide are shown for a control specimen. The
unetched microstructure shows micropores which are located primarily at grain
boundary triple points as revealed in the etched microstructure. The failure
origin for this specimen which failed at 60,700 psi is a processing-related
unbonded SiC inclusion. In addition to this flaw type, voids in the range of
70 to 200 μm were also seen to be failure causing in many other specimens. No
machining was performed for these control specimens and also all CVD coatings
were deposited on the as-fired surfaces of injection molded and sintered alpha
silicon carbide. In Figure 132, the nature of the coatings is examined via opti-
cal and scanning electron microscopy for MTC-coated specimens. The cauliflower-
like appearance of the deposit indicates the size of individual grains. Good
adhesion is evident with the absence of micropores in CVD SiC compared to sin-
tered silicon carbide. The columnar growth of β-SiC grains during the CVD pro-
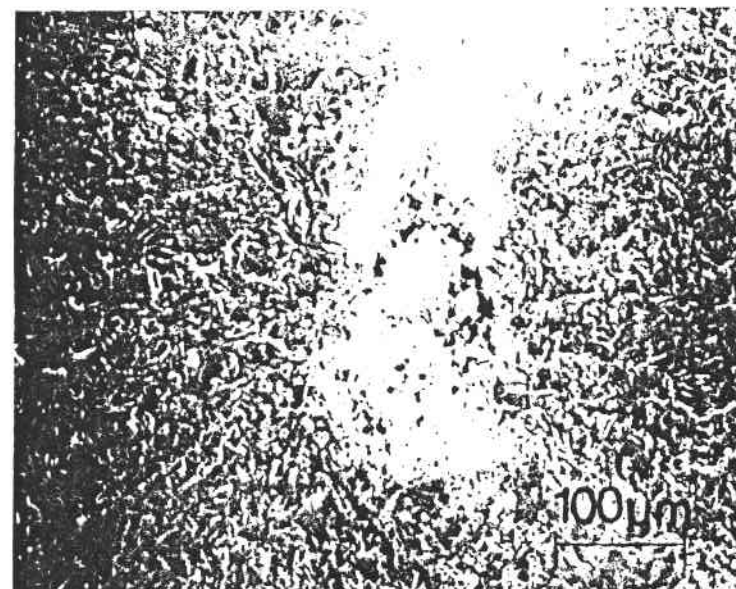cess can also be seen in one of the figures. MTC samples appeared to have the

163
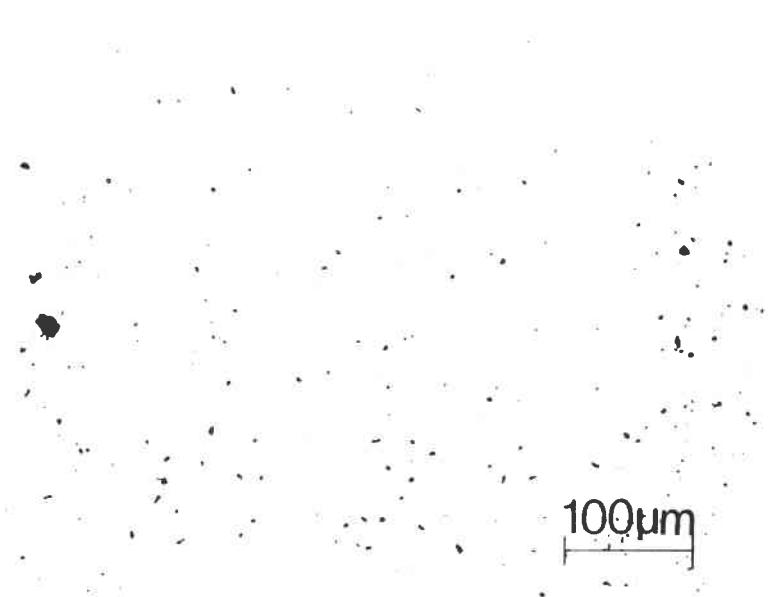
Unetched Microstructure
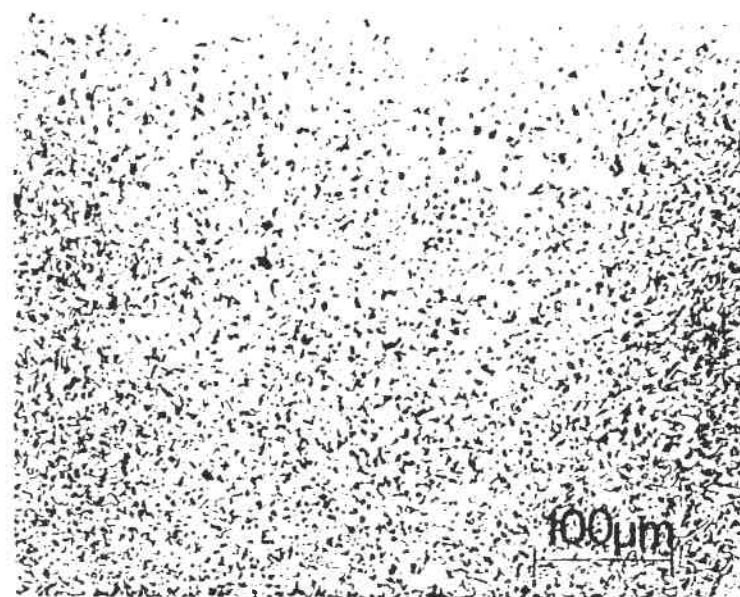
Etched Microstructure
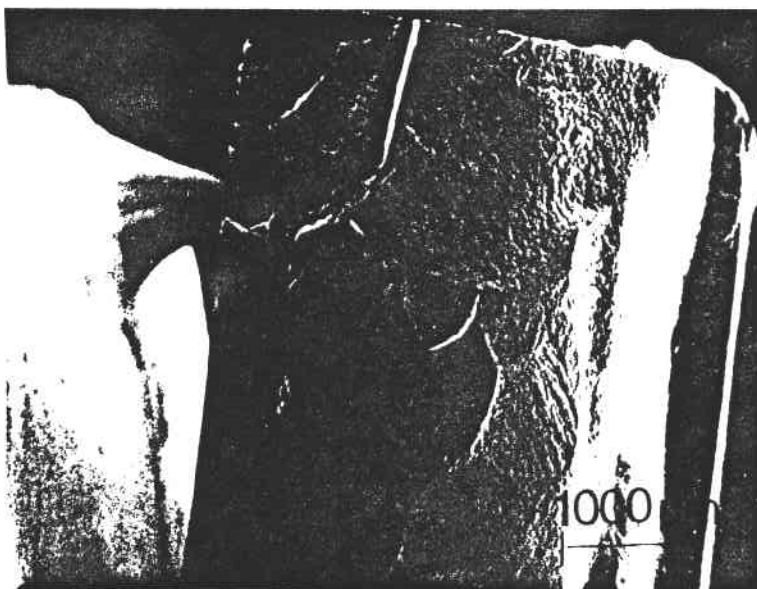
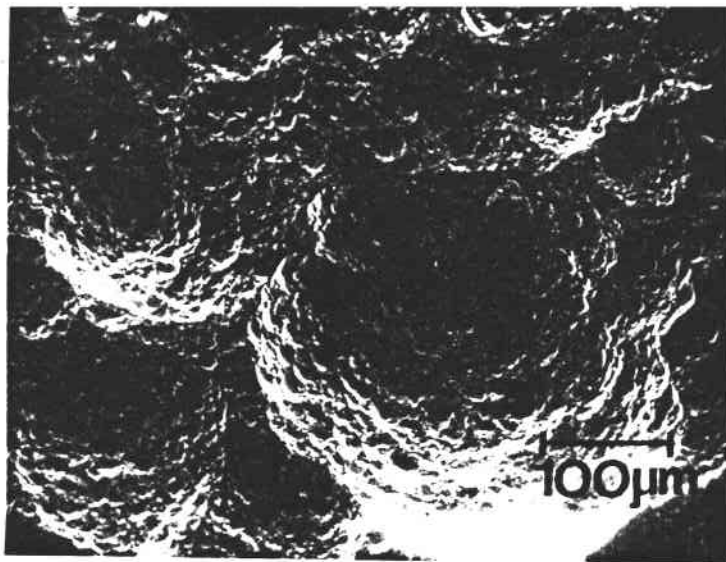
Specimen edge

Fracture Surface under SEM

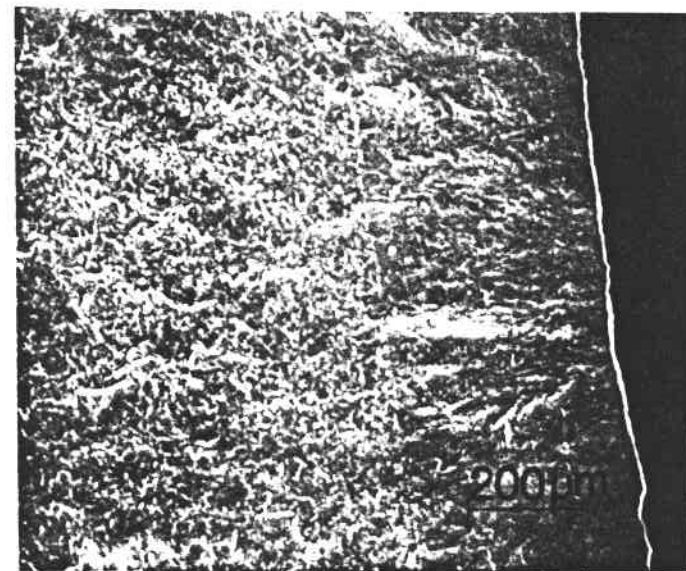Room temperature strength = 60,700 psi
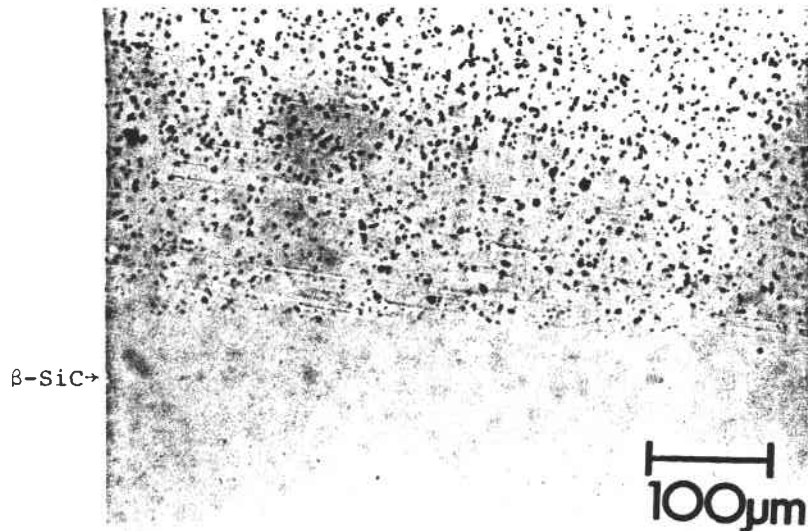S. No. 710

Internal processing-relating unbonded inclusion

Fig. 131 - Microstructures and Failure Origins for Injection Molded SiC Specimen Used as
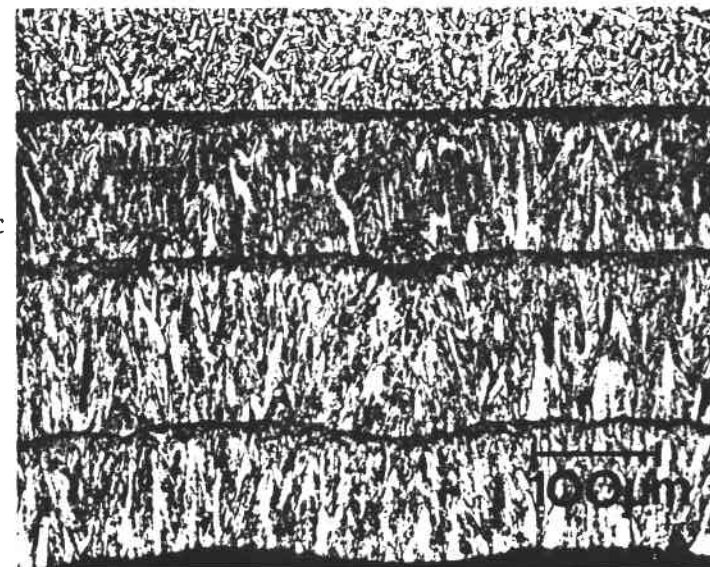
as-deposited surface (SEM)

fracture surface (SEM) σ_f=35,820 psi

←α-SiC

β-SiC→

α-SiC

← CVD β-SiC

(Unetched) Microstructure

(Etched) Microstructure
σ_f=51,970 psi

Fig. 132 - Coating Evaluation for MTC-Coated Specimens

CVD coating applied three times. On the fracture shown, no obvious processing defect can be identified despite the low strength of 35,820 psi.

In Figure 133, the coatings established by DCI are examined. Good CVD adhesion is evident. Some isolated micropores can be seen in the CVD SiC layer. The as-deposited CVD β-SiC surface shows that there exists a range of distribution of size of the CVD-SiC spheres deposited. The columnar growth of these spheres can also be seen in one of the figures. The failure origin for a specimen with a strength of 55,000 psi is shown as an internal processing-related 3-dimensional void.

The coating established by Refractory Composites, Inc. is shown in Figure 134. The as deposited surface shows the spheres smaller than the earlier cases reported. The etched microstructure confirms this hypothesis. The deposit seems to be broken at several places. The grain size and distribution of CVD β-SiC is very similar to that of α-SiC so that it is very difficult to visualize the boundary or the interface. The failure origin for a specimen shown in the figure is a processing-related internal void ($\sigma_f = 63,770$ psi).

The CNTD coating produced by San Fernando Laboratories is examined in Figure 135. The surface appearance of the coating indicates that the CNTD coating proces deposits a smoother layer of β-SiC on α-SiC substrates than other CVD processes examined. Examination of the microstructure in the unetched condition indicates good adhesion of the CNTD coating to the α-SiC substrate. The absence of micropores in the CNTD coating is noticeable. The etched view indicates that the etching conditions are not optimum for the CNTD β-SiC. The fracture origin for a specimen ($\sigma = 65,590$ psi) is shown in one of the figures to be a small void (approximately 50 μm) lying in the interior.

In summary, microscopy investigations on several selected CVD-coated specimens from different vendors have shown that:

(a) Coating thicknesses vary vastly from specimen to specimen (even among the same vendor).

(b) Coating adherence, in general, is very good.

(c) No advantage in strength enhancement is seen even in cases where fracture origin seems to be in the CVD SiC region.

Possible residual stresses introduced during the coating process can influence the fracture strengths significantly. Because no annealing was performed prior to strength testing for possibly removing or minimizing residual stresses, the absence of strength enhancement by CVD coating can be expected. In addition, in many cases processing-related voids control fracture of CVD coated bars. However, the completely dense microstructure of the coatings indicates they can perform useful sealing functions.

as-deposited surface (SEM)

CVD ⟷ ⟶ α-SiC
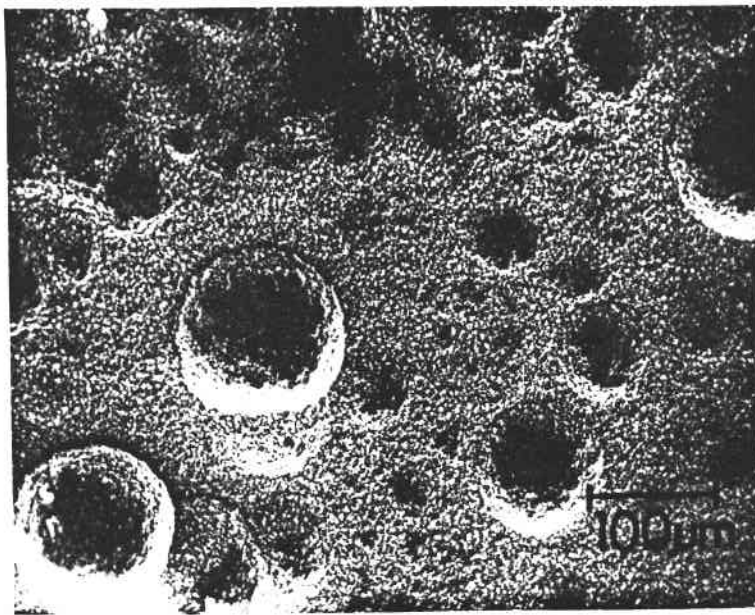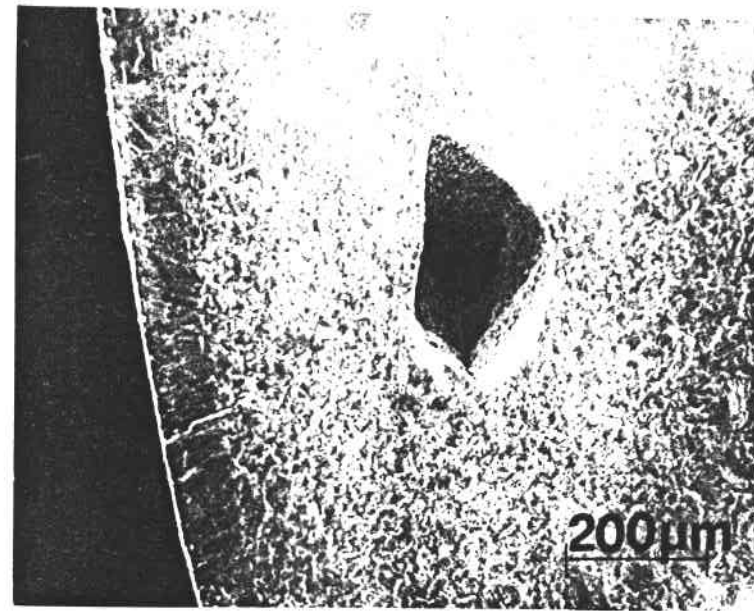
fracture surface (SEM)
σ_f=55,000 psi
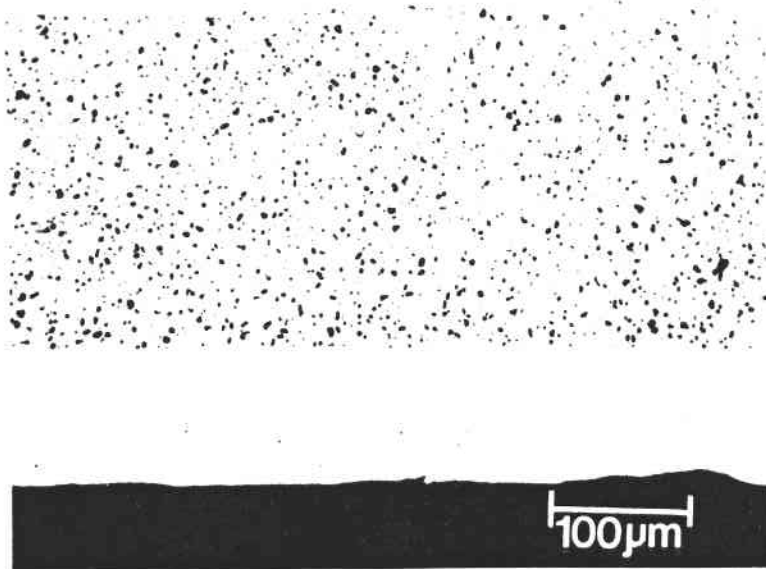
←α-SiC

←β-SiC

(Unetched) Microstructure
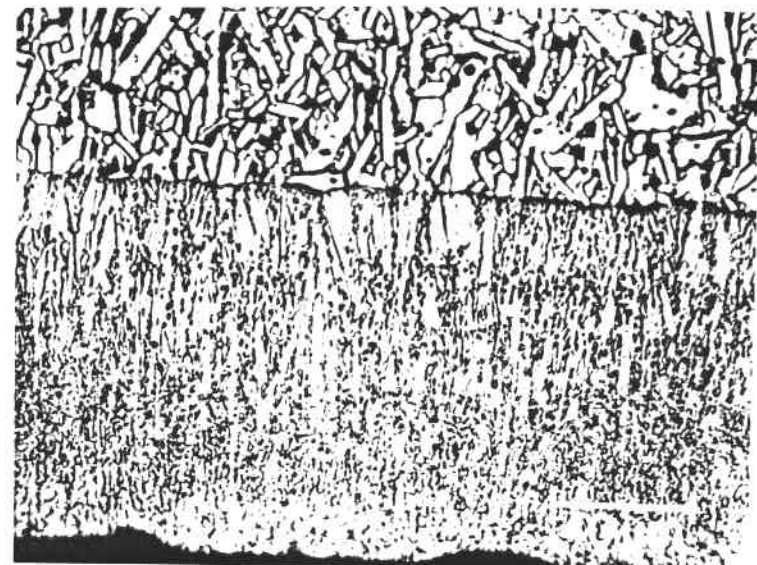
←α-SiC

CVD
←β-SiC

(Etched) Microstructure
σ_f=48,790 psi

Fig. 133 - Coating Evaluation for DCI-Coated Specimens
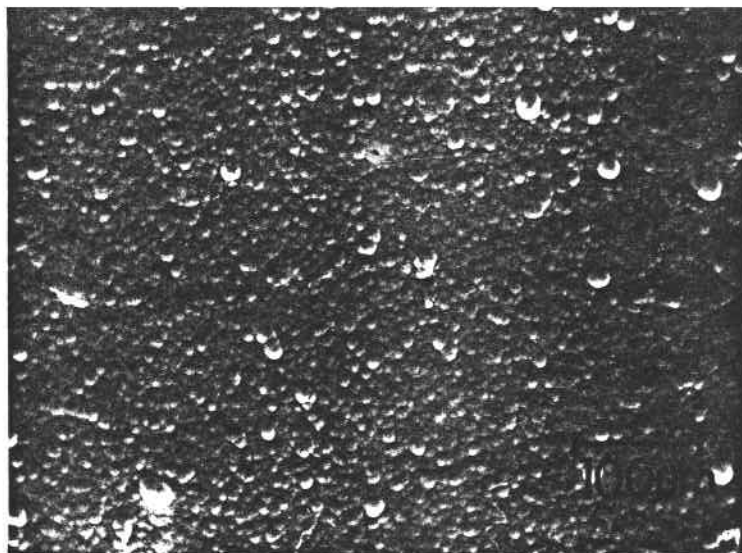
as-deposited surface (SEM)
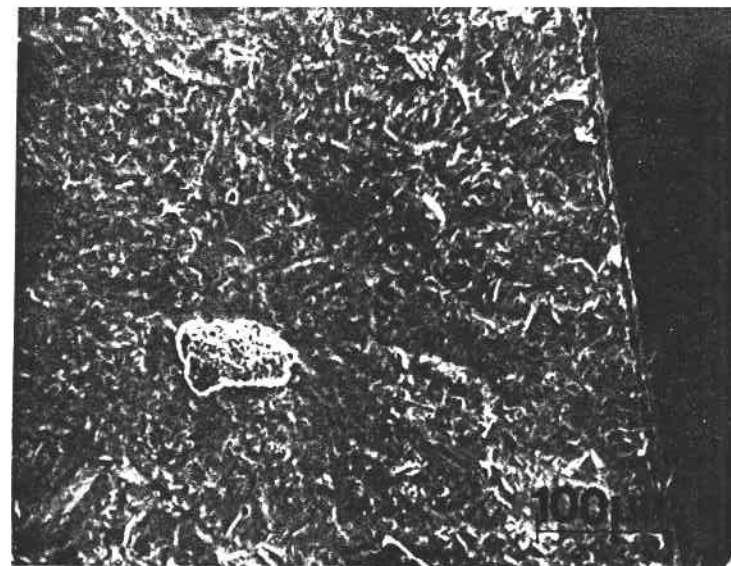
fracture surface (SEM)

σ_f=63,770 psi

CVD
Coating

← α-SiC →

← CVD
β-SiC

40μm

(Unetched) Microstructure

← CVD
β-SiC
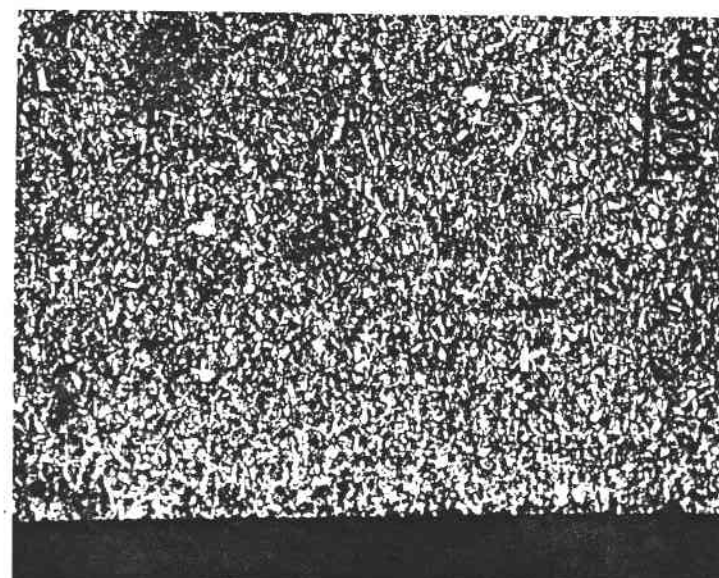
(Etched) Microstructure

σ_f = 58,540 psi

Fig. 134 - Coating Evaluation for RCI-Coated Specimens

as-deposited surface

|← CNTD coating →| ←——— α-SiC
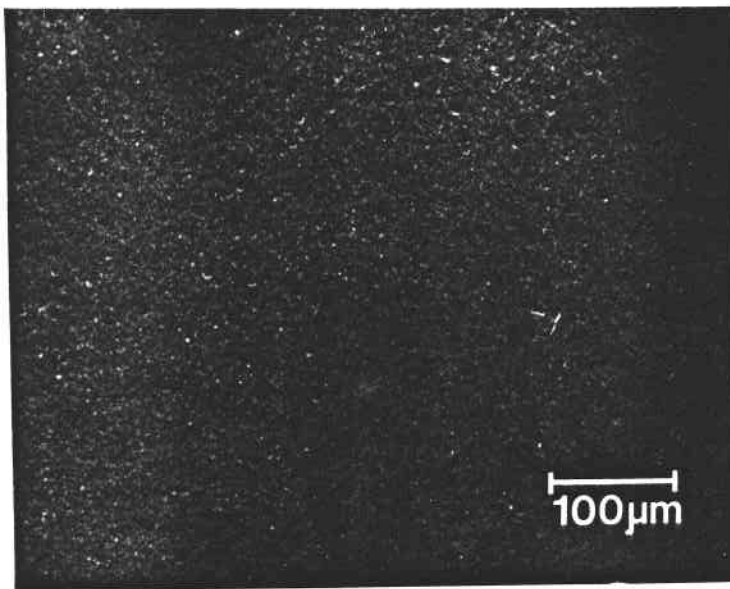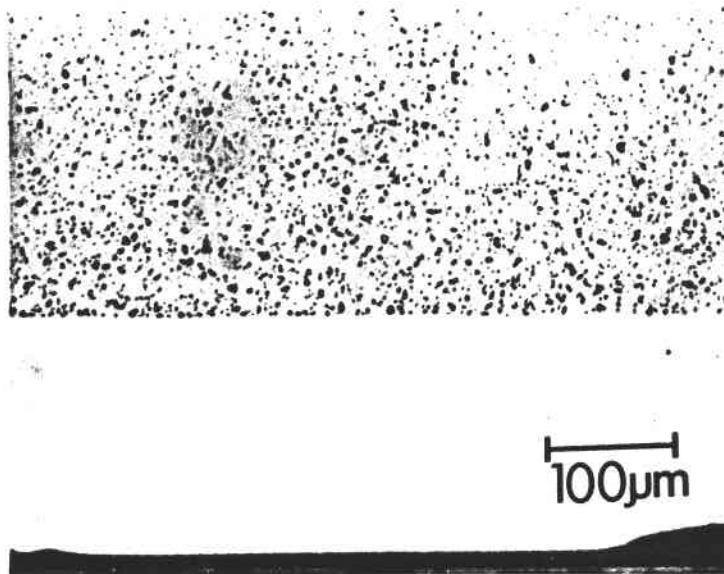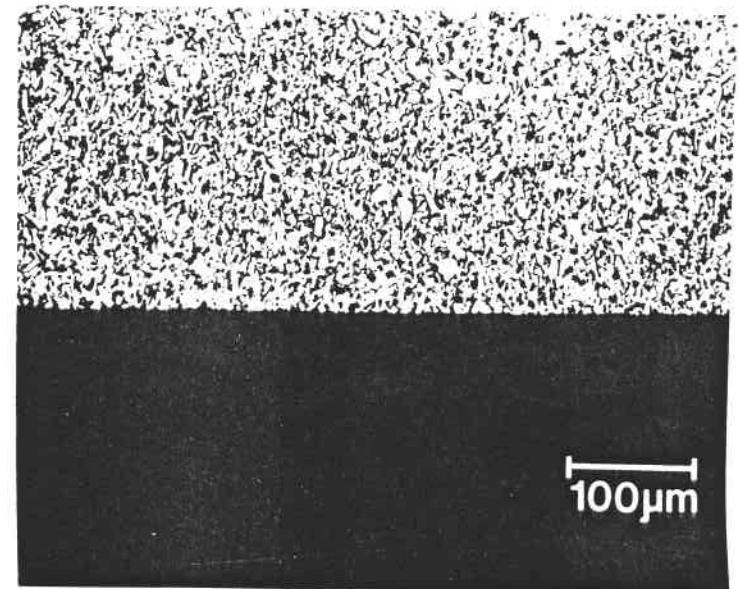Fracture Surface (SEM)
σ_f=65,590 psi

← α-SiC →

← CNTD →
Coating

(Unetched) Microstructure

Internal processing-related unbonded inclusion
σ_f = 63.640 psi

Fig. 135 – San Fernando Laboratories CNTD-Coating Evaluations

4.7 - Hot Isostatic Pressing (Hipping)

Application of hot pressing techniques to powdered ceramics normally makes densification possible at lower temperatures with fewer additives. Hipping typically yields a finer, denser, more homogeneous microstructure with minimal grain boundary phases and concomitant higher strength and enhanced high temperature properties. Hot isostatic pressing has been extensively developed for metal and carbon-carbon composite processing with significant property improvements. Application of this technique to ceramics has been restricted by the lack of high temperature (greater than 1500°C) autoclaves and appropriate non-reactive canning techniques. This program will take advantage of rapidly developing technology and the latest high temperature vessels. The first phase of the program will evaluate densification by the "open" process by processing partially sintered silicon carbide with various densities and hence decreasing amounts of open porosity.

Earlier in the program, a microstructural analysis was completed on hipped bars which were earlier hipped at NASA. The results have indicated that:

(a) No apparent microstructural improvement over "as-received" material for specimens hipped at 1750°C or 1850°C;

(b) Some indication of pore shrinkage in specimens hipped at 1950°C; and

(c) No excessive grain growth at any of the temperatures utilized in hipping.

The microstructural examination indicated that future hipping effort should perhaps be directed to higher temperatures (+1900°C) with varying hold times.

Additional experiments were attempted at 1900-2000°C at 15-30 ksi using NASA-Lewis facilities.

Several plates of sintered alpha silicon carbide supplied by Carborundum were returned by NASA after hot isostatic pressing at Lewis Research Center. The details of hipping are given in Table 22. Hipping did improve the bulk density of initially 88-92 percent dense sintered alpha SiC. For plates which were initially 98 percent dense, hipping further increased the density by approximately 1 percent. The water accessible surface-connected porosity decreases significantly by hipping even on low density (88-92% theoretical) plates-- indicating potential for surface flaw healing by hipping. Densities of plates hipped at 2050°C are very impressive.

Test bars, 0.125" x 0.250" x 2.6", were cut from hipped plates. Careful bar location identifications in the plate were kept and the bars were returned to NASA for SLAM NDE and correlation with NDE of plates. After the bars were received subsequently from NASA, they were tested in 4-point bend with an inner span of 0.75 in. and an outer span of 1.50 in. at 25°C and 1200°C. Fifteen (15) specimens were tested at each temperature to serve as control. The 25°C

170

Table 22 – Results of Hipping Plates of Presintered Alpha Silicon Carbide

Plate No.	Hip Conditions	Initial Density (gm/cc)			Hipped Density (gm/cc)		
		Carbo	NASA	Apparent Porosity (%)	Carbo	NASA	Apparent Porosity (%)
D646-14-2	2050°C, 20K, 2 hrs	2.836	2.820	10.27	2.842	2.821	3.24
646-33-2	2050°C, 20K, 2 hrs	2.927	2.950	4.62	3.012	2.991	0.36
D646-18-1	2050°C, 20K, 2 hrs	3.084	3.063	0.27	3.172	3.161	0.00
D646-11-4	1950°C, 20K, 2 hrs	3.162	3.134	0.04	3.180	3.164	0.01
D646-12-7	1950°C, 20K, 2 hrs	3.153	3.131	0.00	3.179	3.162	0.01
D646-13-8	1950°C, 20K, 2 hrs	3.160	3.142	0.00	3.177	3.167	0.01
D646-13-9	2050°C, 20K, 2 hrs	3.155	3.136	0.00	3.187	3.173	0.00
D646-13-10	2050°C, 20K, 2 hrs	3.152	3.126	0.00	3.187	3.168	0.00
D646-13-11	2050°C, 20K, 2 hrs	3.154	3.132	0.00	3.188	3.172	0.00

NOTE: Carborundum densities measured by water immersion method. NASA used dimensional method.

flexural strength was 48.51 ± 6.51 ksi while at 1200°C, the strength was 54.07 ± 6.33 ksi. The specimens had an average density of 3.15 g/cc (98 percent theoretical). Ten (10) bars of hipped material (1950°C, 20 ksi, 2 hours) have an average flexural strength of 48.04 + 7.47 ksi under similar test conditions. Thirteen (13) bars of hipped material (2050°C, 20 ksi, 2 hours) exhibited an average strength of 50.85 ± 6.82 ksi. Based on these data, it thus appears that an improvement in room temperature strength cannot be achieved for initially 98 percent theoretically dense sintered alpha silicon carbide. Similar results have been reported by G. Watson of NASA Lewis Research Center, Cleveland.†

4.8 - Major Conclusions in Rotor Fabrication Effort

(a) Molding, baking, and sintering of rotor segments made with the modified tool were achieved with a minimum of visual defects. These segments were used for joining development studies by hot pressing.

(b) For sintered alpha SiC, thick section binder removal technology has not been demonstrated using the injection molding tooling available for the common program.

(c) Successful joining of rotor segments was achieved by hot pressing using an extrudable silicon carbide mix at the interface. Consistently high densities (3.13 g/cc) for the final assembly were obtained. Grain growth across the joint interface was also observed by optical microscopy. In test bars, base material or joint material failure occurred in many instances rather than the joint failure. (Caution: Testing was 4-point bend, and not tension).

(d) Significant progress was made in the thixotropic casting of reaction bonded silicon carbide rotors. Using a mix with an optimized carbon content resulted in crack-free casting, and curing and complete siliconization.

(e) A shaft attachment to a thixocast reaction bonded silicon carbide rotor by using a thixocast reaction bonded silicon carbide mix was successfully demonstrated. Visual examination revealed the bonding to be excellent.

(f) It was demonstrated that hot pressing is a viable approach to achieve higher strength in a rotor core.

---

† Most recent results are contradictory, however. This discrepancy has been attributed to surface contaminaton of the earlier bars during hipping (G. Watson, personal communication, May 1981).

(g) Hipping of an initially 98 percent theoretically dense sintered alpha silicon carbide can increase the bulk density of approximately a percentage point; however, no improvement in room temperature strength was demonstrated.

(h) The chemical vapor deposition (CVD) coatings of SiC on injection molded sintered alpha silicon carbide test bars did not change the resulting strength significantly. However, excellent adherence of CVD and CNTD SiC to substrate alpha SiC was observed.

5 - NON-DESTRUCTIVE EVALUATION

One of the objectives of the advanced NDE effort in the AGT common pool was to apply the existing advanced NDE technology for flaw detection, and characterization to candidate SiC materials. The NDE tasks involve the fabrication of seeded defect specimens and evaluation by different NDE techniques such as x-ray radiography, high frequency ultrasonics, scanning laser acoustic microscopy, and scanning photoacoustic spectroscopy.

5.1 - Seeded Defect Disks

Because voids, carbon, and boron carbide inclusions are the critical defects which limit the as-fabricated strengths of sintered alpha silicon carbide, these were the defects which were intentionally seeded in disks of thicknesses ranging from 0.1 to 0.5 inches. Initially, we also had a specimen fabrication effort with small defects (25-50 μm) in the program. However, the seeding of individual defects of this size proved to be impossible by using the existing techniques. It was then decided that because of the fact that there exist many naturally occurring defects of this small size in sintered alpha silicon carbide, an examination of control specimens will yield useful NDE information.

5.2 - Microfocus X-Ray

Disks with intentionally fabricated voids, B_4C and carbon inclusions were examined with microfocus x-ray. The results are given in Table 23.

The results are very encouraging, especially in the 50-125 μm size defects. Destructive sectioning of a 0.1-inch thick seeded defect (void) disk was continued in order to correlate with the microfocus x-ray indications. This disk was seeded with voids in the range of 50 to 125 μm. The maximum defect lengths (in the x-ray direction) have been 110 μm, 130 μm, 160 μm, and 190 μm for a series of five (5) defects (Figure 136). In addition, two voids of 90 μm maximum diameter were also seen on sectioning which were not detected by microfocus x-ray. These observations have confirmed our detection sensivity to be 4.3-3.5 percent of section thickness examined. However, this detection capability is at the cost of time. At 30 kV, the shots take about 22.5 minutes at a 15-inch focal spot to film distance. At 45 kV, the time drops to 4 minutes at a 20-inch focal spot to film distance. The 50-125 μm voids are clearly seen at 30 kV source voltage and the indications are only vague at 45 kV.

Table 23 - Detection of Defects in Seeded Disks of Sintered
Alpha SiC by Microfocus X-ray

Disk Thickness (inch)	Void Size (μm)		Carbon Inclusion Size (μm)		B$_4$C Inclusion Size (μm)	
	50-125	125-250	50-125	125-250	50-125	125-250
0.1	D	D	D	D	PI	D
0.125	D	D	D	D	ND	D
0.25	ND	D	--	D	--	D
0.50	--	D	--	D	--	D

D = Detected
ND = Not Detected
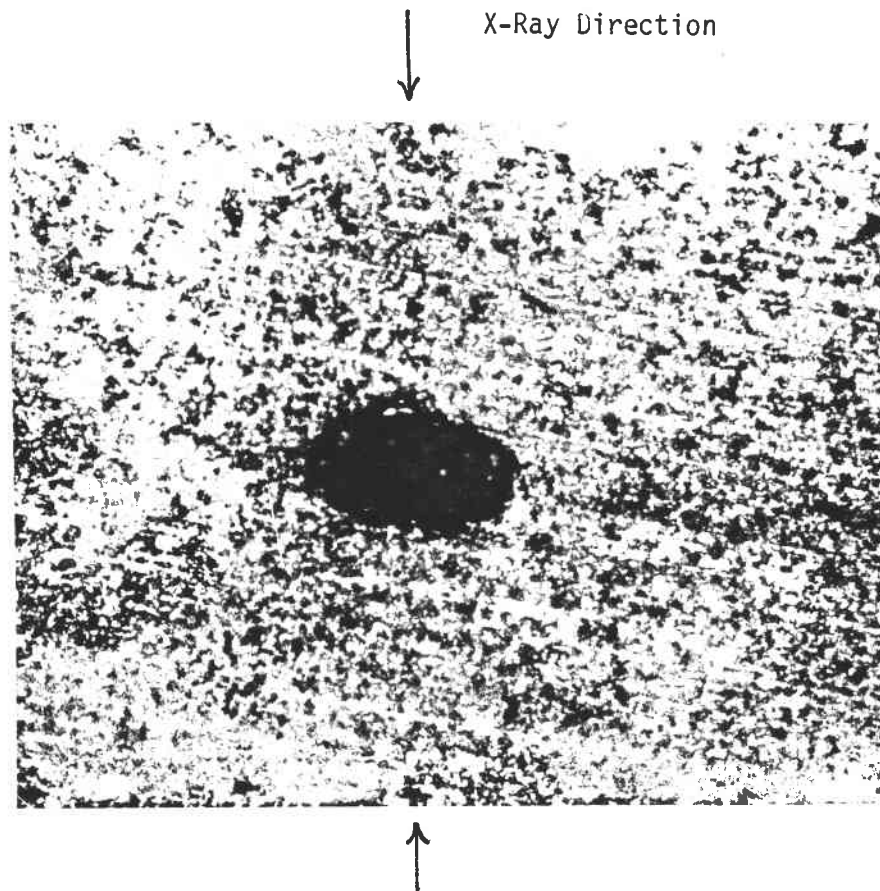PI = Possible Indication

X-Ray Direction

Fig.136 - Appearance of a 100 μm Void Detected by Microfocus X-ray

5.3 - Ultrasonics

Two seeded disks were examined by an ultrasonics technique using a 50 MHz beam. The results of a C-scan and some selected areas of an A-scan are shown (Figures 137 and 138). The disks were examined two times each and excellent reproducibility in defect imaging was seen. Many more defects were detected in addition to the seeded defects. The defect location of the seeded defects was the same as the expected location in some cases, and in some cases it was not.

A 2" x 2" x 0.37" plate of sintered alpha silicon carbide which was fabricated with large voids (approximately 250 μm) was examined both by microfocus x-ray and high frequency pulse-echo ultrasonics. At 55 kV and 0.5 ma, with a focal spot to film distance of 28 inches and a 15-minute exposure, no x-ray defect indications could be identified. However, when this plate was examined with 36 MHz ultrasonics, several defect indications were observed as seen in Figures 139 and 140.

The plate was scanned from both sides and for each side, two successive scans were made to ascertain reproducibility. Therefore, in the copy reproduction, two indications may actually correspond to one single defect due to slight differences in recorder pen repositioning. The two scans often overlapped. Very good correspondence was thus observed. In order to document the consistency in the defect locations, some defects were marked with edges marked with numbers for proper superimposition.

All the indications in the C-scans may not always be due to the existence of defects. In fact, because of the nonparallel specimen surfaces of the as-fired sample, the gate location was affected with respect to the front and back surface. The non-equal distances at different points (ultrasound travel length) of the front and back reflections causes the echo to move back and forth in the time domain of the gate (A-scan) and can trigger the pen (exceeding the peak threshold detection) on the X-Y plotter (C-scan). This can be observed as long lines in Figures 139 and 140. It should be noted that the C-scan is larger than the plate cross section by virtue of the magnification obtained by using the plotter range calibration. Because the beam width was 2 mm and the pen in the plotter dictates the size of dots in the C-scan, the general size of the flaw indication should not be construed as being representative of the actual flaw size.

The streaks observed in the C-scan depend very much on the attenuation characteristics. For example, in one test bar which was examined (Figure 141), a one-digit change in attentuation dramatically changed the number and the length of the indications in the C-scan. Until plates are cut through indicated defects and correlated, these defect indications should be interpreted with caution.
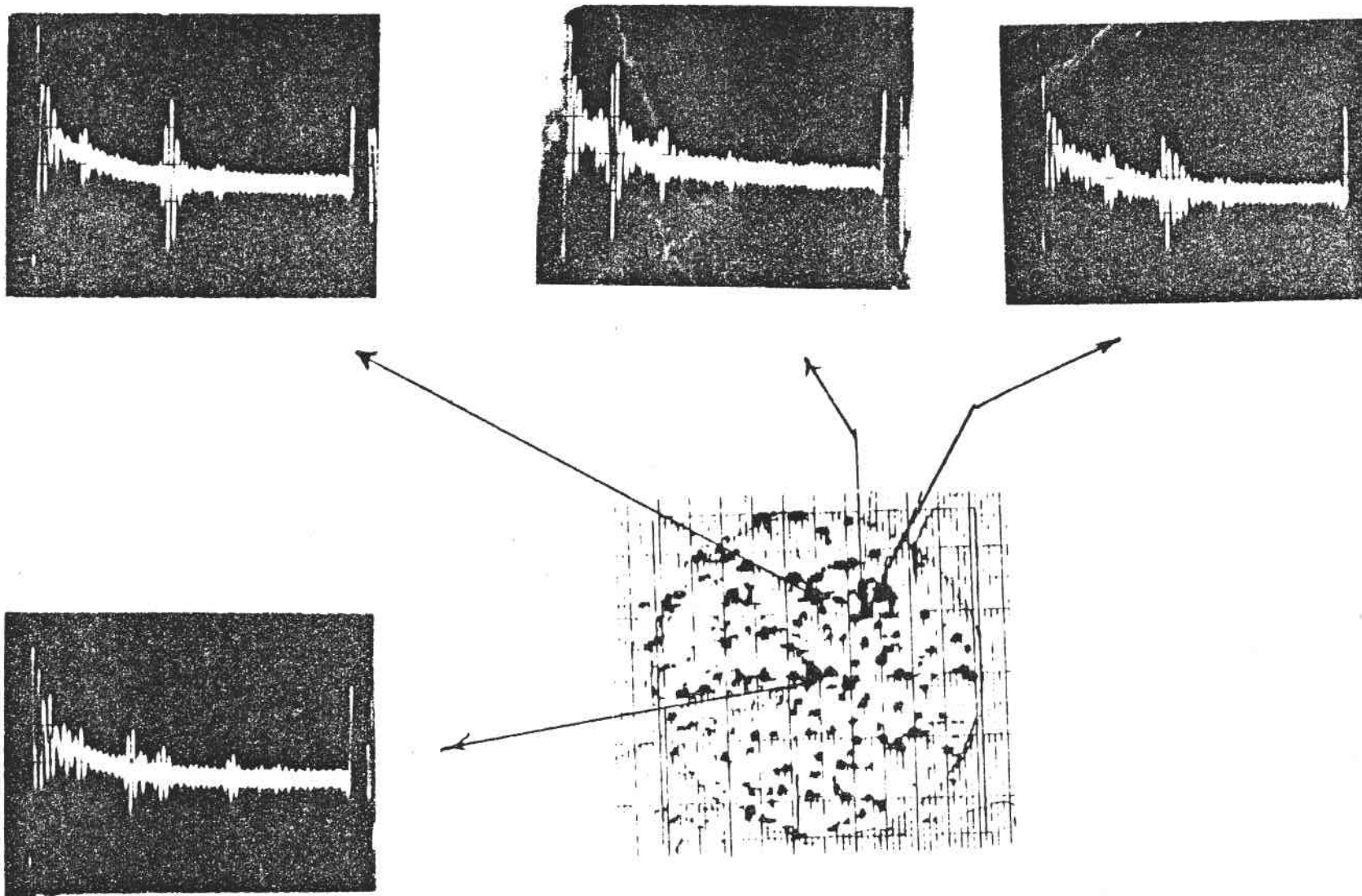
176

Fig. 137 - Ultrasonic A- and C-Scans for 0.50" Thick Disk of Alpha SiC Containing Seeded
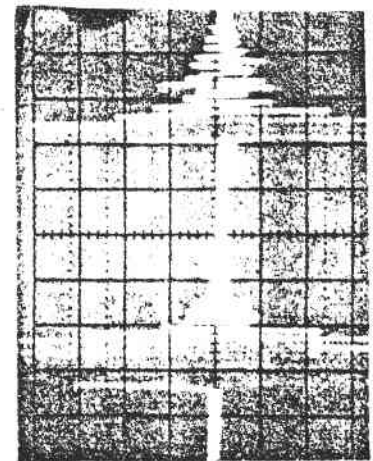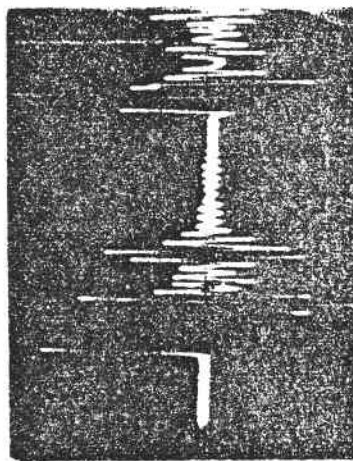125-250 μm Voids. Longitudinal Wave Velocity, $V_\ell = 11.80 \times 10^3$ m/s
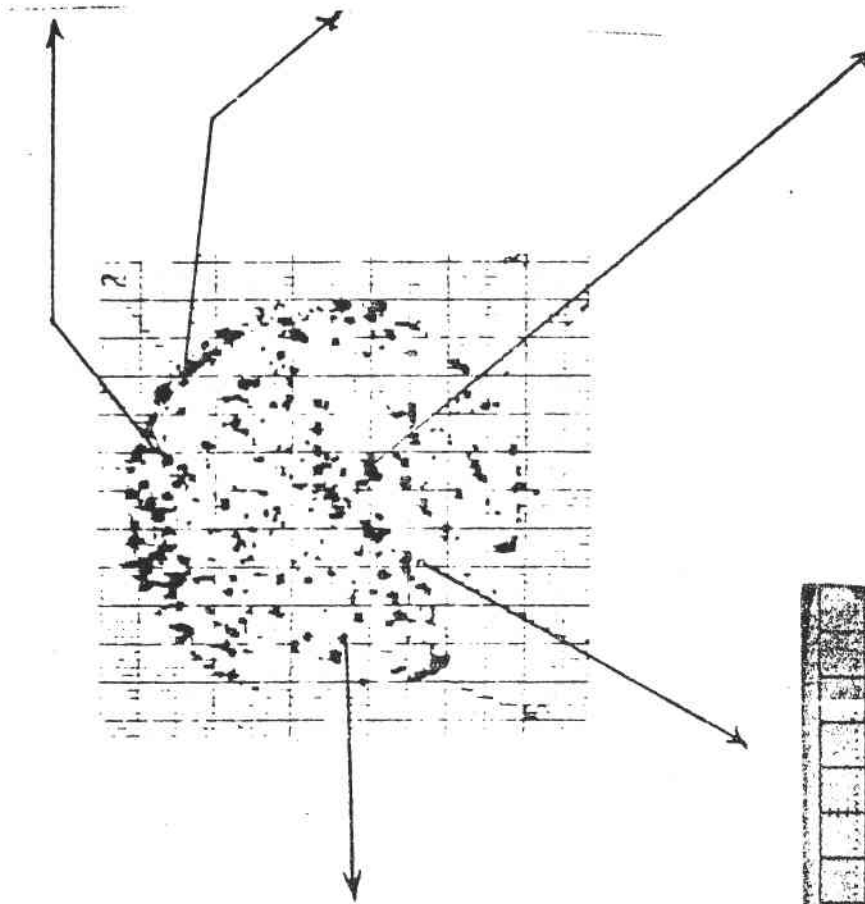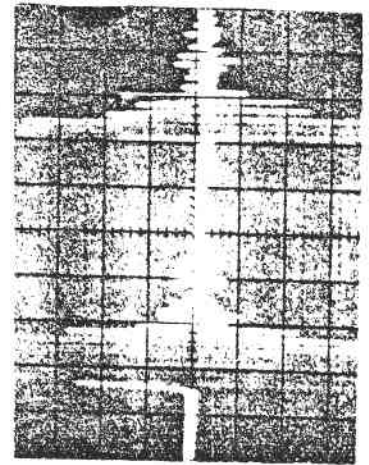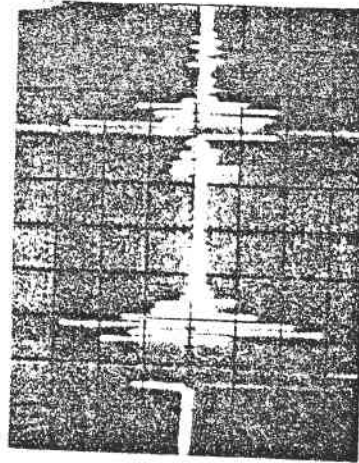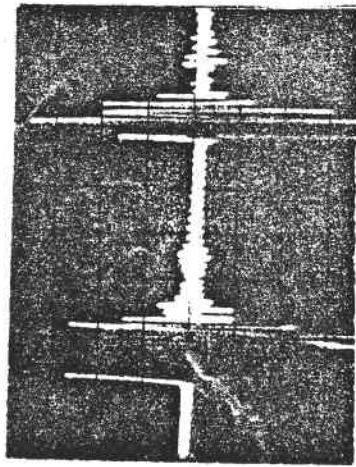
Fig. 138 - Ultrasonic A- and C-Scans for 0.25" Thick Disk of Alpha SiC Containing Seeded
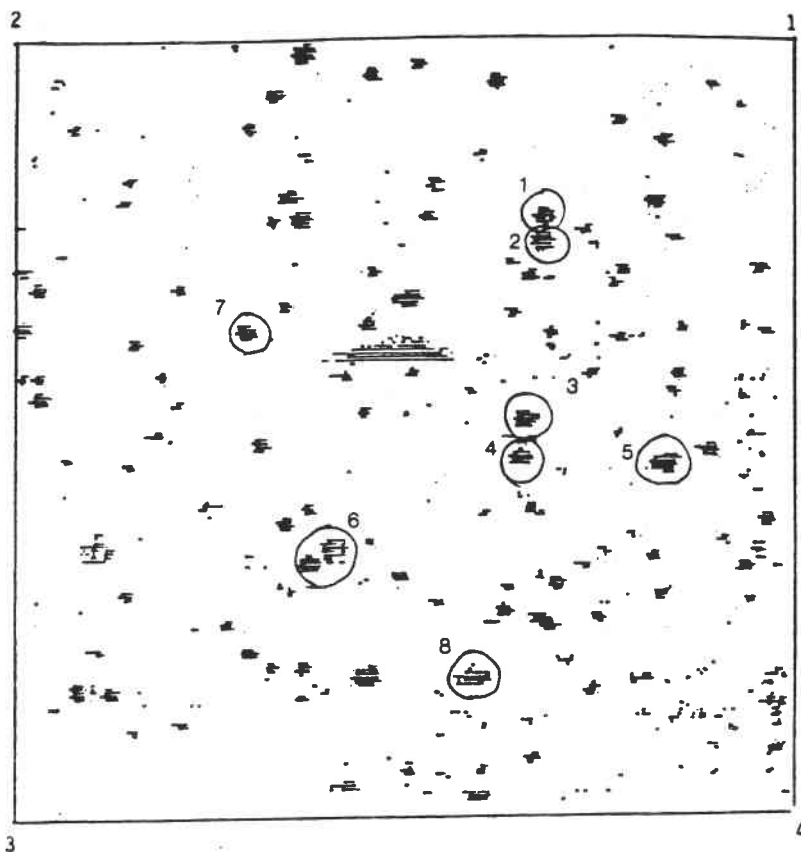
178

Fig. 139 – Ultrasonic C-Scan of Seeded Void Plate at 36 MHz.
The Scan Was Performed Twice and Good Consistency in
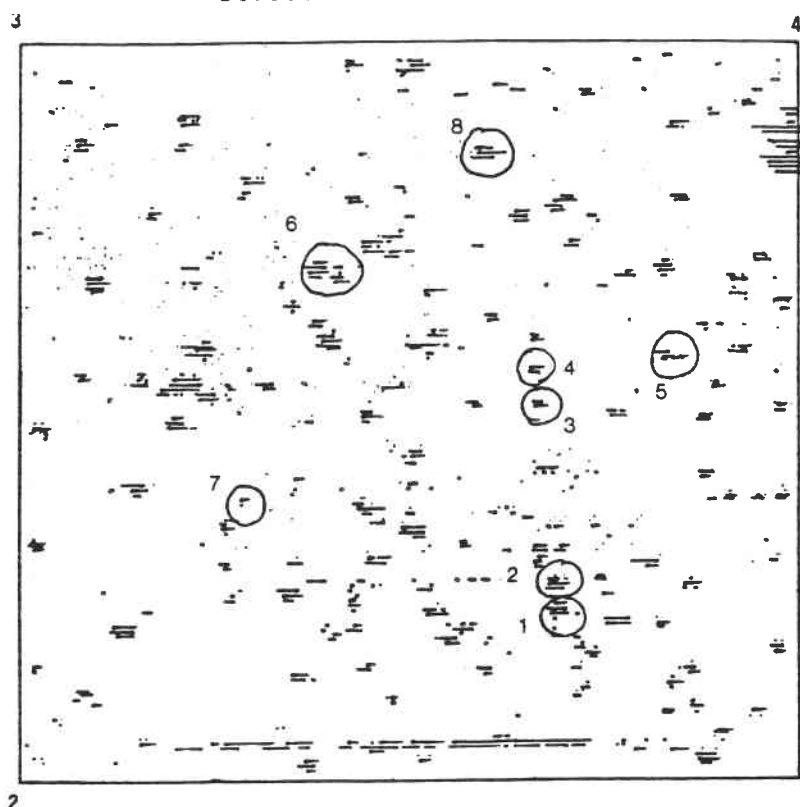Defect Detection Was Seen

Fig. 140 – Ultrasonic C-Scan of Seeded Void Plate at 36 MHz
Corresponding to Figure 139 With Transducer on the Opposite Face
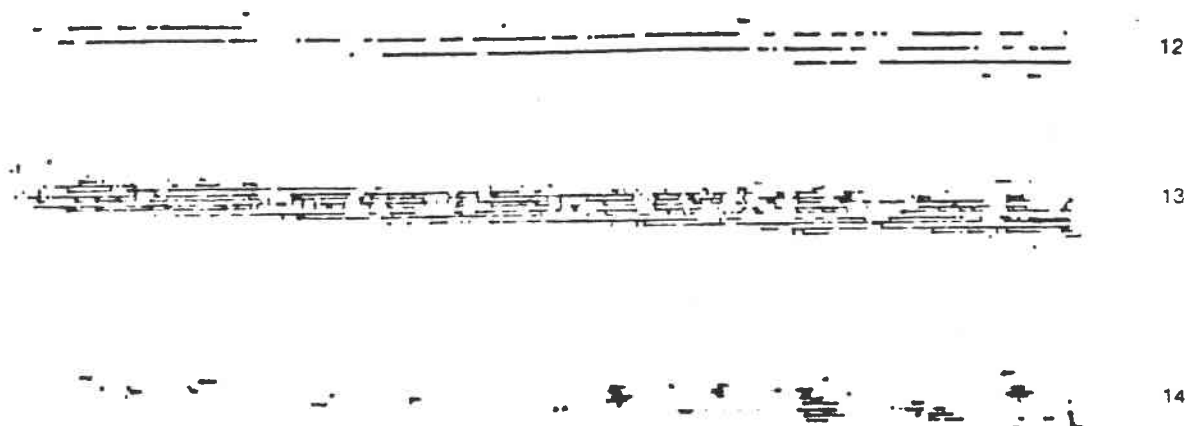of the Plate

179

12

13

14

Fig. 141 – Effect of Attenuation Selection Characteristics on the C-Scan Indications for Alpha Silicon Carbide Test Bar

5.4 – Scanning Laser Acoustic Microscopy (SLAM)

The SLAM work was performed by Sonoscan, Inc. on a separate subcontract. Sonoscan examined the following silicon carbide articles:

I. Flexural Bars
    (a) Reaction sintered
    (b) Sintered

II. Seeded Disks (Sintered Alpha)

III. Turbine Components
    (a) Reaction bonded vanes
    (b) Injection molded alpha SiC vanes
    (c) Injection molded alpha SiC blades

5.4.1 – Reaction Bonded Flexural Bars

All samples were found to be compatible with the SLAM operating at 100 MHz and high resolution images were obtained.

All samples contained a large linear flaw which is typically a millimeter wide and several millimeters in length, oriented parallel to the bar's long axis. This flaw was peculiar in that its visibility was sensitive to the insonification direction.

180

Acoustic background structure in the bars is substantially "cleaner" than that found in the seeded disks, but similar to that of the RBSiC vanes.

In the ten samples investigated, surface flaws, buried flaws and microstructural variations were located and photodocumented. Flaw density was 3 to 4 flaws per bar (data on a 1.0-inch long segment centered on the bar).

An example of the documentation is shown in Figure 142.

The sketch presented indicates the location of flaws found in flexural bar 175. Micrographs illustrating the typical structure, as well as two zones containing flaws are presented in Figures 143 and 144. In addition to the documented features, several small surface pits were also observed. Those that were most visible acoustically are presented in the sketch (the dots).

It should be noted that unless otherwise stated, the micrographs were obtained at a sound frequency of 100 MHz. The field of view is 2.3 by 3.0 mm.

5.4.2 - Sintered Alpha SiC Flexural Bars

All samples were found to be compatible with the SLAM operating 100 MHz and high resolution images were obtained.

No major microstructural changes or peculiar flaws (like that of RBSiC bars) were found.

Acoustic background structure is substantially "cleaner" than that of the seeded discs, but similar to that of the sintered blades and vanes.

In the ten samples investigated, surface flaws, and buried flaws were located and photodocumented. Average detected flaw density is 2 to 3 per bar (data on an 1.0-inch long segment centered on the bar).
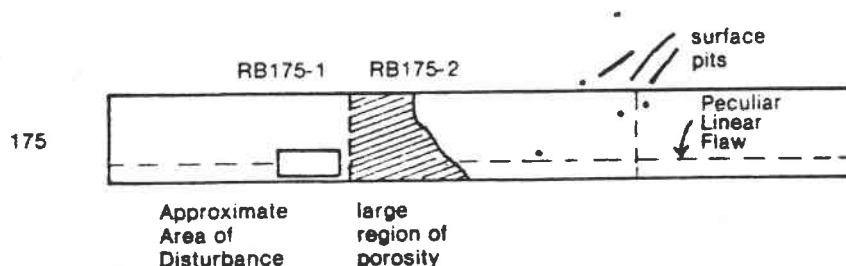
Fig. 142 - RBSiC Bar 175
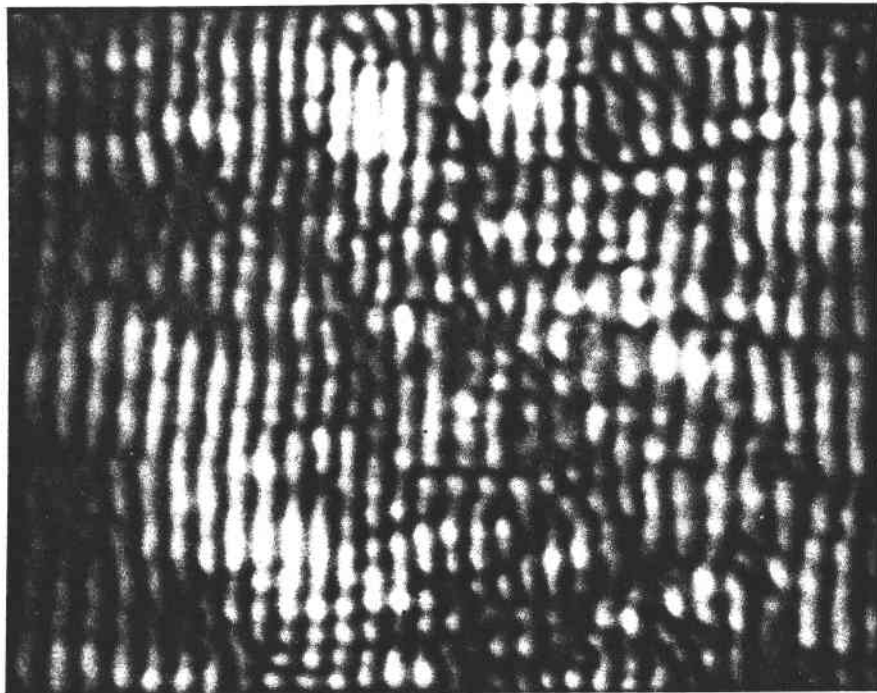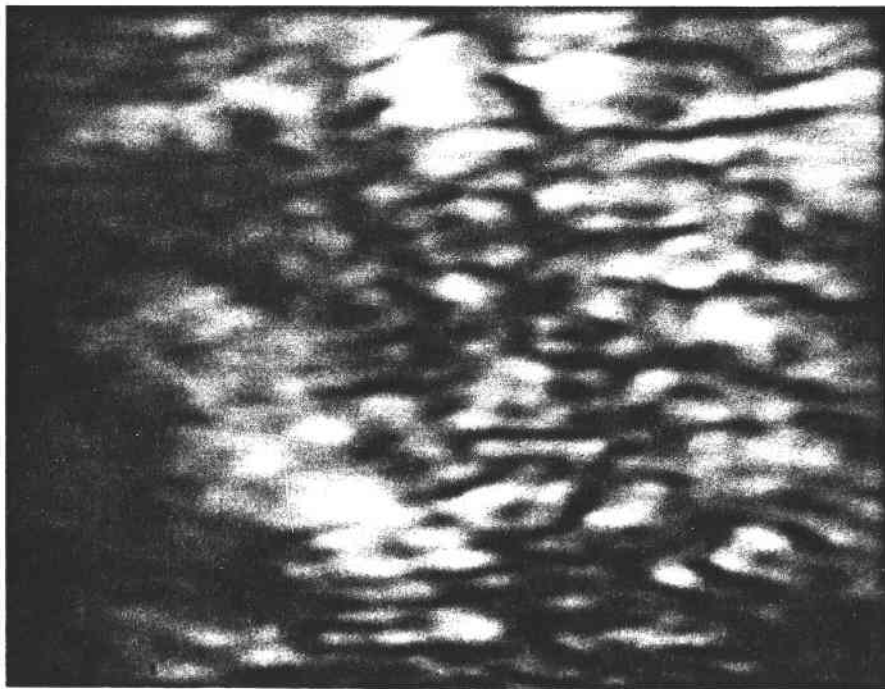
Fig. 143 - Acoustic Micrographs - Bar 175, Outside Region

Figure 143 was taken in the region outside of the central area of the bar. This zone contains considerable structure and a scrambling of the interferogram fringes. This may correspond to a region of unreacted material.

182

Fig. 144 - Acoustic Micrographs - Bar 175, Central Region

Figure 144 shows a zone of transmission variation found in the central zone of Bar 175. This zone contains little acoustic speckle and is interpreted as a zone of increased porosity.

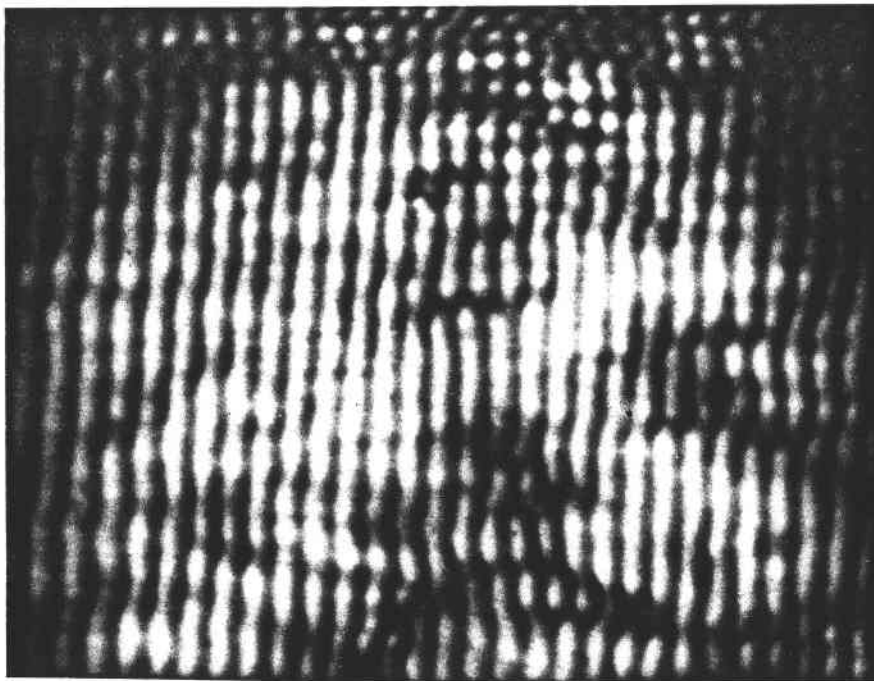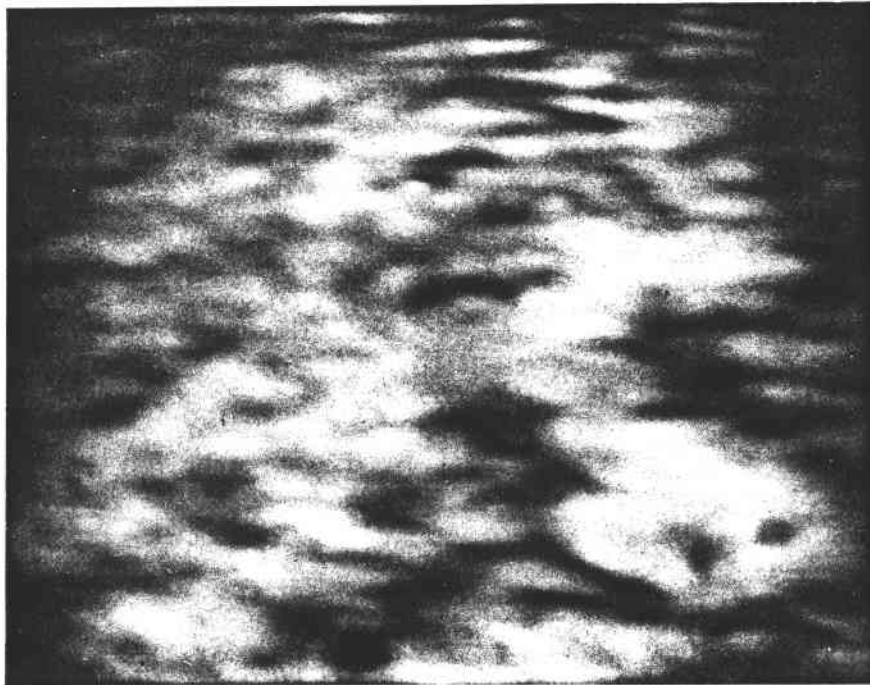All samples were examined at 100 MHz using both shear and compressional waves. Flaw visibility was generally better using shear waves. Micrographs showing a typical structure and illustrating some of the flaw types are presented (Figures 145 and 146). Detailed flaw maps were also documented with an example as shown in Figure 147.

Flaws were detected in all four of the 100 MHz compatible seeded disks. In some cases the flaw location correlates with penciled marks on the surface, in other cases they do not.

5.4.3 - Seeded Defect Disk Examination

Acoustic background structure and acoustic attenuation properties of the disks differ substantially from the flexural bar samples. Typically the disks exhibit more background structure and increased attenuation.

A carbon coating on the disc samples were found to increase acoustic attenuation and produce a very "busy" acoustic background which complicates the detection of small flaws. Removal of carbon improves the technique.

Utilization of these samples as calibration sample requires:

- Further documentation and confirmation of type, size, and location of implanted flaws.

- Understanding of the origin of the flaws which are detected but not implanted.

- Delineation of the differences in material properties between the disks and the bars.

The flaw location information was provided to Carborundum in the manner described in Table 24.

5.4.4 - Reaction Bonded Silicon Carbide Vanes

Vanes can be imaged and micrographs obtained using standard in-sonification stages at 100 MHz.

Routine testing of the vanes will require fixturing in order to make the test systematic and improve testing speed.

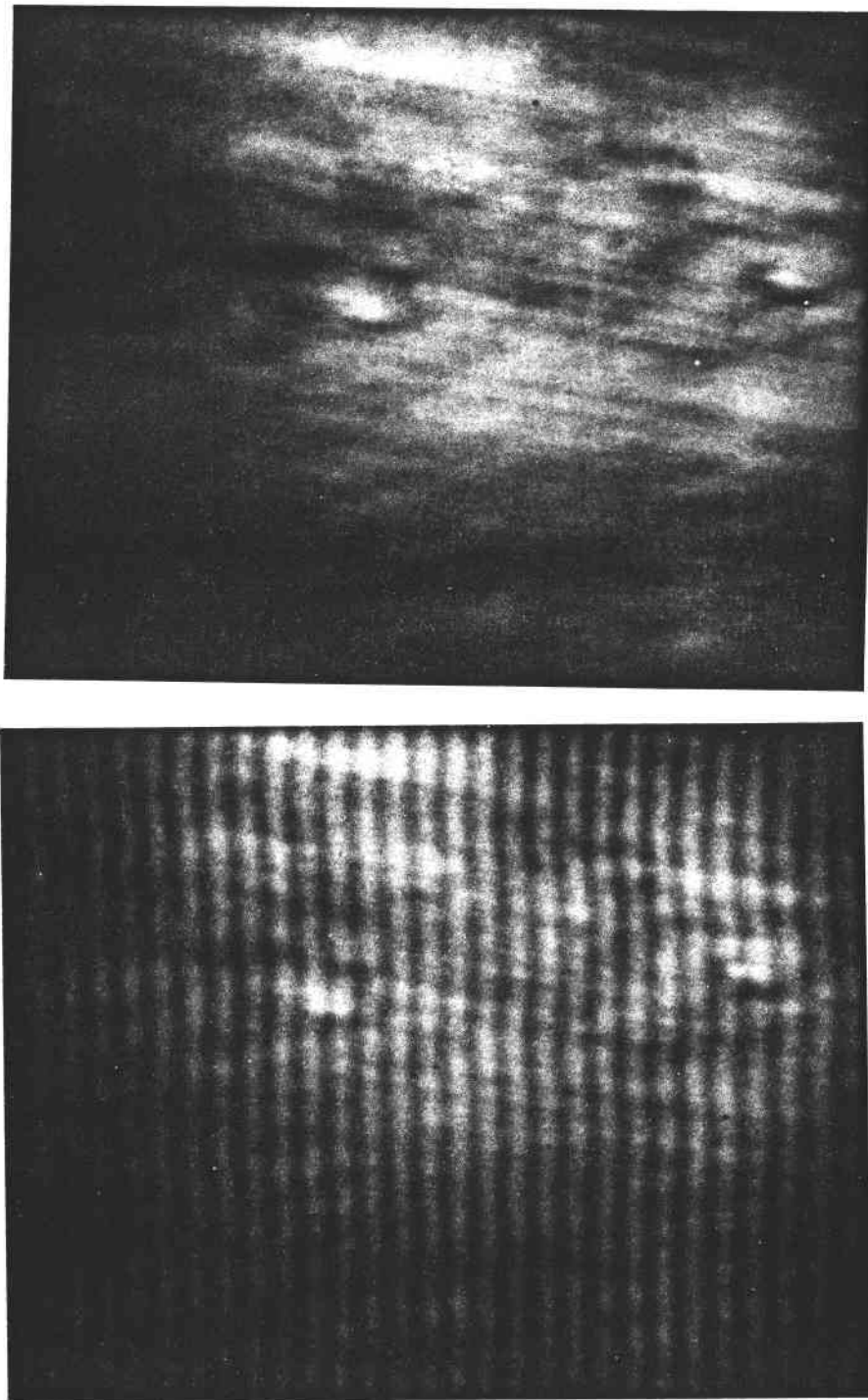The quality of SLAM images obtained on the vanes is comparable to that obtained on the flat bars.

Fig. 145 - Acoustic Micrographs Showing Two Low Contrast Flaws
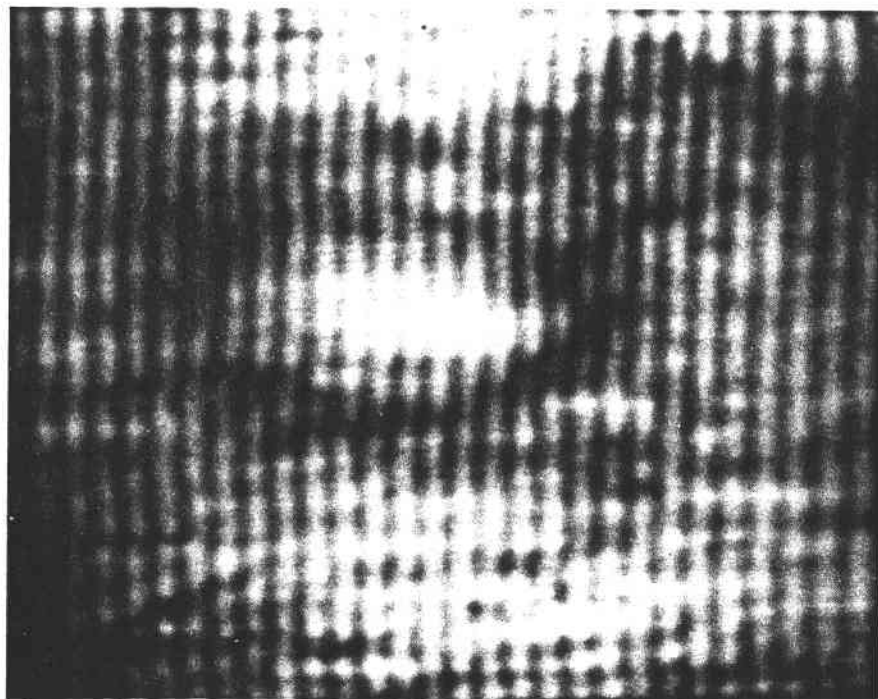in Bar 39-1

Fig. 146 - Acoustic Micrographs Showing Large High Contrast Flaw Found in Sample 39-1

DESCRIPTIONS

(1) Low Contrast Circular ≈ 1200µ below marked surface
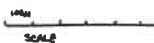
(2) Very Low Contrast, Circular ≈ 500µ below surface

(3)(4)(5) Group of Non Distinct Low Contrast Features

(5) Ring Pattern

(6) Group of Low Contrast Circular Features

(7) Large, Low Contrast, Dark Edges, Bright Center (very deeply embedded)
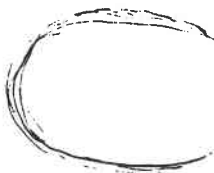
(8) Extremely Low Contrast Large Circular Lying Deep Below the Surface
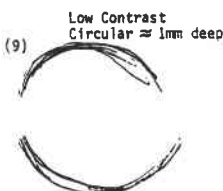
(9) Low Contrast Circular ≈ 1mm deep

Fig. 147 - Example of Documented Detailed Flaw Maps

Table 24 - Flaw Location -- Seeded Disks

Figure	Sample	Comments
SD-1	V2-3	See diagram accompanying micrograph (in the original report).
SD-2	V2-3	See diagram accompanying micrograph (in the original report).
SD-3	V2-3	See diagram accompanying micrograph (Figure 20).
SD-5	V5-3	(a) Marked on sample in green (b) Marked in orange
SD-6	V7-2	Circled in green on sample
SD-7	C3-2	Circled in green on sample
SD-8	C3-2	Circled in orange on sample.
SD-10	B6-2	2 similar areas marked on sample with green dots.
SD-11	B8-2	Marked on sample with green dot.

Background structure, flaw characteristics, and microstructural variations imaged in the vanes are similar to those found in flat bars. Thus, the results on bars are directly applicable to the vanes.

Vanes are more susceptible to microstructural variations attributed to pockets of unreacted material (relative to the RBSC bars).

An example of a defect appearance for Vane 184 is shown in Figure 148.

5.4.5 - Injection Molded Vanes and Blades

Vanes and portions of the blades can be imaged and micrographs obtained using standard insonification stages at 100 MHz.

Routine testing of the vanes and blades will require fixturing in order to make the test systematic, improve test speed, and eliminate sound reverberation artifacts.

SLAM images of the vanes and blades are of a quality comparable to those obtained on bars.

Background structure, and flaw characteristics of the vanes and turbines is similar to that of the bars. Thus, results obtained on the bars are directly applicable to components.

Surface flaws, bumps and pits were detected but do not appear to interfere with visibility of buried structures.

Methods - Five injection molded vanes were examined using the standard 100 MHz soundcells and no special fixturing was required. Without fixturing, it was possible to cover 90 percent of the total blade volume. In some cases and in some areas of the vanes, the micrographs show a number of imaging artifacts resulting from sound reverberation. These artifacts which depend on both the vane geometry and insonification angle are easily distinguished from buried flaws because the SLAM has real-time imaging capabilities. However, artifacts may confuse the reader on the static micrographs and are noted in the figure captions. With appropriate fixturing and sample insonification, the reverberate artifacts can be eliminated from the images.

The flaw locations were identified on the specimens and returned to Carborundum (Table 26). Some typical defect appearances in SLAM are shown in Figures 148 through 152.
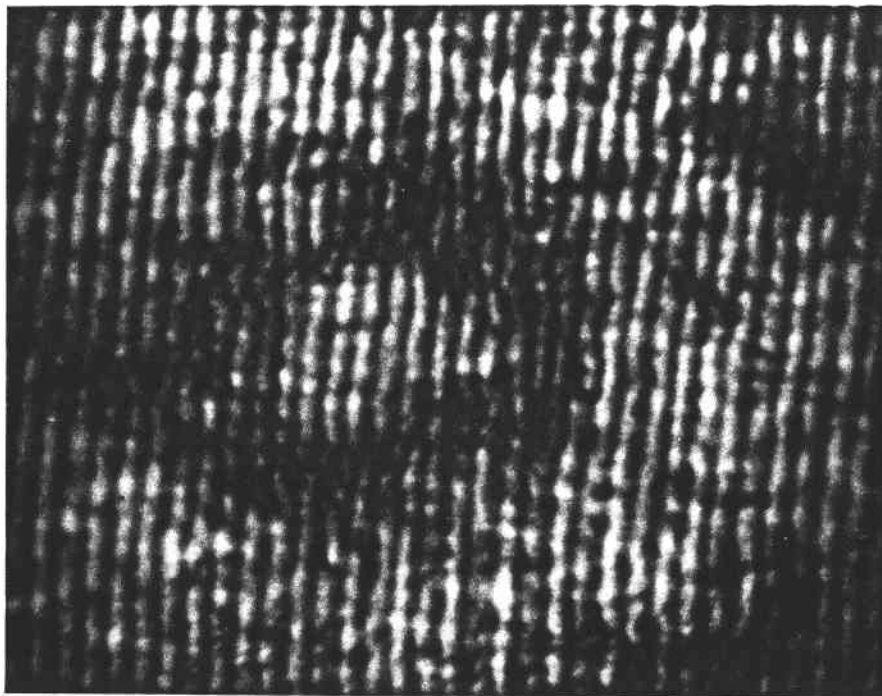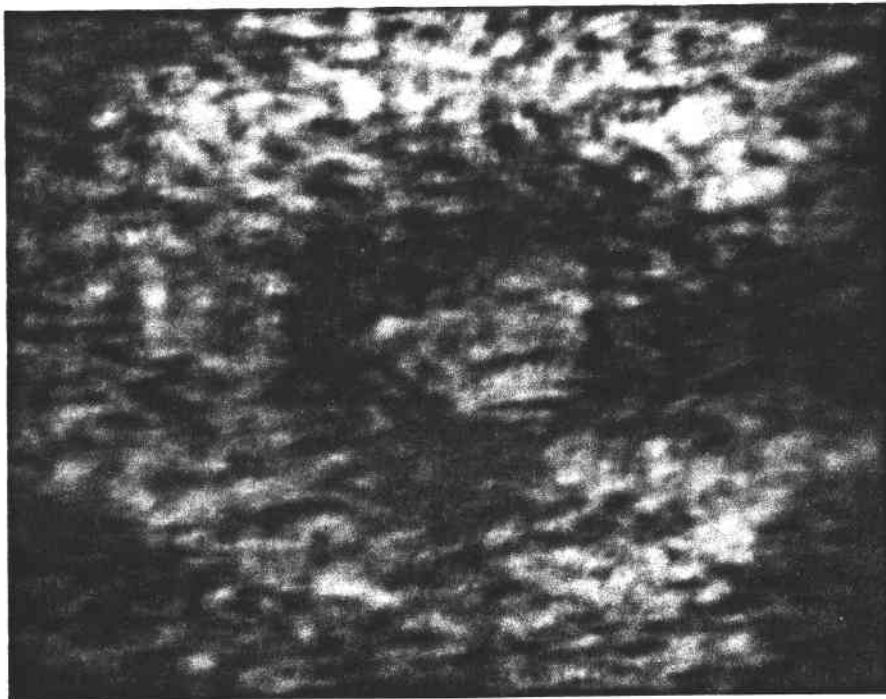
Fig. 148 – Acoustic Micrographs – Vane 184

The above figures are AM and I modes of structures found in another zone in the airfoil of 184. This dark ring pattern is 1.5 mm across (field of view is 3 mm horizontally). Several structures like this one were found and the areas of the vanes were circled in pencil.
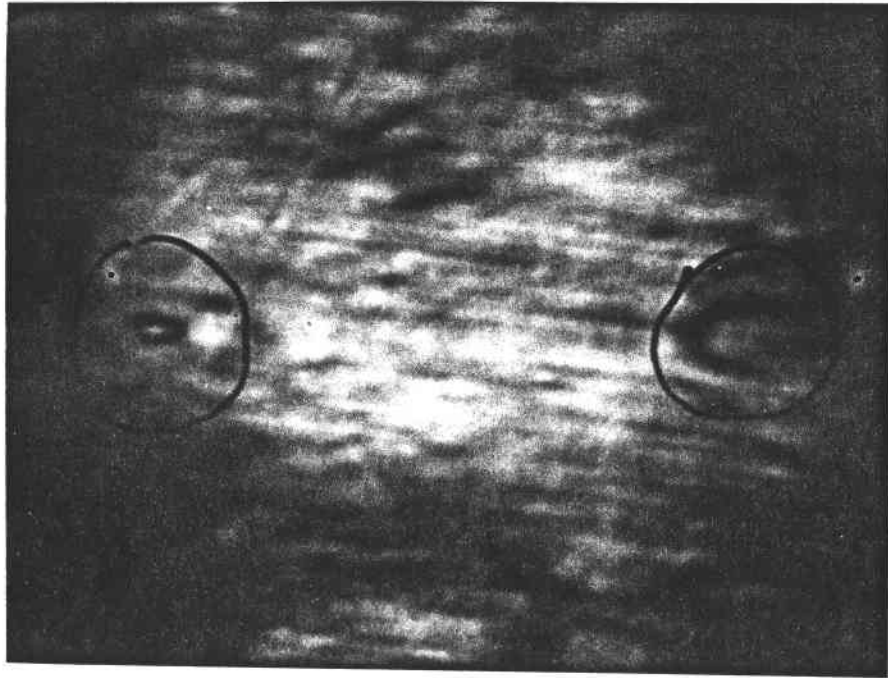
Fig. 149 - Acoustic Micrograph - Sample V2-3

Figure 149 was taken on Sample V2-3. This amplitude micrograph shows two flaws found with the raster over the circled dot mark of the sample (circled).

Table 25 - Flaw Locations

Figure	Sample	Sample Marked
RBV-1	DDA Vane 186	Circle on airfoil
RBV-2	DDA Vane 184	Circle
--	DDA Vane 183	Surface bumps circled
--	DDA Vane 183	2 circles airfoil
--	DDA Vane 175	X marked on airfoil
1MB-5	DDA Blade 24	Large crack in root visible
1MB-4	DDA Blade 16	**Not Marked** (inclusion in root)
1MB-2	DDA Blade 17	Circled tip of airfoil
1MB-3	DDA Blade 445	Large crack in root
1V-V-1	Vane 142	Square area on airfoil
1MV-3	Vane 321	Square area on airfoil and leading edge
RS91-1	Alpha SiC 39-1	Flaw 6 in drawing
RS91-2	Alpha SiC 39-1	Flaw 7 in drawing
RS95-9	Alpha SiC RS95-9	In group of surface flaws near upper edge
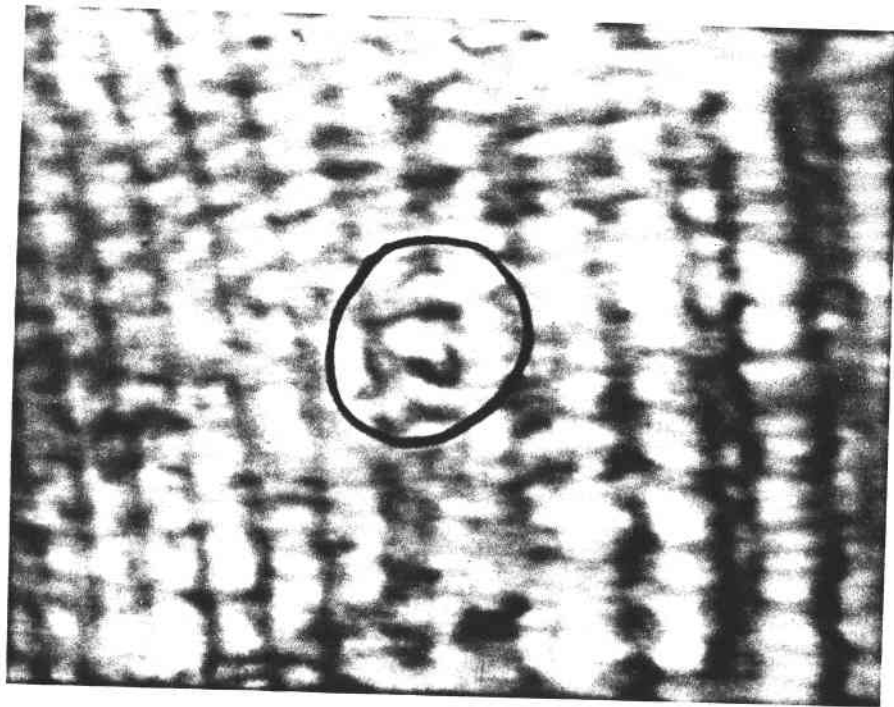
Fig. 150 - Acoustic Micrograph - Vane 142

Figure 150 shows an amplitude micrograph from the airfoil region of Vane 142. The micrograph shows an isolated pore (circled) and its location was marked on the sample. Similar features were found throughout the vane. (The vertical lines are sound reverberation artifacts).
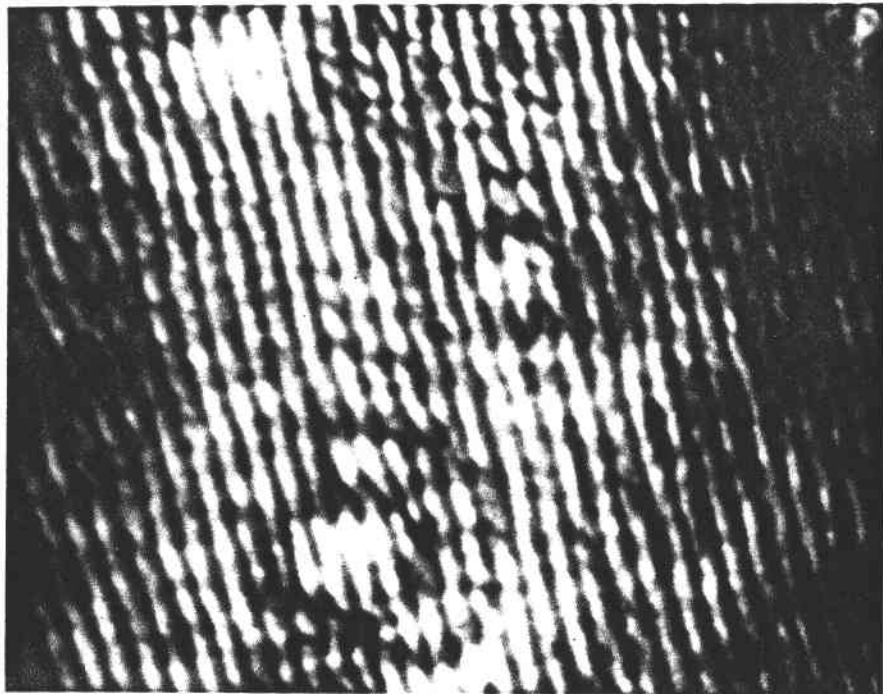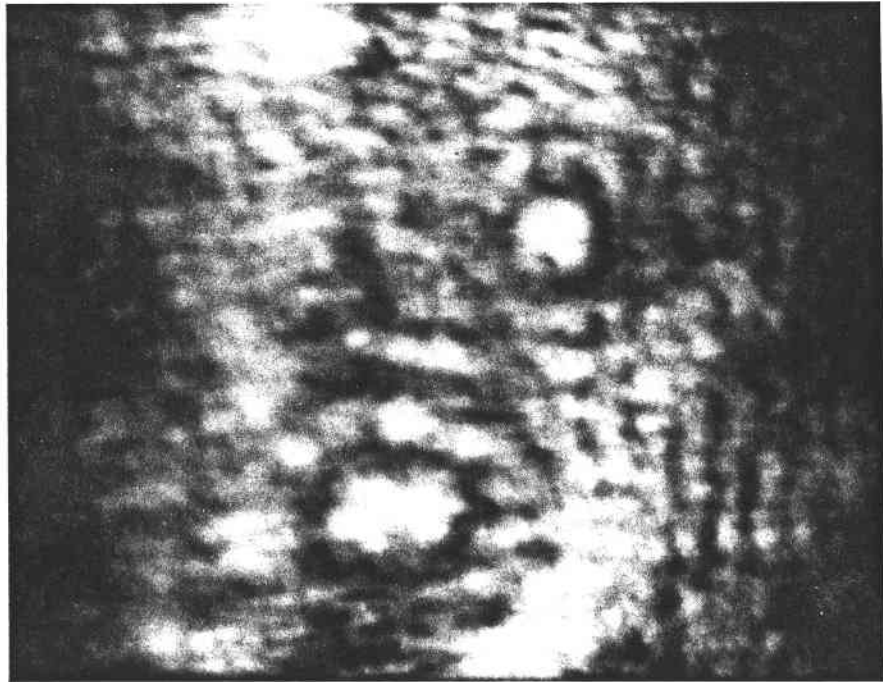
Fig. 151 - Acoustic Micrographs - Blade 17

Figure 151 shows two circular structures found near the tip of the airfoil in Blade 17. Similar structures were found in Blade 94.
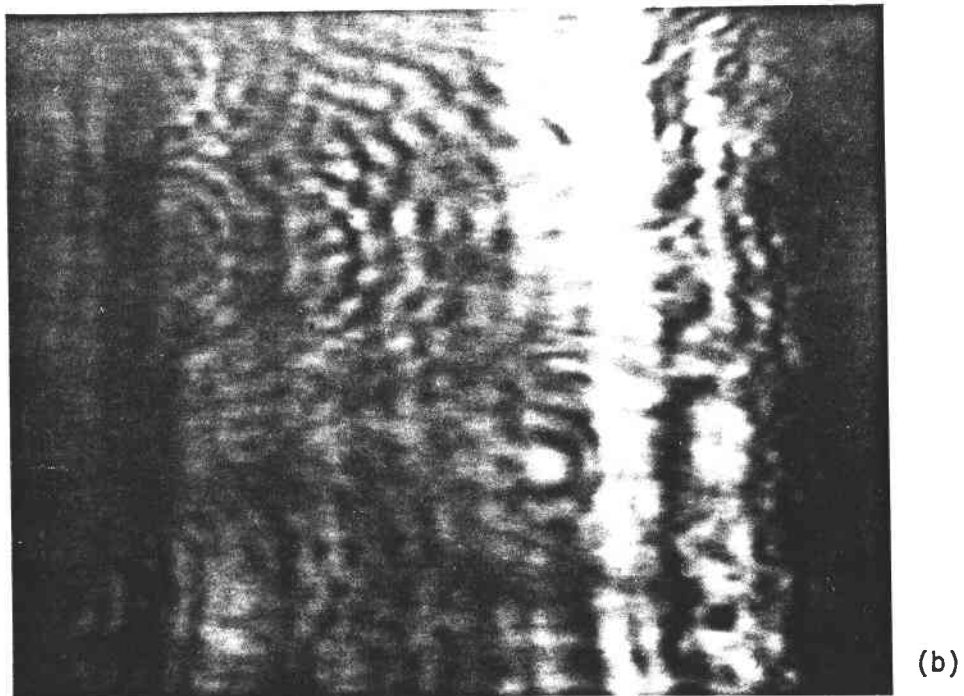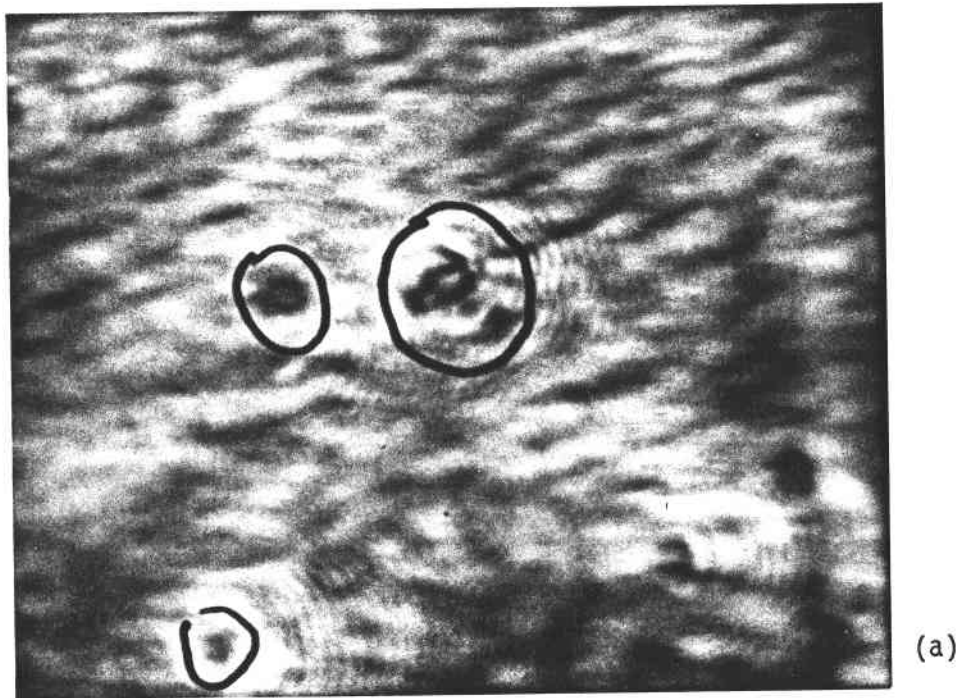
Fig. 152 - Acoustic Micrographs - Vane 321

Figure (a) was taken in an area of the airfoil of Vane 321 with many surface pits (circled), while (b) was taken near the leading edge. Several large, isolated pores lead to the ring patterns observed in this micrograph.

5.5 – Scanning Photoacoustic Spectroscopy (SPAM)

The scanning photoacoustic spectroscopy (SPAM) of silicon carbide materials was performed at the Physics Department of Wayne State University under the direction of Prof. R. L. Thomas.

The alpha silicon carbide specimens were polished and Knoop indentations were made ranging from 1 kg to 3.5 kg loads (90 to 170 μm flaw radius).

5.5.1 – Preparation for SPAM

The SiC ceramic disks (both No. 13 and 8) were sectioned into pieces that would be accommodated by the PAS-cell (see Figure 153). (The same PAS-cell and microphone were used for both the study of the unpolished and the polished SiC surfaces.) Each Knoop flaw was positioned with respect to the edges of its respective sectioned piece and examined optically to determine length, width at mid-point, relative depth at mid-point, and also occurrence of visible surface cracks extending beyond the length of the Knoop flaw (see Table 26). Optical photographs were made of each Knoop flaw and the surrounding sample surface structure. There was good correspondence between Knoop load and length, relative depth, and frequency of surface cracking; correspondence between load and width was not good and in several cases difficult to determine due to side chips occurring at or near the indentation mid-point, particularly for Knoop loads exceeding 2.0 kg.

5.5.2 – SPAM Processing and Data Analysis

Figure 153 describes a block diagram of the system and the PAS cell used to study the polished SiC samples. An Argon beam was chopped at 1 KHz, then focused onto the sample with a beam spot size of approximately 10 μm. The sample was mounted on a mechanical stage which allowed the beam to scan the sample surface in both the x and y directions to produce area scan traces on an x-y plotter. Traces were made of each sample covering a 2.54 mm x 2.54 mm area surrounding the Knoop flaw. The Knoop flaws were located using the sectioned sample edges measured with respect to the mid-point of the Knoop flaw, and also observing the speckle and diffraction patterns produced by the flaws. Repeatibility in locating the Knoop flaws in this manner was excellent.

All traces were made on the same scale for comparison. In addition, the same time constant was used (30 ms) for each sample with the exception of No. 7 where a 100 ms time constant was used due to a higher noise level. The Signal-to-Noise was good for all samples, the background signal from the samples being between 150 μv - 170 μv for all samples at a laser

DIGITAL SCANNING, DATA ACQUISITION AND DISPLAY
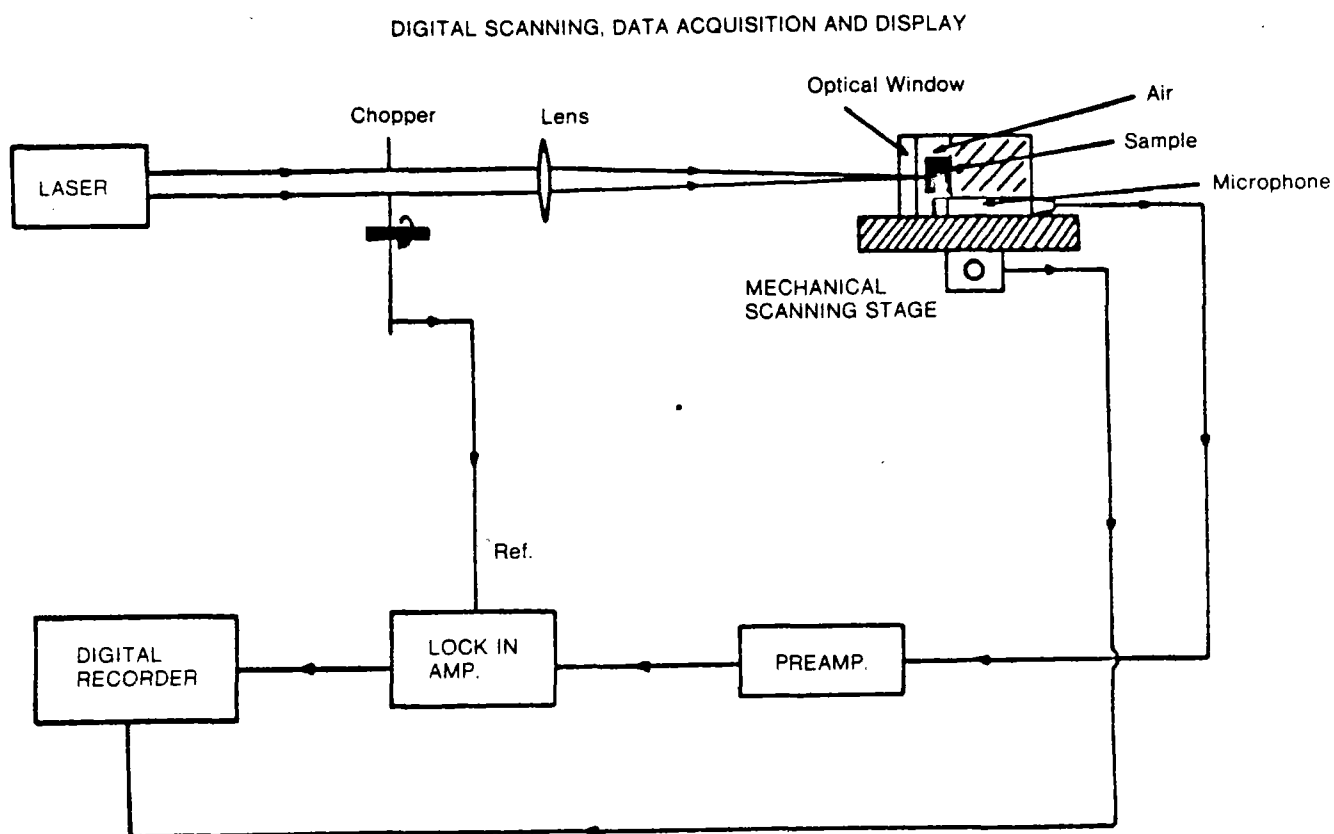
Fig. 153 - Block Diagram of the Apparatus

Table 26 - Knoop Flaws

Knoop Flaw Number	Load (kg)	Length (μm)	PAS-Length (μm)	Width (μm)	PAS-Width (μm)	Surface Cracks Number
1	1.0	79	143	9	160	0
4	1.5	97	170	9	130	1
7	2.0	110	160	12	190	2
16	3.5	167	310	16	280	2
17	3.5	160	260	17	140	2
18	3.5	154	270	16	140	3

current of 14.5A. The power incident on the sample was measured to be approximately 45 mW. The noise level for all samples was approximately ± 1 µv. Repeatability of the traces was excellent for all samples with the exception of No. 7 where the noise level was higher.

Figure 154 shows a photo of a 1 kg load Knoop indentation along with the corresponding PAS signal traces. The blocked area drawn on the signal traces shows the boundaries of the photograph (marked A, B). The Knoop flaw and its signal are marked K, and a large surface structure below the flaw and its signal are marked S. Note that the signal due to the Knoop flaw is larger than the signal due to the surface structure. This was also the case for flaw No. 18 (see Figure 155). The small inset at the left of the photo is a reduced area scan with less expansion in the y-direction to give a more 3-dimensional view of the flaw. Note: there were no surface cracks for any of the 1.0 kg load Knoop indentations. Knoop flaw No. 18 (Figure 155) had the most extensive amount of surface chipping and the most number of cracks. The large chips extending, from the side of the flaw were deeper than the flaw itself. The photo shows the Knoop flaw (k) with a large surface structure(s) below it. Note the corresponding photo-acoustic signal for the surface structure is much smaller than the signal for the Knoop flaw.

Figure 156 shows Knoop flaw No. 7 with a 2.0 kg load. The noise level was highest for this sample (± 1 µv) and the photoacoustic background signal was not as reproducible for this sample as for the others. The signal due to the Knoop flaw was very reproducible, however.

Figure 157 shows traces and a photograph made from the unpolished back surface of one of the SiC sample pieces where there is no Knoop flaw but the surface structure was similar to the previous unpolished Knoop indented surfaces. Note that the surface structure gives rise to a more structured photoacoustic signal.

5.6 - Summary of NDE Task Accomplished

The applicability of microfocus x-ray, high frequency ultrasonics, SLAM, and SPAM technology to detecting defects in silicon carbide materials has been evaluated. Further work is needed in areas of:

(a) Flaw characterization (type, size, shape, and location).

(b) Destructive evaluation -- NDE signal coupling.

(c) Evaluation of different methods to detect and characterize the same flaw.

(d) Acoustic emission studies.

PAS signal traces corresponding to the photo at the right. Each increment in the y-direction is 13mm.
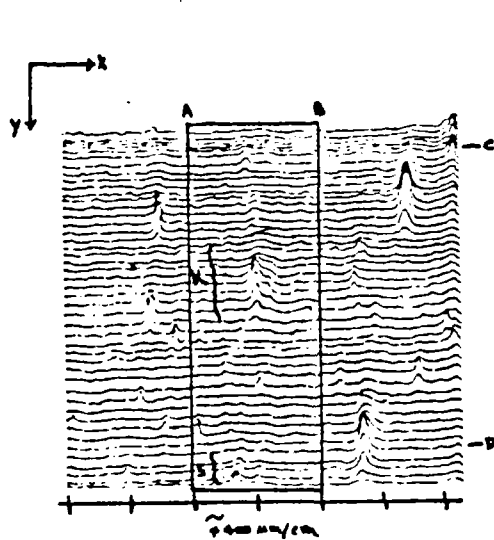
Signal length = 143 μm.

Signal width = 160 μm.
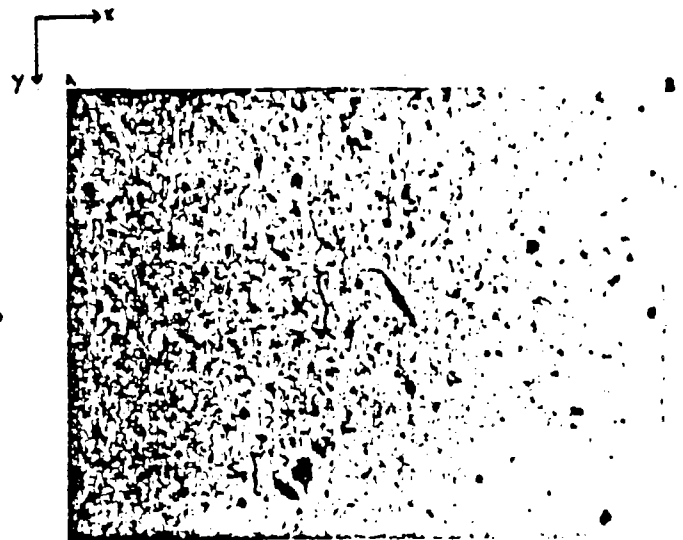
Length = 78 μm.

Width = 9 μm.

Load = 1.0 kg.

Relative depth = 2

Cracks: none

Fig. 154 - Polished SiC Knoop Flaw No. 1

PAS signal traces corresponding to the photo at right. Each increment in the y-direction is 13mm.
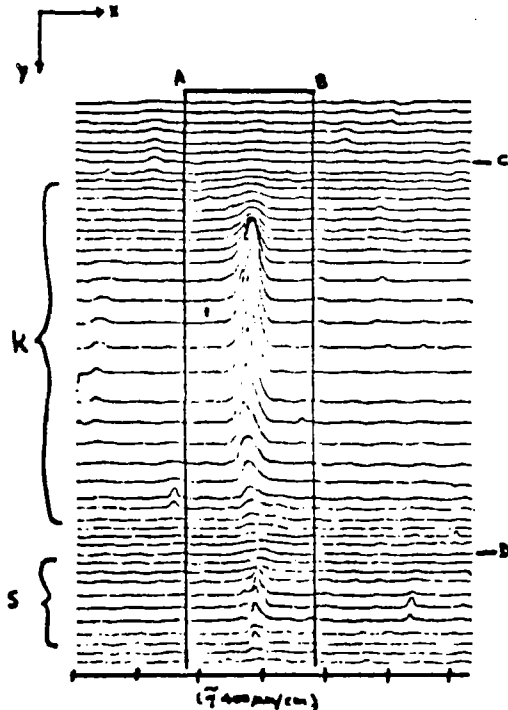
Signal length ≐ 270 μm.

Signal width ≐ 240 μm.

Length ≐ 154 μm.

Width ≐ 12 μm.

Load ≐ 3.5 kg.

Relative depth ≐ 4.2.

Cracks: (3)

Fig. 155 - Polished SiC Knoop Flaw No. 18
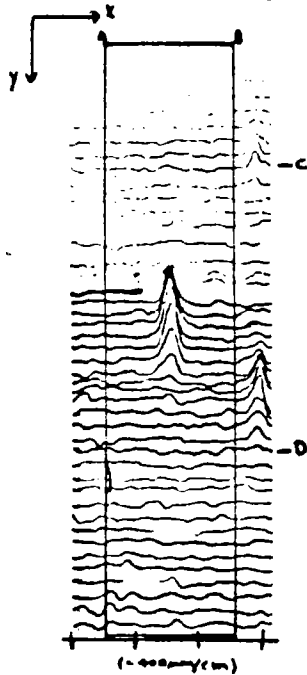
Signal length ≐ 160 μm.

Signal width ≐ 190 μm.
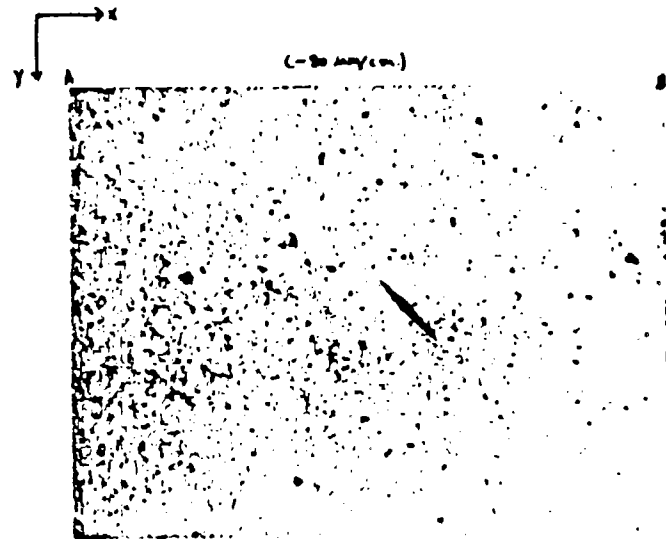
Length ≐ 110 μm.

Width ≐ 12 μm.

Load ≐ 2.0 kg.

Relative depth ≐ 3

Cracks: (2)

Fig. 156 - Polished SiC Knoop Flaw No. 7

Unpolished SiC Surface
(no Knoop flaw).

198
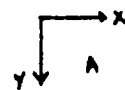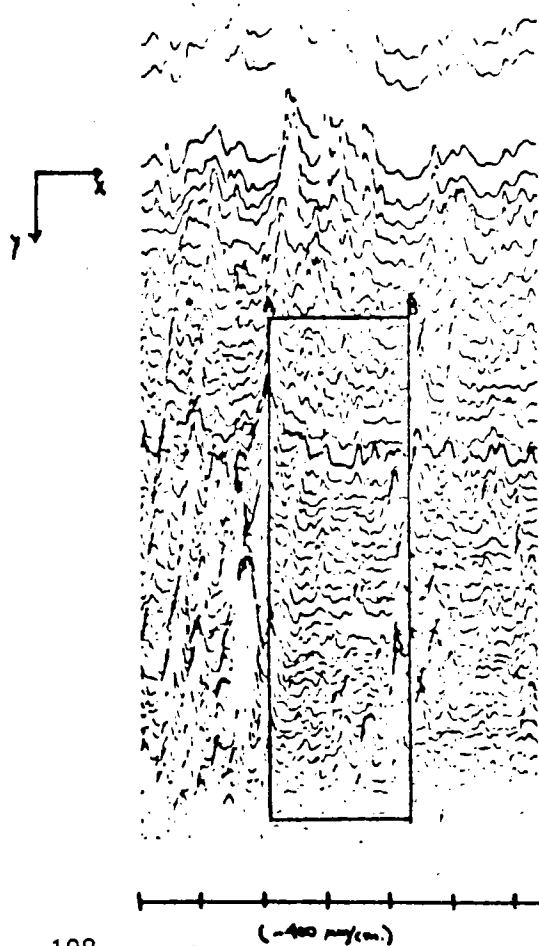
Fig. 157 - Unpolished SiC Surface (No Knoop Flaw)

6 - MECHANICAL PROPERTIES

6.1 - Baseline Properties Determination

The baseline properties data of both sintered alpha silicon carbide and fine grain reaction sintered SiC manufactured by different processes are summarized in Figure 158 and Table 27.

The specimen cross section was 1/8" x 1/4" and a total of 30 specimens were tested per each baseline datum. Tests were done in the 4-point bend mode using a 0.75-inch inner span and a 1.5-inch outer span.

The strength data obtained for injection molded specimens were obtained for an as-fired surface. The cold pressed, isopressed, and slip cast specimens of alpha SiC as well as compression molded and thixocast RBSiC specimens were machined. The test bars were annealed for 2 hours in an inert atmosphere (at 1500°C for alpha SiC and at 1200°C for RBSiC) prior to flexure test.

Strength levels reported here for both cold pressed alpha SiC and fine grain reaction sintered SiC are lower than previously observed. In earlier investigations, strength levels corresponding to the shaded area have been reported for cold pressed sintered alpha SiC and for fine grain reaction sintered SiC. For fine grained reaction sintered SiC, the shaded high temperature area corresponds to test done at 1300°C (2372°F). The Weibull modulus was 10.9 at this temperature and 9.6 at room temperature. The lower strengths observed in the present investigation have been traced back to improper furnacing during specimen preparation.

The baseline data were analyzed by various statistical treatments in order to extrapolate tensile strength data from bend results.

Because of the fact that an optimum sampling may not still be established even though 30 specimens were tested per each condition, a construction of confidence bands for the Weibull least-square regression estimate is useful for design purposes and in reliability analysis. Therefore, 90% confidence bands have been constructed for the different Weibull plots.

6.1.1 - Failure Analysis of Test Bars

Failure analysis, via SEM, was conducted on broken test bars of sintered alpha silicon carbide manufactured by both injection molding and slip casting. The majority of failure-causing flaws were processing-related 3-dimensional voids lying at or close to tensile surface. (See Tables 28 to 30.)

Charactertistic Strength, ksi

Weibull
Modulus
m

| | 10 | 20 | 30 | 40 | 50 | 60 | 70 | 80 |

8.8 25°C (77°F)   100%   Isopressed
7.1 1200°C (2192°F)

8.4 25°C (77°F)   107%   Dry Pressed
7.9 1200°C (2192°F)

5.8 25°C (77°F)   99%   Injection Molded
6.0 1200°C (2192°F)

4.8 25°C (77°F)   110%   Slip Cast (Regular)
6.7 1200°C (2192°F)

4.5 25°C (77°F)   100%   Slip Cast Bimodal
5.5 1200°C (2192°F)

(a) Sintered Alpha Silicon Carbide

Characteristic Strength, ksi

Weibull
Modulus
m

| | 10 | 20 | 30 | 40 | 50 | 60 | 70 | 80 |

5.5 25°C (77°F)   100% Compression
5.9 1200°C (2192°F)   Molded

3.1 25°C (77°F)   134% Thixocast
17.0 1200°C (2192°F)

(b) Fine Grain Reaction Sintered Silicon Carbide

Fig. 158 – High Temperature Strength Retention

200

Table 27 – The Strength Results of Silicon Carbides Manufactured by Different Methods

Method of Manufacture	Temperature °C(°F)	Average Strength (ksi)	Characteristic Strength (ksi) (k=1, for sp. volume)	Weibull Modulus (m)
Sintered Alpha Silicon Carbide				
Isopressed	25(77)	46.28 $\pm$ 5.29	48.85	8.8
	1200(2192)	44.58 $\pm$ 6.43	47.55	7.1
Dry Pressed	25(77)	48.05 $\pm$ 6.25	50.78	8.4
		66.56 $\pm$ 6.33	69.34	12.3[1,2]
	1200(2192)	51.21 $\pm$ 7.09	54.30	7.9
		65.25 $\pm$ 5.58[2]		
Injection Molded	25(77)	61.52 $\pm$ 11.05	66.19	5.8
	1200(2192)	57.46 $\pm$ 10.31	61.85	6.0
Slip Cast (Regular)	25(77)	54.46 $\pm$ 11.39	59.40	4.8
	1200(2192)	61.15 $\pm$ 9.71	65.38	6.7
Slip Cast (Bimodal)	25(77)	42.53 $\pm$ 10.15	46.58	4.5
	1200(2192)	42.00 $\pm$ 7.49	45.46	5.5
Reaction Sintered SiC				
Compression Molded	25(77)	57.34 $\pm$ 11.20	62.02	5.5
		67.69 $\pm$ 8.08	71.22	9.6[3]
	1200(2192)	58.14 $\pm$ 10.99	62.64	5.9
	1300(2372)	71.87 $\pm$ 7.41	75.23	10.9[3]
Thixocast	25(77)	36.92 $\pm$ 10.27	41.69	3.1
	1200(2192)	54.05 $\pm$ 3.16	55.68	17.03

---

1. M. Srinivasan and R. H. Smoak, "Elevated Temperature Fracture Toughness Determinations of Sintered Alpha SiC," Proc. of Intl. Conf. of Fracture Mechanics in Engineering Applications, Bangalore, India, March 26-30 (1979).
2. Data Sheet, Carborundum Company (1978).
3. S. M. Hudson, M. A. Janovicz, and F. A. Rockwood, "Ceramic Applications in Turbine Engines," NASA Report CR-1159865, May (1980).

Table 28 - Defect Types and Distributions in Flexural Strength Specimens

Injection Molded SASC - Tested at 25°C

Type	Number	Percent
Surface Flaws*	17	57
Internal Flaws	7	23
Corner Flaws**	4	13
Others***		
Total	30	100

Table 29 - Distribution of Failure Origins

Injection Molded SASC - Tested at 1200°C

Type	Number	Percent
Surface*	23	77
Internal	4	13
Corner	2	7
Others***	1	3
Total	30	100

Table 30 - Distribution of Failure Origins

Slip Cast SASC - Tested at 25°C

Type	Number	Percent
Surface*	21	70
Internal	6	20
Corner**	2	7
Others***	1	3
Total	30	100

---

* Includes subsurface voids located within 100 μm from the tensile surface.
** Includes chamfer damage
*** No apparent fracture origin noticed

Some of the typical microstructures and the failure origins for sintered alpha silicon carbide and reaction sintered silicon carbide are given in Appendix IV.

The strength distribution of the thixocast reaction bonded silicon carbide at 1200°C (2192°F) is interesting. A limited failure analysis investigation failed to reveal any clues with respect to fracture originating flaws.

It is possible that because of the very low room temperature fracture toughness of this material, machining without introducing subsurface damage is difficult. At 1200°C, however, oxidation crack blunting is a possibility which would increase the strength and minimize the distribution in strength. Because of the high potential of this material for complex shape fabrication, the elevated temperature strength distribution is an aspect which merits further consideration.

6.2 - Fracture Mechanics

In room temperature K_{IC} determination, the single-edge notched-beam method gave K_{IC} - 5.0 to 5.5 MPa $\sqrt{m}$ for specimens machined from a plate of cold pressed sintered alpha SiC. The chevron notched beam yielded a K_{IC} = 3.4 to 4.3 MPA $\sqrt{m}$ when the height of the triangular cross section was approximately 75 percent of specimen depth. A value for K_{IC} = 3.0 MPa $\sqrt{m}$ was obtained by D. Munz (then at DFVLR) on similar specimens. In another inherently high strength specimen population, the SENB method yielded a value of K_{IC} = 5.5 to 5.8 MPa $\sqrt{m}$, where as chevron notched specimens (from the same population) in which the height of the triangular cross section was equal to the specimen depth yielded a value of K_{IC} 6.0 to 9.0 MPa $\sqrt{m}$.

The initial efforts indicate that further development and optimization of notch configuration are needed for application of chevron beam method to alpha SiC.

No detailed fracture mechanics tests could be conducted due to the early termination of the contract.

6.3 - High Temperature Structural Modification

6.3.1 - Oxidation Effects

Oxidation studies were conducted with fine grain reaction sintered silicon carbide. Flexural bars of 2.0" long and 0.125" x 0.25" cross

section were exposed to 1260°C (2300°F) and 1371°C (2500°F) in a tube furnace with a flowing stream of air for up to 500 hours. Room temperature flexural strengths were determined in 4-point bend and the results are shown in Figure 159.

The room temperature strength of the control population is lower than the baseline data reported in Section 6.1. This discrepancy is due to the machining parameters for this particular batch of specimens. Improper machining can introduce considerable subsurface microcracks which result in lower room temperature strength, in general. Oxidation at 1260°C, essentially blunts the severity of these cracks, thereby increasing the strength.

Bars prepared from the same lot of material but machined under optimum conditions gave an average room temperature strength of 64,000 psi. The question whether an inherently high strength population of reaction sintered silicon carbide can be improved with respect to strength by selective oxidation treatment remains unanswered. The results do indicate that the room temperature flexural strength of inherently low strength fine grain reaction sintered silicon carbide can be increased by up to 63 percent by selective oxidation treatments. The oxide scale of 1260°C-oxidized specimens was investigated by optical microscopy. The appearance is complex with seemingly different oxidation products in the free silicon and SiC regions. Some pitting was observed in the 500-hour oxidized specimens which would explain the low strength.

The observed decrease in strength due to 1371°C (2500°F) oxidation can be explained when the oxidation weight change data, shown in Figure 160 is examined. The weight loss (due to pitting, and, perhaps, vaporization of the free silicon) at 1371°C becomes very rapid after approximately 100 hours.

The oxidation studies were not conducted with sintered alpha silicon carbide due to the termination of the contract.

6.3.2 - Stress Rupture Effects

An established method to elucidate time-dependent slow crack growth effects in ceramics is the static fatigue or the long-term creep stress rupture experiments. A variation of this common method is the stepped up stress rupture tests in which either the temperature is incrementally increased at a given applied stress at regular intervals or the applied stress is incrementally increased at constant temperature and the survivability of the specimen under these test conditions is examined. Although no quantitative failure predictions can be extracted from the latter experiment, it may be useful in identifying temperature regions in which a material may exhibit poor loadbearing ability owing to microstructural modifications.
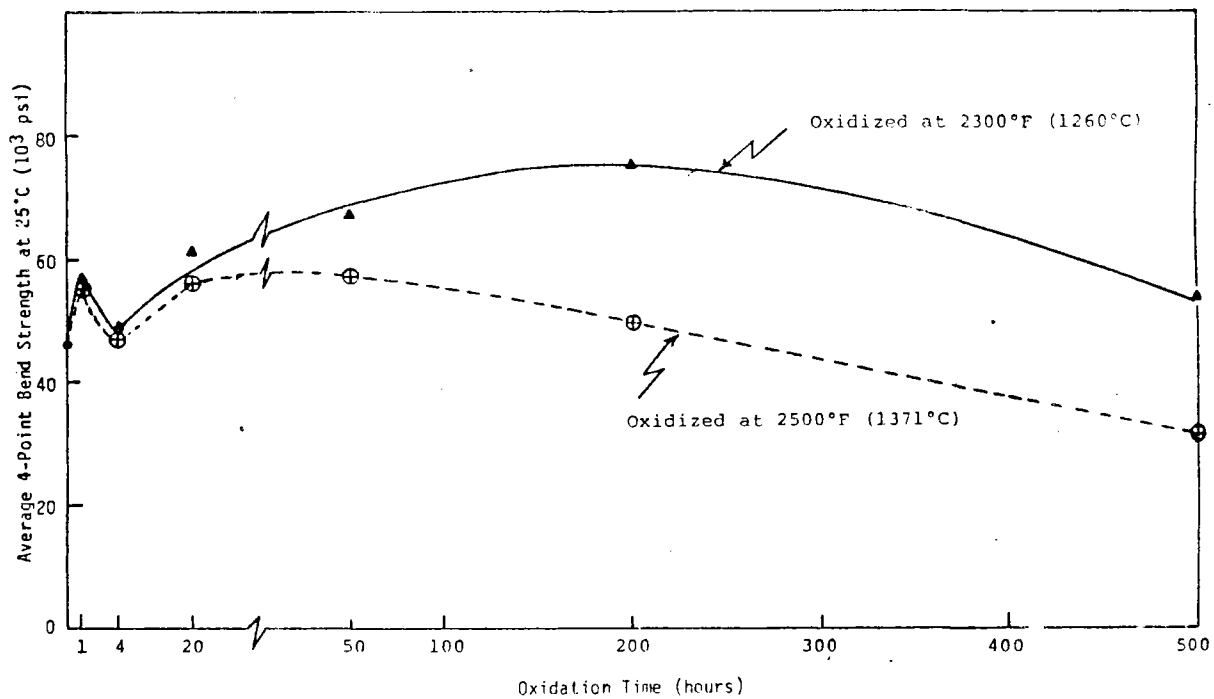
Fig.159 - The Effect of Oxidation on the Room Temperature Strength Of
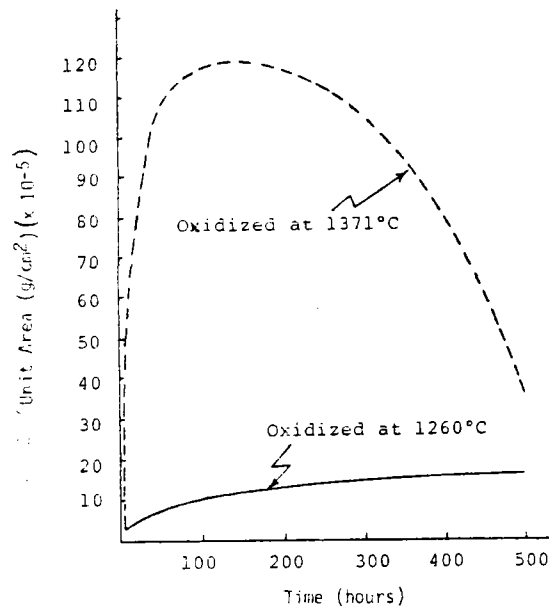Fine Grain Reaction Bonded SiC

Fig. 160 - The Oxidation Weight Gain as a Function of Time
for Fine Grain Reaction Sintered SiC

6.3.2.1 - Stepped-Up Stress Rupture Tests

Tests were conducted from 800°C to 1500°C at 100°C intervals at different loads corresponding to applied stress levels of 40,000 psi to 50,000 psi on a population of cold pressed sintered alpha SiC which had a room temperature baseline strength of 65.9 ± 11.7 ksi. The static loading lasted for 24 hours at each temperature.

The results are shown in Table 31 and Figure 161. Early, 800°C failures were observed for two specimens, one loaded to 40,000 psi and the other to 55,000 psi. However, one specimen survived the cycle to 1500°C at which temperature failure occurred in approximately 2.5 hours. At σa = 50 ksi, two failures occurred at 1300°C, and one at 1100°C.

Failure analysis was conducted on these specimens, aided by a scanning electron microscope. The specimens that broke after exposure to temperatures above 1300°C (namely, 4-11, 5-3, and 4-6) showed some fuzzy intergranular fracture region perhaps indicative of slow crack growth (via grain boundary sliding, for example) occurring at these temperatures (Figure 162). The nature of the failure origins for other specimens were not significantly different from those normally observed for alpha SiC broken at room temperature, indicating that no critical flaw modification occurs below the temperatures where slow crack growth became predominant.

6.3.2.2 - Stress Rupture Tests

Static creep stress rupture tests were conducted with compression molded fine grain reaction sintered silicon carbide in air at 1832°F and 2192°F in 4-point bend. In 100 hours of testing, failure occurred at and above 55,000 psi of applied stress at 2192°F. No failure occurred for stresses up to 56,000 psi at 1832°F (Figure 163). Creep deflections were seen during the stress rupture test, especially at 2192°F (Table 32 and Figure 164). Based on the static fatigue data, the slow crack growth deformation aspect for these materials seems to be insignificant at these temperatures and very high applied stress levels.

The specimens which failed during the test were examined for possible slow crack growth regions on the fracture surface.

Figure 165 shows the microstructure and the fracture surface appearance of a specimen tested at 1200°C. Failure occurred in 17.45 hours at an applied stress of 55,000 psi. This stress level is within the standard deviation of the baseline population at this temperature. The fracture surface appearance is unusual in that there are several regions or pockets which show pull out and poor packing. No specific slow crack growth region is discernable. The fracture surface

Table 31 - Failure Analysis of Bars Tested
By Stepped-Up Rupture Test

No.	Stress, σ_f, 10^3 psi	Comments
2-1	55.0	Chamfer damage; failure occurred at 800°C after 0.8 h.
8-5	55.0	Surface-connected semi-elliptical void with surrounding porous region; a = 30 μm; c = 120 μm. Failure occurred at 800°C after 4.1 h.
5-7	55.0	Surface-connected semi-elliptical processing void; surrounding porous region. a = 26 μm; c = 120 μm. Failure occurred at 900°C after 7.35 h.
1-6	55.0	No obvious fracture origin. The specimen failed at 1100°C in 22.8 h.
4-11	50.0	Semi-elliptical surface void. a = 60 μm; c = 90 μm. Failed at 1300°C after 17.7 h.
5-3	50.0	Chamfer damage. Failed at 1300°C after 23.6 h.
4-6	40.0	Semi-circular poorly-bonded region. Failed at 1500°C after 2.1 h.

Table 32 - Permanent Deflections in Fine Grain Reaction
Sintered SiC in Stress Rupture Expts.

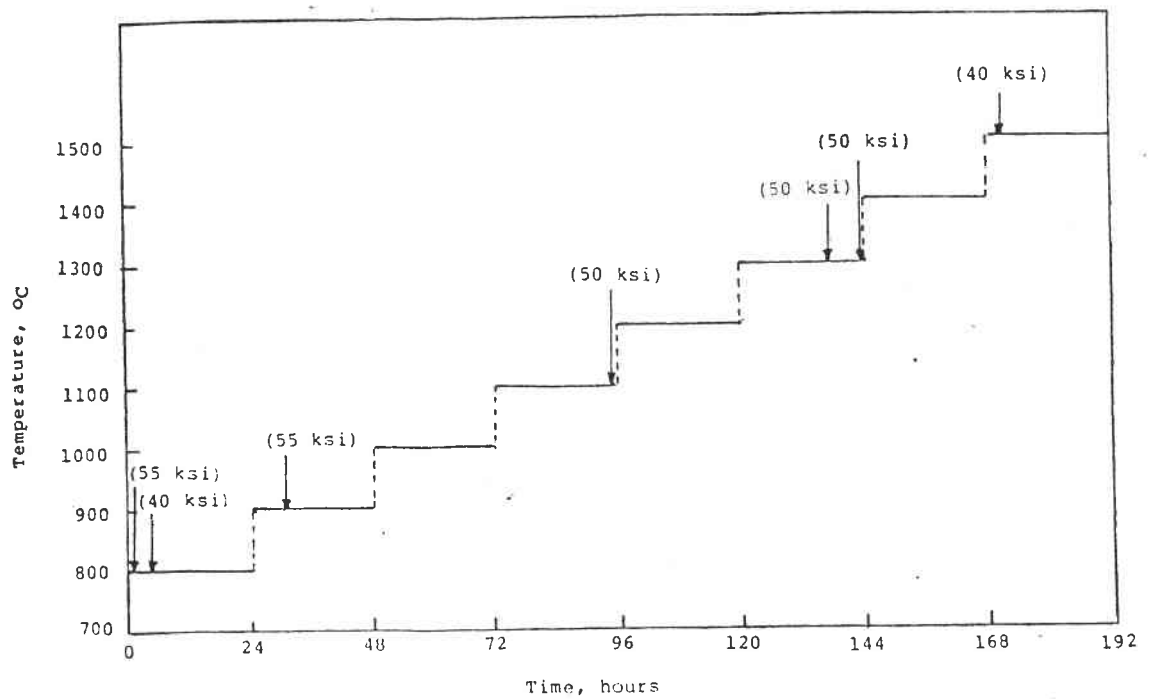| Applied Stress, (σ_a, ksi)	Time (hours)	Deflection (inches)
40	113	0.0155
45	114	0.0259
50	113	0.0235
51	160	0.0163
55	113	0.0059*(anomaly)
56	100	0.0135

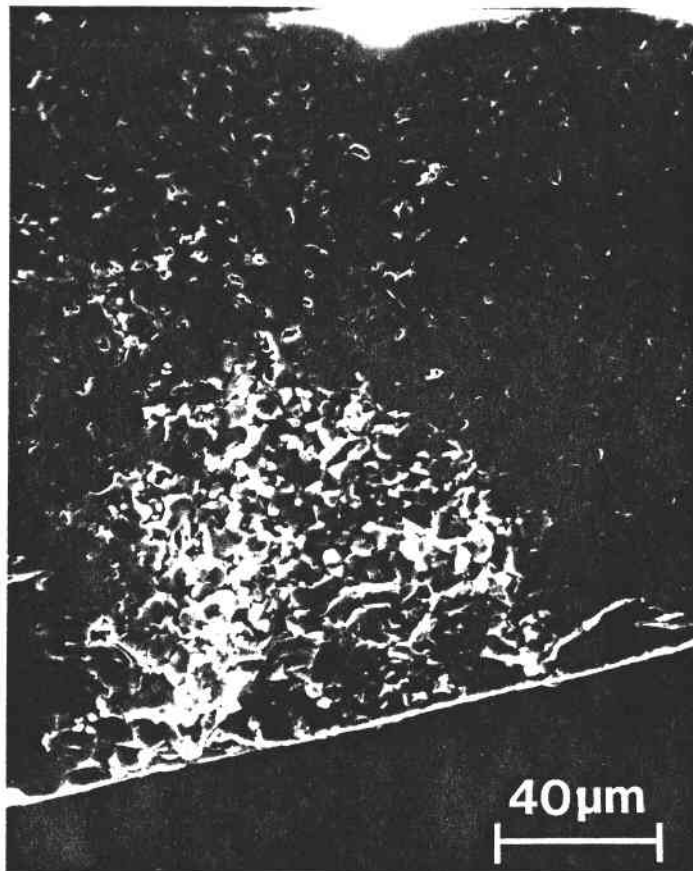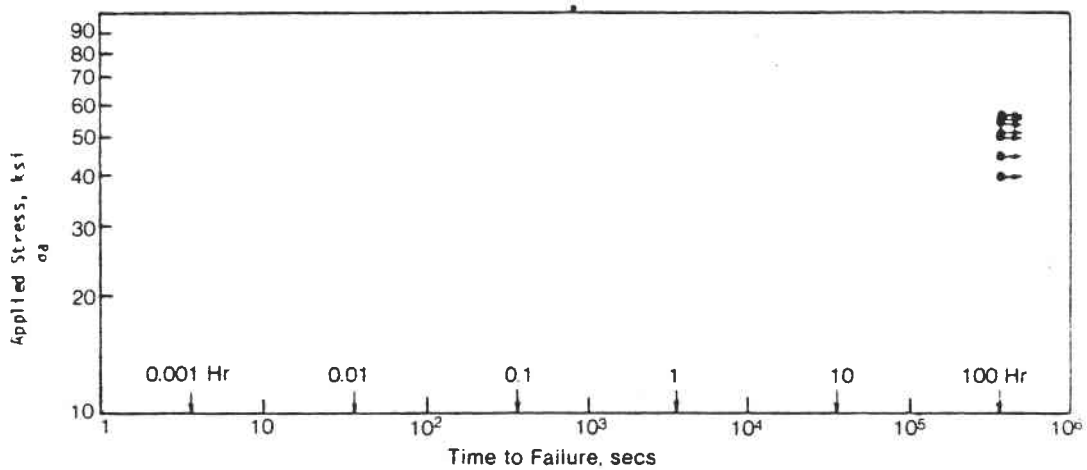Fig. 161 – Stepped-Up Stress Rupture of SASC Bars

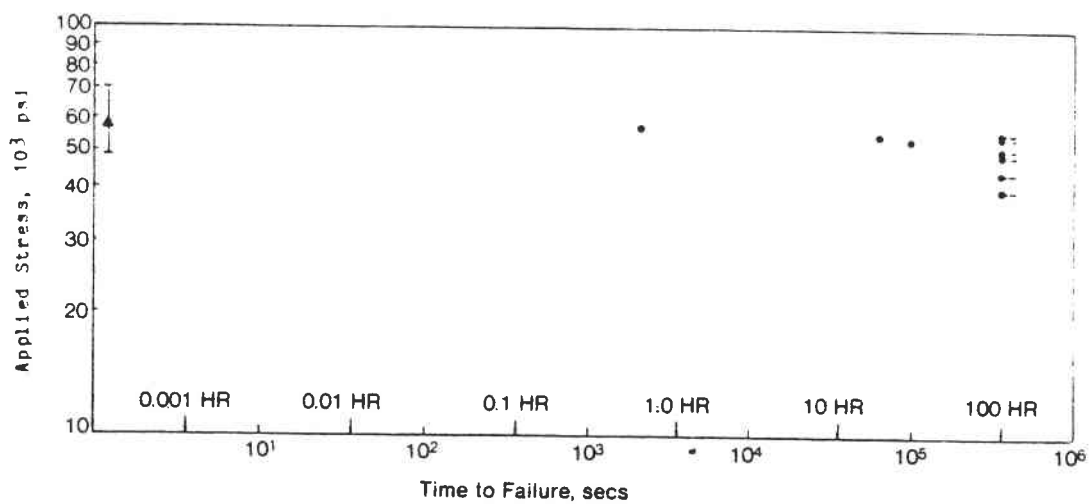

Fig. 162 – Failure Origin for   No. 4-11.   Failed at 1300°C After 17.7 h. Survived 24 hours successively at 800°C through 1200°C at 100°C Intervals
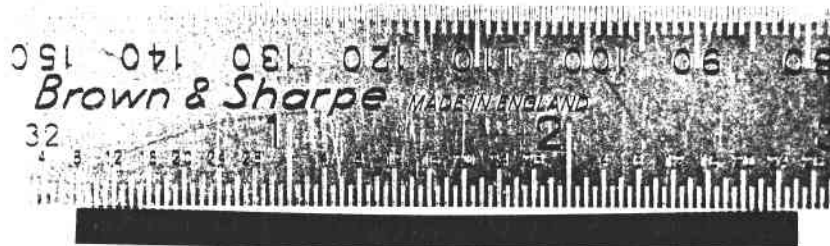
Fig. 163 – Static Stress Rupture Plots for Compression Molded Reaction Bonded
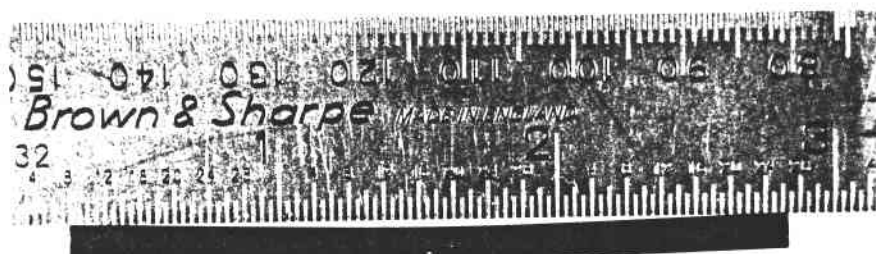SiC (a) at 1000°C and (b) at 1200°C in Air in 4-Point Bend

Compression Molded RS-SiC

23-1 σ_f=50 ksi   112.5 hrs

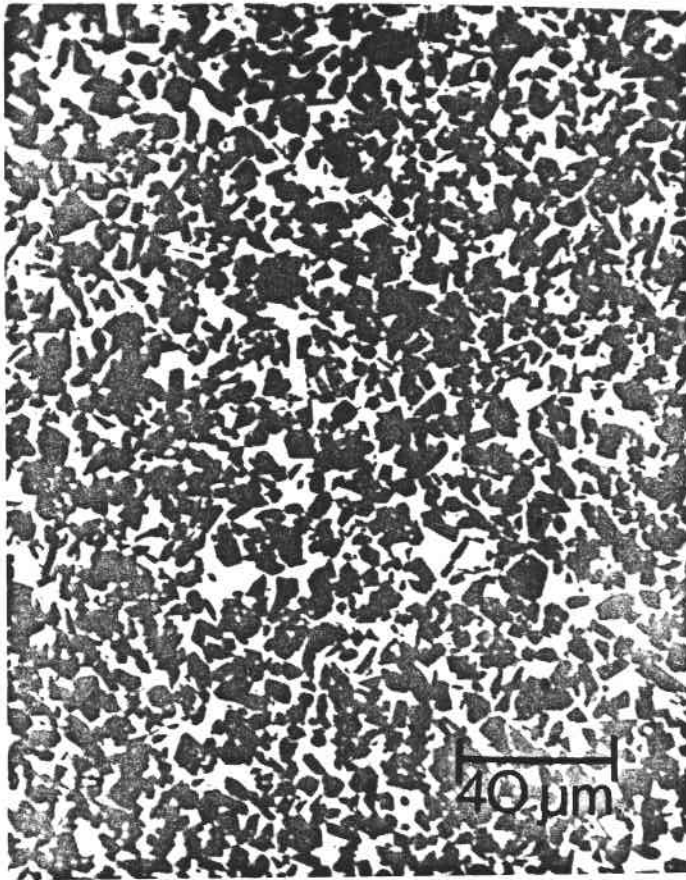235 μ - in. deflection

(a)

Compression Molded RS-SiC

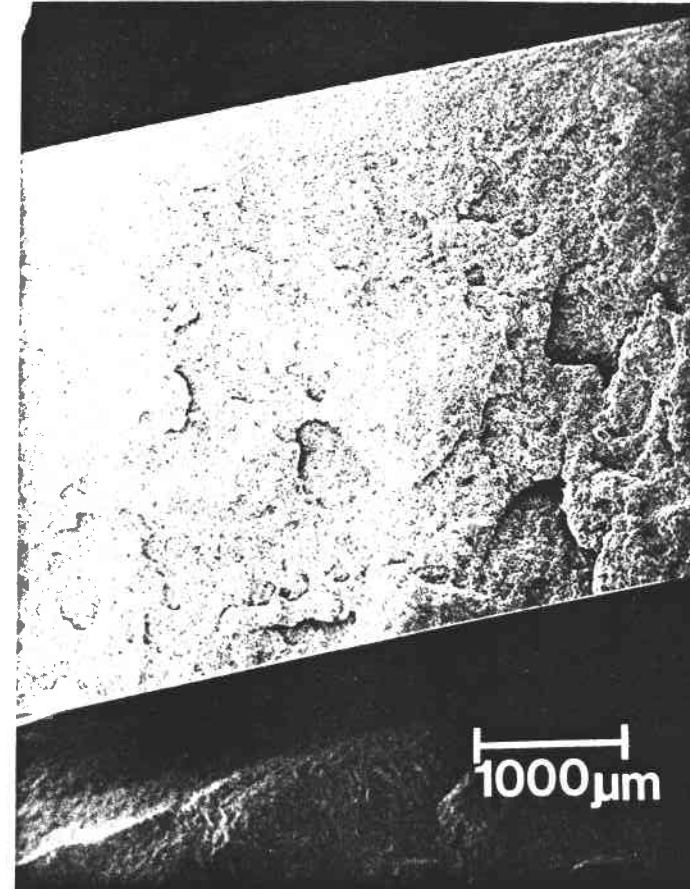108-8 σ_f=45 ksi   113.5 hrs.

258.5 μ-in. deflection

(b)

Fig.164 - Creep Deflection = (a) 0.0235 inch
            (1260°C)   (b) 0.0259 inch

(a)
Optical Microstructure

(b)
SEM Fracture Surface Appearance

Fig. 165 — Microscopy Results for a Specimen Subjected to Stress Rupture Test at
1200°C (2192°F) at an Applied Stress of 55,000 psi —   No. 19-12

appearance of another specimen (Figure 166) is very different. Here again, no obvious slow crack growth region exists although the fracture surface contains contaminants. This specimen failed in 36 minutes at an applied stress of 57,000 psi.

The stress rupture (static fatigue) experiments were conducted on dry pressed sintered alpha silicon carbide at 1500°C (2732°F) in flexural bend. The results are shown in Figure 167. The two survived specimens showed some creep deflection--approximately 3800 micro inches for an applied stress of 35,000 psi and approximately 4000 micro inches for an applied stress of 40,000 psi.

A SEM failure analysis was conducted on failed specimens. Two examples of fracture surface appearance are shown in Figure 168. In both instances, processing-related crack-like voids caused fracture. Although 40-60 hours expires in the test, no oxidation-related slow crack growth region around the main flaw can be seen.

These results have indicated the difficulties which are encountered in applying the traditionally known life predictions established via stress rupture tests in ceramics to the failure of SiC ceramics. A more fundamental understanding with respect to mechanisms causing the stress rupture of silicon carbide materials needs to be established before undertaking life predictive data reduction.

6.3.3 - Creep Experiments

High temperature creep tests were conducted with silicon carbides under this contract. The deflection of beams (0.125" x 0.25" cross section) in 4-point bend was measured as a function of time by using a 3-point probe and a LVDT set-up. The creep strain is then calculated from the beam formula:

$$\varepsilon = 16 \frac{dy}{L^2}, \quad \text{where}$$

d = specimen depth, ε = creep strain
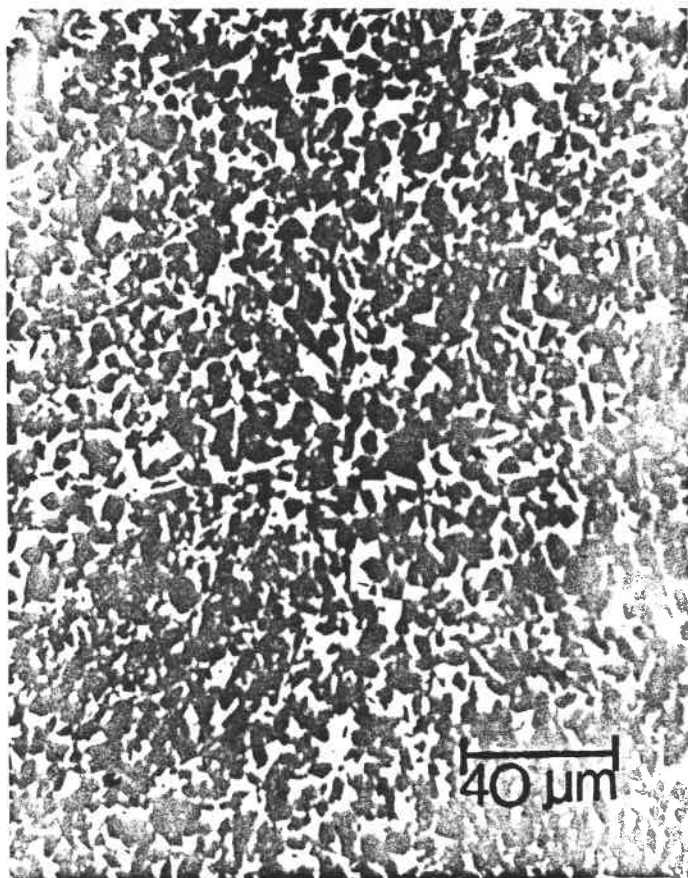y = deflection, and
L = outer span length.

A quadratic curve fit is made between the product of strain and time versus time:

$$\varepsilon t = A + Bt + Ct^2 . \qquad \text{Or}$$

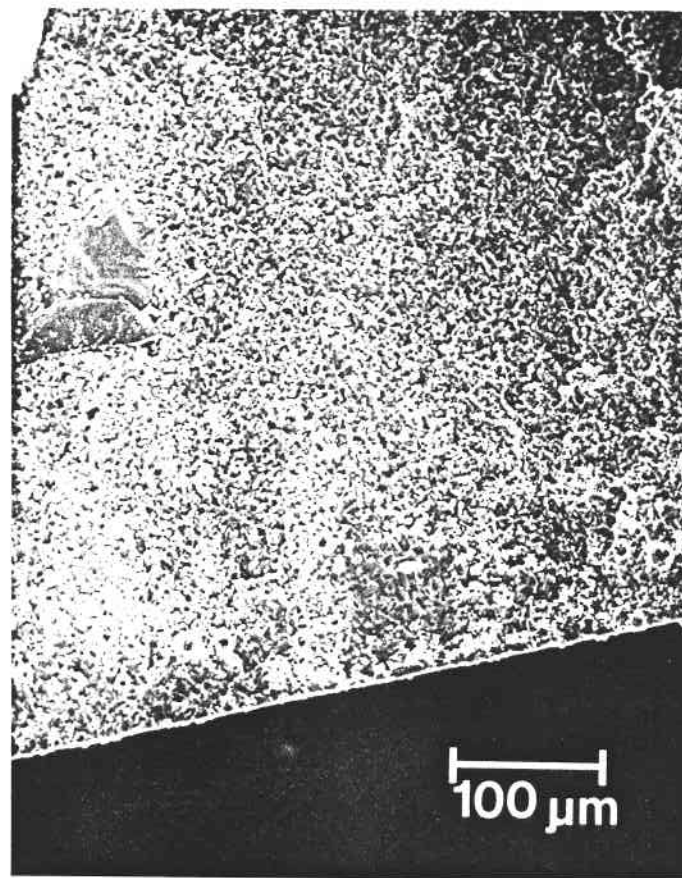$$\varepsilon = B + Ct + \frac{A}{t} .$$

t = time

A, B, C = equation constants

212

(a)
Optical Microstructure

(b)
SEM Fracture Surface Appearance

Fig. 166 - Microscopy Results for a Specimen Subjected to Stress Rupture Test at
1200°C (2192°F) at an Applied Stress of 57,000 psi - No. 106-6
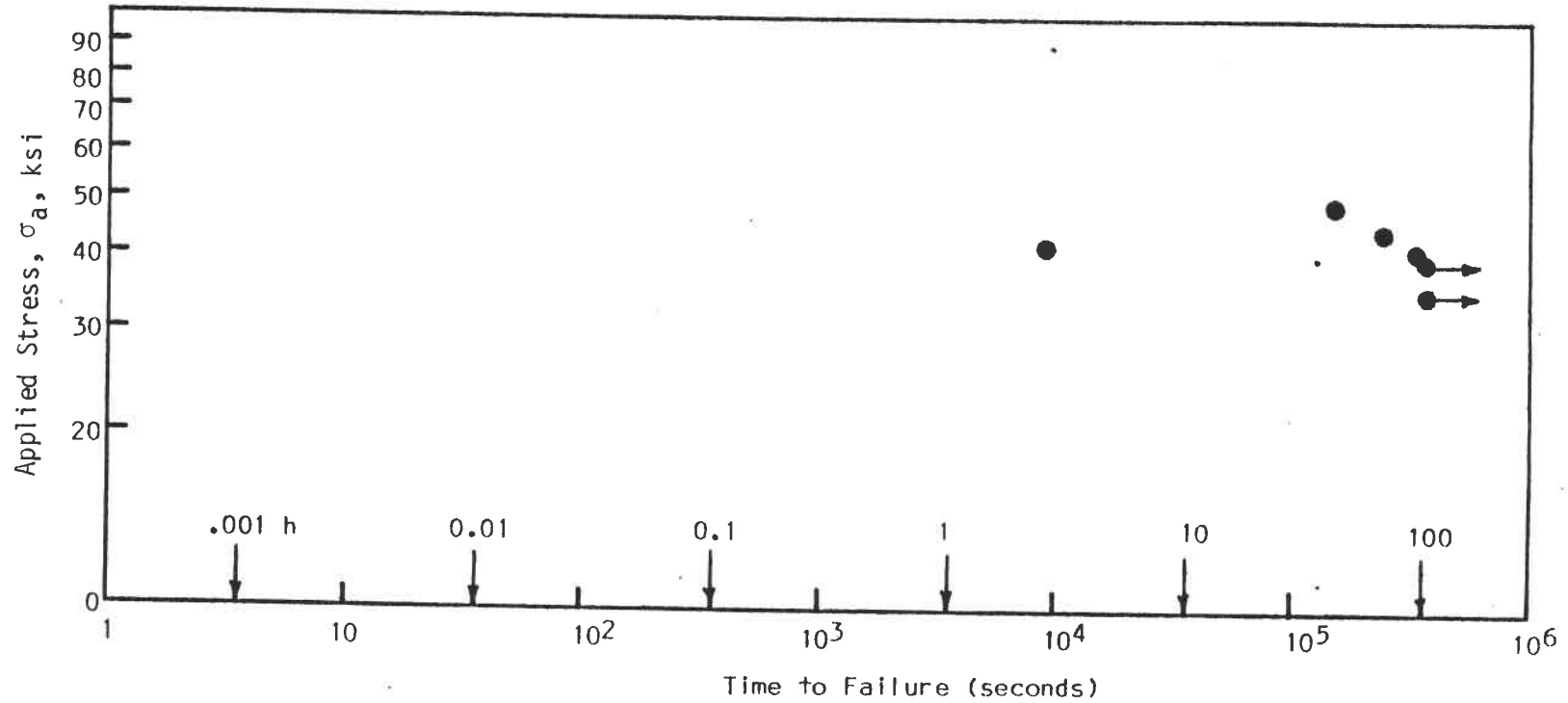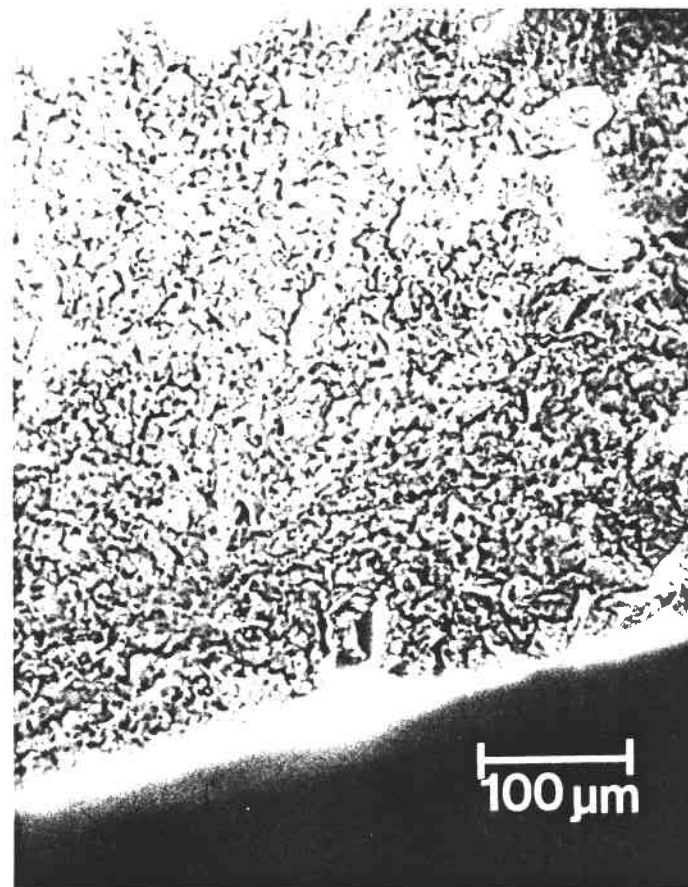
Fig. 167 – Static Stress Rupture Plot for Sintered Alpha Silicon
Carbide at 1500°C (2732°F)

(a)

No. D-9. σ_a = 45,000 psi; L_f = 65.5 h

(b)

No. H-4. σ_a = 50,000 psi; L_f = 41.5 h

Fig.168 - SEM Results for Sintered Alpha SiC Specimens Subjected
To Stress Rupture Test at $27\overline{}0^0$C (2732^0F)

Then the first differential gives the strain rate,

$$\dot{\epsilon} = C - \frac{A}{t^2} \; .$$

The $\dot{\epsilon}$ decreases with time during primary creep regime and stays fairly constant during the steady state regime. In computer calculations, the onset of steady state creep is defined to be when the second differential, $\ddot{\epsilon} = 0.001$ (that is 0.1 percent change in strain rate). In the above equation, the minimum creep rate is equal to C (that is, $\dot{\epsilon}$ at $t = \infty$).

For compression molded reaction bonded SiC, steady state creep was observed to begin between 30 and 40 h at 1200°C at applied outer fiber stress levels of 30, 45, and 50 ksi. Minimum strain rates at these stress levels were 0.741×10^{-6} in/in-h, 3.311×10^{-6} in/in-h, and 3.432×10^{-6} in/in-h respectively.

The creep curves are shown in Figure 169 and the strain rate dependence with time at $\sigma_a = 50$ ksi in Figure 170. The dependence of steady-state creep rate on applied stress is plotted in Figure 171 and the line has a slope of approximately 3. The stress exponent, n, value of 3.0 usually represents lattice mechanisms which occur independently of the presence of grain boundaries such as dislocation glide and climb. These results should be considered strictly preliminary, and an additional datum point or two between 30 and 40 ksi is highly desirable.

The bulk density was measured before and after the creep experiment and the results are given in Table 33:

Table 33 – Density Changes After Creep of RBSiC at 1200°C

Applied Stress, σ_a, ksi	Time, hours	Density, g/cc		$\frac{\Delta\rho}{\rho}$ X 100
		Initial	After Creep	
45	97	2.962	2.921	-1.4
30	114	2.966	2.958	-0.3
30	75	2.990	2.935	-1.8
50	89	2.970	2.928	-1.4

The consistent decrease in densities indicates, perhaps, cavitation during creep.
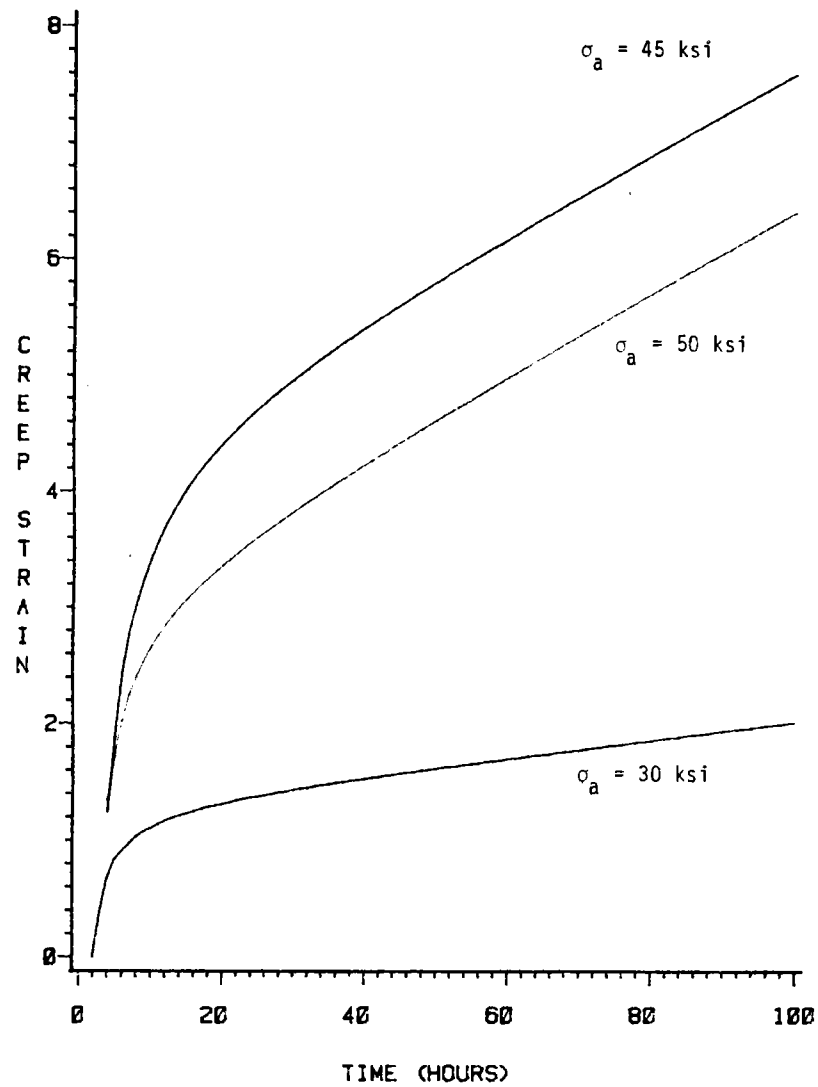
X 10**−4

Fig.169 – Creep Curves for Reaction Bonded Silicon
Carbide, Obtained by Flexural Bend
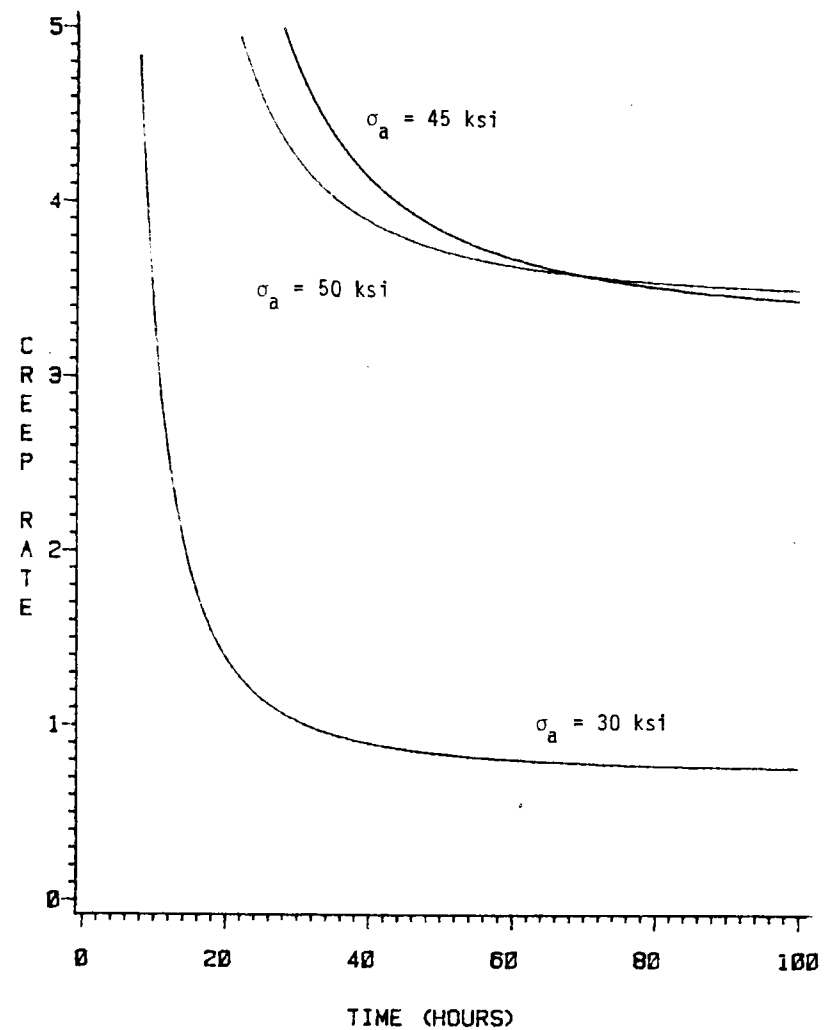Experiment in Air at 1200°C (2192°F)

X 10**−6/HR

Fig.170 – On-Set of Steady State Creep
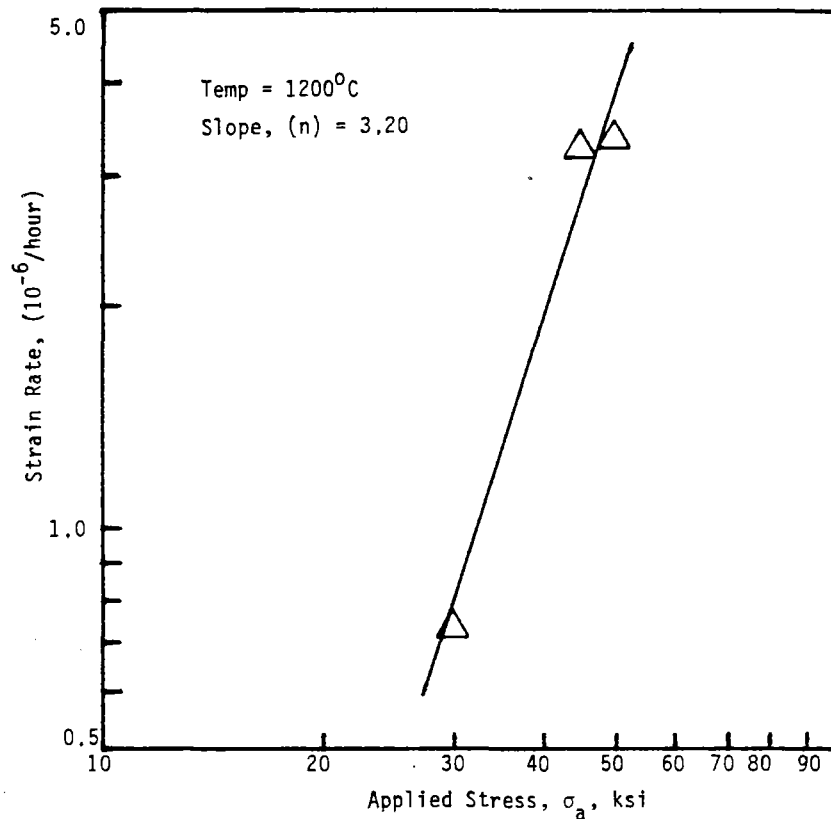for RBSiC at 1200°C

Fig. 171 - **Stress Dependence of Steady-State Creep Rate For
Fine Grain Reaction Bonded SiC at 1200°C (2192°F)**

Creep tests were also conducted for reaction bonded SiC at 1000°C and
cold pressed sintered alpha SiC at 1500°C. The results are as given below:

Compression Molded Reaction Sintered SiC at 1000°C

$\sigma_a = 35$ ksi $\qquad \dot{\varepsilon} = 1.967 \times 10^{-6}$ in/in-h
$\sigma_a = 45$ ksi $\qquad \dot{\varepsilon} = 1.918 \times 10^{-6}$ in/in-h

Essentially no change in the creep rate is observed even though the
applied stresses were different. A re-run of the experiment is suggested.

Cold Pressed Sintered Alpha SiC at 1500°C

$\sigma_a = 30$ ksi $\qquad \dot{\varepsilon} = 2.523 \times 10^{-6}$ in/in-h $\quad \Delta\rho/\rho_{\text{initial}} = -0.5\%$
$\sigma_a = 40$ ksi $\qquad \dot{\varepsilon} = 5.170 \times 10^{-6}$ in/in-h $\quad \Delta\rho/\rho_{\text{initial}} = -0.1\%$

218

6.4 - Summary of Mechanical Properties Investigations

1. Baseline statistical strength distributions were established for fine grain reaction sintered silicon carbide and alpha silicon carbides manufactured by different processes.

2. The silicon carbides exhibit excellent hot strength retention characteristics at 2192°F.

3. The thixocast reaction sintered silicon carbide exhibits unique high reliability characteristics (very high Weibull modulus) at 2192°F.

4. Extensive failure analysis investigations have established that the strength-limiting critical defects for sintered alpha silicon carbide are processing related voids and SiC agglomerates.

5. Limited slow crack growth experiments have indicated that this aspect has a minimal effect on the long term mechanical strength of the silicon carbides at high stresses and temperatures. The failures which occur in limited times cannot be explained by conventional slow crack growth concepts; however, statistical flaw and stress distribution analysis may partly explain the observed behavior. Life time predictions for these materials in service must be made with extreme caution after establishing high temperature fracture mechanisms.

6. Limited creep tests were also performed for the two silicon carbides in flexure. The alpha silicon carbide possesses excellent creep resistance even at 1500°C.

7. Oxidation, at 1260°C (2300°F), for reaction sintered SiC increases the room temperature strength for oxidation periods up to 200 hours. Considerable pitting reduces the strength, however, when the same material is oxidized at 1371°C (2500°F).

8. Because of the early termination of the contract, a more complete understanding of the mechanical effects could not be established for the silicon carbides in the areas of:

    (a) Strength distribution as a function of temperature,
    (b) Dynamic fatigue slow crack growth effects,
    (c) Kinetics and mechanisms of creep,
    (d) Oxidation of alpha silicon carbide,
    (e) Effects of elevated temperature proof tests,
    (f) Fracture mechanics,
    (g) Thermal shock,
    (h) Effect of oxidation on subsequent long term slow crack growth aspects, and
    (i) Failure prediction methodology.

It is recognized that some of the above aspects are extremely important from a practical consideration of the ceramic automotive gas turbine engine. Therefore, it is highly recommended that more important aspects of the above list be studied in greater detail when more favorable economic conditions prevail.

220

7 - PHYSICAL PROPERTIES

During the contract tenure, only the thermal diffusivity and the specific heat were measured as a function of temperature for the two silicon carbides.

7.1 - Thermal Diffusivity

Thermal diffusivity measurements were made by using l a laser flash method for both sintered alpha SiC (Figure 172(a)) and reaction bonded SiC (Figure 172(b)) at Virginia Polytechnic Institute.
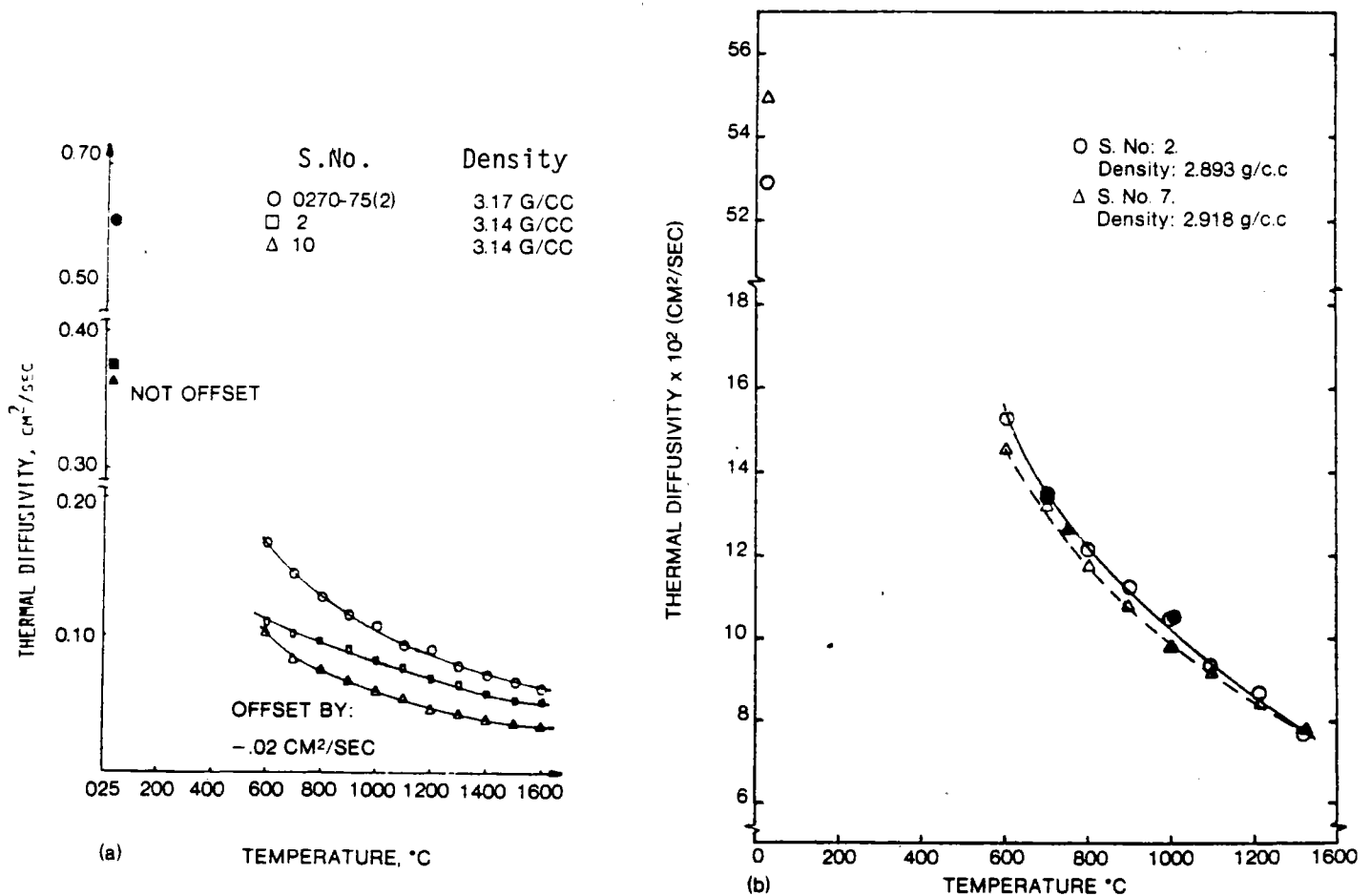

Fig.172 - Thermal Diffusivity Measurements for (a) Sintered Alpha SiC and (b) Reaction Bonded Silicon Carbide

7.2 - Specific Heat

The specific heat measurements were made through Prof. J. Brown of the Virginia Polytechnic Institute, Blacksburg. The results are shown in Figures 173 and 174.
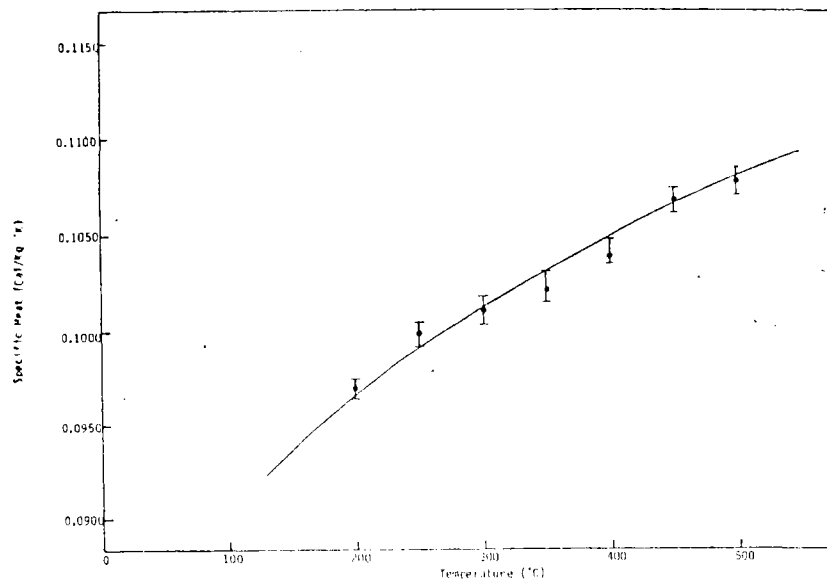

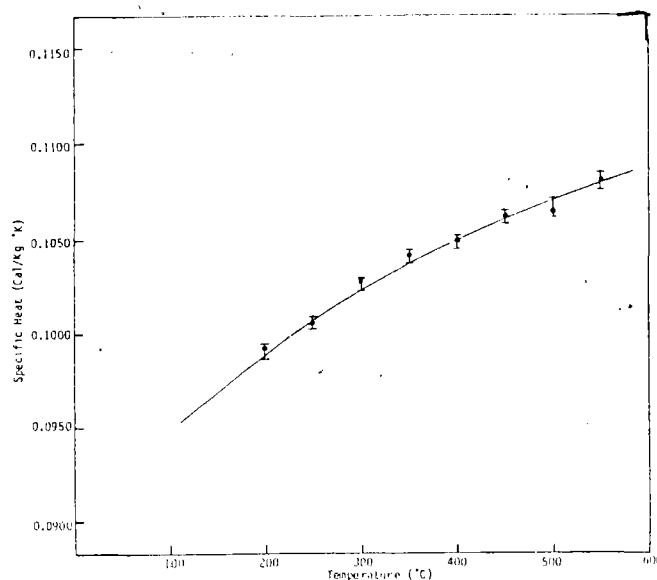**Fig. 173 - Specific Heat of Sintered Alpha Silicon Carbide**

Fig. 174 - The Specific Heat Data for Fine Grain Reaction Bonded Silicon Carbide

1. Report No. CR-180871	2. Government Accession No.	3. Recipient's Catalog No.
4. Title and Subtitle Advanced Gas Turbine (AGT) Technology Development Project, Ceramic Component Development		5. Report Date November 1987
		6. Performing Organization Code
7. Author(s) Ms. M.O. Ten Eyck, Mssrs J.W. MacBeth and T.B. Sweeting Standard Oil Engineered Materials Company, Niagara Falls N.Y.		8. Performing Organization Report No. 31-3725(13)
		10. Work Unit No.
9. Performing Organization Name and Address Standard Oil Engineered Materials Company, Niagara Falls, New York, subcontractor to: Garrett Auxiliary Power Division, Phoenix, Arizona A Unit of Allied-Signal Aerospace Company		
		11. Contract or Grant No. DEN3-167
		13. Type of Report and Period Covered Topical, October 1979 – July 1987
12. Sponsoring Agency Name and Address Department of Energy, Office of Transportation Systems, Heat Energy Propulsion Division, Washington, D.C. 20585		
		14. Sponsoring Agency Code DOE/NASA/0167-13

15. Supplementary Notes

Topical Report under Interagency Agreement
Project Manager Mr. T.N. Strom, Propulsion Systems Division
NASA-Lewis Research Center, Cleveland Ohio 44135

16. Abstract

This topical report summarizes the ceramic component technology development activity conducted by Standard Oil Engineered Materials Company while performing as a principal subcontractor to the Garrett Auxiliary Power Division for the Advanced Gas Turbine (AGT) Technology Development Project (NASA Contract DEN3-167). The report covers the period October 1979 through July 1987, and includes information concerning ceramic technology work categorized as common and unique. The common work pertains to ceramic development applicable to two parallel AGT projects established by NASA contracts DEN3-168 (AGT100) and DEN3-167 (AGT101), whereas the unique work solely pertains to Garrett directed activity under the latter contract.

The AGT101 Technology Development Project is sponsored by the U.S. Department of Energy (DOE) and administered by NASA-Lewis Research Center, Cleveland, Ohio. Project Management is provided by Mr. T.N. Strom of the NASA Propulsion System Division.

Standard Oil, acting as a principal subcontractor and supplier of ceramic components, directed its efforts toward the development of ceramic materials in the silicon-carbide family. Various shape forming and fabrication methods, and non-destructive evaluation techniques were explored to produce the static structural components for the ceramic engine. This enabled engine testing to proceed without program slippage, and developed the approaches for producing low-cost, production quantity processes. Standard Oil contributed to the acceptance of ceramics as a viable approach for auto-motive gas turbine engines and to the advancement of this vital ceramic technology.

17. Key Words (Suggested by Author(s)) Advanced Gas Turbine Single Shaft Engine Ceramic Turbine Turbine Transmission	18. Distribution Statement Unclassified – Unlimited Star Category 85 DOE Category UC-96		
19. Security Classif. (of this report) Unclassified	20. Security Classif. (of this page) Unclassified	21. No. of Pages 237	22. Price* All

* For sale by the National Technical Information Service, Springfield, Virginia 22161

NASA-C-168 (Rev. 10-75)